Evaluating vital components of elasmobranch assessment and spatial conservation

by

Manuel Dureuil

Submitted in partial fulfilment of the requirements
for the degree of Doctor of Philosophy

at

Dalhousie University
Halifax, Nova Scotia
August 2019

“Specialists are the animals that remind us what an incredible fluke it is that our world exists at all”

Rob Stewart

To my parents who have always supported and believed in me.

Table of contents

List of tables

List of figures

Abstract

Elasmobranchs (sharks, skates and rays) have been important predators in marine ecosystems for over 400 million years. However, many species experience an elevated risk of extinction today due to the effects of fishing and bycatch. Yet, scientific information to inform stock assessments and spatial conservation efforts is often scarce and of poor quality. This thesis evaluates (1) how important life history parameters can be estimated more reliably to improve data-poor stock assessments for better fisheries management, and (2) whether existing marine protected area (MPA) networks can act as an additional conservation strategy for threatened elasmobranchs. A new approach is presented to estimate somatic growth parameters from mark-recapture tagging data. This information can be utilized to estimate individual ages indirectly from body length. Another parameter that is crucial to stock assessments is natural mortality. Through comparative analysis, a unified estimator of natural mortality for elasmobranch and teleost (bony fish) is developed that reliably predicts natural mortality from maximum age, as well as a new measure, the length after which natural morality can be assumed constant. On this basis, different approaches to estimate juvenile natural mortality were tested. In cases where independent estimates of natural mortality and growth cannot be obtained this thesis shows that the ratio of natural mortality over growth can be predicted in elasmobranchs, by utilizing more available data on length at maturity and maximum length. The results are critically discussed with regards to life history theory and potential applications in data-poor assessments. Finally, existing MPA networks across northern Europe were evaluated to determine if their increased coverage translated into increased conservation for data-poor and threatened elasmobranch species. It was shown that industrial trawl fishing is 38% higher within MPAs, on average, and that the relative abundance of elasmobranchs within an area decreases significantly with the intensity of trawl fishing. These findings suggest that low protection standards of investigated MPAs undermines conservation outcomes for these and potentially other threatened species. To conclude, this thesis provides approaches to obtain improved ecological insights, stock assessments and spatial protection for elasmobranchs, in order to facilitate more effective fisheries management and conservation.

Acknowledgements

First and foremost, my thanks go to my main supervisor, Boris Worm. I cannot even put in words how thankful I am for your support. Maybe I start with some so-called “side projects” to my PhD that are still ongoing, projects that I really wanted to do, and that you supported me to pursue. These include an elasmobranch conservation and research project in Cabo Verde, the foundation of Sharks of the Atlantic Research and Conservation Centre (ShARCC) and the Assistant Professor position to co-teach the sharks, rays and skates class at Dalhousie. Even though without those projects I would, without any doubt, have had more time to sleep at nights during my PhD, I would not have been able to develop the many skills that I am so happy to have and the many experiences that I’m glad I didn’t miss. You understand passion, so thank you for teaching me how to handle it and teaching me that there is a life beside (not without!) sharks, rays and skates. Your incredible talent for seeing the bigger picture, asking the right questions and formulating everything in the most understandable and compact way before communicating it taught me so much. I could have not asked for more or better in my PhD. Thank you Boris.

Furthermore, I would like to thank my co-supervisor Rainer Froese. I am so grateful, Rainer, for being your student and being trained by someone with your expertise and knowledge. What I took away from our discussions or some of your challenging tasks is beyond words. You are playing a significant role in the way I do science, how I address problems and the way I critically question things. I am learning from you the art of logic and reasoning to produce sound science. I cannot put into words how grateful and honored I am for everything you have done for me.

A special thanks also to my committee members, Fred Whoriskey and Mike Dowd, and my external examiner Neil Hammerschlag. Fred, thank you so much for all your trust in me and all your support, with the shark class and with Cabo Verde. Thank you for having an open ear and giving the best and calming advice in stressful situations. Mike, thank you for the most helpful advice on statistics, in particular for the natural mortality chapter. It is always very refreshing to chat with you. Neil, I am very thankful your comments and feedback, this improved the thesis a lot. Thank you for being such an inspiration.

Also, I would like to give a special thank you to my third unofficial supervisor, mentor and shark class co-instructor Chris Harvey-Clark. Chris, what I have learned from you is unbelievable. You are an inspiration and I enjoyed every second that I could spend with you. You taught me shark tagging and so many other things. I am forever grateful.

I would also like to thank everyone that played a critical part in this journey: Art Gaetan for showing me my first blue shark and for sharing some of the most memorable moments in my life with me; Brendal Townsend for all your support from day one. You made so much possible for me and I will never forget that; William Aeberhard for being a friend and a stats tutor. Thank you for all your statistical advice, for providing your expertise, not giving up on me, the improved R code for the simulation analysis and the implementation of the growth methods, in particular the maximum likelihood and Bayesian methods in Chapter 3; Alison Towner and Lothar Beck, my professional shark journey started with you. Ali, you showed me my first live shark, and always supported me, something I will always appreciate; To OTN, especially Joe, for your help in Cabo Verde and during the shark class, and for sharing some pretty amazing memories, and to Anja and Nikki for your amazing support; To the Animal Ethics lab, in particular Jennifer Wipp, for all your help over the years and the nice chats during my irregular visits, and Jennifer Devitt for teaching me how to stitch up a shark; To my most wonderful previous office mates Nina, Silvia, Jan and Nazli, for all your support and good company for many years now; To Henning Winker for the most engaging discussions; To Warren Joyce, Heather Bowlby and Dave Kulka for all the helpful discussions, your great support in the shark class and for sharing your incredible expertise with me. I am honored learning from you all. To Mason for being an incredible lawyer and starting ShARCC with me. To Rob Stewart, the most passionate and incredible human being I have ever met. Your legacy will live on.

A special thanks to my office mates and the Worm Lab associates (current and past); Kristina, Beth and Laurenne you are amazing; and to Aurelie and Greg for being amazing as well, and for teaching me so much; to Rodrigo, Christine, Derek and Heike, for stimulating discussion (mostly about sharks, even about German sharks and sometimes stats); and Nakia for becoming the best shark buddy on the other side of the planet.

Thanks to everyone else who accompanied this journey, to all the teachers and all the guest lecturers in the shark class, I learned a lot. To all the shark class students as well, you may have taught me more than I could teach you. To all my friends, from back home and all the friends that I made during this journey, from Cabo Verde, South Africa, Mexico, Brazil, to just mention a few, and of course to all the dear friends I made in Canada.

I would also like to thank James A. Thorburn, Ken Collins and Jim Ellis for providing me your tope tagging data; Rory McAuley for providing me with your sandbar shark tagging

data; Bob Hueter and John Tyminski for providing the bonnethead shark length frequencies and time at liberty records; Bryan Frazier for providing information on bonnethead growth and the very helpful feedback and comments; Heath Stone for providing me with length frequency data for skates and sharks from Eastern Canada and for all your help and support; and Thorsten Werner for providing your expertise on European marine conservation; and to everyone else who provided me with feedback and helpful comments, in particular during the European Elasmobranch Conferences.

I am very grateful for the support from the Sobey Fund for Oceans, the Nova Scotia Innovation and Research Entrance Graduate Scholarship, the Dalhousie University Department of Biology and the Transatlantic Ocean System Science and Technology program that made many collaborations possible and introduced me to wonderful places and people. I also gratefully acknowledge the open data policy from the Centre for Environment, Fisheries and Aquaculture Science, Global Fishing Watch, the World Database on Protected Areas, the International Council for the Exploration of the Sea, and the Information and Data Centre at Commonwealth Scientific and Industrial Research Organisation (CSIRO) Oceans and Atmosphere, Australia.

Lastly, but most importantly, I would like to thank my family, my partner and my Luna. Thank you Luna for always cheering me up and giving me a meow and attention when needed. Thank you mum and dad for the best support of all; to my sister, my niece and brother in law for being always there; and to Kirsti and my new second family I found here. Kirsti I cannot even put in words how much I appreciate all the sharky discussions and late night debates and all your incredible help, thank you for being my partner and best friend.

Without all of you this thesis would have not been possible.

Chapter 1
Introduction

1.1 General introduction

Elasmobranchs (sharks, skates and rays) are a group of predominantly marine fish that evolved more than 400 million years ago with a diversity of about 1,150 species today (Ebert & Stehmann, 2013; Last et al., 2016). These species have become of increasing conservation concern over the past few decades because of dramatic population declines around the globe (Baum et al., 2003; Baum & Myers, 2004; Ferretti et al., 2008, 2010; Roff et al., 2018), and are now considered one of the most threatened group of animals on the planet (Dulvy et al., 2014; www.iucnredlist.org).

This precarious conservation status of elasmobranchs today is largely due to increased anthropogenic mortality, either through incidental bycatch or as targeted catch predominantly for fins, meat and liver oil (Stevens et al., 2000; Dulvy et al., 2014). The global catch of sharks alone is estimated to be around 100 million individuals per year, with the majority stemming from discarded bycatch (Worm et al., 2013). In addition, elasmobranchs commonly display low productivity due to their life history characteristics being slow growth, late maturity and few albeit large offspring (Hoenig & Gruber, 1990; Camhi et al., 1998; Cortes, 2000; Dulvy et al., 2014). Although, large offspring have higher survival rates, they are also associated with greater parental investment, such as long generation times and reduced numbers of pups. This, in turn, selects for slow growth, long life spans, larger adult body sizes and increased adult survival (Kindsvater et al., 2016).

Due to their low productivity and slow life history pattern most elasmobranchs cannot withstand perturbations (such as fishing) well (Kindsvater et al., 2016). Consequently, even mild exploitation can deplete populations relatively fast, whereas recovery rates are very slow (Ward-Paige et al., 2012). To prevent further depletion and aid recoveries, necessary fisheries management strategies and conservation measures need to be based on the best scientific advice. However, elasmobranchs have among the highest proportion of data-deficient species of any animal group, with almost half of all species having insufficient information to assess their status (Dulvy et al., 2014; www.iucnredlist.org), yet many of those are predicted to be threatened (Dulvy et al., 2014; Fernandes et al., 2017). The problem of data deficiency is often two-fold: a scarcity of data combined with low data quality where information exists. For example, ages are now considered to be systematically underestimated in many elasmobranchs (Harry, 2017;

Natanson et al., 2018), but such age information forms the basis of many stock assessments.

A fundamental aspect of scientific assessment requires good information on the dynamics of a population, conceptualized in Fig. 1.1. In a closed population, i.e. assuming no emigration or immigration, reproduction (or recruitment), growth and natural mortality are the key processes determining population size under natural conditions. In exploited populations fishing mortality is added to the natural mortality rate (Fig. 1.1). Hence, it is these natural processes that hold information about a population's intrinsic capacity to withstand exploitation. Therefore, knowledge on natural mortality, growth and reproduction are vital in order to inform stock assessments and gain information about a species' resilience. Consequently, methods that can reliably estimate these vital processes from the often limited information are not only benefiting the general understanding of elasmobranch ecology, but are also critical to improve existing assessments and allow for more species to be assessed. On this basis, scientific advice for fisheries management and conservation could be generated more comprehensively for sharks, skates and rays.

Another suitable management and conservation tool in data-poor situations are spatial protection measures such as dedicated fisheries closures, shark sanctuaries, or marine protected areas (MPAs) (Johannes, 1998; Ward-Paige & Worm, 2017). The latter is a form of spatial conservation aiming to protect parts or the entirety of a habitat or ecosystem. Given their increasing popularity and ocean coverage (Worm, 2017), and the many studies that have suggested that MPAs can have positive effects on elasmobranchs (Garla et al., 2006; Claudet et al., 2010; Bond et al., 2012; Knip et al., 2012a; Le Port et al., 2012; Bond et al., 2017; Da Silva et al., 2013; Edgar et al., 2014; Espinoza et al., 2014; Escalle et al., 2015; Graham et al., 2016; Ward-Paige & Worm, 2017; White et al., 2017; Davidson & Dulvy, 2017; Speed et al., 2018; Boerder et al., 2019; Germanov et al., 2019; Carlisle et al., 2019), they could be another important conservation tool for sharks, rays and skates. Therefore, MPAs can be viewed as a vital component in the spatial conservation of elasmobranchs. Yet, MPAs and entire MPA networks can have different standards and guidelines (Reker et al., 2015). Hence, whether the increasing coverage of MPAs also translates into increasing conservation of elasmobranchs is largely unknown, particularly in temperate waters.

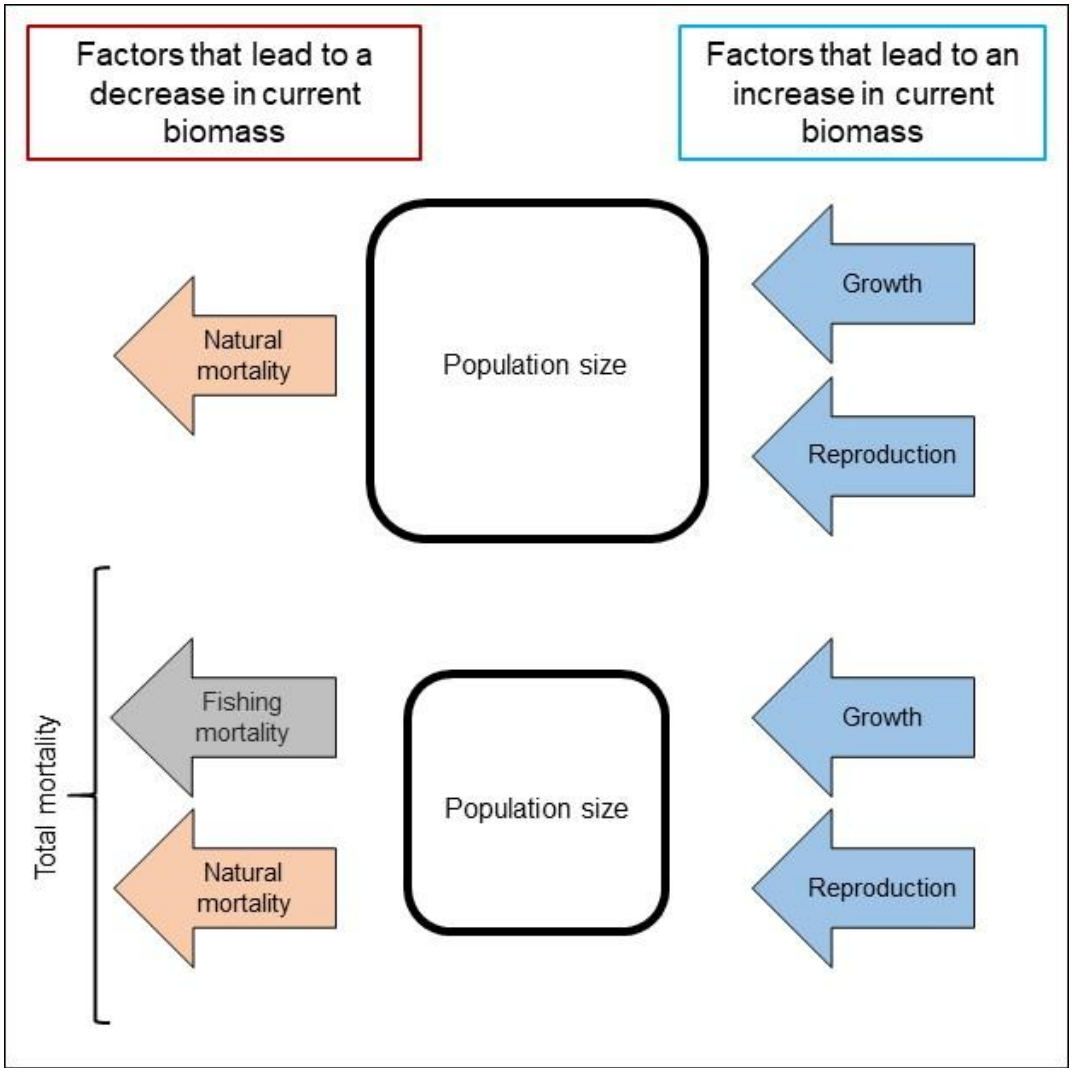

Fig. 1.1: Schematic representation of factors affecting the dynamics of populations.

In this context, the overarching objective addressed by this thesis is to critically evaluate and help improve vital components of elasmobranch assessment and spatial conservation. The ultimate goal is to contribute to improved fisheries management and effective conservation for elasmobranchs, especially in the absence of detailed biological and fisheries data. More specifically this thesis asks (1) how reliable life history parameters can be obtained in data-poor situations to inform stock assessment and fisheries management, while gaining more detailed insights into the ecology of elasmobranchs, and (2) whether existing MPA networks act as a suitable conservation tool for threatened elasmobranchs?

1.2 Thesis outline

This thesis is organized into 5 publication-format chapters that evaluate vital components of elasmobranch assessment and spatial conservation, beginning with an introductory chapter and ending with a concluding chapter that describes the main findings, discusses ecological and conservational implications and management applications, as well as suggestions for future research directions. In Chapter 2, a comparative study was designed to investigate different methods that estimate growth parameters from mark-recapture tagging information on a dataset from the threatened Northeast Atlantic tope shark (*Galeorhinus galeus*). A combination of empirical and simulated data was utilized to identify the best performing approach given the limited information available. In Chapter 3, a new methodology is suggested to estimate growth from limited mark-recapture information for elasmobranch species, in general. Here, different methods were tested on empirical mark-recapture data from various elasmobranch species and on simulated data. A best performing methodology to estimate growth from limited mark-recapture information in elasmobranchs is presented. Chapter 4 focuses on the natural mortality rate, one of the most difficult life-history parameters to estimate, but crucial for scientific assessments. The aim of Chapter 4 is to present a method that reliably predicts adult and juvenile natural mortality from more available life history parameters in elasmobranchs. Therefore, a dataset was generated first that contained available direct observations of elasmobranch natural mortality and life history parameters. This information was then compared to the information available for teleosts (bony fish) to investigate if common relationships exist. Based on information on observed natural mortality, maximum age and proportion of survivors to maximum age for both taxa, a new natural mortality estimator was developed and compared to other commonly applied

estimators. Furthermore, approaches to estimate maximum age from growth were also investigated, and an approach is presented that allows the estimation of natural mortality if observations on longevity are absent. In Chapter 5, the predictability of the ratio of natural mortality over growth for elasmobranchs is investigated. This ratio is important in many data-poor assessments. Commonly, it has been assumed invariant, but collective evidence suggests it to be variable, yet predictable. Based on the dataset generated in Chapter 4, length at maturity and maximum length were evaluated as possible predictors. An interim approach is presented that might be utilized until more accurate information becomes available, limitations and applications are critically discussed, and future research directions proposed. In Chapter 6, existing marine protected area networks across northern Europe are evaluated to determine if their increased coverage translates into increased conservation for elasmobranch species inhabiting the region. Evaluation was based on the relative abundance of elasmobranchs within an MPA, as well as the quantity of industrial trawl fishing, a major threat to these species. Chapter 6 reveals current limitations and identifies standards and guidelines needed for MPAs to be an effective conservation tool for elasmobranchs.

1.3 Statement of authorship

The 5 data chapters (Chapters 2 – 6) are organized as manuscripts intended for publication, or have already been published in peer-reviewed scientific journals, with an introduction, materials and methods, and a results and discussion section. In the following the current publication status is listed. For all published chapters the author of this thesis was the main contributor to the design, the research and the writing.

Chapter 2: **Dureuil, M.,** & Worm, B. (2015). Estimating growth from tagging data: an application to north-east Atlantic tope shark Galeorhinus galeus. Journal of fish biology, 87(6), 1389-1410.
https://onlinelibrary.wiley.com/doi/abs/10.1111/jfb.12830

Chapter 3: Re-evaluating methods to estimate growth from tagging data in elasmobranchs. Unpublished.

Chapter 4: A unified natural mortality estimator for marine fish. Unpublished.

Chapter 5: Relationships between mortality, growth and reproduction in elasmobranchs. Unpublished.

Chapter 6: **Dureuil, M.,** Boerder, K., Burnett, K. A., Froese, R., & Worm, B. (2018). Elevated trawling inside protected areas undermines conservation outcomes in a global fishing hot spot. Science, 362(6421), 1403-1407.
https://science.sciencemag.org/content/362/6421/1403

Chapter 2
Estimating growth from tagging data: an application to north-east Atlantic tope shark *Galeorhinus galeus*

2.1 Abstract

This study addresses the inherent uncertainty when estimating growth from limited mark-recapture information. A selection procedure was developed utilising 18 competing growth estimation methods. The optimal method for a given dataset was identified by simulating the length at capture and length at recapture under different scenarios of measurement error and growth variability while considering the structure of the observed data. This selection procedure was applied to mark-recapture data for 37 female and 16 male tope sharks *Galeorhinus galeus* obtained from tagging studies in the north-east Atlantic. Parameter estimates differed strongly among methods, showing the need for careful method selection. The selection approach suggested that best estimates for males and females were given by James' weighted least squares approach with a fixed asymptote. Given an average size at birth of 28 cm, the von Bertalanffy growth function of north-east Atlantic *G. galeus* would be $L_t = 200.85 - (200.85 - 28)e^{-0.076t}$ for females and $L_t = 177.30 - (177.30 - 28)e^{-0.081t}$ for males. The resulting age estimates were up to 11 years lower when compared to previous estimates derived from highly uncertain vertebrae readings. More generally, this procedure can help identify optimal estimation methods for a given dataset and therefore aid in estimating more reliable growth parameters from mark-recapture information.

2.2 Introduction

Growth of individuals is a key aspect in fisheries science as it determines the gain of biomass for a particular stock. In 1938, von Bertalanffy published a model that allows predicting the length of an organism from its age, which has become the most commonly used approach to estimate growth of both bony and chondrichthyan fish (Cailliet & Goldman, 2004). In sharks, most growth studies use length at age data obtained from growth band deposition in vertebrae which assumes periodic ring formation (Cailliet & Goldman, 2004). Although the periodicity of ring formation is often not tested, many sharks are believed to have annual band deposition (Cailliet & Goldman, 2004; Cailliet, 2015).

Dureuil, M. and Worm, B., 2015. Estimating growth from tagging data: an application to north-east Atlantic tope shark *Galeorhinus galeus*. Journal of fish biology, 87(6), pp.1389-1410. https://onlinelibrary.wiley.com/doi/abs/10.1111/jfb.12830

For some shark species however, age obtained from vertebrae band readings can be misleading due to irregular formation or decay of annual growth bands (Natanson & Cailliet, 1990; Kalish & Johnstone, 2001; Natanson et al., 2002, 2014; Ardizzone et al., 2006; Francis et al., 2007; Andrews et al., 2011; Hamady et al., 2014). Tope shark *Galeorhinus galeus* (Linnaeus 1758) is considered to be such a species (Kalish & Johnstone, 2001), requiring alternative approaches to estimate growth.

Although tagging studies primarily focus their research on distribution and movement, these studies can also provide information on a variety of biological aspects, including growth (Kohler & Turner, 2001). Approaches for estimating growth based on mark-recapture tagging data use differential length measures (Gulland & Holt, 1959; Fabens, 1965; Francis, 1988b) and have been applied to several shark species (e.g. Simpfendorfer, 2000; Skomal & Natanson, 2003; Meyer et al., 2014). However, these methods can produce different results for the same dataset and can give biased results if growth is variable, time at liberty is short, or the sample size is small, outlier contaminated or not representative of all age classes (Sainsbury, 1980; Francis, 1988a; Maller & deBoer, 1988; Kimura et al., 1993; Wang & Thomas, 1995; Simpfendorfer, 2000; Natanson et al., 2002, 2006; Skomal & Natanson, 2003; McAuley et al., 2006; Eveson et al., 2007). Presently, it remains unclear which method performs best for a given data set, in particular when only limited data is available.

Here, a procedure to help select the best performing growth estimation method for a given mark-recapture dataset was developed. A simulation analysis with known input parameters for growth was used, which considered sample size, length and time at liberty distributions, i.e. the structure of the data, as well as individual growth variability (GV) and measurement error (ME). From this, the best performing method was identified and applied to a small dataset containing tagging information for *G. galeus* in the north-east Atlantic.

The north-east Atlantic stock of *G. galeus* ranges from the North Sea to north-west Africa and the Mediterranean Sea (ICES, 2009). In this region, this species is classified as *Data Deficient* on the IUCN Red List (Walker et al., 2006) and an analytical assessment is missing (ICES, 2014). Despite reliable catch data, information about life history of *G. galeus* is also lacking. Growth studies have been undertaken for *G. galeus* stocks elsewhere (Grant et al., 1979; Ferreira & Vooren, 1991; Moulton et al., 1992; Francis & Mulligan, 1998; McCord, 2005), but to date only one study has examined age structure of this stock based on vertebral samples of four males (Henderson et al., 2003). Therefore,

the aim of this study was to determine growth parameters of *G. galeus* in the north-east Atlantic. This can aid in future assessment and may help to better understand this species' resilience to exploitation.

2.3 Materials and methods

2.3.1 Growth estimation methods

All growth curves were fitted using the von Bertalanffy growth function (von Bertalanffy, 1938):

$$L_t = L_\infty - (L_\infty - L_0)e^{-kt}, \quad (2.1)$$

where L_t is the total length (cm) at age t (years), L_∞ is the asymptotic total length, L_0 is the total length at birth and k is a curve parameter describing how fast L_∞ is approached. Capape et al (2005) found L_0 for *G. galeus* to range between 24 cm and 32 cm with a mean of 28.05 ± 2.68 cm, thus L_0 was set to 28 cm. In total, 18 different variants of the von Bertalanffy growth function were considered, based on seven broader growth estimation methods for mark-recapture data (Table 2.1). The Gulland and Holt method (Gulland & Holt, 1959) uses the graphical interpretation of annual growth increments and mean length to estimate von Bertalanffy growth parameters (VBGP). This method was applied as described in Sparre & Venema (1999). The Fabens method (Fabens, 1965) uses a least squares method to estimate growth parameters k and L_∞. James (1991) proposed to use a weighted least squares approach of the Fabens method, instead of ordinary least squares. The weighting factor of the Weighted Fabens method is the inverse variance. In addition to the Fabens method, which solves for length increments, a transformed version was tested, the *Delta t* method. This method minimises the residual sum of squares between the observed and predicted time at liberty. The James method is another estimator suggested by James (1991) to obtain unbiased parameters by solving two equations simultaneously instead of using a least squares approach. A joint solution for both equations was obtained by the Newton-Raphson method of the *rootSolve* package (Soetaert, 2009) in the statistical software *R* (R Core Team, 2013). The Wang method (Wang, 1998) considers GV by letting the asymptotic length vary. Therefore, an additional parameter to Fabens' equation is introduced. The Francis method (Francis, 1988b) is an extension to the Fabens method by using a maximum likelihood approach. This function includes two estimated mean growth rates g_{L1} and g_{L2} at two user selected reference lengths L_1 and L_2. These reference lengths should lie within the length at capture range.

In this study, the mean of the three smallest and largest values of length at capture were used for the smaller and larger reference lengths respectively. The Francis method also allows the estimation of GV, the mean and standard deviation of MEs (*m* and *s*), the probability of outlier contamination (*p*) and the seasonality of growth. The latter was not considered here. Overall, up to six parameters were estimated by the this method (model 1: g_{L1}, g_{L2} and *s*; model 2: g_{L1}, g_{L2}, *s* and GV; model 3: g_{L1}, g_{L2}, *s*, GV and *m*; model 4: g_{L1}, g_{L2}, *s*, GV, *m* and *p*). The simplest model (model 1) was investigated first and parameters were added successively up to model 4. The Akaike Information Criterion (AIC) was used to investigate an improvement of the model by adding parameters. In this study, time at liberty for Francis method was added to an arbitrary time at capture, because the exact date was lacking for three individuals. The analysis of Francis method was performed in *R* software by using a modified *grotag* function of the *fishmethods* package (Nelson, 2013). In addition to these seven broader growth estimation methods, it was investigated if a fixed value of the asymptotic length L_∞ can reduce bias in parameter estimates for methods that did not consider GV. For the methods that did not consider heteroscedasticity, it was investigated whether a multiplicative error structure (ln – ln transformation) can produce better parameter estimates. The value used as fixed asymptotic length for *G. galeus* was obtained from the species' maximum length L_{max}, determined by the average length of the three largest (or heaviest) specimens caught in the north-east Atlantic. If only total body weight, *W*, (gram) was given, total length was estimated via the inverted length-weight relationship of *G. galeus* for the north-east Atlantic for females

$$L = [W(0.0029^{-1})]^{3.1^{-1}} \quad (2.2)$$

and males

$$L = [W(0.0042^{-1})]^{3.01^{-1}} \quad (2.3)$$

respectively (Dureuil, 2013). Asymptotic length was estimated from its relationship to maximum length (Froese & Binohlan, 2000):

$$L_\infty = 10^{(0.044+0.9841 \log L_{\max})}. \quad (2.4)$$

The 95% confidence limits of L_∞ were based on the standard error estimates given by the authors.

Table 2.1: Summary of the different methods considered to estimate growth from tagging data. In total, 18 different approaches were investigated, based on seven broader growth estimation methods. The equations of the latter are provided. For the methods that did not consider growth variability, it was investigated if variants with a fixed value of the asymptotic length L_∞ (*fix*) can reduce bias in parameter, in addition to the basic methods. The value used as fixed asymptotic length was obtained from its relationship to the species' maximum length L_{max}. For the methods that did not consider heteroscedasticity, it was investigated if variants utilising a natural logarithm (ln – ln) transformed error structure (*e*) can produce better parameter estimates, in addition to the basic methods. Note that the *Delta t* method with a fixed asymptote (*dtfix*) requires the lengths at capture and recapture to be smaller than L_∞, the ln – ln transformed Fabens and Gulland and Holt methods with a fixed asymptote (*fabfixe*, *GHfixe*) require the length at capture to be smaller than L_∞.

Symbol	Name	Equations*	Variants	Fixed Parameters	Estimated Parameters	Reference
GH	Gulland and Holt method	$\frac{dL}{dt} = a + bL_{\text{mean}}$ $L_{\text{mean}} = (L_r + L_c)2^{-1}$ $k = -b, L_\infty = -ab^{-1}$	*GHe* *GHfix* *GHfixe*	 L_∞ L_∞	L_∞, *k* *k* *k*	Sparre & Venema (1999)
fab	Fabens method	$dL = (L_\infty - L_c)(1 - e^{(-kdt)})$	*fabe* *fabfix* *fabfixe*	 L_∞ L_∞	L_∞, *k* *k* *k*	Fabens (1965)
wfab	Weighted Fabens method	$\sum\left\{\left[L_r - L_c - (L_\infty - L_c)\left(1 - e^{(-kdt)}\right)\right]^2 (1 + e^{(-2kdt)})^{-1}\right\}$	*wfabfix*	L_∞	*k*	James (1991)
dt	Delta t method	$dt = -k^{-1} ln[(L_\infty - L_r)(L_\infty - L_c)^{-1}]$	*dte* *dtfix* *dtfixe*	 L_∞ L_∞	L_∞, *k* *k* *k*	This study
jam	James method	$\sum\left[L_r - L_c - (L_\infty - L_c)\left(1 - e^{(-kdt)}\right)\right] = 0,$ $\sum dt\left[L_r - L_c - (L_\infty - L_c)\left(1 - e^{(-kdt)}\right)\right] = 0$			L_∞, *k*	James (1991)
wan	Wang method	$dL = [L_\infty + \beta(L_c - \bar{L_c}) - L_c](1 - e^{(-kdt)})$	*wane*		L_∞, *k*	Wang (1998)
fra	Francis method	$L = \left[\left(L_2 g_{L_1} - L_1 g_{L_2}\right)\left(g_{L_1} - g_{L_2}\right)^{-1} - L_c\right]\left\{1 - \left[1 + \left(g_{L_1} - g_{L_2}\right)(L_1 - L_2)^{-1}\right]^{dt}\right\}$ $k = -ln\left[1 + \left(g_{L_1} - g_{L_2}\right)(L_1 - L_2)^{-1}\right]$ $L_\infty = (L_2 g_{L_1} - L_1 g_{L_2})(g_{L_1} - g_{L_2})^{-1}$			L_∞, *k*	Francis (1988b)

*Descriptions: All length *L* are total length (cm). The variable dL is the growth increment, *dt* is the time at liberty (years), *b* is the slope, *a* the intercept, L_c is the length at capture, L_r is the length at recapture, *k* is the von Bertalanffy growth constant, L_∞ is the asymptotic length, the parameter ß allows L_∞ to vary, $\bar{L_c}$ is the mean length at capture, and g_{L1} and g_{L2} are estimated mean growth rates at two user selected reference lengths L_1 and L_2.

2.3.2 Data

Information on north-east Atlantic *G. galeus* sex, date of release and recapture and length or weight at capture and recapture was extracted from the literature (Holden & Horrod, 1979; Stevens, 1990) and provided by the Centre for Environment, Fisheries and Aquaculture Science (CEFAS) tagging database, the UK Shark Tagging Programme and the Scottish Sea Angling Conservation Networks (SSCAN) Shark Tagging Programme. Duplicate records were deleted. Values for length obtained from weight by Stevens (1990) were back-calculated to weight by the formula he applied. Equations (2.2) and (2.3) were then used to calculate length whenever weight was given instead of length or when length values were erroneous. Data on growth rates from tagging data can be subject to significant MEs (Holden & Horrod, 1979; Stevens, 1990) of the inherent variability in body weight or imprecise measurements. Therefore, negative growth rates and biologically questionable data points were excluded. The latter were identified by using the assumption of a linear decrease when plotting growth per year against the mean length (Gulland & Holt, 1959). This method is believed to be strong in detecting data points that deviate from the von Bertalanffy growth model (Sparre & Venema, 1999). Outliers were identified by using the *influence plot* function of the *car* package in *R* (Fox & Weisberg, 2011), which combines Studentized residuals, hat values, and Cook's distance. Values showing a large Cook's distances and deviating more than three times the average hat value and/or ± two times the Studentized residuals were discarded. In total, four female and three male data points were considered as outliers and removed from the analysis, giving a final sample size of 37 female and 16 male individuals. Details on outlier removal are provided in Appendix A.

Table 2.2: Simulation runs executed in this study. Small errors were simulated with a standard deviation of 0.01 and large errors with a standard deviation of 0.05. Here, the standard deviation was multiplied with the length to simulated size dependent errors. Growth variability was simulated with a standard deviation of 1 or 5 for small or large variability respectively.

Simulation	Error (*E*)	Variability (*V*)	Name
Run 1	small	small	Run *ev*
Run 2	large	large	Run *EV*
Run 3	large	small	Run *Ev*
Run 4	small	large	Run *eV*

2.3.3 Method selection

The best performing method for the given data was identified via a simulation analysis with known growth parameters, executed in *R*. From the basic growth relationship, 1000 random bootstrapped datasets were generated with either small or large GV, and small or large ME. In total four simulation runs were executed (Table 2.2). The complete simulation analysis was run twice, for males and females independently. If not stated otherwise above, the optimizer command was used for fixed L_∞ approaches, and the *optim* command was used for all other approaches. A commented *R* script for the simulation analysis is provided in Appendix A. The method selection procedure via the simulation analysis involves the following steps:

Define true von Bertalanffy growth parameters

The true value of the asymptotic length $L_{\infty true}$ was set equal to the asymptotic length obtained from the maximum size, as described above. The true value of the growth constant k_{true} was set at 0.092 y^{-1} for males and 0.075 y^{-1} for females, obtained from growth studies of *G. galeus* in southern Brazil (Ferreira & Vooren, 1991).

Consider the sample size

The number of individuals was set equal to the observed number of individuals in the *G. galeus* tagging database, to account for the sample size of the given data.

Calculate a true age at capture

The user selected true VBGP were used to calculate the true age at capture for each individual t_{ci} from the observed length at capture L_{ci}, to reflect the length distribution of the sampled data: $t_{\mathrm{ci}} = {k_{\mathrm{true}}}^{-1} ln[(L_{\infty\mathrm{true}} - L_0)(L_{\infty\mathrm{true}} - L_{\mathrm{ci}})^{-1}]$, where L_0 was assumed to be 28 cm.

Introduce growth variability in the length at capture

Individual GV was introduced by letting the asymptotic length of each individual $L_{\infty i}$ vary. The effect of small and large GV was considered by sampling from a normal distribution with zero mean μ and a standard deviation σ of 1 and 5 respectively:

$$L_{\infty\mathrm{i}} = L_{\infty\mathrm{true}} + \mathcal{N}(\mu = 0, \sigma = 1 \; or \; 5). \quad (2.5)$$

A new length at capture was then simulated to account for individual GV: $L_{t_{\mathrm{ci}}} = L_{\infty\mathrm{i}} - (L_{\infty\mathrm{i}} - L_0)(e^{(-k_{\mathrm{true}} t_{\mathrm{ci}})})$.

Introduce measurement errors in the length at capture

Random MEs in the individual length at capture were introduced by sampling from a normal distribution with zero μ and a σ of 0.01 and 0.05 for small and large ME respectively. The standard deviation σ was multiplied by length, to account for the possibility that ME increases with size, e.g. because large sharks might be more difficult to straighten out. The individual length at capture accounting for GV and ME l_{tci} was then calculated:

$$l_{t_{\mathrm{ci}}} = L_{t_{\mathrm{ci}}} + \mathcal{N}(\mu = 0, \sigma = 0.01 L_{t_{\mathrm{ci}}} \; or \; 0.05 L_{t_{\mathrm{ci}}}). \quad (2.6)$$

Calculate the true age at recapture

The true age at recapture t_{ri} was obtained by adding the observed time at liberty dt to the true age at capture t_{ci}: $t_{\mathrm{ri}} = t_{\mathrm{ci}} + dt$, to reflect the time at liberty structure of the sampled data.

Introduce growth variability and measurement errors in the length at recapture

The length at recapture for each individual with GV accounted for was simulated as: $L_{t_{\mathrm{ri}}} = L_{\infty \mathrm{i}} - (L_{\infty \mathrm{i}} - L_0)\left(e^{(-k_{\mathrm{true}} t_{\mathrm{ri}})}\right)$ and the ME was introduced by:

$$l_{t_{\mathrm{ri}}} = L_{t_{\mathrm{ri}}} + \mathcal{N}(\mu = 0, \sigma = 0.01 L_{t_{\mathrm{ri}}} \; or \; 0.05 L_{t_{\mathrm{ri}}}). \quad (2.7)$$

To avoid biologically unreasonable negative growth increments l_{tri} was forced to be larger l_{tci}, by calculating the absolute values of the simulated individual growth increments: $dl_{\mathrm{i}} = \left| l_{t_{\mathrm{ri}}} - l_{t_{\mathrm{ci}}} \right|$ and recalculating the length at recapture: $l_{t_{\mathrm{ri}}} = dl_{\mathrm{i}} + l_{t_{\mathrm{ci}}}$.

2.3.4 Evaluate method performance

To evaluate the performance of each method the simulated length at capture l_{tci} and length at recapture l_{tri} were used as input data for the different growth estimation methods and the results were investigated via bias-precision-accuracy plots. We followed the definitions of Walther & Moore (2005) and their recommendation to use scaled measures, which allow comparison between males and females or other studies. Accordingly, average bias over all four simulation runs was defined as relative bias: $relative\ bias = (An)^{-1} \sum_{\mathrm{i}=1}^{n} (\theta_{\mathrm{i}} - A)$, where A is the known growth parameter ($L_{\infty true}$, k_{true}) and θ_i is the single bootstrap value which was computed n = 1000 times for each simulation run. Average precision over all four simulation runs was defined as the coefficient of

variation *CV*: $CV = 100\left[\sqrt{n^{-1}\sum_{i=1}^{n}(\theta_i - \bar{\theta})^2}\right]\bar{\theta}^{-1}$, where $\bar{\theta}$ is the mean of the bootstrap values. Average accuracy over all four simulation runs was defined as scaled mean squared error *SMSE*: $SMSE = (A^2 n)^{-1}\sum_{i=1}^{n}(\theta_i - A)^2$. Means were calculated as trimmed means with 1% of the largest and smallest values removed, to decrease the influence of extreme values which may arise from numerical instabilities during the simulation analysis. Smaller values for *relative bias*, *CV* and *SMSE* indicated better performance and the best performing method was selected as the method with the lowest *SMSE* value, as this measure incorporates bias and precision. The best performing method was subsequently utilised to estimate VBGP from tagging data of north-east Atlantic *G. galeus*. Confidence limits of the obtained parameters were estimated as the 2.5% and 97.5% percentiles of a bootstrapped dataset. Therefore, 1000 replicates were generated by random selection with replacement from the original *G. galeus* dataset, each with the original sample size of males or females respectively.

2.3.5 Growth comparison among *G. galeus* populations

Estimated VBGP of *G. galeus* from the north-east Atlantic were compared with other regions via an auximetric grid. In an auximetric grid, log *k* values are plotted against log L_∞ values, to investigate the growth performance of different populations across geographical areas. Different populations typically cluster in log – log space (Pauly et al., 1996).

2.3.6 Age at maturity and longevity

The age at maturity was estimated from length at 50% maturity by using the rearranged form of equation (2.1) solving for age instead of length. Longevity t_{max} was estimated as the time span required to attain 99% of the asymptotic length following Skomal & Natanson (2003) and Manning & Francis (2005):

$$t_{\max} = k^{-1} ln\{(L_\infty - L_0)[(1 - 0.99)L_\infty]^{-1}\}, \quad (2.8)$$

as well as Fabens (1965), who defined the time required to attain > 99% of the asymptotic length as:

$$t_{\max} = 5ln(2)k^{-1}. \quad (2.9)$$

2.4 Results

2.4.1 Data

In males, three observations were considered biologically questionable. This included two individuals with annual growth rates of over 20 cm and one individual with a size at recapture of 184 cm. In females, four observations were considered outliers. This included three individuals with annual growth rates larger than 17 cm and one individual with an annual growth rate of only 7 cm at a mean size of 45.5 cm. The influence plots are provided in Appendix A. The final dataset contained capture-recapture information of 16 male and 37 female sharks. The annual growth ranged from 0.15 cm to 14 cm in females, with a mean of 5 cm, and from 0.6 cm to 11 cm in males, with a mean of 4 cm. Length ranged from 84 cm to 175 cm in females and 126 cm to 168 cm in males. The time at liberty of females ranged from 64 days to 6.7 years, with a mean of 2.2 years. In males, the shortest time at liberty was 70 days and the highest 10.9 years, with a mean of 2.7 years.

2.4.2 Asymptotic length

The largest or heaviest female *G. galeus* caught in the north-east Atlantic were 200.00 cm (Capapé & Mellinger, 1988), 37.4 kg (EFSA, 2013) and 36.7 kg (SSTP, 2010). These weights correspond to a length of 196.69 cm and 195.53 cm. The largest or heaviest male *G. galeus* caught in the north-east Atlantic were 177.80 cm, 22.7 kg and 22.3 kg (Stevens, 1990). These weights correspond to a length of 172.45 cm and 171.49 cm. Therefore, the asymptotic length obtained from the average maximum size via equation (2.4) was 200.85 cm (with 95% confidence limits of 171.72 and 229.98) for females and 177.30 cm (151.58 and 203.01) for males. These values were subsequently used for the fixed asymptotic length and as true values in the simulation runs.

2.4.3 Method selection

The overall performance of each method was evaluated via bias-precision-accuracy plots derived from the simulation analysis considering all four scenarios of GV and ME. For both, female and male data, the overall best performing method in estimating the growth constant was the Weighted Fabens method with a fixed asymptote (Figs. 2.1; 2.2), whereas the Fabens method performed best in estimating the asymptote (Figs. 2.3; 2.4). The detailed results for each of the four simulation runs are provided in Appendix A. Performance in estimating the asymptote was generally better than performance in estimating the growth constant, but none of the methods performed best for both

parameters. Accordingly, the error associated with estimating the growth constant was larger. In addition, the estimated fixed asymptotic lengths using equation (2.4) were not significantly different to the methods that performed best in estimating the asymptote (Table 2.3 and Table 2.4). Therefore, von Bertalanffy growth estimates from the Weighted Fabens method with a fixed asymptote were selected as growth parameters for male and female *G. galeus* in the north-east Atlantic. The fit of the mark-recapture information to the selected VBGP is shown in Fig. 2.5.

2.4.4 Growth comparison among *G. galeus* populations

The VBGP of *G. galeus* for the north-east Atlantic were compared with estimates for populations of other geographical areas via an auximetric grid (Fig. 2.6). Growth performance was more closely related to New Zealand and southern Brazil stocks, than to Australian and South African stocks. The slope of all growth estimates combined was -2.05 and therefore close to the expected value of -2 (Pauly et al., 1996).

2.4.5 Age at maturity and longevity

The length at which 50% of the individuals are mature was summarised by Dureuil (2013) from the literature as 155 cm in females and 121 cm in males. From this it follows that age at maturity is 17 years in females and 12 years in males. Longevity estimates ranged from 46 to 59 years in females and from 43 to 55 years in males using equations (2.9) and (2.8) respectively.

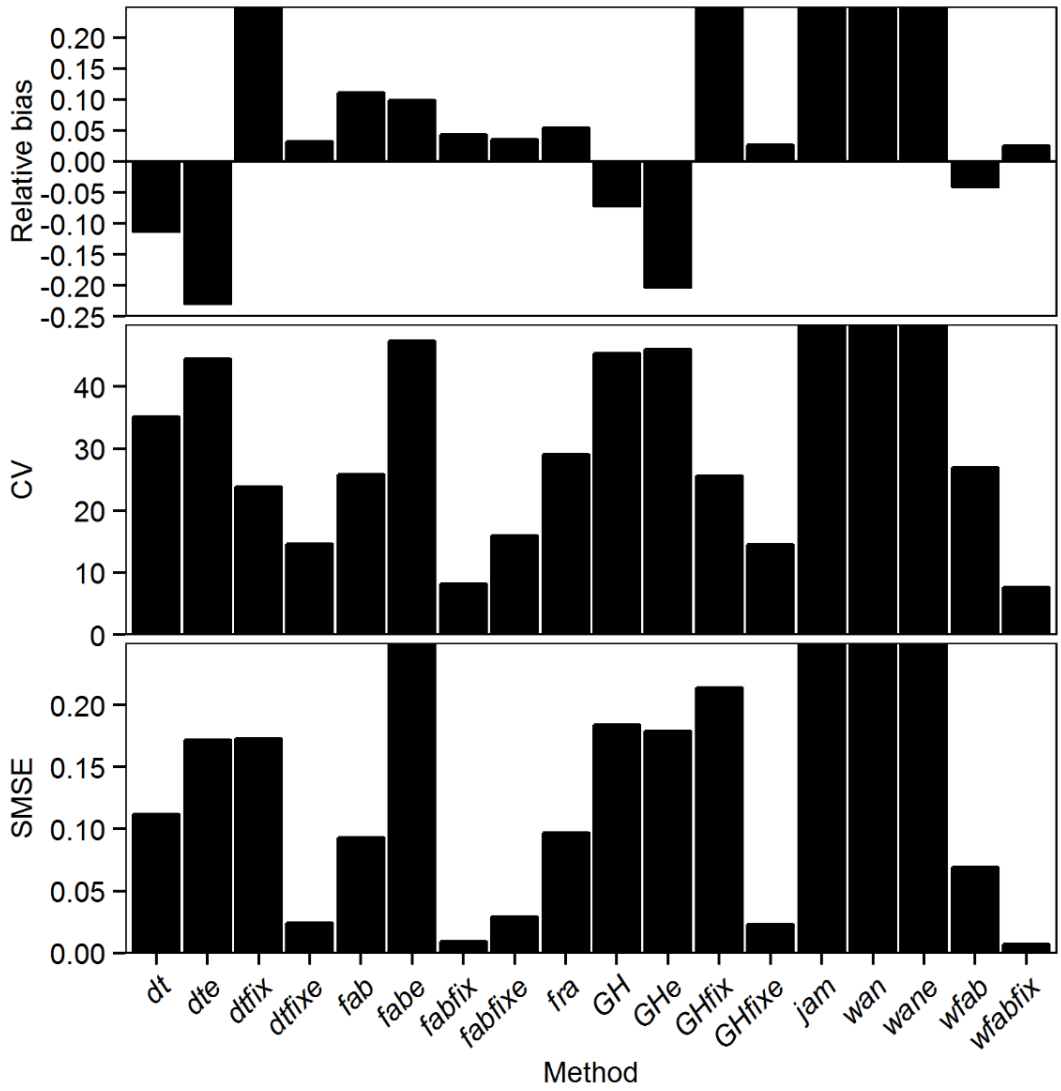

Fig. 2.1: Simulation results for the growth constant *k* (female data). The *relative bias*, precision (coefficient of variation; *CV*) and accuracy (scaled mean squared error; *SMSE*) of mean estimates is contrasted for 18 different methods. Simulations considered the structure of the *Galeorhinus galeus* data and different magnitudes of growth variability and measurement error. Lower values indicate better performance. Methods abbreviated as in Table 2.1.

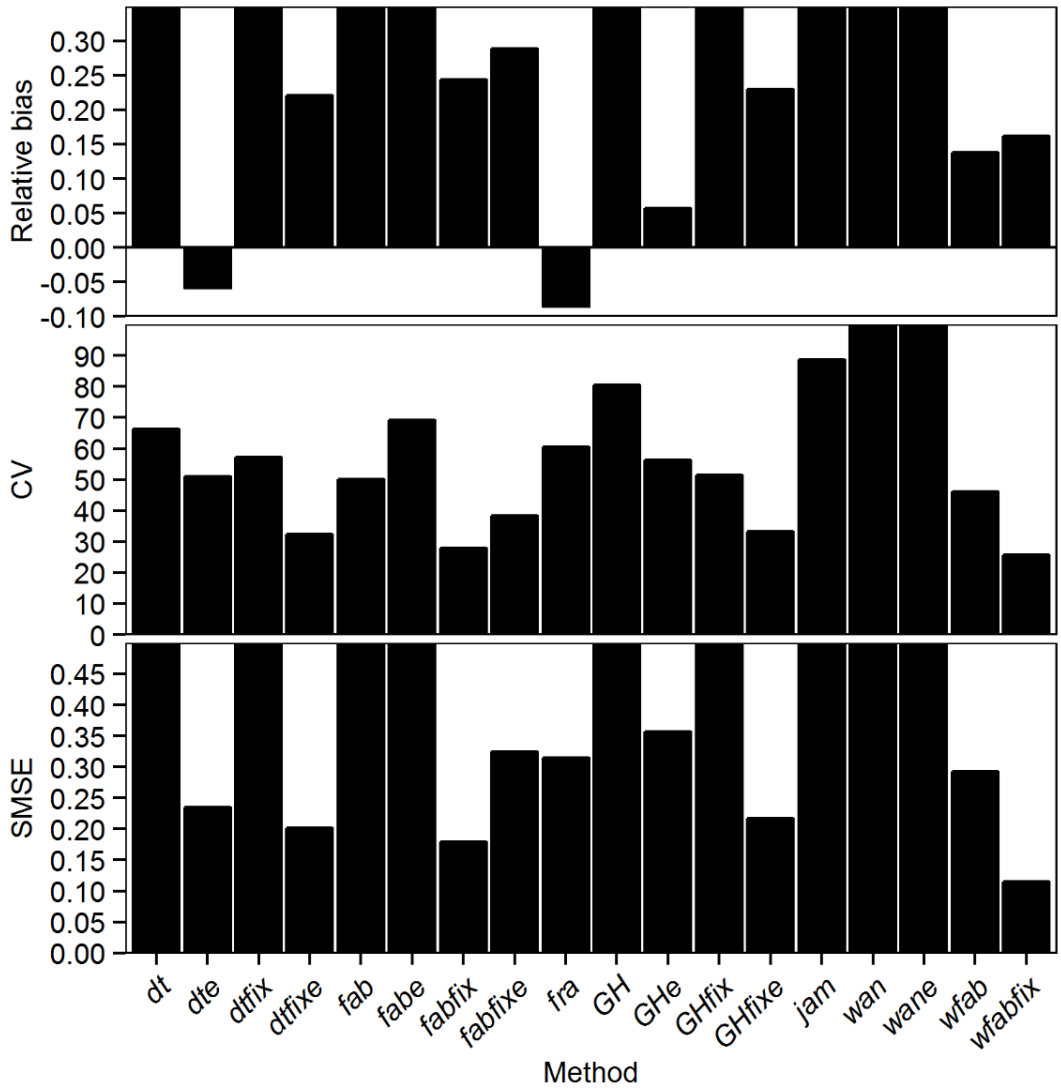

Fig. 2.2: Simulation results for the growth constant *k* (male data). Symbols and abbreviations as in Fig. 2.1.

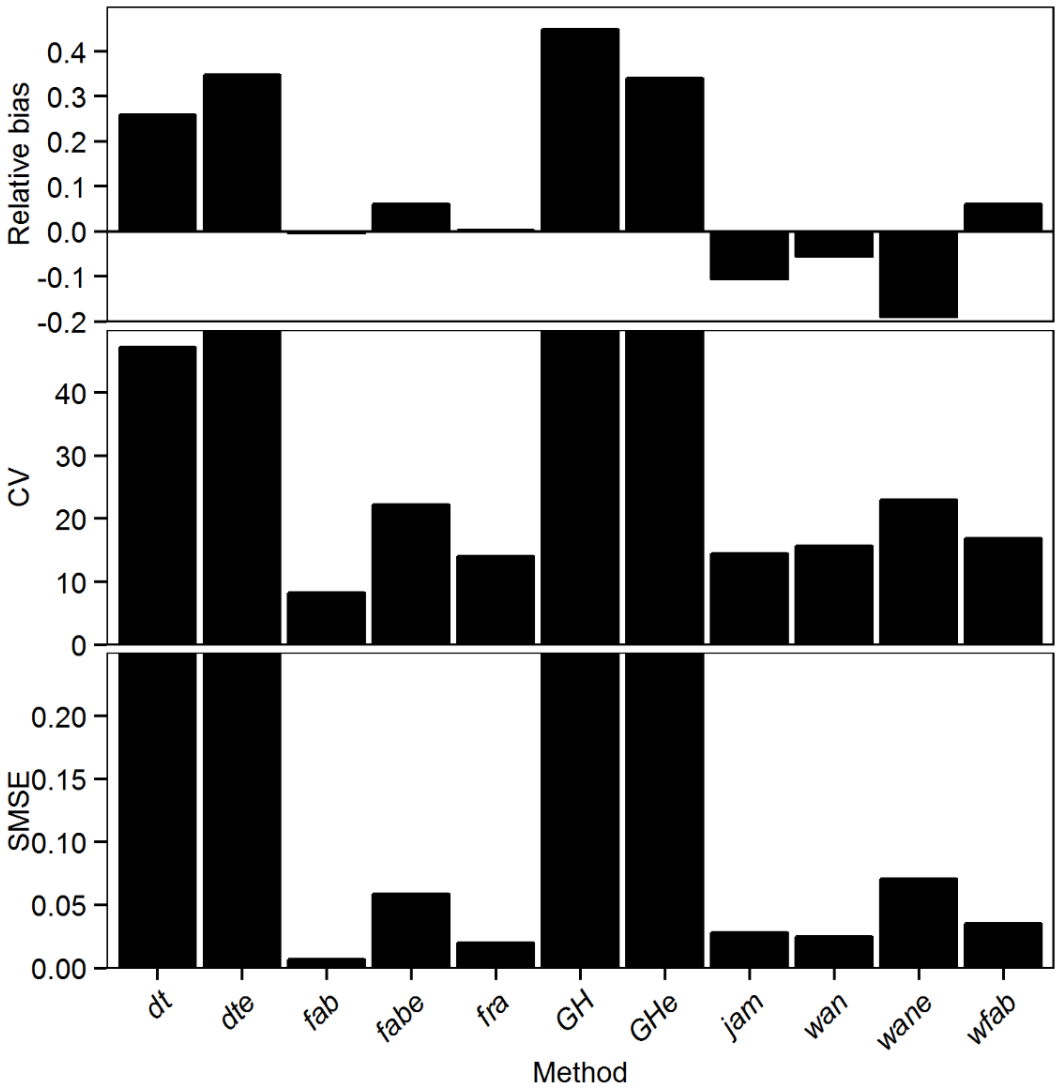

Fig. 2.3: Simulation results for the asymptotic length L_∞ (female data). Symbols and abbreviations as in Fig. 2.1

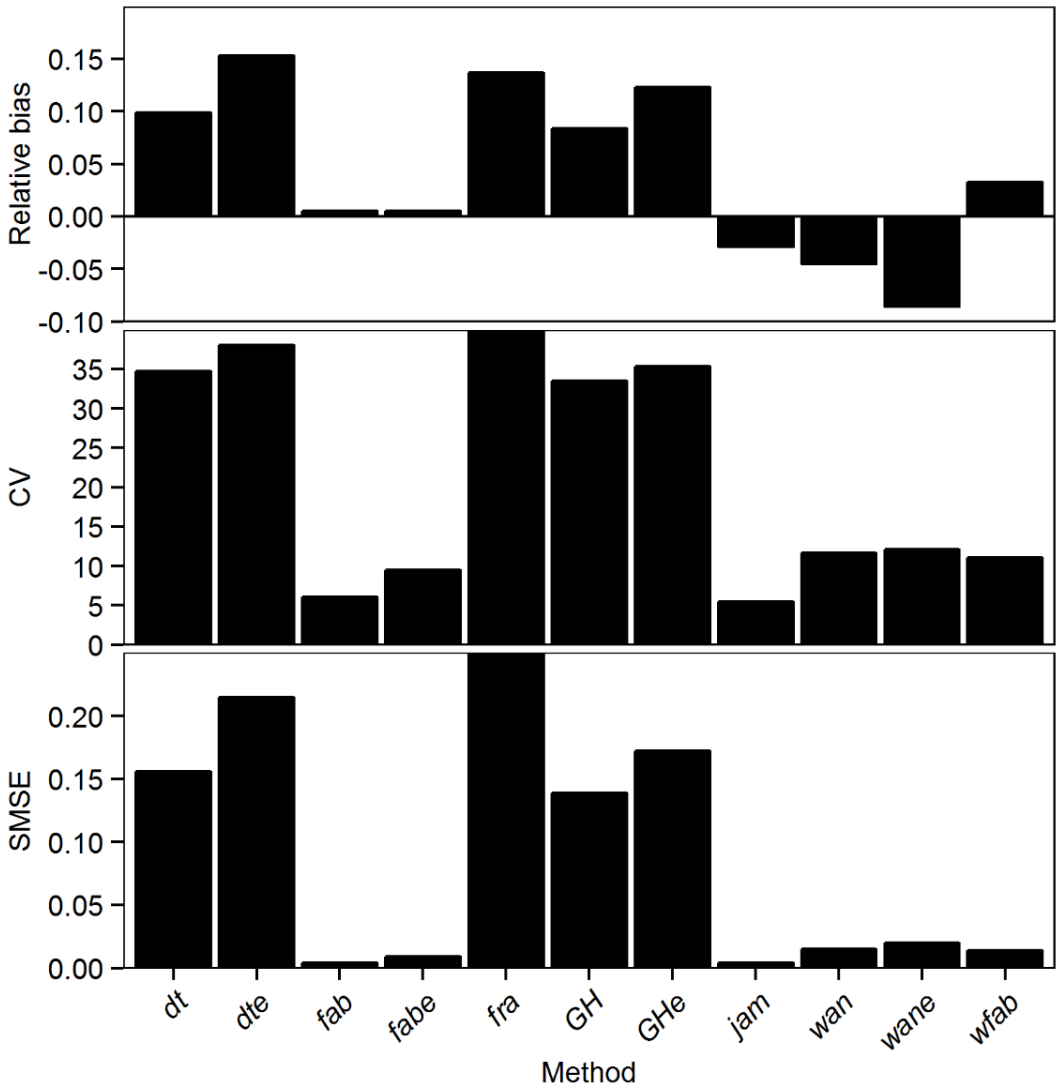

Fig. 2.4: Simulation results for the asymptotic length L_∞ (male data). Symbols and abbreviations as in Fig. 21.

Table 2.3: Von Bertalanffy growth estimates of female *Galeorhinus galeus.* The asymptotic length L_∞ and the growth constant *k* from 37 mark-recapture data points for all methods with lower (*LCL*) and upper (*UCL*) 95% confidence limits. In bold is the method from which the parameters were chosen. This method performed best for the given data according to the simulation analysis. The ln – ln transformed method of Wang (1998) did not converge. Methods abbreviated as in Table 2.1.

Method	L_∞	*LCL* L_∞	*UCL* L_∞	*k*	*LCL k*	*UCL k*
fra	200.27	166	280	0.071	0.028	0.140
wan	196.89	144	333	0.081	0.026	0.385
wane	NA	NA	NA	NA	NA	NA
jam	220.05	-449	914	0.058	-35.926	0.215
GH	246.78	177	900	0.043	0.007	0.097
GHe	209.58	157	1060	0.049	0.004	0.133
GHfix	200.85	172	230	0.069	0.057	0.082
GHfixe	200.85	172	230	0.055	0.041	0.071
fab	182.25	162	234	0.106	0.051	0.161
fabe	183.09	154	371	0.072	0.017	0.179
fabfix	200.85	172	230	0.078	0.061	0.091
fabfixe	200.85	172	230	0.054	0.040	0.070
wfab	191.87	163	307	0.088	0.028	0.147
wfabfix	**200.85**	**172**	**230**	**0.076**	**0.059**	**0.089**
dt	243.15	179	662	0.057	0.013	0.123
dte	216.69	168	1181	0.045	0.004	0.092
dtfix	200.85	172	230	0.100	0.074	0.132
dtfixe	200.85	172	230	0.055	0.041	0.072

Table 2.4: Von Bertalanffy growth estimates of male *Galeorhinus galeus*. The asymptotic length L_∞ and the growth constant k from 16 mark-recapture data points for all methods with lower (*LCL*) and upper (*UCL*) 95% confidence limits. In bold is the method from which the parameters were chosen. This method performed best for the given data according to the simulation analysis. Methods abbreviated as in Table 2.1.

Method	L_∞	*LCL* L_∞	*UCL* L_∞	k	*LCL k*	*UCL k*
fra	176.38	-295	830	0.085	-0.027	0.133
wan	152.86	144	177	0.444	0.083	3.200
wane	148.51	143	160	1.122	0.200	4.851
jam	166.78	150	174	0.157	0.084	0.646
GH	179.56	162	400	0.117	0.014	0.255
GHe	177.47	165	312	0.100	0.017	0.216
GHfix	177.30	152	203	0.124	0.086	0.171
GHfixe	177.30	152	203	0.100	0.071	0.142
fab	174.33	161	223	0.096	0.030	0.209
fabe	170.90	160	211	0.134	0.046	0.280
fabfix	177.30	152	203	0.085	0.066	0.116
fabfixe	177.30	152	203	0.105	0.073	0.152
wfab	177.41	163	281	0.081	0.019	0.172
wfabfix	**177.30**	**152**	**203**	**0.081**	**0.065**	**0.110**
dt	171.83	164	305	0.142	0.021	0.279
dte	178.39	165	323	0.097	0.017	0.196
dtfix	177.30	152	203	0.097	0.078	0.157
dtfixe	177.30	152	203	0.101	0.072	0.143

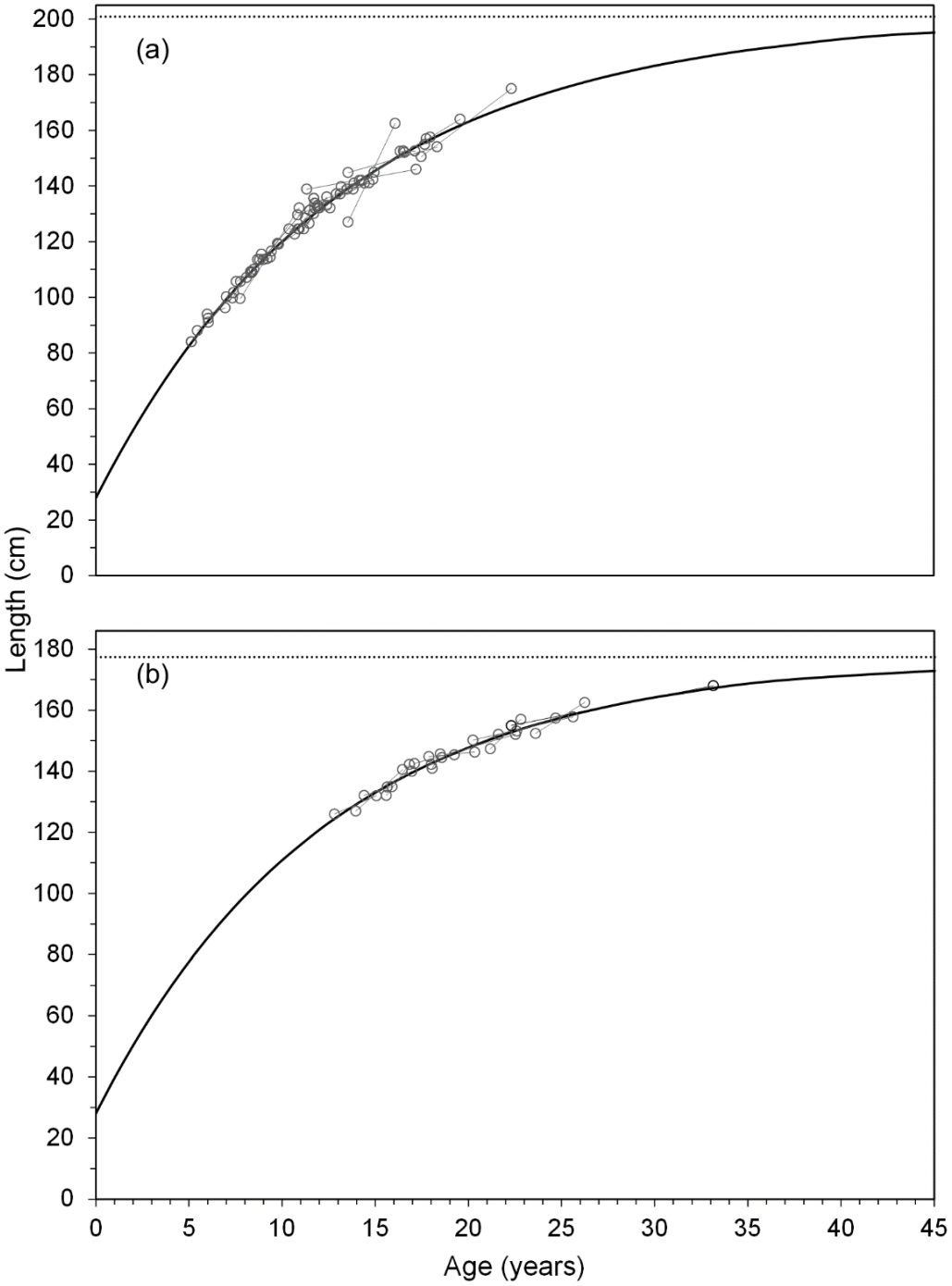

Fig. 2.5: Growth curves. Shown are the von Bertalanffy growth curve of female *Galeorhinus galeus* (a) and male *Galeorhinus galeus* (b) obtained from the method that performed best in the simulation analysis, the Weighted Fabens method introduced by James (1991) with a fixed asymptote. The grey open circles represent the capture and recapture data, where the data of each individual is connected by a grey solid line. The dotted line represents the asymptote.

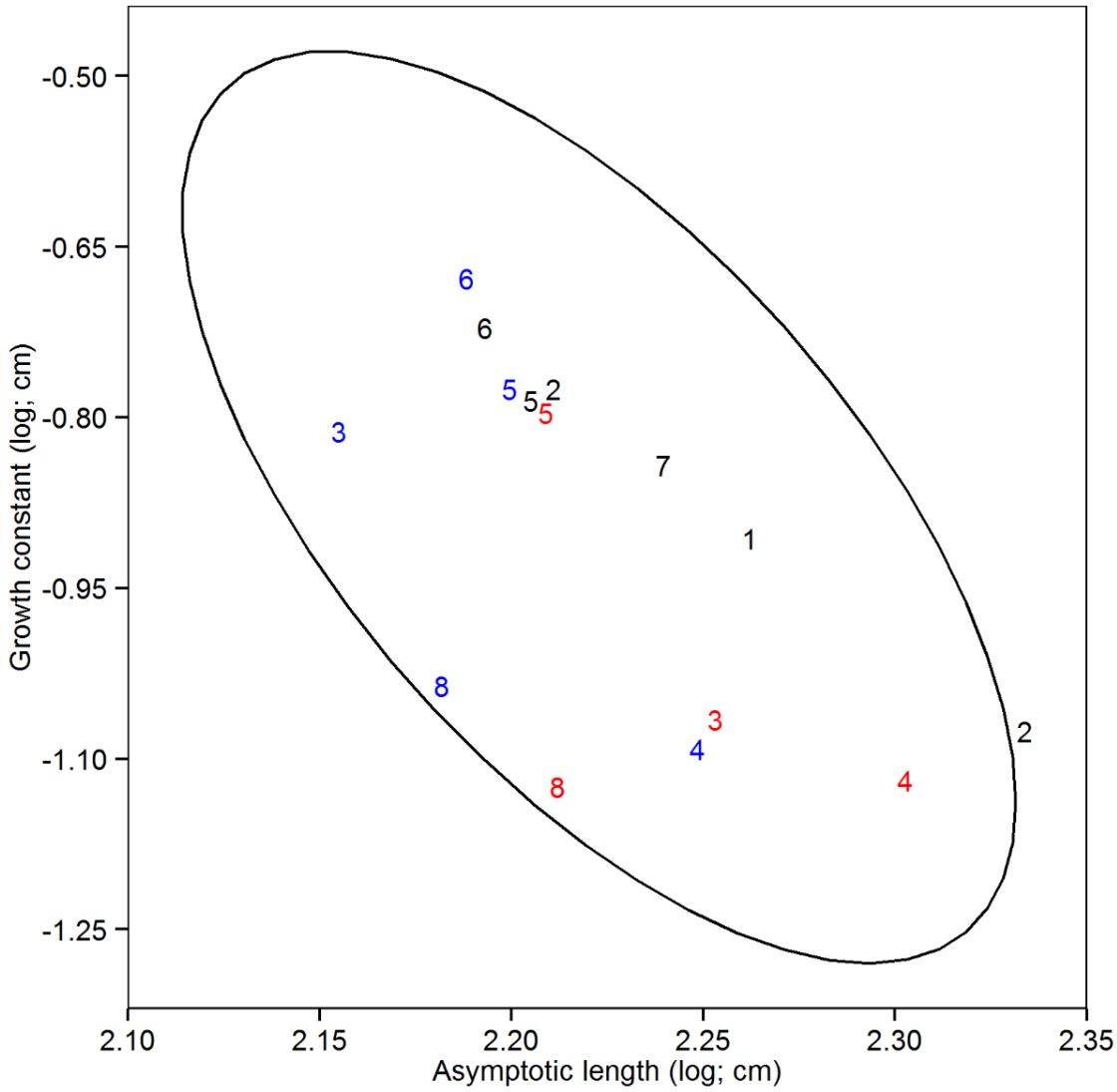

Fig. 2.6: Growth of *Galeorhinus galeus* in various regions. Growth parameters are shown in red for females, in blue for males and in black for combined sexes. The circle represents the 95% confidence ellipse. The numbers refer to the regions: 1 Australia (Moulton et al., 1992); 2 Bass Strait, Australia (Moulton et al., 1992); 3 New Zealand (Francis & Mulligan, 1998); 4 north-east Atlantic (this study); 5 south-eastern Australia (Grant et al., 1979); 6 South Africa (McCord, 2005); 7 Southern Australia, (Moulton et al., 1992); 8 Southern Brazil (Ferreira & Vooren, 1991).

2.5 Discussion

This study presented a structured selection procedure which helped identify the best performing method to estimate growth for a small mark-recapture sample of *G. galeus*. Parameter estimates differed strongly among methods, showing the need for careful method selection. In the present study, the majority of tagged and recaptured individuals were mid-sized sharks. Maximum and mean time at liberty was larger for males, but the sample size was smaller for males than for females. In males, some capture and recapture information was present for larger individuals, but lacking for small individuals. In females, the length distribution was more representative, although data for small and very large individuals was also scarce (Fig. 2.5). In order to find the best method for estimating growth parameters from this limited tagging information, the performance of the three commonly utilised methods from Gulland & Holt (1959), Fabens (1965) and Francis (1988b) were tested, as well as 15 attempts to improve these models. Therefore, small and large GV and MEs were simulated while considering the structure of the data (i.e. sample size, observed length distribution and time at liberty).

In agreement to the findings in this study, previous studies have shown bias in the commonly utilised methods. From validated age data for sandbar sharks it was shown that large differences can occur when comparing growth parameters obtained by direct aging methods with those obtained from the Francis method, with the latter likely to overestimate the VBGP *k* and to underestimate the asymptote (McAuley et al., 2006). McAuley et al (2006) suggested that the bias was due to variability in growth, especially when time at liberty was short and the sample size was small and outlier contaminated. Other studies found that if old sharks were absent in the sample, the Francis method can produce higher *k* and lower asymptote values (Natanson et al., 2002) or higher values in both parameters (Skomal & Natanson, 2003). The Gulland and Holt and the Fabens methods may fail if time at liberty is short and GV is high (Simpfendorfer, 2000). It is well described that the Fabens method can produce bias estimates when individual growth is variable (Sainsbury, 1980; Francis, 1988a; Maller & deBoer, 1988; Kimura et al., 1993; Wang & Thomas, 1995; Eveson et al., 2007) or MEs are high (Eveson et al., 2007), which can lead to an overestimation of mean length at age (Sainsbury, 1980). Our findings indicated that the Francis method tended to be the least biased out of the commonly utilised methods, in particular when the sample is larger and both smaller and larger individuals are present. The Fabens method showed higher bias and was particularly sensitive to MEs, and the Gulland and Holt method was biased even when ME and GV were small (Appendix A).

The best performing method for both sexes was the Weighted Fabens method with a fixed asymptotic length.

The lack of small individuals in the data, as well as a small sample size, may positively bias the results and lead to a higher uncertainty and larger errors in the parameter estimates in general. Overall, MEs had the largest effects on the performance of all methods, which is indicated by the larger errors in Run *Ev* than in Run *eV* (Appendix A). The simulated GV had a mean of zero and ranged from about ± 3 cm to ± 15 cm for small and large variability respectively, and the simulated MEs had a mean of zero and ranged from about ± 5 cm to ± 25 cm for small and large errors respectively (Appendix A). Thus the standard deviation estimates utilised in equations (2.5), (2.6) and (2.7) for GV and MEs were considered to be reasonable for a shark species with a maximum size of 200 cm. Factors leading to ME can include the accuracy of the measurement (especially for larger sharks being measured alive), the method (measuring board or tape measure) and the type of measurement, e.g. total or fork length (Francis, 2006). Therefore, it should be recommended that measurements are done as accurately as possible. In addition, length measurements should be preferred over measurements in weight, as the latter might be more variable. Finally, it should be explicitly stated which type of length measurement was utilised. Individual GV may become a more important issue if the capture-recapture data are seasonally biased (Simpfendorfer, 2000). Therefore, it can be necessary to include seasonal effects to account for the fact that growth might slow down at certain times of the year (Pauly et al., 1992). In our study, the division of the total days individuals spent at liberty during spring and summer by the total days individuals spent at liberty in fall and winter was 1.01 for females and 0.99 for males. Therefore, no effect of seasonality was expected. If this is not the case, growth models allowing for seasonality may be applied (e.g. Pauly & Gaschutz, 1979; Francis, 1988b; Somers, 1988; Wang, 1999) or the sample might be adjusted to become equally distributed among seasons.

The natural logarithm (ln – ln) transformation had no consistent positive effect on method performance, whereas fixing the asymptote generally increased the performance of the methods. It has been shown previously that the Weighted Fabens method produces only unbiased results when observational errors occurred, whereas variability in the asymptote produced biased results (Kimura et al., 1993). The findings of the present study suggest that fixing the asymptote can help overcome this problem.

When applying the 18 different methods to the observed data, significant difference in VBGP where found (Table 2.3; 2.4), which in turn resulted in considerably different

growth curves among the methods for females and males (Fig. 2.7). This demonstrates that it is important to select the method which performs best for a given data structure. Although the simulation analysis revealed that for the given data none of the methods performed best in estimating both parameters, accuracy in estimating the growth constant was lower and the associated error higher. In addition, the values for the fixed asymptotic length were similar to the results of the methods performing best in estimating the asymptote. Therefore, methods were selected according to their performance in estimating the growth constant.

The results of the selected method should also be discussed in terms of biological reasonability. Hence, estimated growth parameters from this study were compared to those from *G. galeus* populations in other regions. The comparison of the growth performance of different populations revealed that growth parameters of the north-east Atlantic stock were more similar to those from New Zealand and southern Brazil stocks, than to Australian and South African stocks. The female asymptotic length of 200.85 cm is larger than the 162 cm reported from south-eastern Australia (Grant et al., 1979), the 179 cm reported from New Zealand (Francis & Mulligan, 1998) and the 163 cm from southern Brazil (Ferreira & Vooren, 1991). Likewise, male asymptotic length of 177.30 cm was found to be larger than the 143 cm reported from New Zealand (Francis & Mulligan, 1998), 154 cm from South Africa (McCord, 2005), 152 cm from southern Brazil (Ferreira & Vooren, 1991) and 158 cm from south-eastern Australia (Grant et al., 1979). This comparison suggest that the asymptotic length tend to increase with latitude for the same species, a pattern that has been described before (Kimura, 2008). The VBGP *k* found in this study of 0.076 y^{-1} for females and 0.081 y^{-1} for males, was close to the Southern Brazil stock, where *k* was estimated at 0.075 y^{-1} for females and 0.092 y^{-1} for males (Ferreira & Vooren, 1991). In females, *k* was most different from the south-east Australia stock, where it was estimated at 0.16 y^{-1} (Grant et al., 1979). In males, the South African stock showed least agreement, where *k* is believed to be 0.21 y^{-1} (McCord, 2005). The high growth constant found for *G. galeus* in South Africa might be an artefact of vertebral readings, the high growth constant for *G. galeus* from Australia might be an artefact of the method chosen to estimate growth from tagging information. Grant et al (1979) used the Fabens method, which in the present study produced large bias, particularly for the growth constant.

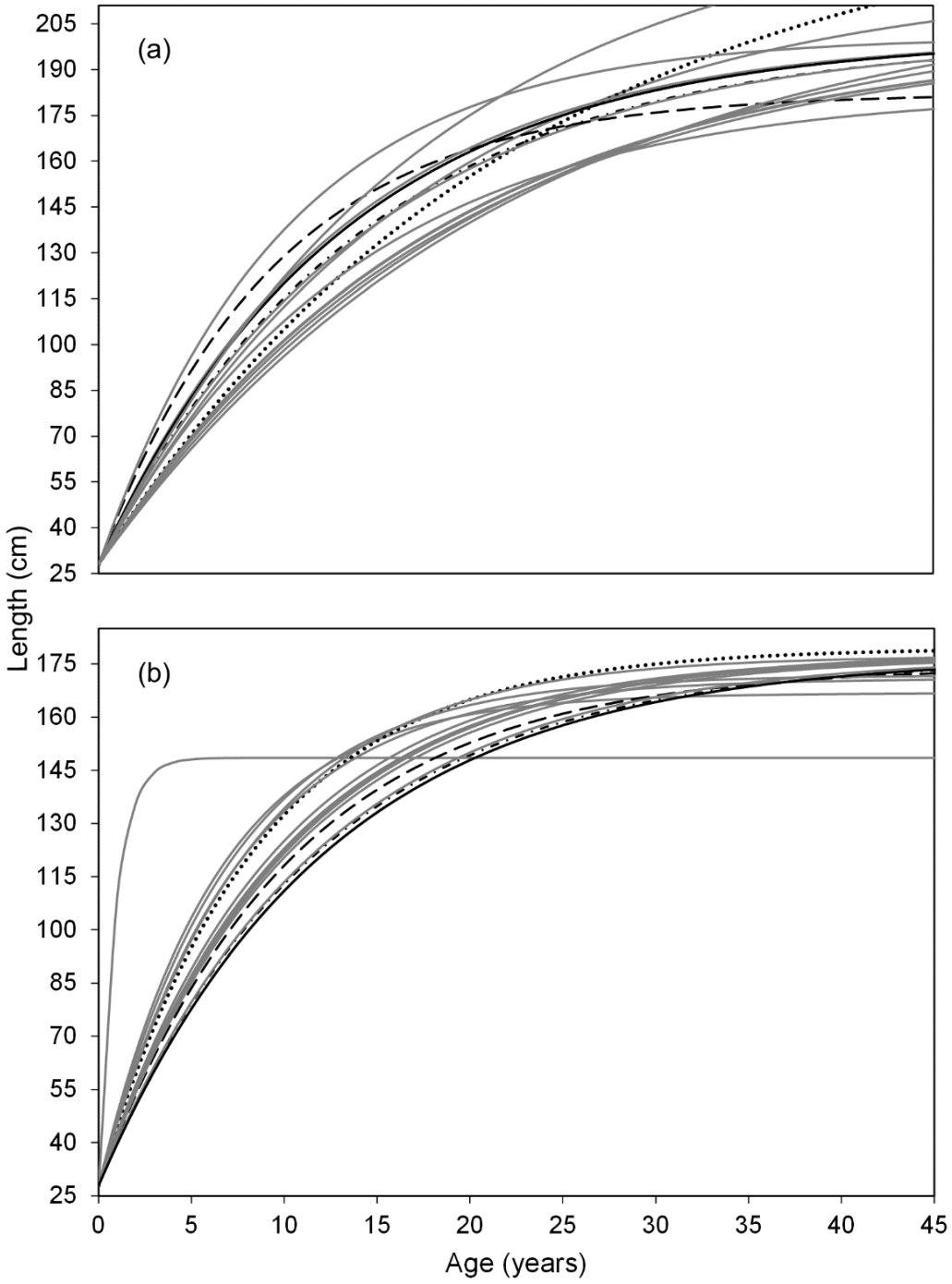

Fig. 2.7: Growth curve comparison. Von Bertalanffy growth functions for female (a) and male (b) *Galeorhinus galeus* with the parameters derived from each of the 18 methods are shown. The best method, the Weighted Fabens method (James, 1991) with a fixed asymptote, is indicated by the black solid line. The other commonly used methods are indicated as follows: the black dotted line shows the results of the Gulland & Holt (1959) method; the black dashed line shows the results of Fabens (1965) method; and the black dotted-dashed line shows the results of Francis (1988b) method. The ln – ln transformed method of Wang (1998) did not reach convergence for female data and therefore could not be shown.

Overall, the comparisons of the VBGP are in agreement with the general pattern, that organisms grow faster towards a lower asymptote in an environment with higher temperature (von Bertalanffy, 1960), because the asymptote and *k* are negatively correlated (Kimura, 1980). From the VBGP, age at maturity for the north-east Atlantic stock was estimated at 17 and 12 years for female and male *G. galeus* respectively. In other stocks, female age at maturity was reported to be 10 years in Australia (Olsen, 1954), 16 years in southern Brazil (Peres & Vooren, 1991) and 13 – 15 years in New Zealand (Francis & Mulligan, 1998). For males, age at maturity was reported to be 11 years in southern Brazil (Peres & Vooren, 1991), 12 to 17 years in New Zealand (Francis & Mulligan, 1998), 6 years in South Africa (McCord, 2005) and 8 years in Australia (Olsen, 1954). Like growth performance, age at maturity in the north-east Atlantic is most similar to the southern Brazil stock. These findings are in agreement with the general finding that slower growth results in later maturation (Roff, 1984; Jensen, 1996). Longevity estimates ranged from 46 – 59 years in females and from 43 – 55 years in males using equations (2.9) and (2.8), respectively. These values include the suggested maximum age of 53 years for females (Olsen, 1984) and 45 years of males, the latter estimated based on tag returns (Moulton et al., 1989). In summary, the comparison of the growth performance, the age at maturity and longevity estimated in this study to other regions suggests that the results are reasonable, despite being based on a small sample size. Hence, the productivity of north-east Atlantic *G. galeus* is low, increasing the species risk of extinction (Musick, 1999).

To conclude, this is to our knowledge the first comparative study of methods to estimate growth from tagging information in a shark species and the first applying the Weighted Fabens approach from James (1991) for this group of animals. Results reinforce the need to apply different approaches on a given dataset and to verify the method used to estimate growth. Obtaining growth estimates from mark-recapture data can be particularly important for species like *G. galeus*, where vertebral readings may not represent an adequate procedure to estimate age (Kalish & Johnstone, 2001). The results of the present study were compared to the only available age data of *G. galeus* in the north-east Atlantic, obtained from vertebrae (Henderson et al., 2003). Their preliminary age estimates of four male specimens with a length of 141 cm, 148 cm, 149 cm and 152 cm were 10 year, 12 year, 10 years and 11 years, respectively. Our estimates would suggest ages of 17 year, 20 years, 21 years and 22 years for the same length. Hence, the

estimated ages from the growth parameters obtained in this study were up to 50% higher than to those reported by Henderson et al (2003), which would support previous concerns that vertebral readings can underestimate age in this species (Officer et al., 1996; Kalish & Johnstone, 2001). The presented method selection procedure can aid in obtaining less biased growth parameters from mark-recapture tagging data by finding the best performing method for a given dataset, especially if the sample size is small. More accurate growth parameters will in turn improve stock assessments. However, the results of the selection procedure are limited to the chosen methods. Hence, it is important to test a variety of different growth estimation methods. Future studies should ideally include new growth estimation methods in the selection procedure, such as Bayesian methods, to make the method selection more reliable. In particular a Bayesian version of the Francis method could be promising, as this method was designed to account for measurement errors, growth variability and the proportion of outliers within the data. In addition, future studies should include both age- and length-based approaches to gauge the robustness of either.

Chapter 3
Re-evaluating methods to estimate growth from tagging data in elasmobranchs

3.1 Abstract

The body (somatic) growth of individuals is a vital process that governs many aspects of a species' life history. Thus, knowledge about growth parameters is critical in many stock assessment methods. Such growth parameters are derived by relating individual length to age, with the latter commonly estimated from growth bands formed in calcified structures. Recent research, however, suggests that these structures cannot be used for aging in many elasmobranchs (sharks, rays and skates). Alternative methods from mark-recapture tagging data have been proposed in the past, but have not been rigorously tested on this group of species. Therefore, the performance of seven different methods in estimating von Bertalanffy growth parameters for elasmobranchs was investigated here. The performance of the methods were evaluated in two ways: 1) Estimated growth parameters from simulated datasets that considered individual growth variability, measurement error and different scenarios for the length at capture, times at liberty and sample size were compared to the true growth parameters in the simulation; 2) Growth parameters were estimated from empirical mark-recapture tagging data for 15 different elasmobranch stocks and compared to literature growth parameters obtained from length-at-age information. There was a high variability in performance across methods. The only method that performed reasonably well in all scenarios was a Bayesian implementation of Fabens original method (BFa) with informative priors on the growth parameters. This method gave biologically plausible results for all stocks, even in cases with very few tagged individuals. The prior information was obtained from observed maximum length. Different prior ranges are discussed, and it is shown that too narrow priors can bias the parameter estimates. Hence priors should be selected wide enough to account for individual variability in the asymptotic maximum length. In conclusion, the results suggest that BFa could become a full alternative to conventional length-at-age methods in elasmobranchs and therefore aid the reliability and quality of stock assessments and life history studies.

3.2 Introduction

Somatic growth is a fundamental parameter for the understanding of life history characteristics and for accurate assessment of fish populations (Haddon, 2011). Typically, growth parameters are obtained from length-at-age data, with ages coming from readings of rings formed in calcified structures (Cailliet & Goldman, 2004). Length and age are then related by a growth function, with the von Bertalanffy growth function most commonly utilized for fish (Cailliet & Goldman, 2004).

In bony fishes accurate age estimates have been obtained from the growth zones that form in both otoliths (earbones) and scales. Elasmobranchs (sharks, rays and skates) lack otoliths and their placoid scales do not form distinguishable bands (Campana, 2001, 2014). Instead, the alternating opaque and translucent growth bands that stem from mineralization in the vertebral centra have been used most commonly in elasmobranch aging, often assuming annual band pair deposition (Cailliet, 1990; Cailliet & Goldman, 2004; Campana, 2014). However, not all elasmobranch species form such bands (Cailliet, 2015) and there is considerable uncertainty in assigning ages to growth bands in species due to the following: Growth band formation might not be consistent throughout the lifespan in some elasmobranch species (Francis et al., 2007; Natanson et al., 2014; Cailliet, 2015); Bands can become too narrow to be reliably distinguishable with the slowing growth in adult individuals (Natanson et al., 2002, 2014; Francis et al., 2007; Cailliet, 2015); Different preparation techniques can lead to different results; Band formation can change due to different ontogenetic stages, different habitats occupied (vertically and horizontally), or different exploitation levels (Cailliet, 2015). As a result, many elasmobranchs have not been aged reliably (Cailliet & Goldman, 2004; Goldman et al., 2012; Cailliet, 2015; Harry, 2017), and it has recently been shown that ages derived from vertebral growth bands are systematically underestimated in these species (Harry, 2017). Furthermore, it has been found that these bands are not related to age and time, but to swimming mode, body girth and structural vertebrate properties, with the number of growth bands changing along the vertebral column, at least for some species (Ingle et al., 2018; Natanson et al., 2018).

A bias in age estimation translates directly into bias of the derived growth parameters (Natanson et al., 2014; Harry, 2017), which can have serious consequences. For example, in elasmobranch assessments, individuals are commonly aged indirectly from length by using previously established growth functions; hence, biased growth parameters would affect any age-structured assessment model. Likewise, age at maturity

is commonly estimated indirectly from inverse growth functions and length at maturity (Cortes, 2000). Furthermore, underestimated longevity might give overly optimistic estimates of the natural mortality rate (Chapter 4), which could result in a mismanagement of species. Growth has also been used to define the productivity and extinction risk of a population, with von Bertalanffy growth constants of > 0.3 $year^{-1}$, between 0.3 to 0.16 $year^{-1}$, between 0.15 to 0.05 $year^{-1}$ and < 0.05 $year^{-1}$ defining high, medium, low and very low productivity respectively (Musick, 1999). Moreover, Harry (2017) pointed out that consequences resulting from underestimated ages are not straightforward, but can be rather complex: greater maximum ages would suggest lower natural mortality rates and thus lower productivity and resilience to exploitation, but longer lifespans can also lead to greater net reproductive rates which would suggest faster population doubling times and hence greater productivity. Given the threatened status of many elasmobranch species (Dulvy et al., 2014) it is important to prevent mismanagement, and therefore alternative approaches to estimate reliable growth parameters in elasmobranchs are required.

Methods that utilize the change in body length over time from mark-recapture tagging data have been suggested as such alternative approaches (Cailliet et al., 1992; Cailliet, 2015; Harry, 2017). Several methods have been proposed in the past, but these have been shown to give potentially highly biased parameter estimates (Sainsbury, 1980; Francis, 1988a; Maller & deBoer, 1988; Kimura et al., 1993; Wang & Thomas, 1995; Simpfendorfer, 2000; Natanson et al., 2002, 2006; Skomal & Natanson, 2003; McAuley et al., 2006; Eveson et al., 2007). Recently, Dureuil & Worm (2015) proposed a selection procedure to identify the best method for estimating growth parameters from mark-recapture tagging data of the tope shark (*Galeorhinus galeus*) and suggested that future studies should include Bayesian approaches in the selection procedure.

The present study builds on these previous investigations and aims to identify robust methods that provide unbiased parameter estimates across different species and data sources. In total, the performance of the following seven methods were investigated: the three most commonly applied conventional methods from Gulland & Holt (1959), Fabens (1965) and Francis (1988b); a modification of the Fabens (1965) method by James (1991); a Bayesian version of Fabens (1965); a random effect model fitted by maximum likelihood (Laslett et al., 2002); and a Bayesian random effect model (Zhang et al., 2009). Bayesian methods allow the inclusion of prior information, and here informative, less informative (referred to as semi-informative) and vague priors on the growth parameters were tested.

The performance of each method was assessed using an extensive Monte Carlo simulation study and evaluation testing. The simulations with known growth trajectories considered both, individual growth variability, and measurement errors in body length. Based on the known growth trajectories, the effects of different length distributions of individuals at capture, different times at liberty between a capture and recapture event, and different sample sizes were investigated. In addition, each method was evaluated by applying it to empirical mark-recapture tagging data of 11 different elasmobranch species from 15 different stocks. The results from the evaluation analysis were compared to von Bertalanffy growth parameters estimated via conventional methods using length-at-age data, obtained from the literature for the same species and stock. This is the first study to rigorously test the performance of methods that estimate growth parameters from mark-recapture tagging data in elasmobranchs. Best approaches are identified, and the use of different prior information and data is discussed.

3.3 Materials and methods

3.3.1 Framework and notation

The growth estimation framework considered in this study is directly based on the von Bertalanffy equation (von Bertalanffy, 1938):

$$L_t = L_\infty - (L_\infty - L_0)e^{-kt}, \quad (3.1)$$

which can also be formulated as follows (Haddon, 2011):

$$L_t = L_\infty(1 - e^{-(k(t-t_0))}), \quad (3.2)$$

where L_t represents the length at age t, L_∞ is the asymptotic maximum length, k is the Brody coefficient (or 'growth constant'), describing the steepness of the growth curve at time t_0, L_0 is the length at birth, and t_0 is the theoretical age at which the fish has length zero. All parameters refer to an average individual in a population. The theoretical time, t_0, is smaller than the age of birth, t_b, which is 0. The von Bertalanffy growth function can also be expressed as the change in body length, ΔL, over time, ΔT, between a capture and recapture event. The length increment between length at capture, L_{T1}, and length at recapture, L_{T2}, is $\Delta L = L_{T2} - L_{T1}$, with the corresponding time increment $\Delta T = T_2 - T_1$ (Fabens, 1965):

$$L_{\mathrm{T2}} - L_{\mathrm{T1}} = \Delta L = (L_\infty - L_{\mathrm{T1}})(1 - e^{(-k\Delta T)}). \quad (3.3)$$

Times of capture and recapture are denoted T_1 and T_2, respectively. Hence, $T_b<T_1<T_2$, where T_b is time of birth. The associated age at capture will be detonated as t_1 and the

age at recapture as t_2. All lengths are given as total length (cm), all ages are given in years and times are given either in days or years.

3.3.2 Simulation design

In order to find the best performing method in estimating von Bertalanffy growth parameters from mark-recapture data under a variety of controlled scenarios, a Monte Carlo simulation study was performed. The simulated data was generated using the following steps:

Step 1: Select true growth parameters

First, the true growth parameters, $trueL_\infty$ and *truek*, were selected. Here, the information provided by Farrell et al (2010) for the Northeast Atlantic female starry smoothhound shark (*Mustelus asterias*), a typical elasmobranch, with L_∞ at 123.5 cm and k at 0.146 year^{-1}, was utilized. Note, that species with different growth trajectories have the same growth curves if they grow according to the von Bertalanffy model (Fig. B1). Therefore, the von Bertalanffy growth parameters $trueL_\infty$ and *truek* can be chosen arbitrarily with similar simulation results expected.

Step 2: Simulate true lengths at capture

Second, lengths at capture were randomly generated. These lengths consisted of a sample of length measurements of n fish, all independent from each other, with the index i used to refer to individual fish. Considering fish are randomly sampled at capture without replication, and are all coming from the same population, the individual lengths are independent and identically distributed (*iid*), with a distribution specified by a mean, μL_{T1}, and a standard deviation (sd), σL_{T1}. Different distributions were considered for the lengths at capture to mimic different length structures in the data, e.g. caused by gear selectivity or the occurrence of only certain life stages. The following distributions were specified:

a) A symmetric length at capture distribution with the peak number of individuals between minimum and maximum length and the same number of young and old individuals, on average. This was specified by a normal distribution with $\mu L_{T1} = (trueL_{max}+trueL_0)/2$ and $\sigma L_{T1} = 0.3\mu L_{T1}$. The $trueL_0$ was obtained from equation (3.2) with age = 0 and with $truet_0$ obtained from its relationship to L_∞ and k (Pauly, 1979):

$$truet_0 = 10^{(-0.3922-0.2752\log10(trueL_\infty)-1.038\log10(truek))}. \quad (3.4)$$

The value for $trueL_{max}$ was set at 95% of $trueL_{\infty}$ (Taylor, 1958).

b) A positively skewed length at capture distribution (right skewed) with predominately young individuals at capture, and only a few old individuals. This was specified by a gamma distribution with a shape parameter of $1+((trueL_0+\mu L_{T1})2)/4$ and a scale parameter of 4;

c) A negatively skewed length at capture distribution (left skewed) representing a sample of predominately old individuals at capture and only a few young individuals. This was specified by a normal distribution with the mean, $\mu = ((trueL_{max}+\mu L_{T1})/2)^2$, and the sd, $\sigma = 0.3\mu$;

d) A bimodal length at capture distribution used to mimic cases where young and old individuals dominate the captured sample, with very few individuals representing the ages in between. This was specified by two normal distributions, the first with a mean, $\mu_1 = ((trueL_0+\mu L_{T1})2)$, a sd $\sigma_1 = 0.15\mu_1$ and $n = n/2$, and the second with a mean, $\mu_2 = ((trueL_{max}+ \mu L_{T1})/2)$, the second sd $\sigma_2 = 0.15\mu_2$ and $n = n/2$.

Typical simulation results for the four different length at capture distributions are shown in Figure 3.1.

Step 3: Calculate true ages at capture, and ages and lengths at recapture

Next, the individual ages at capture were calculated:

$$t_{1,i} = -\frac{\ln\left(1-\frac{L_{T1,i}}{trueL_{\infty}}\right)}{truek} + truet_0, \qquad (3.5)$$

and from this, the ages at recapture for each individual, t_{2i}, by adding the time difference in years between capture and recapture, ΔT_i, to the age at capture, t_{1i}. These time differences, ΔT_i, were independently simulated from a gamma distribution with a common scale parameter set to 1 and a shape parameter varying between individuals. The shape parameters were computed so that the $(1\text{-}0.01/n)^{th}$ quantile of the resulting gamma distribution equals the time difference corresponding to an age at recapture that matches the true maximum age:

$$truet_{max} = truet_0 - \frac{\ln\left(1-\frac{trueL_{max}}{trueL_{\infty}}\right)}{truek}. \qquad (3.6)$$

Thus, ΔT_i was automatically negatively correlated with age at capture and it was ensured the true maximum age, $truet_{max}$, was very rarely attained in any sample. From these ages at recapture the corresponding lengths at recapture were calculated for each individual using equation (3.2), $L_{T2,i} = trueL_{\infty}(1 - e^{-\left(truek(t_{2,i}-truet_0)\right)})$.

Step 4: Introduce individual growth variability and measurement error

Based on the exact individual lengths and ages at capture and recapture individual growth variability and measurement errors were implemented. First, individual growth variability (gv) was introduced. Individual values for the asymptotic length, $L_{\infty,I}$, were assumed to be normally distributed with an average variability of ± 20% of the (constant) $trueL_{\infty}$. This was achieved by randomly simulating from a normal distribution using a mean, μ_{∞}, of 0 and a standard deviation, σ_{∞}, of 0.067 times the $trueL_{\infty}$:

$$L_{\infty,i} = trueL_{\infty} + N(\mu_{\infty} = 0, \sigma_{\infty} = 0.067 trueL_{\infty}). \quad (3.7)$$

The individual asymptotic maximum lengths were then used to derive the corresponding individual values for the growth constants, $k_{i,}$ by first calculating the true growth performance index, $true\Theta$, which relates L_{∞} and k (Pauly & Munro, 1984; Moreau et al., 1986):

$$true\Theta = log10(truek) + 2log10(trueL_{\infty}), \quad (3.8)$$

and:

$$k_i = 10^{(true\Theta - 2\log10(L_{\infty,i}))}. \quad (3.9)$$

Individual variability in t_0 was introduced by calculating $t_{0,i}$ via equation (3.4) with $L_{\infty,i}$ and k_i as input.

Given that each individual now has its own von Bertalanffy growth parameters, each individual also has its own maximum length, $L_{max,i} = 0.95L_{\infty,i}$, and maximum age, $t_{max,i} = t_{0,i} - \frac{\ln\left(1-\frac{L_{max,i}}{L_{\infty,i}}\right)}{ki}$. Consequently, the previously computed ΔT_i values could now imply ages at recapture beyond the true maximum age, and therefore needed adjustment. This was achieved by simulating a new time at liberty which accounted for individual growth variability, $\Delta T_{gv,i}$. This was simulated as described above, but the parameters in equation (3.6) were substituted with the individual parameters. The negative correlation between length at capture and the derived time at liberty was maintained and is shown in Figure 3.1.

The individual ages at recapture with growth variability, $t_{2,gv,I}$, were obtained by adding $\Delta T_{gv,i}$ to the individual ages at capture, $t_{1,i}$. The lengths at capture and recapture accounting for individual growth variability, $L_{T1,gv,i}$ and $L_{T2,gv,I}$, were calculated via $L_{T1,gv,i} = L_{\infty}i(1 - e^{-(ki(t_1 i - t_0 i))})$ and $L_{T2,gv,i} = L_{\infty,i}(1 - e^{-\left(ki\left(t_{2,gv,i} - t_{0,i}\right)\right)})$, respectively. Cases with the simulated length at recapture, $L_{T2,gv,I}$, smaller than the simulated length at capture, $L_{T1,gv,I}$, were discarded as they would result in negative growth.

Measurement errors (ME) are likely to occur in practice and were simulated by adding some Gaussian noise to the simulated lengths, allowing for an average error of ± 10% of the true individual length at capture, $L_{T1,i}$:

$$Lerror_{T1,i} = N(\mu = 0, \sigma = 0.033 L_{T1,i}) \quad (3.10)$$

$$L_{T1,ME,i} = L_{T1,i} + Lerror_{T1,i} \quad (3.11)$$

Following Laslett et al (2002) it was assumed that the measurement error was smaller at capture, because researchers tagging the individuals were assumed to measure more accurately. The error in the lengths at recapture was assumed to be larger, on average ± 20% of the true individual length at recapture, $L_{T2,i}$, because recaptures are often provided by persons not involved in the tagging:

$$Lerror_{T2,i} = N(\mu = 0, \sigma = 0.067 L_{T2,i}) \quad (3.12)$$

$$L_{T2,ME,i} = L_{T2,i} + Lerror_{T2,i}. \quad (3.13)$$

Again, when accounting for ME, cases with the simulated length at recapture, $L_{T2,ME,I}$, smaller than the simulated length at capture, $L_{T1,ME,I}$, were discarded as this would result in negative growth.

The simulated lengths at capture and recapture accounting for both, growth variability and measurement error, $L_{T1,gv,ME,i}$ and $L_{T2,gv,ME,I}$, were finally calculated for each individual, *i*:

$$L_{T1,gv,ME,i} = L_{T1,gv,i} + Lerror_{T1,i} \quad (3.14)$$

and:

$$L_{T2,gv,ME,i} = L_{T2,gv,i} + Lerror_{T2,i}. \quad (3.15)$$

Note that again individuals with negative growth ($L_{T1,gv,ME,I} > L_{T2,gv,ME,i}$) were discarded. The deviance from $L_{T1,gv,ME}$ to L_{T1}, i.e., the simulated length with growth variability and measurement error versus the length with no variability or error, and the deviance from $L_{T2,gv,ME}$ to L_{T2} is shown in Figure 3.1.

Step 5: Allow for on average short or long times at liberty

The average time at liberty may impact parameter estimates, especially when the average time at liberty is short (Simpfendorfer, 2000; McAuley et al., 2006). To mimic shorter or longer times at liberty in the data, a scale factor of 2 was used in the gamma distribution to simulate on average shorter times at liberty (Figs. 3.1; B3) and a scale factor of 1 to simulate on average longer times at liberty (Figs. B2; B4).This corresponds to an approximate median time at liberty of 0.25 years and 1.35 years for the two time-at-liberty scenarios, respectively.

Step 6: Allow for different sample sizes

The sample size was varied, starting with a moderate sample size of n = 20 individuals. However, mark-recapture data on elasmobranchs is generally very sparse and a small sample size of n = 5 individuals was also investigated.

Step 7: Simulate data

Mark-recapture data based on the starry smoothhound characteristics with the above simulation design were simulated for 200 random independent data sets (samples), here referred to as the number of replicates. Altogether, 16 different scenarios were simulated, all with growth variability and measurement error, and with different length at capture distributions (normal, right skewed, left skewed, bimodal), overall short or long times at liberty and moderate or very small sample sizes (Table 3.1).

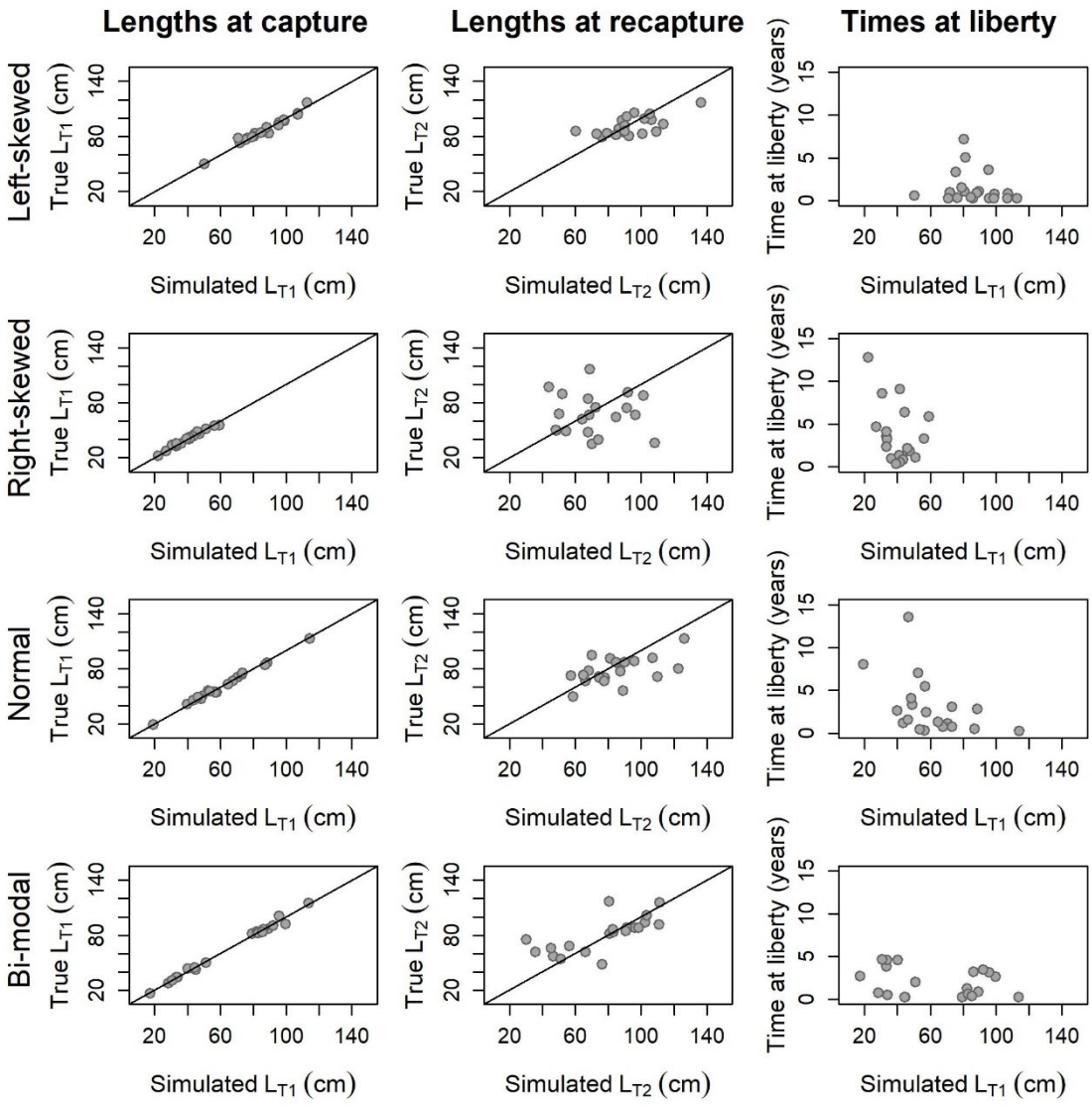

Fig. 3.1: Simulation design to mimic mark-recapture tagging data. Shown are the lengths at capture (L_{T1}, left column), lengths at recapture (L_{T2}, middle column) and times at liberty (right column) under different length at capture distributions (rows). The black lines indicate the 1:1 line between the true lengths versus the simulated lengths where growth variability and measurement error were introduced. The negative correlation implemented between lengths at capture and the times at liberty is presented in the third column. All scenarios shown here were simulated with a sample size of 20 individuals and on average short times at liberty.

Table 3.1: Simulation analysis scenarios. Shown are the 16 different simulation runs used to generate mark-recapture tagging data under pre-specified conditions: samples sizes of either 20 or 5 individuals; overall long or short times at liberty; and normal, right-skewed, left-skewed or bi-modal length at capture distributions. All runs were simulated with growth variability and measurement error, with 200 replicates (random datasets). Based on the known true growth parameters, the performance of the investigated methods in estimating von Bertalanffy growth parameters were tested.

Run	Sample size	Time at liberty	Distribution
1	5	long	normal
2	5	short	normal
3	5	long	right
4	5	short	right
5	5	long	left
6	5	short	left
7	5	long	bi-modal
8	5	short	bi-modal
9	20	long	normal
10	20	short	normal
11	20	long	right
12	20	short	right
13	20	long	left
14	20	short	left
15	20	long	bi-modal
16	20	short	bi-modal

3.3.3 Growth parameter estimation methods

In total, 7 different approaches to estimate von Bertalanffy growth parameters from mark-recapture tagging data were investigated. For mark-recapture tagging data, the most commonly applied parameterizations of the von Bertalanffy growth model are:

a) The Fa method (Fabens, 1965), which relates mark-recapture tagging data to length increments, ΔL, length at tagging, L_{T1}, and the time at liberty, ΔT:

$$\Delta L_i = (L_\infty - L_{\mathrm{T1,i}})(1 - e^{(-k\Delta T_i)}) + \varepsilon_i, \quad (3.16)$$

where ΔL is the length at recapture minus the length at capture, $L_{T2} - L_{T1}$, and ΔT is the time at recapture, T_2, minus the time at capture, T_1, and the epsilon, ε_i, is an error term with independent and identically distributed (*iid*) errors which have an expectation (mean) of zero and constant variance (sigma^2).

b) The Ja method, proposed by James (1991), which uses a weighted least squares approach of the Fa method, instead of ordinary least squares, with the inverse variance as a weighting factor:

$$\sum\left\{\left[L_{\mathrm{T2,i}} - L_{\mathrm{T1,i}} - \left(L_\infty - L_{\mathrm{T1,i}}\right)\left(1 - e^{(-k\Delta T_i)}\right)\right]^2 / (1 + e^{(-2k\Delta T_i)})\right\}. \quad (3.17)$$

This method was found to be the best performing among several methods applied to a mark-recapture dataset of the tope shark (Dureuil & Worm, 2015) and was therefore included here.

c) The Gh method (Gulland & Holt, 1959; Sparre & Venema, 1999) which relates mark-recapture tagging data to length increments, mean length, L_{mean}, and the time at liberty via regression analysis:

$$\frac{\Delta L_i}{\Delta T_i} = a + bL_{mean,i} + \varepsilon_i, \quad (3.18)$$

where a is the intercept, b is the slope, $L_{mean} = (L_{T2} + L_{T1})/2$, $k = -b$ and $L_\infty = -a/b$.

d) The Fr method (Francis, 1988b), which is an extension to the Fabens method using a maximum likelihood approach. This method includes two estimated mean growth rates, g_{L1} and g_{L2}, at two user selected reference lengths, L_1 and L_2:

$$\Delta L_i = \frac{\left[\left(L_{2,\mathrm{i}} g_{L_{1,\mathrm{i}}} - L_{1,\mathrm{i}} g_{L_{2,\mathrm{i}}}\right)/\left(g_{L_{1,\mathrm{i}}} - g_{L_{2,\mathrm{i}}}\right) - L_{\mathrm{T1,i}}\right]}{\left\{1 - \left[1 + \left(g_{L_{1,\mathrm{i}}} - g_{L_{2,\mathrm{i}}}\right)/(L_{1,\mathrm{i}} - L_{2,\mathrm{i}})\right]^{\Delta T_i}\right\}} + \varepsilon_i, \quad (3.19)$$

where epsilon, ε, is following a normal distribution and k and L_∞ can be estimated as follows (Francis, 1988b, 1988a):

$$k = -ln\left[1 + \left(g_{L_{1,\mathrm{i}}} - g_{L_2,i}\right)/\left(L_{1,\mathrm{i}} - L_{2,\mathrm{i}}\right)\right], \quad (3.20)$$

$$L_\infty = (L_{2,\mathrm{i}} g_{L_{1,\mathrm{i}}} - L_{1,\mathrm{i}} g_{L_{2,\mathrm{i}}})/(g_{L_{1,\mathrm{i}}} - g_{L_{2,\mathrm{i}}}). \quad (3.21)$$

In addition to the above commonly applied methods the following methods were also investigated here:

e) The La method (Laslett et al., 2002), which models the lengths at capture and recapture jointly, rather than modeling only the differences in length, with an explicit (measurement) error term. The joint modeling is done by assuming both lengths are conditionally independent and normally distributed. This method also specifies random effects for L_∞ and the relative age at tagging, A, to take into account individual variability in growth and age. Random effects can be cast in both a frequentist and Bayesian approach and generally serve the purpose of modeling extra variability not accounted for by available covariates (also called fixed effects), and yet can be attributed to some grouping factor (e.g. the mean L_∞ of the entire population) as long as repeated measurements are available, see e.g. McCulloch & Searle (2000). The random effect of L_∞ is assumed to be Gaussian independent and identically distributed, while the random effect of A is assumed to be independent and log-normally distributed. The relative age at tagging, A, is derived from the time at tagging, T_1, minus t_0, the theoretical age at 0 length. The model can be summarized as follows:

$$L_{T1,i} = L_{\infty,i}(1 - e^{(-kA_i)}) + \varepsilon_{T1,i} \quad (3.22)$$

$$L_{T2,i} = L_{\infty,i}(1 - e^{(-k(A_i+T_{2,i}-T_{1,i}))}) + \varepsilon_{T2,i} \quad (3.23)$$

$$\varepsilon_{T1,i} \sim idd\ N(0, \sigma\varepsilon^2)$$

$$\varepsilon_{T2,i} \sim idd\ N(0, \sigma\varepsilon^2)$$

$$L_{\infty,i} \sim idd\ N(\mu_\infty, {\sigma_\infty}^2)$$

$$A_i \sim idd\ logN(\mu_A, {\sigma_A}^2),$$

for $i = 1, \ldots, n$, where $logN(\mu, \sigma^2)$ stands for a log-normal distribution with mean, μ, and variance sigma^2 both on the log scale. The two measurement error terms, $\mathcal{E}_{T1}$ and $\mathcal{E}_{T2}$, are independent of each other but share the same variance. The two random effects, $L_{\infty,i}$ and A_i, depend on fixed parameters (the population means) which need to be estimated along with k and sigmaepsilon^2 ($\sigma\varepsilon^2$). The method of Laslett et al (2002) was implemented in the TMB *R* package, where the Laplace approximation was used for integrating out both random effects L_∞ and A.

f) The BFa method, a Bayesian formulation of the original Fa method, which involves a likelihood assumption (i.e. assuming a Gaussian probability distribution for the errors in the main equation) and extra information about the values of L_∞ and k in the form of prior distributions:

$$\Delta L_i = L_\infty - \left(L_\infty - L_{T1,i}\right)e^{(-k\Delta T_i)} + \varepsilon_i \quad (3.24)$$

$\varepsilon_i \sim iid\ N(0, \sigma^2)$

$L_\infty \sim unif[lb.L_\infty, ub.L_\infty]$

$k \sim unif[lb.k, ub.k]$

$\sigma \sim unif[lb.\sigma, ub.\sigma]$,

for i = 1, …, n, where epsilon, $\mathcal{E}_i$, is again an error term with independent and identically distributed (*iid*) errors, but assuming a full distribution. From a Bayesian perspective, the three parameters L_∞, k and sigma, σ, are no longer single numerical values but random variables, and their distribution represents the uncertainty one has about such parameters independent of the data at hand (see e.g. Gelman et al., 2014). As new data are collected, the distribution of the parameters is updated by computing posterior distributions and simple numerical summaries, such as mean and mode, which often serve as reference points for comparison with frequentist (i.e. non-Bayesian) point estimates. In the Bayesian implementation of the Fabens method described here, uniform priors were considered and specified by the user as lower and upper bounds for all parameters; see section on prior information below on how such bounds were set. The ADNUTS and TMB *R* packages (Kristensen et al., 2016) were used to draw samples from the posterior distributions in an efficient manner thanks to automatic differentiation (see Kristensen et al., 2016) and the no-U-turn Hamiltonian Monte Carlo sampling algorithm (Hoffman &Gelman, 2014).

g) The Zh method, a Bayesian method from Zhang et al (2009) denoted as "Model 1" in the source publication. This method also models the lengths at capture and recapture jointly, assuming both are normally distributed, and involves three random effects: L_∞, k and age at capture, A. Thus, this model resembles the Laslett et al (2002) method presented above, although it adds a third random effect for k and specifies slightly different distributions, with L_∞ and k assumed Gaussian independent and identically distributed, and age at tagging assumed independent and gamma distributed. The following equations summarize the model assumptions:

$$L_{T1,i} = L_{\infty,i}(1 - e^{(-k_i A_i)}) + \varepsilon_{T1,i} \quad (3.25)$$

$$L_{T2,i} = L_{\infty,i}(1 - e^{(-k_i (A_i + T_{2,i} - T_{1,i}))}) + \varepsilon_{T2,i} \quad (3.26)$$

$\varepsilon_{T1,i} \sim iid\ N(0, \sigma\varepsilon^2)$

$\varepsilon_{T2,i} \sim iid\ N(0, \sigma\varepsilon^2)$

$L_{\infty,i} \sim iid\ N(\mu_\infty, {\sigma_\infty}^2)$

$k_i \sim iid\ N(\mu_k, {\sigma_k}^2)$

$A_i \sim iid\ gamma(shapeA, rateA)$,

where gamma (*shapeA*, *rateA*) stands for a gamma distribution with shape parameter *shapeA* and rate (inverse of scale) parameter *rateA*. The prior specifications of Zhang et al (2009) were modified to accommodate uniform priors as outlined below:

$\mu_\infty \sim unif[lb.\mu_\infty, ub.\mu_\infty]$

$\sigma_\infty \sim unif[lb.\sigma_\infty, ub.\sigma_\infty]$

$\mu_k \sim unif[lb.\mu_k, ub.\mu_k]$

$\sigma_k \sim unif[lb.\sigma_k, ub.\sigma_k]$

$shapeA \sim unif[lb.shapeA, ub.shapeA]$

$rateA \sim unif[lb.rateA, ub.rateA]$

$\sigma\mathcal{E} \sim unif[lb.\sigma\mathcal{E}, ub.\sigma\mathcal{E}]$.

For all non-Bayesian methods, the standard error, SE, estimated from the data, was used to estimate 95% confidence intervals, CI, with CI = mean ± 1.96SE. For Bayesian methods, the 95% credible intervals were computed from the 2.5th and 97.5th percentile of the posterior distribution.

3.3.4 Prior information

The Bayesian methods to estimate von Bertalanffy growth parameters from mark-recapture data, BFa and Zh, allow the inclusion of prior knowledge for the parameters. Here, uniform prior distributions were enforced, with reasoning that there is a biologically meaningful range of values a parameter can take for a given species, but that no particular value within that range can be favored beforehand. Three different prior approaches were tested.

In the first approach informative priors were set. Given historical information on the largest individual for a particular species and population, an estimate of the asymptotic length, L_∞^*, can be computed following Froese & Binohlan (2000):

$$L_\infty^* = 10^{(0.044+0.9841*\log10(L_{max}))}. \quad (3.27)$$

The maximum total length, L_{max}, can be taken from literature and was set at 133 cm for the simulation analysis, which is the maximum length of female starry smoothhound sharks in the Northeast Atlantic (Farrell et al., 2010). The lower and upper uniform bounds for L_∞^* were assumed to be between $0.9L_{max}$ and $1.2L_{max}$ (Taylor, 1958; Froese & Binohlan, 2000; Nadon & Ault, 2016; Froese et al., 2019).

The bounds for *k* were based on the growth performance index theta, Θ, which relates L_∞ and *k* (Pauly & Munro, 1984; Moreau et al., 1986, see also equation (3.8)). To calculate Θ, all L_∞ and *k* estimates from all fish species with the same body shape were first extracted from FishBase. This was done because only species with the same body shape can be compared using the growth performance index (Pauly & Munro, 1984). Only studies with total length present, marked as non-doubtful and not from captive fish were included. Then, the minimum and maximum of all available Θ values were used as lower and upper references (lb. Θ and ub.Θ). From this, the lower and upper bounds for *k* were computed as:

$$lb.k = 10^{(\mathrm{lb.}\Theta - 2\log 10(L_\infty{}^*))} \quad (3.28)$$

and:

$$lb.k = 10^{(\mathrm{ub.}\Theta - 2\log 10(L_\infty{}^*))}. \quad (3.29)$$

Methods utilizing this first approach with informative priors on L_∞ and *k* are labelled with numeric *I* and abbreviated BFaI.

In the second approach semi-informative priors were utilized by setting the lower and upper uniform bounds for $L_\infty{}^*$ between $0.5L_{max}$ and $1.5L_{max}$. Methods utilizing the second approach with semi-informative priors on L_∞ and *k* are labelled with numeric *II* and abbreviated BFaII.

In the third approach vague priors were utilized for the asymptotic maximum length and the growth constant, with L_∞ between 0 cm and 2000 cm and *k* between 0 $year^{-1}$ and 20 $year^{-1}$, reflecting the largest known values for any fish (Boettiger et al., 2012; Froese & Pauly, 2018). Methods utilizing the third approach with a vague prior are labelled with numeric *III* and abbreviated BFaIII.

The priors on variance, shape and rate parameters were left fairly wide in all three approaches, and thus uninformative, covering a numerically sensible interval such as 10^{-4} to 10^4 for a standard deviation.

3.3.5 Evaluation of methods' performance

To evaluate the performance of each method a deterministic approach was applied first, i.e. all methods were applied to the simulated data without any growth variability or error. Here, 20 datasets were simulated using a sample size of 5, a normal distribution for length at capture and overall shorter times at liberty. Based on this, the methods should find the true growth parameters used as inputs in the simulation study. Methods that were exceeding a relative error of 5% for either L_∞ or *k* more than once

(>5%) were not included in the following simulation analysis. For the Bayesian methods vague priors were used for the deterministic analysis. The Bayesian methods were run with one chain, 2000 iterations and a warm-up phase of 1000 iterations. This means that the first 1000 iterations were discarded and only the following 1000 iterations were used to estimate the parameters.

All methods with a relative error for the growth parameters of less than 5% in the deterministic analysis were applied to the simulated mark-recapture data for each of the 16 different combinations, i.e. considering different length at capture distributions, times at liberty and sample sizes. The number of replicates was set to 200 for each simulation run. The performance of each method for the simulated data was evaluated graphically by comparing boxplots of the estimated parameters with the true parameters. Note, that technically all methods are mis-specified, because the simulation design does not follow any of the investigated methods exactly, but rather came from first principles to mimic realistic data. Hence, no method would be expected to have zero bias in all scenarios.

In addition, all methods were tested on observed mark-recapture tagging data for 11 different elasmobranch species totaling 15 different stocks. The mark-recapture tagging data was obtained from the International Commission for the Conservation of Atlantic Tunas (ICCAT) database of conventional tagging data (https://www.iccat.int/en/accesingdb.htm) and provided by the Centre for Environment, Fisheries and Aquaculture Science (CEFAS) Tagged Fish Database. Only length information with known units and measurement methods were utilized and transformed to cm. Measurements in fork length were transformed to total length using published relationships. Mark-recapture data can be subject to significant measurement errors, and to minimize the impact of outliers the following steps were applied in the given order: 1) First, only observations with times at liberty of > 90 days were included, because of the large variability and influence on errors for shorter time periods (Simpfendorfer, 2000; McAuley et al., 2006); 2) Then, growth rates in cm per year exceeding the interquartile range of all growth rates in cm per year for a particular species and stock were excluded; and 3) Lastly, negative growth rates were excluded. The Bayesian methods were run with one chain, 2000 iterations and a warm-up phase of 1000 iterations.

The maximum total length, L_{max}, needed to obtain the prior information was taken from Ebert & Stehmann (2013) for all species. The performance of the methods in estimating growth from mark-recapture data was then evaluated by comparing the results obtained from the mark-recapture methods with growth parameters obtained from

literature using conventional length-at-age methods. Growth parameters can be different for the same species but different stocks, and therefore only studies for the same species and stock were considered. For visualization purposes, the Bayesian methods with different prior approaches were compared independently and only the overall best performing approach, as identified in the simulation analysis, was applied for the comparison with non-Bayesian methods. The influence of different prior information on the parameter estimates is discussed.

3.4 Results

Only five out of the eight methods identified the true growth parameters of L_∞ = 123.5 cm and k = 0.146 year^{-1} at all times when applied to 20 replicated datasets, each with a sample size of 5 individuals, a normal distribution for length at capture, overall shorter times at liberty, and no growth variability or measurement error. For the Zh, Gh and Fr methods, either the estimated asymptotic length or the von Bertalanffy growth constant were outside a 5% relative error range in at least 6 of the 20 replicates (Table B1). Consequently, these three methods were not applied to the simulated data with growth variability and measurement error.

Of the methods applied in the simulation analysis, which utilized four different length at capture distributions, sample sizes of 5 or 20 individuals and overall short (median ≈ 0.25 years) or long (median ≈ 1.35 years) times at liberty, the Bayesian implementation of Fabens (1965) method with informative priors (BFaI) performed best across all controlled scenarios (Fig. 3.2). For all methods, the variability in the growth constant was greater than the variability in the asymptotic maximum length. Additionally, increasing the sample size from 5 to 20 individuals reduced the variability around the parameter estimates for some methods, particularly for BFaI (Figs. B5; B6). Generally, the estimates of the asymptotic maximum length were closer to the true value when times at liberty were long for non-Bayesian methods and for BFaI, but mixed results were found for the weaker priors in scenarios BFaII and BFaIII. Estimates were also generally closer to the true value for normal or bimodal distributed lengths at capture (Fig. B5). The growth constant was usually estimated higher across methods when times at liberty were long, but all methods, except BFaI, performed poorly in estimating k (Fig. B6), with the relative bias being larger than for L_∞ (Figs. B5; B6). In the scenario of right skewed distributions, only BFaI and Ja found reasonable results for both growth parameters, with the latter method only giving reasonable results if times at liberty were long. All method except BFaI

performed poorest when lengths at capture were right skewed and times at liberty on average short (Figs. B5; B6). The BFaI method also performed generally best for left skewed distributions (Figs. B5; B6).

All methods (BFa, Fa, Fr, Gh, Ja, La, Zh) were tested on empirical tagging data. Given that BFaI performed best in the simulation analysis, the two Bayesian methods, Zh and BFa, were only tested with informative priors (ZhI and BFaI; Table B2). Mark-recapture information (Table 3.2) and growth parameters obtained from direct length-at-age information (Table 3.3) were available for 11 elasmobranch species from 15 different stocks, with mark-recapture data taken from the ICCAT and CEFAS databases and growth parameters from direct aging data taken from literature. The final sample sizes after outlier exclusion ranged from 4 individuals for the blue skate (*Dipturus batis*) and small-eyed ray (*Raja microocellata*) to 968 individuals for the thornback ray (*R. clavata*) (Table 3.2). The sample size for literature-derived growth parameters ranged from 61 individuals to 4788 individuals (Table 3.3). With the exceptions of the starry ray (*Amblyraja radiata*), blonde ray (*Raja brachyura*) in the North Sea/West of Scotland, and thornback ray West of Scotland, the time periods when the mark-recapture data were taken overlapped with the time periods when the data were sampled in the literature studies. The lengths at capture distributions could generally be described in a similar manner to those tested in the simulation analysis, i.e. normal, right skewed, left skewed, or bimodal, although some distributions were multimodal (Fig. B7). Times at liberty tended to be negatively correlated with length at capture for most species and were on average approximately one year (Fig. B8).

The two Bayesian methods, BFaI and ZhI, were the only methods with biologically reasonable estimates for the asymptotic maximum length for all species and stocks (Fig. 3.3A). Estimates for the growth constant were more variable, and here only the BFaI method gave biologically reasonable results for all stocks (Fig. 3.3B). In most cases, the resulting von Bertalanffy growth curves indicated slower growth from BFaI compared to curves derived from direct aging information, with all of the other methods failing for at least one of the 15 stocks (Figs. 3.4; 3.5).

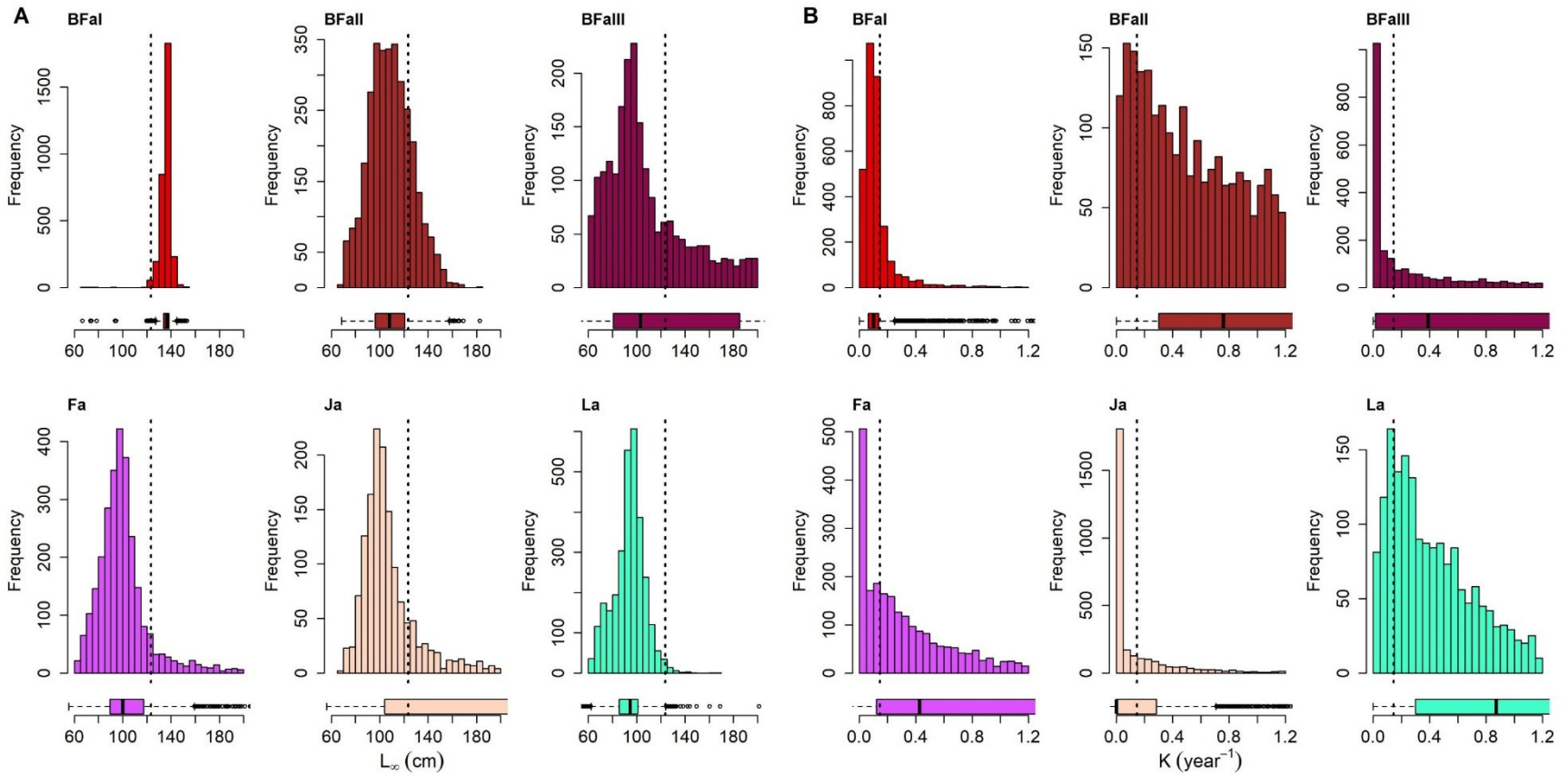

Fig. 3.2: Overall performance in estimating growth parameters from simulated mark-recapture tagging data. A) True asymptotic maximum lengths, L_∞, at 123.5 cm and **B)** true growth constant, k, at 0.146 year^{-1} (dotted vertical lines) compared to growth parameters estimated with: a Bayesian implementation of Fabens (1965) method using informative (BFaI), semi-informative (BFaII) or vague (BFaIII) prior information; the Fabens (1965) method (Fa); the James (1991) method (Ja); or the Laslett et al (2002) method (La). Results are given over all controlled scenarios for length at capture distributions, sample size and overall times at liberty (simulation runs 01 – 16). For details see table 3.1. Histograms show the frequency distribution of the estimates and boxplots show the median estimate and the variability over all simulation runs.

Table 3.2: Species, stock discrimination, sample size and time periods for the investigated elasmobranch species. Information on stock ID was obtained from http://stockdatabase.ices.dk, ICES (2017) and Campana et al (1999). All information was for combined sexes, except for stock rjh.27.4a6, where information is for females. The sample size, n, refers to total sample size with the numbers in parenthesis showing the data points identified as outliers. These values would need to be subtracted from the total sample size to get the final sample size used in this study. The time period is given as the minimum and maximum sampling years.

Species	Common name	Stock ID	Location	n	Time period
Amblyraja radiata	Starry ray	rjr-234	Norwegian Sea, North Sea, Skagerrak, Kattegat	18 (3)	1959 − 1963
Dipturus batis	Blue skate	rjb.27.67a-ce-k	Celtic Seas, western English Channel	4 (0)	1965 − 2014
Isurus oxyrinchus	Shortfin mako	North Atlantic	North Atlantic Ocean	97 (5)	1976 − 2015
Lamna nasus	Porbeagle	Northwest Atlantic	Western North Atlantic	58 (2)	1983 − 2005
Leucoraja naevus	Cuckoo ray	rjn.27.678abd	West of Scotland, southern Celtic Seas, western English Channel, Bay of Biscay	27 (2)	1963 − 2012
Prionace glauca	Blue Shark	North Atlantic	North Atlantic	386 (39)	1966 − 2017
Raja brachyura	Blonde ray	rjh.27.4a6	North Sea, West of Scotland	36 (5)	1963 − 1970
		rjh.27.7afg	Irish Sea, Bristol Channel, Celtic Sea North	36 (4)	1964 − 2012
Raja clavata	Thornback ray	rjc.27.3a47d	North Sea, Skagerrak, Kattegat, eastern English Channel	1023 (37)	1959 − 2016
		rjc.27.6	West of Scotland	14 (0)	1963 − 1968
		rjc.27.7afg	Irish Sea, Bristol Channel, Celtic Sea North	339 (13)	1964 − 2013
Raja microocellata	Small-eyed ray	rje.27.7fg	Bristol Channel, Celtic Sea North	4 (0)	1964 − 2013
Raja montagui	Spotted ray	rjm.27.3a47d	North Sea, Skagerrak, Kattegat, eastern English Channel	72 (5)	1959 − 2014
		rjm.27.7ae-h	southern Celtic Seas, western English Channel	165 (7)	1964 − 2013
Squalus acanthias	Spurdog	dgs.27.nea	Northeast Atlantic	1035 (59)	1960 − 2014

Table 3.3: Literature based growth estimates for the investigated elasmobranch species. von Bertalanffy growth parameters L_∞ (cm) and k ($year^{-1}$) for 15 North Atlantic elasmobranch stocks obtained from literature (Aging). All parameters were estimated from conventional aging methods using length-at-age information. If available, 95% confidence intervals were extracted and are given in parenthesis. All growth parameters were for combined sexes, except for the stock rjh.27.4a6, where information is for females. The mean was used between sexes and time periods if applicable, and fork length was transformed into total length using published relationships. The sample size, n, refers to total sample size and the time period is the minimum and maximum sampling year.

Species	Stock ID	L_∞	k	n	Time period	Source
Amblyraja radiata	rjr-234	68.7 (56 − 82)	0.125 (0.066 − 0.184)	531	1991 − 1995	Walker (1999)
Dipturus batis	rjb.27.67a-ce-k	254 (197 − 311)	0.057 (0.036 − 0.078)	126	<1978	Du Buit (1977)
Isurus oxyrinchus	North Atlantic	379.1 (312 − 447)	0.084 (0.058 − 0.110)	258	1662 − 2004	Natanson et al (2006); ICES (2017)
Lamna nasus	Northwest Atlantic	278.2 (266 − 290)	0.100 (0.085 − 0.115)	780	1961 − 2004	Campana et al (1999); Cassoff et al (2007)
Leucoraja naevus	rjn.27.678abd	79.3 (71 − 87)	0.246 (0.189 − 0.302)	560	1996 − 1998	Gallagher et al (2005)
Prionace glauca	North Atlantic	338.8 (334 − 352)	0.170 (0.160 − 0.180)	411	1966 − 2001	Skomal & Natanson (2003); ICES (2017)
Raja brachyura	rjh.27.4a6	144.3	0.190	61	1987 − 1988	Fahy (1989)
	rjh.27.7afg	150.3 (90 − 211)	0.137 (0.029 − 0.245)	268	1996 − 1998	Gallagher et al (2005)
Raja clavata	rjc.27.3a47d	108	0.155	92	1992 − 1995	Walker (1999)
	rjc.27.6	112.2	0.175	469	1987 − 1988	Fahy (1989)
	rjc.27.7afg	123 (77 − 169)	0.114 (0.039 − 0.189)	258	1996 − 1998	Gallagher et al (2005)
Raja microocellata	rje.27.7fg	137	0.086	2592	1974 − 1976	Ryland & Ajayi (1984)
Raja montagui	rjm.27.3a47d	77.2 (62 − 92)	0.200 (0.073 − 0.327)	165	1991 − 1995	Walker (1999)
	rjm.27.7ae-h	75.4 (68 − 83)	0.280 (0.204 − 0.356)	468	1996 − 1998	Gallagher et al (2005)
Squalus acanthias	dgs.27.nea	93 (85 − 102)	0.120 (0.096 − 0.141)	4788	1959 − 1998	Dureuil (2013)

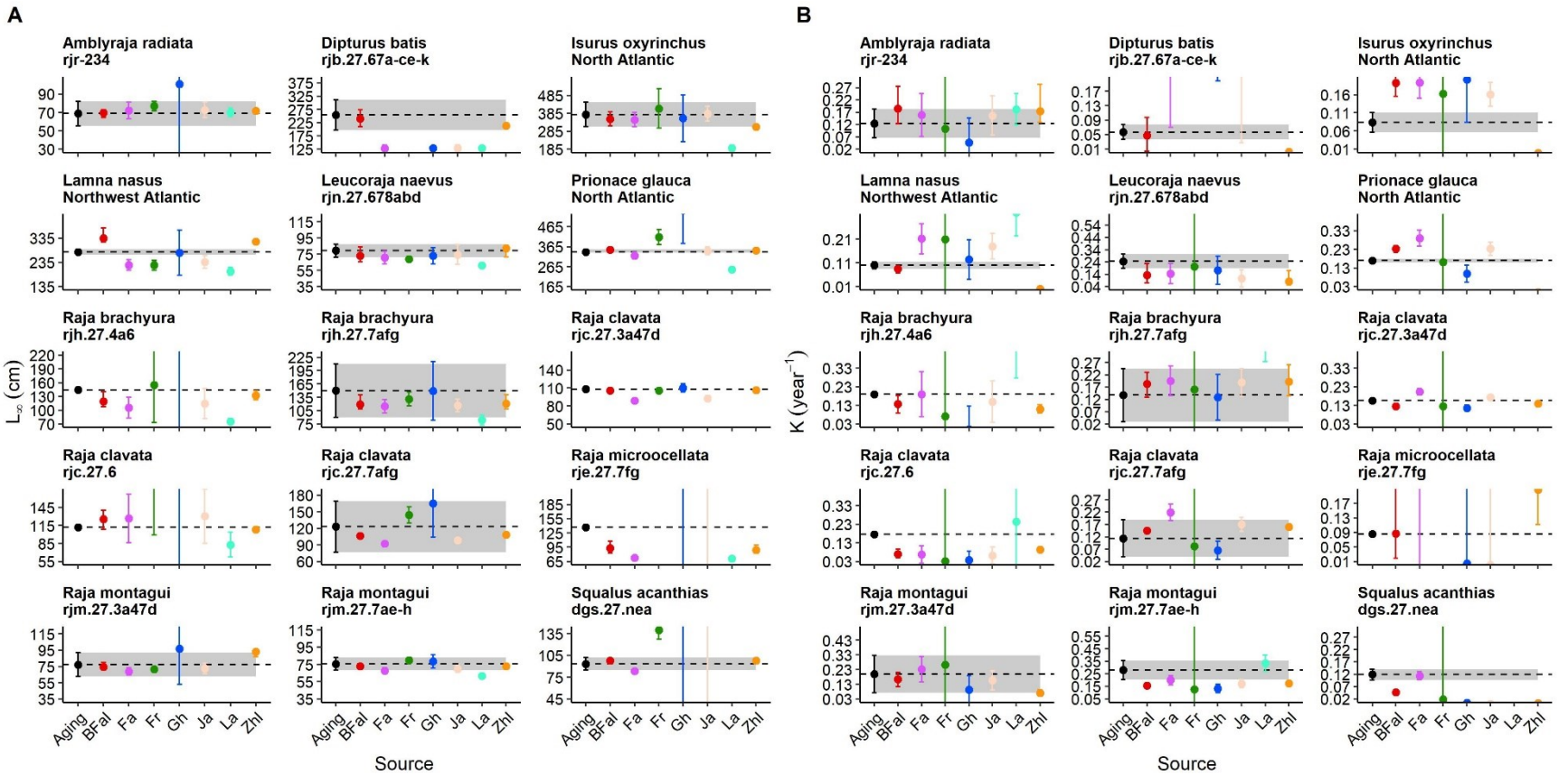

Fig. 3.3: Growth parameter estimates for 15 North Atlantic elasmobranch stocks from various methods. A) Asymptotic maximum lengths, L_∞ (cm), and **B)** von Bertalanffy growth constant, k (year^{-1}). The dotted vertical line indicates growth parameters obtained from literature (Aging), all of which were based on conventional length-at-age information. If available, 95% confidence intervals were extracted and are shown here as error bars. All other methods utilized mark-recapture tagging data: a Bayesian implementation of Fabens (1965) method using informative priors (BFaI); the Fabens (1965) method (Fa); the Francis (1988b) method (Fr); the Gulland & Holt (1959) method (Gh); the James (1991) method (Ja); the Laslett et al (2002) method (La); and the Zhang et al (2009) method (ZhI), for which the same informative priors as in BFaI were utilized. For the mark-recapture methods the error bars show either 95% confidence intervals, or 95% credible intervals, in the case of the Bayesian methods. Elasmobranch species names and stock ID's are given above each panel.

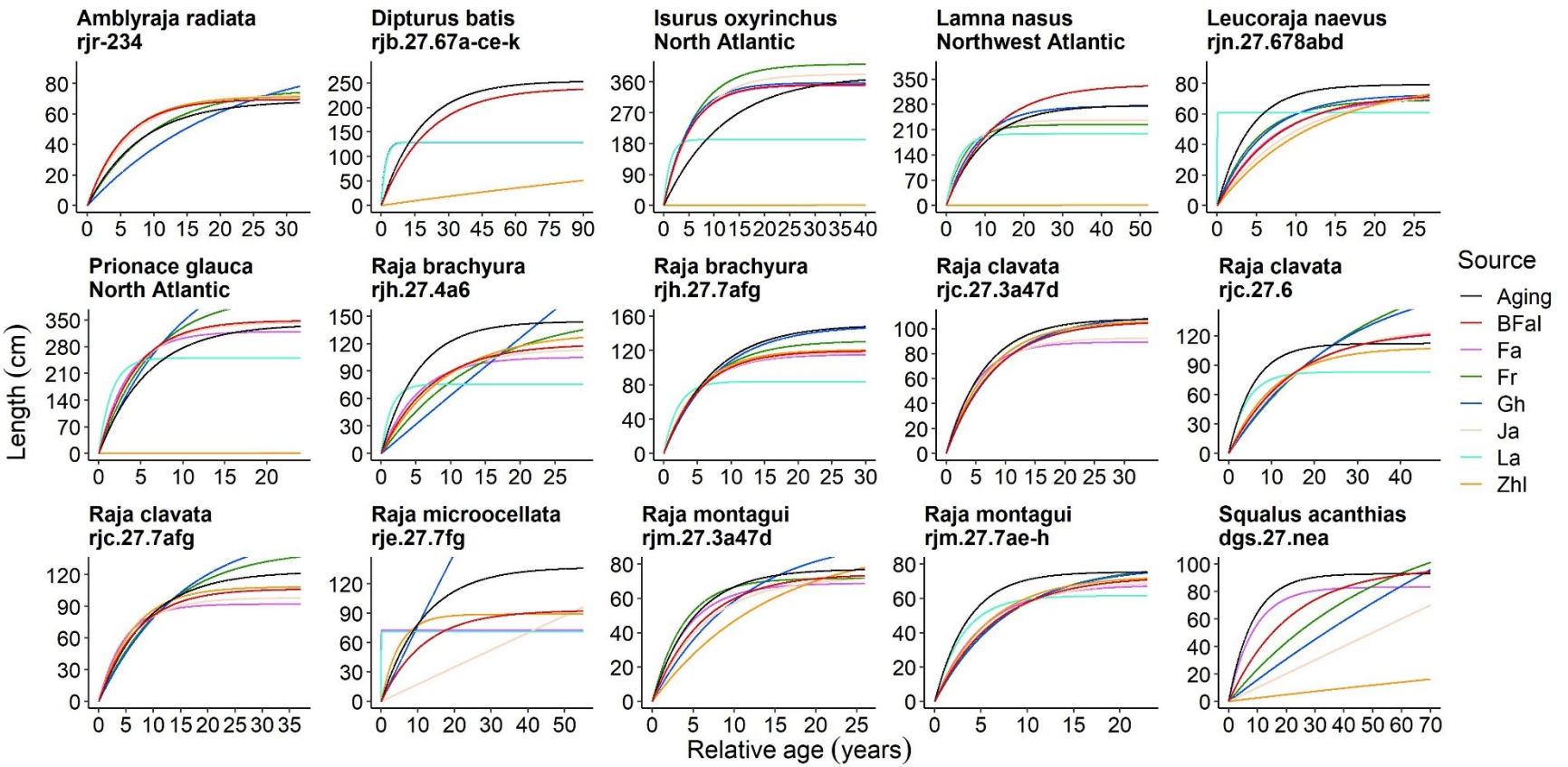

Fig. 3.4: von Bertalanffy growth curves for 15 North Atlantic elasmobranch stocks from various methods. Shown are von Bertalanffy growth curves obtained from literature using conventional length-at-age information (Aging, black line) and obtained from the following methods, all utilizing mark-recapture tagging information (colored lines): a Bayesian implementation of Fabens (1965) method using informative priors (BFal); the Fabens (1965) method (Fa); the Francis (1988b) method (Fr); the Gulland & Holt (1959) method (Gh); the James (1991) method (Ja); the Laslett et al (2002) method (La); and the Zhang et al (2009) method (Zhl), for which the same informative priors as in BFal were utilized. Elasmobranch species names and stock ID's are given above each panel. Ages are relative due to the absence of the von Bertalanffy parameters length at birth or time at zero length.

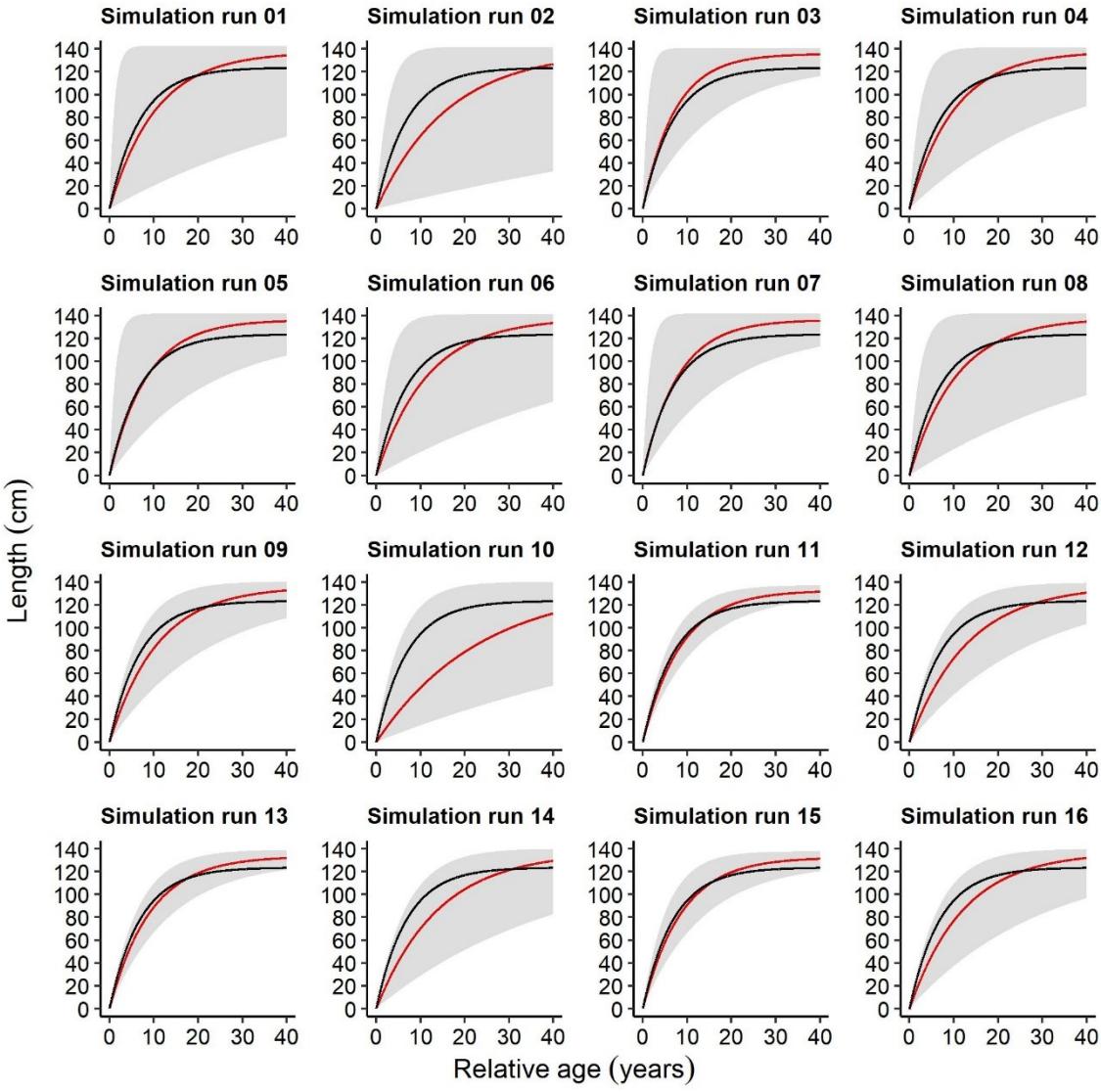

Fig. 3.5: Comparison of true and simulated von Bertalanffy growth curves from mark-recapture tagging data. Shown are the true von Bertalanffy growth curves (black line) and simulated curves as the median over all 200 replicates (red) from the Bayesian implementation of Fabens (1965) method with informative priors (BFaI), under different controlled scenarios for length at capture distributions, sample size and overall times at liberty (simulation runs 01 – 16). For details see table 3.1. The 95% credible intervals of the BFaI method are shown in grey. Ages are relative due to the absence of the von Bertalanffy parameters length at birth or time at zero length.

3.5 Discussion

This study investigated the performance and robustness of different methods to estimate von Bertalanffy growth parameters from mark-recapture tagging data in elasmobranchs. Such methods are urgently needed, as many (or most) elasmobranch species cannot be aged via conventional methods, leading to age underestimation and bias in the derived growth parameters (Harry, 2017; Natanson et al., 2018). Here, simulation testing under different controlled scenarios and evaluation testing with empirical tagging data was used to evaluate seven alternative approaches. Strong differences in the performance of the seven tested methods were found, and only the Bayesian implementation of Fabens (1965) method with informative priors gave largely unbiased growth parameter estimates under all scenarios.

In agreement to our findings, the method from Fabens (1965) is known to produce biased estimates when individuals display variability in growth (Sainsbury, 1980; Francis, 1988a; Maller & deBoer, 1988; Kimura et al., 1993; Wang & Thomas, 1995; Eveson et al., 2007) or when measurement errors occur (Eveson et al., 2007; Dureuil & Worm, 2015), thus overestimating mean length-at-age (Sainsbury, 1980). James (1991) suggested to use weighted least-squares instead, which has been shown to perform well if the asymptotic maximum length is fixed (Dureuil & Worm, 2015), but the findings here suggest that in many circumstances the results are biased. It may, however, perform well when the data is right-skewed or bimodally distributed and the times at liberty are large (Figs. B5; B6). Instead of fixing the asymptotic maximum length, Laslett et al (2002) included individual variability in L_∞ by utilizing two equations, one for the length at capture and one for the length at recapture, instead of one equation that describes the change in the growth increment. They then modelled the length at capture and recapture jointly by maximizing a marginal likelihood. This approach is also addressing critiques that growth parameters have different interpretations in length-at-age and mark-recapture, because the measured length is the expected length in the first model and the observed length in the second model (Francis, 1988a). Furthermore, it allows the error terms of the length-at-capture and recapture to be (conditionally) independent. Laslett et al (2002) tested their model on various simulation designs. In addition, Eveson et al (2007) applied the method from Laslett et al (2002) to simulations with various specifications. However, in both studies the sample size was rather large with at least 100 individuals. Moreover, Laslett et al (2002) used southern bluefin tuna (*Thunnus maccoyii*) as an example, a data-rich species that is believed to not follow a general von Bertalanffy growth curve (Hearn & Polacheck, 2003).

Eveson et al (2007) had no real-world example. Eveson et al (2007) also found that bias in growth parameter estimates became larger when average times at liberty were reduced from 4 years to 2 years, which is almost double the long time at liberty utilized here. Therefore, this rather data-intensive method may not be applicable for many elasmobranchs, as suggested by the findings of this study.

Three of the seven methods, Gh, Fr, and Zh, failed to find the true growth parameters in a simulated dataset even without growth variability or error. It was expected that the Gh method would not return the exact true values, because it is only an approximation of the von Bertalanffy growth function. Why the Fr method failed is less clear, but the arbitrary selection of the reference lengths might be problematic in data-poor situations. Likewise, the Zh method may have failed because it was not possible to estimate three random effects from such limited data. The same methods also gave biologically unreasonable results for some of the 15 stocks (Fig. 3.3). The Gh method (Gulland & Holt, 1959), has been shown to produce biased estimates, even when growth variability and measurement error are small (Dureuil & Worm 2015), and may fail when time at liberty is short or growth variability high (Simpfendorfer, 2000). For the Fr method (Francis, 1988b), it has been hypothesized that biased growth parameters might be produced when growth is variable, measurement errors occur, times at liberty are short and the sample size is small (McAuley et al., 2006), or old individuals are absent (Natanson et al., 2002; Skomal & Natanson, 2003). The third method that failed finding the true growth parameters when applied in simulations without error or growth variability was the Zh method (Zhang et al., 2009). Zhang et al (2009) developed a Bayesian model to be used for a sea snail, the northern abalone (*Haliotis kamtschatkana*), based on the maximum likelihood method from Laslett et al (2002). Their simulation design was mimicking the observed mark-recapture tagging data, with a sample size of > 100, a time at liberty from < 0.07 years to > 3 years, with the majority of individuals at liberty for more than 1 year, and a right skewed (positive or lognormal) length at capture distribution, covering most of the species size range (37mm to 113 mm). The species-specific characteristics of their study may explain why this method did not perform well for elasmobranchs. Three random effects may not be suitable for data-poor approaches because different pairs of L_∞ and k can yield in the same likelihood and would warrant further recaptures of the same individual to be identifiable, as present for northern abalone. The information available for elasmobranchs is often less extensive. Moreover, accurate measurement of body length may be easier to obtain from an abalone shell than

from a live elasmobranch, reducing the error associated with the data. Given the difficulties to measure sharks and rays in the field, methods that are highly sensitive to measurement error are not generally suitable for elasmobranchs. Other methods might have too data-intensive requirements and are therefore not applicable.

Dureuil & Worm (2015) found that fixing the asymptotic size can improve parameter estimates for the tope shark. However, a Bayesian approach that allows for prior information on the asymptotic size within a range of values (or within a distribution) might be preferable over fixing a parameter. The presented Bayesian implementation of Fabens (1965), BFa, method achieved exactly this. As expected, given the findings by Dureuil & Worm (2015), some prior information was needed to obtain reasonable growth parameter estimates under all scenarios. This was realized by using uniform prior bounds in L_∞ and k, derived from the species' observed maximum size, with L_∞ being between $0.9L_{max}$ and $1.2L_{max}$ (method BFaI). In addition, BFa requires less information compared to the other Bayesian method that was tested here from Zhang et al (2009). It does not include random effects nor the age at tagging, A, and therefore has less parameters to be estimated. However, even if BFaI was the overall superior method in both the simulation and evaluation analysis, it tended to consistently underestimate k and overestimate L_∞ in the simulation analysis (Figs. B5; B6). Yet, the estimated ages could still be unbiased, given that von Bertalanffy growth parameters are correlated (Pilling et al., 2002). This would be of great significance, because estimating age indirectly from length via the von Bertalanffy growth function is common in elasmobranchs, due to the difficulties and costs to age individuals directly. However, when using the median of L_∞ and k from BFaI for each simulation run and comparing the derived growth curves with the true growth curves, it can be seen that the resulting curves are still biased, with ages generally overestimated for younger individuals and underestimated for older individuals (Fig. 3.6). Consequently, there is a need to obtain unbiased growth parameter estimates. The BFaI method itself might still produce unbiased parameter estimates, but Bayesian methods can be sensitive to provided prior information (Yin et al., 2019). To investigate this, a range of priors was applied using different L_{max} values with resulting L_∞ values between $0.9L_{max}$ and $1.2L_{max}$ (BFaI), $0.9L_{max}$ and $1.1L_{max}$ (BFaIA), $0.8L_{max}$ and $1.2L_{max}$ (BFaIA), $0.8L_{max}$ and $1.1L_{max}$ (BFaIA), or $0.7L_{max}$ and $1.2L_{max}$ (BFaIA). The resulting growth parameters were indeed, overall, unbiased, if the prior bounds around L_∞ were not too narrow, but in the range of ± 20% of L_{max}, BFaIB, (Figs. 3.6; A.3.9). The effect of the different priors on empirical data was less pronounced (Fig. 3.7; Table 3.4), with similar results between BFaI and BFaIB.

This suggests that it might not be the best approach to make the prior bounds as narrow as possible, but rather to choose the prior bounds wide enough that natural variability in L_∞ among individuals of the same population is taken into account.

The estimated growth parameters from BFaI or BFaIB agreed well with those reported in the literature. All literature studies counted band pairs in the vertebrae to estimate age, except for the spurdog (or spiny dogfish, *Squalus acanthias*) where spines were used. Although these bands are likely not a reliable indicator of age, they could still coincidentally form annually during some parts of an elasmobranch lifespan (Natanson et al., 2018). Hence, it is unknown if the regularly reported underestimation of ages for elasmobranchs (Harry, 2017) also occurred in the literature aging studies that were utilized here. Yet, *S. acanthias* is considered an example for which age estimates appear valid throughout its lifetime (Cailliet, 2015), and the results from the mark-recapture data here suggest slightly slower growth compared to the literature estimates. However, slower growth than previously reported has also been suggested for Northwest Atlantic *S. acanthias* (Campana et al., 2009), and the growth parameters found here agree with growth parameters reported for this species from other areas (Campana et al., 2009; Bubley et al., 2012). In addition, spines wear or break naturally which can cause bias in age estimates (Taylor et al., 2013) that could have affected the literature estimates utilized here. Furthermore, the mark-recapture data consisted of >60% males, which attain smaller asymptotic maximum sizes and have a higher growth constant than females. These factors may in part explain the observed difference between length-at-age and mark-recapture growth parameter estimates reported here.

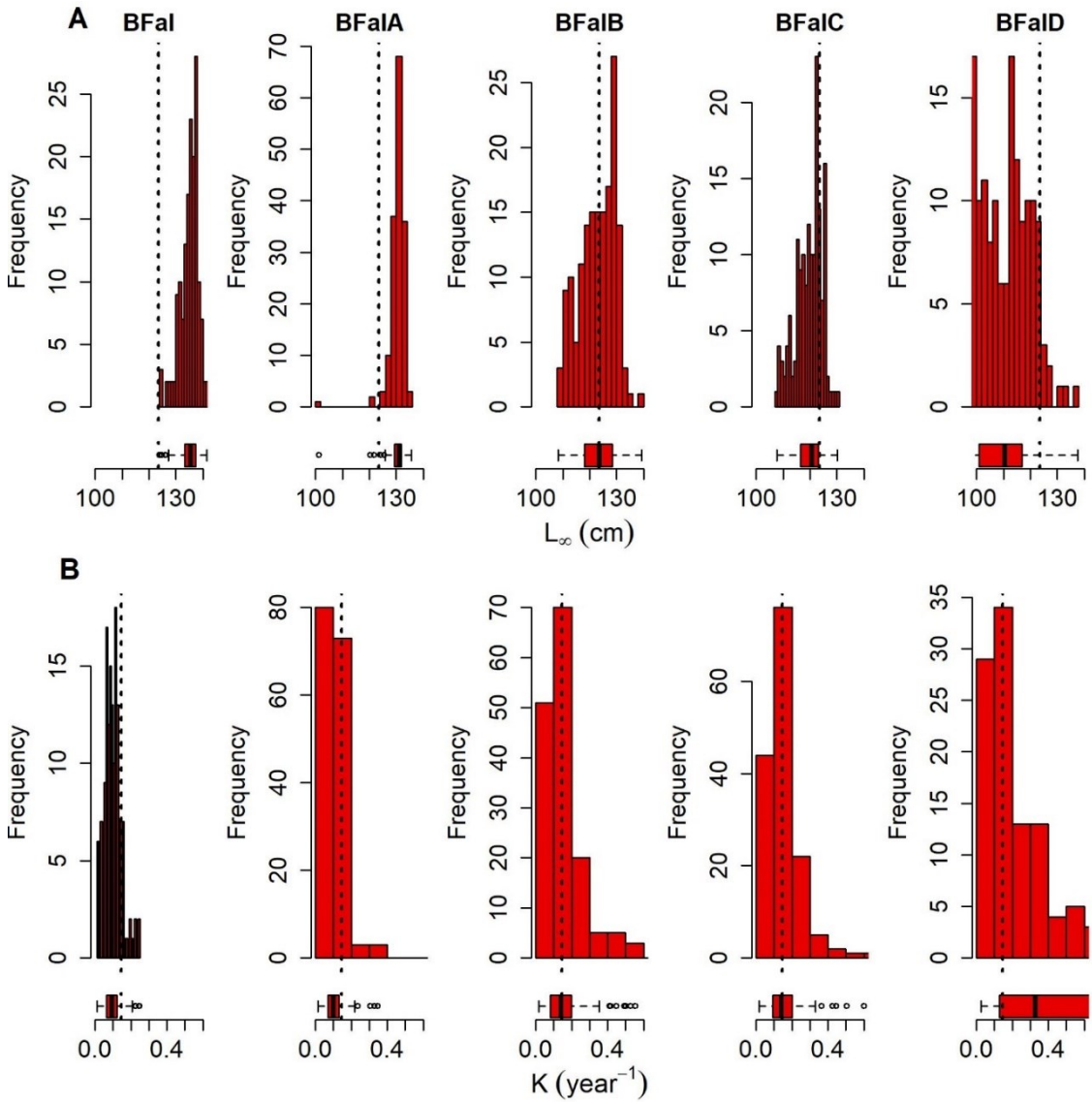

Fig. 3.6: Overall performance of the Bayesian Fabens methods in estimating growth parameters from simulated mark-recapture tagging data under different informative prior scenarios. A) True asymptotic maximum lengths, L_∞, at 123.5 cm and **B)** true growth constant, k, at 0.146 year^{-1} (dotted vertical lines) compared to growth parameters estimated with a Bayesian implementation of Fabens (1965) with informative priors (BFa). The approaches differ in the defined uniform prior bounds around L_∞, obtained from observed maximum length, L_{max}, with $0.9L_{max}$ and $1.2L_{max}$ (BFaI), with $0.9L_{max}$ and $1.1L_{max}$ (BFaIA), with $0.8L_{max}$ and $1.2L_{max}$ (BFaIB), with $0.8L_{max}$ and $1.1L_{max}$ (BFaIC), and with $0.7L_{max}$ and $1.2L_{max}$ (BFaID). Results are given over all controlled scenarios for length at capture distributions, overall times at liberty, with a sample size of 20 individuals for all runs (simulation runs 09 – 16) and 20 replicates per run. For details see table 3.1. Histograms show the frequency distribution of the estimates and boxplots show the median estimate and the variability over all simulation runs.

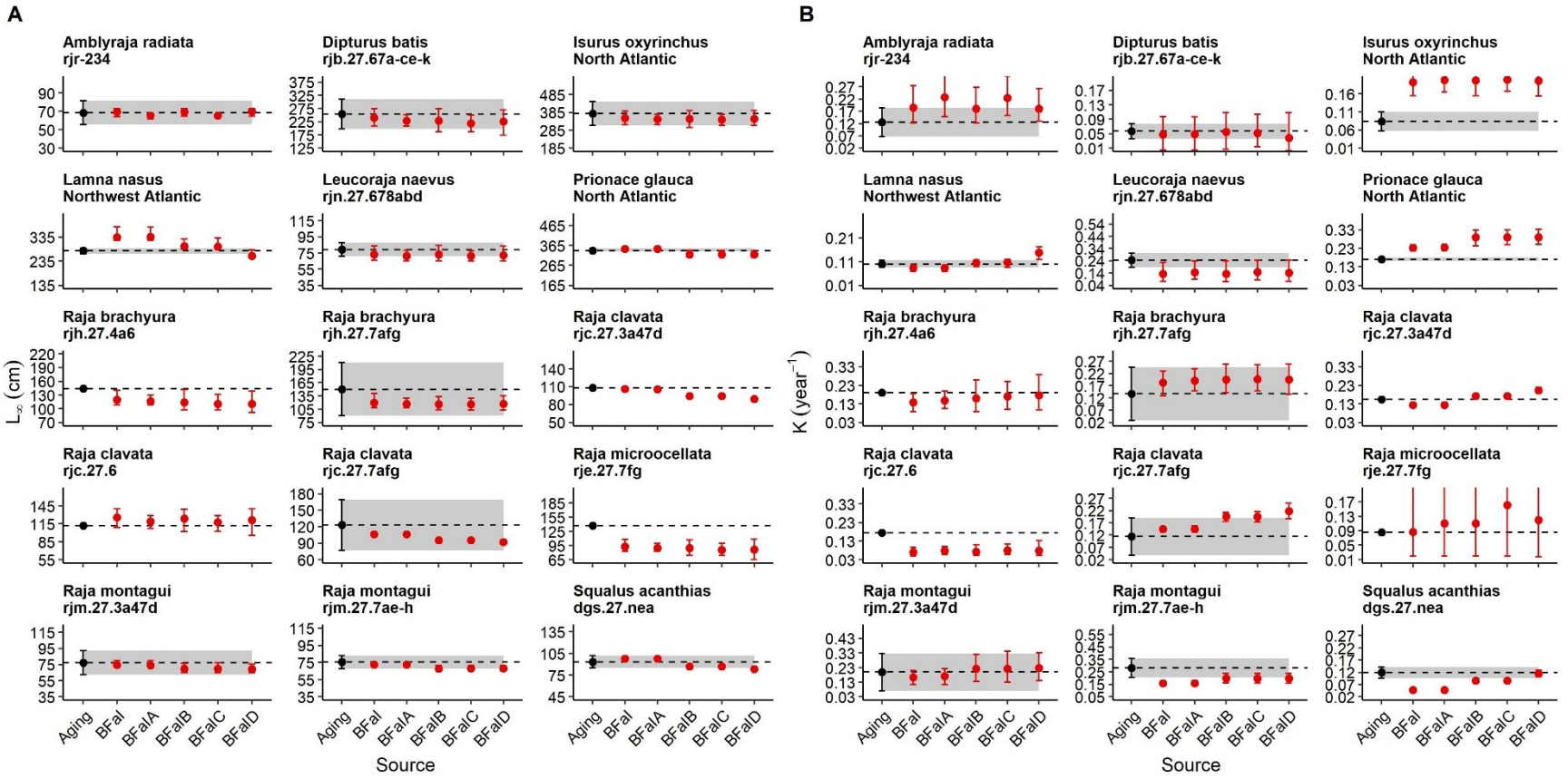

Fig. 3.7: Comparison of growth parameter estimates for 15 North Atlantic elasmobranch stocks obtained from Bayesian Fabens methods under different informative prior scenarios. A) Asymptotic maximum lengths, L_∞ (cm), and **B)** von Bertalanffy growth constant, k (year^{-1}). The dotted vertical lines indicate growth parameters obtained from literature (Aging), all of which were based on conventional length-at-age information. If available, 95% confidence intervals were extracted and are shown as error bars. All other growth parameters were estimated from a Bayesian implementation of Fabens (1965) with informative priors (BFa). The approaches differ in the defined uniform prior bounds around L_∞, obtained from observed maximum length, L_{max}, with $0.9L_{max}$ and $1.2L_{max}$ (BFaI), with $0.9L_{max}$ and $1.1L_{max}$ (BFaIA), with $0.8L_{max}$ and $1.2L_{max}$ (BFaIB), with $0.8L_{max}$ and $1.1L_{max}$ (BFaIC), and with $0.7L_{max}$ and $1.2L_{max}$ (BFaID). For the mark-recapture method the error bars show 95% credible intervals. Elasmobranch species names and stock ID's are given above each panel.

Table 3.4: Bayesian mark-recapture growth estimates. von Bertalanffy growth parameters L_∞ (cm) and k (year^{-1}) for 15 North Atlantic elasmobranch stocks estimated from mark-recapture tagging data using the overall best performing method, a Bayesian implementation of Fabens (1965) with informative priors. The BFaI approach defines uniform bounds around L_∞ at $0.9L_{max}$, the observed maximum size, and $1.2L_{max}$. The BFaIB approach defines symmetrical uniform bounds around L_∞ at $0.8L_{max}$ and $1.2L_{max}$. The 95% credible intervals are given in parenthesis.

Species	Stock ID	BFaI		BFaIB	
		L_∞	k	L_∞	k
Amblyraja radiata	rjr−234	69.67 (64.3 − 73)	0.184 (0.122 − 0.275)	69.84 (64.8 − 73.1)	0.18 (0.122 − 0.268)
Dipturus batis	rjb.27.67a−ce−k	240.41 (209 − 273.9)	0.048 (0.005 − 0.097)	228.15 (186.9 − 274)	0.055 (0.006 − 0.108)
Isurus oxyrinchus	North Atlantic	352.39 (316.2 − 393)	0.193 (0.156 − 0.236)	349.7 (300.3 − 395.9)	0.197 (0.155 − 0.262)
Lamna nasus	Northwest Atlantic	335.16 (320.3 − 377.5)	0.084 (0.068 − 0.094)	297.1 (285.1 − 326.8)	0.106 (0.089 − 0.117)
Leucoraja naevus	rjn.27.678abd	73.11 (65.9 − 84)	0.134 (0.071 − 0.228)	73.2 (65.3 − 84.3)	0.134 (0.068 − 0.238)
Prionace glauca	North Atlantic	348.69 (344.8 − 359.2)	0.233 (0.214 − 0.249)	320.65 (307.7 − 340.9)	0.289 (0.243 − 0.327)
Raja brachyura	rjh.27.4a6	119.57 (108.2 − 140.5)	0.138 (0.088 − 0.184)	114.18 (97.4 − 141.6)	0.161 (0.087 − 0.259)
Raja clavata	rjh.27.7afg	119.55 (108.9 − 140.3)	0.183 (0.128 − 0.23)	116.28 (103.5 − 133.1)	0.195 (0.141 − 0.258)
	rjc.27.3a47d	105.93 (105.8 − 106.4)	0.125 (0.12 − 0.13)	94.31 (94 − 94.9)	0.173 (0.166 − 0.179)
	rjc.27.6	125.58 (109.1 − 140.3)	0.07 (0.05 − 0.096)	124.04 (102.3 − 139.5)	0.072 (0.052 − 0.111)
	rjc.27.7afg	106.51 (105.8 − 108.4)	0.144 (0.133 − 0.155)	95.4 (94 − 98.3)	0.197 (0.175 − 0.213)
Raja microocellata	rje.27.7fg	92.74 (82.5 − 107.7)	0.087 (0.019 − 0.318)	89.53 (73.7 − 106.7)	0.11 (0.02 − 0.601)
Raja montagui	rjm.27.3a47d	74.33 (72.1 − 79.9)	0.164 (0.114 − 0.209)	69.67 (65.2 − 76.4)	0.222 (0.135 − 0.319)
	rjm.27.7ae−h	72.78 (72 − 74.6)	0.157 (0.141 − 0.173)	67.96 (65.1 − 71.7)	0.199 (0.162 − 0.236)
Squalus acanthias	dgs.27.nea	97.86 (97.7 − 98.4)	0.047 (0.045 − 0.05)	87.03 (86.8 − 87.7)	0.086 (0.08 − 0.092)

Northwest Atlantic porbeagle sharks (*Lamna nasus*) have also been subject to extensive age validation studies (Campana et al., 2002; Natanson et al., 2002) and therefore the growth estimates might be considered of higher quality. The estimates from BFaI and BFaIB were similar to the literature estimates for porbeagle and within a 10% range for BFaIB. Only the growth rate of shortfin mako (*Isurus oxyrinchus)* seemed largely overestimated by either BFaI or BFaIB. However, for shortfin mako in the eastern Pacific Ocean it has been shown that band pair deposition changes over the species life from two band pairs per year to one band pair (Wells et al., 2013; Kinney et al., 2016). Although variability in band pair deposition was deemed unlikely, it was not ruled out for North Atlantic mako sharks (Natanson et al., 2006), and variable band pair deposition changing from two to one band pair would result in faster growth rates. This could explain the discrepancy between the length-at-age growth parameters and the growth parameters from mark-recapture tagging data estimated here.

There were also discrepancies when comparing the estimated growth parameters based on the simulation analysis with those estimated from the empirical mark-recapture data. For example, the growth parameter *k* was lower for the *R. clavata* stock rjc.27.6 when compared to the length-at-age literature *k*. When comparing the scenario for this stock with the closest scenario in the simulation design, a sample size of 20 individuals, bimodal distribution of length at capture and long times at liberty, *k* would have been expected to be overestimated by BFaIB. One reason for such a discrepancy could be that the simulation design did not account for multimodal length at capture distributions. Another reason could be that measurement error or growth variability was actually larger or smaller in the empirical tagging data than in the simulation. It is also possible that the literature value itself was biased, as discussed above. This indicates the importance of including both simulation and evaluation testing in studies that estimate the performance of different methods in biological systems. Overall, caution should be taken if the median time at liberty is low (~ 0.25 years), the sample size small and large individuals absent from the mark-recapture tagging data. Yet, even in those circumstances biologically reasonable results were obtained from both, BFaI and BFaIB methods (Fig. 3.3).

The current study provides the most extensive review on estimating growth from mark-recapture tagging data in elasmobranchs to date. In the past, growth parameters estimated from tagging data have been suggested as one of the verification techniques that can be applied during growth estimation (Campana, 2001), and if growth parameters estimated from length-at-age and mark-recapture information are in agreement, it might

indeed be a good indicator that growth for this species and population is well described (Harry, 2017). Yet, given the uncertainty in elasmobranch aging (Harry, 2017; Natanson et al., 2018), full alternatives to length-at-age approaches are urgently needed. The findings here suggest that a Bayesian implementation of Fabens (1965) method, BFa, is promising, particularly because the simulation design did not favor any of the methods before-hand and no method would be expected to have zero bias in all scenarios. In addition, biologically reasonable results were obtained for all empirically investigated stocks. However, prior information should be chosen carefully. Priors on the asymptotic maximum length should be informative, yet wide enough to capture the variability of maximum lengths among individuals.

Future research should test the inclusion of individual variability via random effects. The BFa approach would need one random effect less, compared to Zhang et al (2009), because age at tagging information is not needed when modeling the length increment. Furthermore, a random effect in L_∞ only, might already be sufficient (Eveson et al., 2007; Zhang et al., 2009). Therefore, this approach could display a good trade-off between complexity and the availability and quality of the data in elasmobranchs. The current findings also question the justification of lethal sampling for elasmobranch aging studies, which has been criticized in the past (Hammerschlag & Sulikowski, 2011) and support the development of non-lethal mark-recapture alternatives. Even though mark-recapture tagging data cannot be used to estimate the length at birth, L_0, parameter, the observed length at birth is generally well known in elasmobranchs and could be used instead (Cailliet et al., 2006; Dureuil & Worm, 2015). However, the length at birth should be selected carefully. Pardo et al (2013) showed that the theoretical length at birth only overlapped with the observed length at birth in 60% of the cases when investigating 30 elasmobranch species. Due to the close correlation of the growth parameters (Pilling et al., 2002), the observed length at birth might best be used in cases where L_∞ is also biologically reasonable, for example if L_∞ is close to the average of the largest observed individuals in a population.

Given that the Bayesian implementation of Fabens (1965) method provides biologically reasonable results, it may well be used as a full alternative to obtain more accurate growth parameters in elasmobranchs. Even though the method performed well with only a moderate number of samples, larger sample sizes (e.g. more than 20 recaptures) will result in more reliable parameter estimates. It should also be noted that different growth models could fit the data better (Cailliet et al., 2006) and therefore a

multimodal approach was argued preferable in elasmobranch growth studies (Smart et al., 2016). Hence, future work may include the consideration of other growth models, such as the Gompertz model and the logistic function, rearranged for mark-recapture data (Baker et al., 1991), ideally formulated in a Bayesian framework. Furthermore, alternative approaches to a mark-recapture tagging method may still be required for some species where it is difficult to conduct tagging studies and obtain recaptures, for example this could be the case for some deep-water elasmobranchs.

Chapter 4
A unified natural mortality estimator for marine fish

4.1 Abstract

Natural mortality, *M*, is a key parameter in assessing and managing living resources, yet it is inherently difficult to estimate. Therefore, *M* is often estimated indirectly from life history traits and assumed to be invariant over size, age, and time. Indirect estimators are particularly relevant for data-poor species including many elasmobranchs (sharks, skates and rays). However, these estimators are based almost exclusively on teleost (bony fish) data and consequently their performance for elasmobranchs is unknown. For elasmobranchs it has been suggested to utilize estimators derived for marine mammals instead, due to similar demographic characteristics. However, here it is shown that the relationship between observed maximum age, t_{max}, and adult natural mortality is not significantly different for teleosts and elasmobranchs. Based on updated information and rigorous data quality control, the following estimator can be utilized to obtain adult natural mortality in both taxa: $M = e^{(1.543-1.065*log_e(t_{max}))}$. Furthermore, it is suggested that for juveniles, natural mortality at length can also be estimated from the adult *M* estimator, under the assumption that *M* is inversely proportional to body length: $M_L = e^{(1.543-1.065*log_e(t_{max}))}\frac{L_{ta}}{L}$. The reference length, L_{ta}, is the length at the age after which *M* is assumed to be constant, t_a. This reference length can be estimated from the von Bertalanffy growth function, $L_{ta} = L_\infty - (L_\infty - L_0)e^{-k(\left(\frac{2}{log_e(P)}+1\right)*t_{max})}$, where L_0 is the length at age 0, L_∞ is the asymptotic maximum length, *k* is a growth constant, and *P* is the proportion surviving to maximum age, here shown to be approximately 1 – 2%. If t_{max} is unknown it can be estimated from growth information by assuming that 99.1% of the asymptotic length is reached at maximum age. It is also shown that many of the previously published estimators overestimated *M* in elasmobranchs and teleosts, and as such a species' resilience to fishing. Thus, the updated estimator can help foster more reliable stock assessments of data-poor species.

4.2 Introduction

Globally, many threatened or exploited marine species are lacking scientific assessments, which often impedes sustainable use and conservation (Ricard et al., 2012; Dulvy et al., 2014; Simpfendorfer & Dulvy, 2017). This is also reflected by the proportion of

species listed as data deficient on the International Union for Conservation of Nature (IUCN) red list for marine taxonomic groups that are of major conservation concern. Within these groups, elasmobranchs (sharks, skates and rays) have the highest proportion of data deficiency, with almost half of all species having insufficient information to assess their status (Dulvy et al., 2014; www.iucnredlist.org). To overcome the lack of assessments for such species, data collection can be intensified (Kindsvater et al., 2018), however, this is often very costly. Another solution can be to utilize existing data and investigate if common ecological principles across taxa allow for information to be shared between data-rich and data-poor species (Kindsvater et al., 2018).

The latter has become a common practise to obtain one of the most crucial but difficult to estimate parameter of scientific assessments and the dynamics of populations, the natural mortality rate, *M* (Pauly, 1980; Hoenig et al., 2016). Natural mortality is usually expressed as an instantaneous rate in fisheries assessments and best described by an exponential decay model:

$$N_t = N_0 * e^{-((M+F)*t)}, \quad (4.1)$$

where N_t is the number of individuals at time, t (years), N_0 is the initial number of individuals, M is the instantaneous rate of natural mortality, i.e. the component of total mortality that is not caused by fishing, and F is the instantaneous rate of fishing mortality; both given in year^{-1}. The two mortality components, M and F, sum up to the total mortality rate, Z. Natural mortality in particular affects key reference parameters in fisheries, such as optimal exploitation rates, resilience and productivity (Maunder & Wong, 2011). For example, the rate of natural mortality has been widely used in fisheries management as a proxy for the fishing mortality which produces maximum sustainable yield (Gulland, 1971; Zhou et al., 2012). Given its importance in assessments and for the understanding of population dynamics, it is critical to obtain accurate estimates. Erroneous natural morality rates can highly influence predicted stock size, especially when natural mortality is overestimated (Sims, 1984; Johnson et al., 2015). Higher natural mortality rates translate to higher estimated stock sizes (Cheilari & Rätz, 2009) and reference points (Cheilari & Rätz, 2009; Maunder & Wong, 2011), and underestimate fishing mortality rates (Cheilari & Rätz, 2009). Consequently, incorrect natural mortality estimates can result in biased estimates of stock status (Clark, 1999), increasing the risk of mismanagement.

Ideally, natural mortality is estimated empirically via direct methods, i.e. within stock assessments (Lee et al., 2011), from mark-recapture tagging studies (Hoenig et al., 1998), from telemetry data (Heupel & Simpfendorfer, 2002; Knip et al., 2012b), from catch curves

used to estimate total mortality in unexploited, newly exploited or very lightly exploited populations (Simpfendorfer, 1999), or by extrapolating natural mortality from total mortality and fishing effort (Pauly, 1984). These methods are generally data-intensive and therefore often not applicable for many species within data-poor groups, such as elasmobranchs.

In an unexploited population with no fishing mortality, Hoenig (1983) showed that if the maximum age of a population is defined as the age to which a proportion, *P*, of individuals survives from N_0, equation (4.1) becomes:

$$\frac{N_{t_{max}}}{N_0} = e^{-(M*t_{max})}, \quad (4.2)$$

which can be further simplified:

$$log_e(P) = -M * t_{max} \quad (4.3)$$

and linearized:

$$log_e(M) = \beta_0 + \beta_1 * log_e(t_{max}), \quad (4.4)$$

where β_0 and β_1 are constants (the intercept and slope) to be estimated from a linear regression model. If mortality follows an exponential decay and the proportion surviving from birth to maximum age would be the same for species within different taxonomic groups, then equation (4.4) would become a universal mortality estimator for each species within these taxa. One such universal *M* estimator has been suggested by Hoenig (1983) from a linear regression model of natural mortality estimates found in literature versus observed maximum ages, for molluscs, fish and cetaceans combined. Hoenig's (1983) reasoning to use the combined estimator, instead of one estimator for each of the taxa, was to use the model with the widest range of maximum ages and the highest coefficient of determination. This estimator is an example of an indirect method, where a relationship is developed empirically across species for which natural mortality has been estimated directly (e.g. from catch curves in unexploited populations), and where one or more life history parameters were observed for the same species and same population. This relationship can then be used to obtain an estimate of natural mortality in species where *M* is unknown, but for which the respective life history parameters are known. Many of these indirect natural mortality estimators have been developed (see Kenchington (2014) for a review), and generally require information on maximum age (Hoenig, 1983; Then et al., 2015), age at maturity (Jensen, 1996) or growth (Pauly, 1980; Jensen, 1996; Then et al., 2015).

Additionally, these indirect methods typically assume natural mortality as a constant (Vetter, 1988), i.e. they are age, size and time independent methods. This is a common assumption in fisheries assessments (Vetter, 1998). Age and size independency might well be valid during the adult phase (Brodziak et al., 2011; Deroba & Schueller, 2013; Johnson

et al., 2015), due to a balance between intrinsic and extrinsic mortality factors: Extrinsic mortality decreases as individuals become larger, for example due to fewer predators, while intrinsic mortality increases, for example due to the accumulation of harmful mutations or the higher mortality risk associated with reproduction. However, the same validity cannot be assumed for juveniles. The natural mortality rate during the juvenile phase has been shown to be substantially higher than for adults in both, teleosts (bony fish) and elasmobranchs (Peterson & Wroblewski, 1984; Chen & Watanabe, 1989; Lorenzen, 1996, 2000; Gruber et al., 2001; Gislason et al., 2010; Heupel & Simpfendorfer, 2011). In response to this problem, some indirect methods relating life history to age- and size-dependent natural mortality rates have been developed (e.g. Peterson & Wroblewski, 1984; Chen & Watanabe, 1989; Lorenzen, 1996, 2000; Gislason et al., 2010). However, the empirically derived indirect natural mortality estimators that are available to date utilized almost exclusively information from teleosts, and some of these estimators have been shown to substantially overestimate natural mortality in elasmobranchs, specifically sharks (Powter & Gladstone, 2008; Kenchington, 2014). Consequently, the development of taxon-specific alternatives has been suggested (Kenchington, 2014).

In contrast to many teleosts, elasmobranchs are more generally characterised by low natural mortality rates, slow growth, late maturity, low fecundity, extended reproductive cycles and longer lifespans (Hoenig & Gruber, 1990; Camhi et al., 1998; Cortes, 2000; Dulvy et al., 2014), similar to marine mammals (Smith et al., 1998). Therefore, it has been proposed to use *M* estimators derived from cetacean (whales, dolphins and porpoises) data for elasmobranchs (Cortes, 1998; Simpfendorfer et al., 2005), and this approach has been applied to several species (Cortes, 1998; Mcauley et al., 2007; Heupel & Simpfendorfer, 2011; Hisano et al., 2011; Liu et al., 2015; Lessa et al., 2016; Yokoi et al., 2017). Yet, the lack of adequate data has prevented the detailed investigation of indirect *M* estimators' performance for elasmobranchs (Kenchington, 2014) to date. For example, Hoenig's original estimator had only two data points for elasmobranchs (Hoenig, 1982), with only one estimated using a direct method and the other wrongly specified as direct. Consequently, it is still unclear how good indirect natural mortality estimators perform for elasmobranchs and whether a taxon-specific estimator is needed.

Here, two databases for marine fish (elasmobranchs and teleosts) with direct natural mortality estimates and life history information were assembled; one database for adults and one for juveniles. Original sources containing natural mortality estimates were carefully checked for erroneous estimates before extracting the direct *M* estimates. In addition, newly

collected or previously not considered data were analyzed for elasmobranchs, combined with an extensive literature review, to obtain a greater number of direct natural mortality estimates. On this basis an empirically updated *M* estimator was developed, and it was investigated if taxon-specific *M* estimators are required for teleosts and elasmobranchs. Furthermore, the performance of previously published estimators was compared to the updated estimator. More generally, this study aimed to identify the best performing approach to estimate natural mortality for marine fish in both, juveniles and adults, to improve assessments and scientific management of information-limited species.

4.3 Materials and methods

4.3.1 Data

Given the inclusion of doubtful or erroneous information and the overall uncertainty of direct *M* estimates utilized in previously published data bases (Kenchington, 2014; Then et al., 2015), two new *M* databases were developed, one for adults and one for juveniles (Appendix D). These databases contain direct *M* estimates as well as associated life history information required by many of the indirect estimators.

Adult natural mortality data

Adult natural mortality, *M*, is here defined as a constant annual instantaneous mortality rate estimated for adult individuals.

For teleosts, direct estimates of the adult natural mortality rate, *M*, were obtained from peer-reviewed literature by carefully checking and consulting the original sources utilized in a recently published extensive database, which incorporated other previously published databases (Then et al., 2015). The following selection criteria were applied: (1) Only *M* values derived from direct methods in the original source and from marine species where all data, or the majority of data, used to estimate *M* came from adults were considered; Furthermore estimates were excluded that: (2) were unreliable (e.g. total mortality was smaller than *M*; *M* was guessed; *M* from mark-recapture methods when methods were not considering immigration and emigration, tag loss, reporting rate or tagging mortality); (3) were considered unreliable by the authors in the original study; (4) were based on estimates of total mortality, *Z*, and assumed $Z = M$, but the level of exploitation was unknown or the stock was exploited; and/or (5) had no estimate of corresponding maximum age available. If aware, revised *M* estimates based on more and/or updated data were used.

All references that were excluded from the present study are provided with reasoning (Appendix D). Sex-specific natural mortality estimates were preferred over combined sex estimates, given that the other life history parameters were also available for each sex. In the absence of sex-specific information the average *M* across both sexes was taken. If several direct methods were applied, or the study gave several direct *M* estimates, and the authors did not specifically exclude the validity of a method or estimate, the average across methods or estimates was taken. The average was also taken if a study gave several *M* estimates from an unexploited population from different areas but for the same population or stock.

For elasmobranchs, an extensive literature search including grey literature (such as governmental reports) was additionally conducted, due to the scarcity of direct *M* estimates in previous databases. Direct *M* estimates for elasmobranchs were also obtained from newly collected information and appropriate information previously not considered to estimate natural mortality. Published estimates for which updated information was available were also re-analyzed. When sample size was sufficient, *M* was estimated for males and females independently. One extreme outlying value of elasmobranch *M* was excluded from the analysis (Fig. C1).

Juvenile natural mortality data

Juvenile natural mortality is here defined as an annual instantaneous mortality rate estimated at a certain length, age or weight representative for a juvenile individual. Direct estimates of juvenile *M* were obtained from an extensive literature search applying the same criteria as described above. In addition, only direct rates from wild populations at a juvenile length, weight or age and estimated per one year were included. Juvenile *M* estimates that were overall lower than adult *M* estimates were not considered, because all tested methods assume a declining *M* with age, length or weight. Generally, the underlying samples consisted of juvenile individuals with various length or age classes and therefore juvenile *M* refers here to the instantaneous natural mortality rate at a mean length. If not provided, the mean length at juvenile *M* was calculated as the mean between the minimum and maximum length in the sample. If an age range was given instead then length was calculated using the von Bertalanffy growth function (von Bertalanffy, 1938),

$$L_t = L_\infty - (L_\infty - L_0)e^{-kt} = L_\infty * (1 - e^{-k(t-t_0)}), \quad (4.5)$$

where L_t is the length-at-age t, L_0 is the length at age 0, L_∞ is the asymptotic length, k is a curve parameter describing how fast L_∞ is approached and t_0 is the theoretical age at zero

length. The length at age 0 can be obtained from t_0,

$$L_0 = L_\infty * (1 - e^{-k*t_0}). \quad (4.6)$$

All length measurements are in cm total length and all ages in years.

Life history data

Life history information on observed maximum age, von Bertalanffy growth parameters and age at maturity, t_m, were extracted from the same study, if possible, or obtained from a literature search. For the latter case, only information from the same population or stock as the *M* estimate were considered, and similar time periods and location were preferred. If age at maturity was not available, but length at maturity, L_m, together with growth information was, then age at maturity was calculated using the rearranged von Bertalanffy growth function,

$$t = \frac{log_e \frac{(L_\infty - L_0)}{(L_\infty - L_t)}}{k} = -log_e \left(1 - \frac{L_t}{L_\infty}\right)/k + t_0, \quad (4.7)$$

with $t = t_m$ and $L_t = L_m$. Likewise, if length at maturity was not available, but age at maturity and growth were, then length at maturity was estimated using the von Bertalanffy growth function, equation (4.5). Length at birth was assumed to be 0 if t_0 was not provided. The mean environmental temperature inhabited by the species, *T* (℃), was taken from Then et al (2015) or FishBase (Froese & Pauly, 2018). Weight, *W*, in gram was calculated from the corresponding length class, *L*, using length-weight relationships (Froese, 2006). If the direct *M* estimate was only available for combined sexes, certain areas or time periods then the average of the life history parameters was taken across the corresponding sexes, areas or time periods, if possible. All life history parameters were standardized to the same units. Rates are given in year^{-1}, ages are given in years, and length is given in cm total length throughout. When total length was not given it was estimated from length-length relationships.

The references from which the adult and juvenile direct *M* estimates and the life history information were taken are provided in Appendix D.

4.3.2 Adult natural mortality estimator

In total, four new indirect adult natural mortality estimators were developed:

1) Given the linear relationship between maximum age and natural mortality, equation (4.4), a linear regression analysis of direct *M* estimates versus observed t_{max} from the adult *M* database was developed to estimate the parameters β_0 and β_1. This estimator

is hereafter referred to as *DureuilTmax*. The response variable natural mortality, *M*, and the covariate maximum age, t_{max}, were $\log_e$ transformed.

2) The *DureuilTmax* estimator requires an input of observed maximum age. In the absence of an observed value, maximum age might be estimated from the von Bertalanffy growth function:

$$\hat{t}_{max} = \frac{1}{k} * log_e((L_\infty - L_0)/((1 - X) * L_\infty), \quad (4.8)$$

where *X* is the proportion of the asymptotic maximum length, L_∞, reached at maximum age. Commonly, *X* is assumed to be 0.95 (Taylor, 1958; Ricker, 1979) and the estimated maximum age with *X* = 0.95 was subsequently used as input in the *DureuilTmax* estimator. This estimator is hereafter referred to as *DureuilLinf95*.

3) The proportion of the asymptotic maximum length, L_∞, reached at maximum age was also calculated using all available information on growth and observed t_{max} in the adult *M* database via:

$$X = (L_\infty - (L_\infty - L_0) * e^{(-k*t_{max})})/L_\infty. \quad (4.9)$$

The estimated maximum age with *X* as the median across all species was then used as input in the *DureuilTmax* estimator. This estimator is hereafter referred to as *DureuilLinf*.

4) The adult natural mortality rate can also be estimated from the proportion of the cohort that remains alive at maximum age, equation (4.3). This proportion was estimated as the median across all in the adult *M* database. This estimator is referred to as *DureuilP*.

4.3.3 Juvenile natural mortality estimator

A new indirect juvenile natural mortality estimator was developed based on Lorenzen (2000), who suggested that *M* scales inversely proportional with body length:

$$M_L = M_r \frac{L_r}{L}. \quad (4.10)$$

This estimator needs a constant natural mortality rate, M_r, at a specific reference length, L_r, as input. Here the predicted constant adult natural mortality rate from the *DureuilTmax* estimator was used for M_r. The asymptotic maximum length, L_∞ (Beyer et al., 1999), and the length at maturity, L_m (Brodziak et al., 2011), have both been proposed as reference lengths, but here a new reference length is suggested in addition; the length at the age after which *M* can be considered constant, L_{ta}. This length was derived as follows: The adult constant natural mortality rate is related to the average life expectancy, *E*, in the form:

$$M = \frac{1}{E}. \quad (4.11)$$

Now *E* can be defined as the average life expectancy after the age at which *M* is assumed

constant t_a:

$$E = \frac{t_{max} - t_a}{2}. \quad (4.12)$$

It can be further defined that x is the proportion of t_{max} at which M is assumed constant:

$$E = \frac{t_{max} - (x * t_{max})}{2}, \quad (4.13)$$

and therefore:

$$M = \frac{2}{t_{max} - (x * t_{max})} = \frac{2}{t_{max} * (1-x)} = \frac{\frac{2}{(1-x)}}{t_{max}}. \quad (4.14)$$

This implies that M can be estimated from a constant divided by maximum age, which is equivalent to the definition in equation (4.3):

$$M = \frac{\frac{2}{(1-x)}}{t_{max}} = \frac{-log_e(P)}{t_{max}}. \quad (4.15)$$

From this it follows that:

$$\frac{2}{(1-x)} = -log_e(P), \quad (4.16)$$

which can be solved for x:

$$x = \frac{2}{log_e(P)} + 1, \quad (4.17)$$

and hence:

$$t_a = \left(\frac{2}{log_e(P)} + 1\right) * t_{max}. \quad (4.18)$$

The same empirically derived proportion surviving to maximum age, P, as in *DureuilP* was used here, i.e. the median across all calculated proportions based on the adult M database. Finally, L_{ta} was obtained from t_a via the von Bertalanffy growth function. This estimator, with L_{ta} as a reference length, is referred to as *LorLta*.

4.3.4 Evaluation of estimators

First, the linear regression based indirect adult M estimator *DureuilTmax* was evaluated by validating linear regression assumptions using various methods. Fitted values were plotted against the residuals to check for homogeneity of variances. Then et al (2015) implied that the independence of observations assumption of linear regression might be violated, when M estimates for the same species but different locations, or for male and female, are utilized separately. Therefore, the residuals were tested on auto-correlation graphically via the auto-correlation-function (acf) plot in *R* (R Core Team, 2017). Furthermore, a sensitivity analysis was performed to test the validity of the *DureuilTmax* estimator to use ordinary linear regression, and to use data on teleosts and elasmobranchs combined. First, it was tested if a combined taxa (elasmobranch and teleost) estimator is

valid by applying three approaches: 1) Testing if a linear regression with *taxa* (elasmobranch or teleost) as an additional covariate is an improved model compared to *DureuilTmax*; 2) Comparing the *DureuilTmax* parameters with the parameters from linear regression models for each taxa; and 3) Comparing the *DureuilTmax* parameters with the parameters from a linear regression model, but utilizing only information from species with a maximum age ≥ 3 years, because elasmobranchs attain higher maximum ages than teleosts (Nielsen et al., 2016). A maximum age of 3 years was selected because 3 years is among the lowest maximum ages reported in elasmobranchs (Cailliet & Goldman, 2004). Second, it was tested if the use of ordinary linear regression is valid by comparing the *DureuilTmax* parameters with the parameters obtained from various other linear regression techniques: 1) Robust linear regression to investigate if a few observations have a high influence, using the R package MASS (Venables & Ripley, 2002); 2) Model II major axis regression, because the covariate maximum age is also measured with error, using the lmodel2 package (Legendre, 2018); 3) Random intercept and random intercept and slope models with taxonomic order as random effect, to further investigate dependency among observations, i.e. to estimate model parameters after accounting for potential dependency among taxonomic orders, using the *lme4* package (Bates et al., 2015). Furthermore, to evaluate indirect *M* estimates from *DureuilTmax* against *M* estimates from direct methods, a 10-fold cross validation technique was applied to obtain a prediction error (Then et al., 2015; Hoenig et al., 2016) using the *DAAG* package (Maindonald & Braun, 2015). Here, 10 data points were randomly removed, and the remaining data points were used to re-fit the model to predict the 10 removed observations, providing an estimate on how close the results of *DureuilTmax* are compared to direct methods.

The performance of all newly developed indirect *M* estimators (*DureuilTmax*, *DureuilP*, *DureuilLinf95* and *DureuilLinf*, *LorLta*) were compared against previously published indirect *M* estimators. This was done by evaluating the accuracy and precision of the indirect estimators in predicting the direct *M* estimates in the adult or juvenile *M* database, respectively. For adult *M*, 10 more commonly applied indirect adult *M* estimators were used for comparison (Table 4.1).

For juvenile *M*, comparisons were done using seven more commonly applied age, size or weight dependent indirect *M* estimators (Table 4.2). For estimators using weight instead of length the mean weight in gram was calculated from mean length using length-weight relationships (Froese, 2006). For estimators using age instead of length, mean age was obtained from mean length using the von Bertalanffy growth function, equation (4.7).

To evaluate performance of the different estimators the recommendations of Walther & Moore (2005) were followed, and scaled measures were used. First, the relative error in percent was calculated,

$$Relative\ error = \frac{\widehat{M_i} - M}{M} * 100, \quad (4.19)$$

where *M* is the known parameter, i.e. the *M* value obtained from the direct methods in the *M* databases, and $\widehat{M}$ is the corresponding *i*th estimate from each of the investigated estimators. Boxplots were used to show the variation in the relative error and the median for each estimator. In order to evaluate the performance based on accuracy and precision, two measures were calculated. The scaled median absolute deviation SMAD:

$$SMAD = median(\left|\frac{\widehat{M_i} - M}{M}\right|) \quad (4.20)$$

and the scaled mean absolute error SMAE:

$$SMAE = mean(\left|\frac{\widehat{M_i} - M}{M}\right|). \quad (4.21)$$

Smaller values for the relative error, SMAD and SMAE indicated better performance.

Each estimator was tested on the maximum number of observations, whether all life history information was complete for a particular observation, or not. This can introduce bias and prevent a fair comparison in which outlier species (or stocks) or non-randomness would not affect all estimators the same (Hoenig et al., 2016). Therefore, all estimators were also tested on a common database, where only direct *M* estimates were included for which all other life history information required by any of the estimators were also available. Furthermore, the residuals (direct *M* from databases minus predicted *M* from estimator) were plotted against the predicted *M* from the indirect estimators, to identify estimators with better behaving error structure (Then et al., 2015).

Table 4.1: Indirect estimators of adult natural mortality. Natural mortality, M (year^{-1}), estimators based on maximum age, t_{max} (years), age at maturity, t_m (years), von Bertalanffy growth parameters, k (year^{-1}) and L_∞ (cm), and average water temperature, T (°C), are shown. All estimators are empirically derived and based on direct M estimates, except Jensen's (1996) estimators, which are based on life history theory and Cadima's (2003) estimator which arbitrarily assumes that 5% of individuals survive to maximum age. For Hoenig's t_{max} estimators it is indicated if the estimator is Hoenig's taxa combined (mollusks, fish and cetaceans), cetaceans or fish only estimator. The parameters β_0 and β_1 were obtained from linear regression analysis, the parameter P from the median survival to t_{max} and the parameter X from the median percentage of L_∞ at t_{max}, with information taken from the updated M database.

Name	Formula	Reference
DureuilTmax	$M = e^{(\beta_0+\beta_1*log_e(t_{max}))}$	This study
HoenigAll	$M = e^{(1.44-0.982*log_e(t_{max}))}$	Hoenig (1983)
HoenigCetacean	$M = e^{(0.941-0.873*log_e(t_{max}))}$	Hoenig (1983)
HoenigFish	$M = e^{(1.46-1.01*log_e(t_{max}))}$	Hoenig (1983)
ThenTmax	$M = 4.899{t_{max}}^{-0.916}$	Then et al (2015)
DureuilP	$M = \frac{-log_e(P)}{t_{max}}$	This study
HewittHoenigP	$M = \frac{-log_e(0.015)}{t_{max}}$	Hewitt and Hoenig (2005)
P0.05	$M = \frac{-log_e(0.05)}{t_{max}}$	Cadima (2003)
JensenTm	$M = \frac{1.65}{t_m}$	Jensen (1996)
JensenGrowth	$M = 1.5k$	Jensen (1996)
ThenGrowth	$M = 4.118k^{0.73}{L_\infty}^{-0.33}$	Then et al (2015)
PaulyGrowth	$M = 10^{(-0.007-0.279*log_{10}(L_\infty)+0.654*log_{10}(k)+0.463*log_{10}(T))}$	Pauly (1980)
DureuilLinf95	$M = e^{(\beta_0+\beta_1*log_e\left(\frac{1}{k}*log_e(\frac{(L_\infty-L_0)}{((1-0.95)*L_\infty)})\right))}$	This study
DureuilLinf	$M = e^{(\beta_0+\beta_1*log_e\left(\frac{1}{k}*log_e(\frac{(L_\infty-L_0)}{((1-X)*L_\infty)})\right))}$	This study

Table 4.2: Indirect estimators of juvenile natural mortality. Natural mortality, M (year^{-1}), at length, age or weight estimators based on von Bertalanffy growth parameters, k (year^{-1}) and L_∞ (cm), weight, W (grams), length, L (cm), age, t (years), and age at which senescence (the increase of mortality at old ages) commences, t_s (years), are shown. The method of Lorenzen (2000), *LorL*, requires a constant reference natural mortality rate, M_r, at a reference length. Here, adult M estimated from *DureuilTmax* was utilized as M_r and three reference lengths were tested: the length after which M is assumed constant, L_{ta}, the length at maturity, L_m (Brodziak et al., 2011) and L_∞ (Beyer et al., 1999). The method of Peterson & Wroblewski (1984), *PW*, was derived from dry weights in grams and dry weight was assumed to be 20% of wet weight (Cortes, 2002).

Name	Formula	Reference
LorLta	$M_L = M_r \frac{L_{ta}}{L}$	This study
LorLm	$M_L = M_r \frac{L_m}{L}$	Lorenzen (2000); Brodziak et al (2011)
LorLmax	$M_L = M_r \frac{L_\infty}{L}$	Lorenzen (2000); Beyer et al (1999)
LorW	$M_W = 3W^{-0.288}$	Lorenzen (1996)
PW	$M_W = 1.92(W - (0.2 * W))^{-0.25}$	Peterson & Wroblewski (1984); Cortés (2002)
CW	$M_t = \begin{cases} \frac{k}{1 - e^{-k(t-t_0)}} & t \le t_s \\ \frac{k}{a_0 + a_1(t - t_s) + a_2(t - t_s)^2} & t \ge t_s \end{cases}$ $a_0 = 1 - e^{-k(t_s - t_0)}$ $a_1 = k e^{-k(t_s - t_0)}$ $a_2 = -\frac{1}{2} k^2 e^{-k(t_s - t_0)}$ $t_s = -\frac{1}{k} LN\left\|1 - e^{k * t_0}\right\| + t_0$	Chen & Watanabe (1989)
Cha	$M_L = (\frac{L}{L_\infty})^{-1.5} * k$	Charnov et al (2013)
Gis	$M_L = e^{(0.55 - 1.61 * log_e(L) + 1.44 * log_e(L_\infty) + log_e(k))}$	Gislason et al (2010)

4.4 Results

4.4.1 Adult natural mortality

In total, 120 direct adult natural mortality estimates for marine fish from 70 different sources were utilized for the adult *M* database. Observations from another 70 sources were not considered due to erroneous or highly unreliable estimates (Appendix D). Direct *M* observations came from 105 teleosts and 15 elasmobranchs from 15 taxonomic orders within 39 families, comprising 77 and 12 different teleost and elasmobranch species, respectively. The direct natural mortality observations were estimated primarily from catch curves, i.e. applying a linear regression to the $\log_e$ transformed equation (4.1) in unexploited or slightly exploited populations, so that *M* is approximately *Z*. Direct *M* observations ranged from 7.92 year^{-1} to 0.014 year^{-1}. Maximum ages ranged from 0.73 years to 131.5 years in teleosts and 5.7 years to 73 years in elasmobranchs. The asymptotic maximum lengths ranged from 4.72 cm to 280 cm and the von Bertalanffy growth coefficient *k* ranged from 2.555 year^{-1} to 0.034 year^{-1}. Of the 120 direct natural mortality and maximum age observations, 118 observations had also corresponding von Bertalanffy growth parameters available, and 86 observations had also age at maturity data available.

Based on the updated adult *M* database the *DureuilTmax* estimator is:

$$M = e^{(1.543 - 1.065 * log_e(t_{max}))}. \quad (4.22)$$

This estimator had a 10-fold cross validation prediction error of 0.13. The linear relationship between natural mortality ($\log_e$ yr^{-1}) and maximum age ($\log_e$ yr) was highly significant ($p < 2.2*10^{-16}$; Table 4.3) with a coefficient of variation, R^2, of 0.92. The *DureuilTmax* estimator showed a good fit for both elasmobranchs and teleosts (Fig. 4.1) and there was no significant difference between taxa nor did the model improve with taxa as an additional covariate (p = 0.49; Table 4.3).

Furthermore, the linear regression for each taxon individually, and the linear regression based on comparable maximum ages only, showed similar parameter estimates when compared to *DureuilTmax*, as well as overlapping confidence intervals (Table 4.4). Likewise, the parameter estimates were very similar across various linear regression techniques and all were within the confidence intervals of *DureuilTmax* (Table 4.4).

The variances of the *DureuilTmax* estimator were homogeneous (Fig. C2), the residuals had an approximate normal distribution (Fig. C3; Shapiro-Wilk p = 0.057; Kolmogorov-Smirnov $p < 1*10^{-6}$) and there was no residual auto-correlation (Fig. C4). This suggests that the use of the ordinary linear regression model was appropriate.

In the absence of an observed value for maximum age, maximum age might be estimated using the von Bertalanffy growth function. The percentage of the asymptotic maximum length reached at maximum age *X* was set at 0.95 for the *DureuilLinf95* estimator and estimated from the life history information in the adult *M* database for the *DureuilLinf* estimator. The estimated median *X* was 0.991 and *X* was not significantly different between elasmobranchs and teleosts (Fig. 4.2A; Wilcoxon $p = 0.83$). Hence, the *DureuilLinf* estimator is given by:

$$M = e^{(1.543 - 1.065 * log_e\left(\frac{1}{k} * log_e\left(\frac{(L_\infty - L_0)}{((1-0.991)*L_\infty)}\right)\right))}. \quad (4.23)$$

The proportion of individuals surviving from birth to maximum age was also not significantly different between elasmobranchs and teleosts (Fig. 4.2B; Wilcoxon $p = 0.15$) and the median percentage of individuals remaining alive at maximum age is 1.827%. Therefore, the *DureuilP* estimator is given by:

$$M = \frac{-log_e(0.01827)}{t_{max}}. \quad (4.24)$$

The *DureuilTmax* estimator performed best compared to all other tested indirect methods, across elasmobranchs and teleosts (Fig. 4.3A; Table 4.5), and among each taxon separately (Fig. C5; Table C1). The previously established indirect adult *M* estimators were generally overestimating natural mortality, with average relative errors of up to 100%. From the published indirect adult *M* estimators, the *HoenigFish* estimator performed best (Fig. 4.3A; Table 4.5). Furthermore, the new *DureuilTmax*, *DureuilP* and *DureuilLinf* as well as all estimators from Hoenig (1983) and all estimators based on the proportion surviving to maximum age, *P*, had relative errors that were generally smaller than 50% across all taxonomic orders (Fig. C6), with the *DureuilTmax* estimator performing best (Figs. C7; C8; Table C2).

To test all estimators on a common database, 34 data points were excluded, because these observations were lacking at least one parameter required by any of the adult *M* estimators. Based on the remaining 86 observations, *DureuilTmax* also performed best (Fig. C9; Table C3). When selecting 10 observations randomly from these 86 observations, applying all estimators, calculating the relative error, SMAE and SMAD, and repeating these steps 1000 times, a similar pattern emerged (Fig. C10). The *DureuilTmax* estimator also showed the best residual behavior (Fig. C11).

Table 4.3: Relationship of natural mortality and maximum age between elasmobranchs and teleosts. Shown are the estimated coefficients from linear regression, the 95% confidence intervals and the *p*-values for two models predicting the adult natural mortality rate, M ($\log_e yr^{-1}$). The first model is the *DureuilTmax* estimator with only maximum age t_{max} ($\log_e$ yr) as covariate (bold). The second model has an additional covariate taxa (elasmobranch or teleost). Both models had a coefficient of variation, R^2, of 0.92. The model with only t_{max} as covariate had a slightly lower Akaike information criterion (AIC) of 100 compared to 102 for the model with t_{max} and taxa as covariates.

Model		β	95% confidence intervals	*p*-value
$\log_e(M) = \beta_0 + \beta_1 * \log_e(t_{max})$	**Intercept**	**1.543**	**1.38 – 1.71**	**$< 2.2*10^{-16}$**
	$\log_e t_{max}$	**-1.065**	**-1.12 – -1.01**	**$< 2.2*10^{-16}$**
$\log_e(M) = \beta_0 + \beta_1 * \log_e(t_{max}) + \beta_2 * Taxa$	Intercept	1.477	1.23 – 1.73	$< 2.2*10^{-16}$
	$\log_e t_{max}$	-1.063	-1.12 – -1.01	$< 2.2*10^{-16}$
	Taxa	0.070	-0.13 – 0.27	0.49

Table 4.4: Sensitivity analysis. Shown are the results of different linear regression models used to evaluate if the relationship of natural mortality, M ($\log_e$ yr^{-1}), and maximum age, t_{max} ($\log_e$ yr), is: a) different for elasmobranchs and teleosts (linear regression for each taxa individually, linear regression based on comparable maximum ages (only observations with $t_{max} \geq 3$); b) influenced by a few values (robust regression); c) influenced by errors in maximum age (model II major axis regression); d) dependent on taxonomic order (random intercept and slope models). Maximum age was significant ($p < 2.2*10^{-16}$) for each model. The *DureuilTmax* estimator (base case) with elasmobranchs and teleosts combined is shown in bold.

Method	Model	95% confidence intervals	
		Intercept	Slope
Teleosts	$\log_e(M) = 1.549-1.064*\log_e(t_{max})$	1.40 − 1.70	-1.12 − -1.00
Elasmobranch	$\log_e(M) = 1.419-1.043*\log_e(t_{max})$	1.50 − 1.84	-1.23 − -0.86
Comparable t_{max}	$\log_e(M) = 1.548-1.066*\log_e(t_{max})$	1.29 − 1.81	-1.15 − -0.98
robust regression	$\log_e(M) = 1.549-1.062*\log_e(t_{max})$	1.38 − 1.72	-1.11 − -1.01
Model II regression	$\log_e(M) = 1.673-1.114*\log_e(t_{max})$	0.87 − 1.97	-1.18 − -1.06
Random intercept	$\log_e(M) = 1.627-1.075*\log_e(t_{max})$	1.40 − 1.85	-1.13 − -1.02
Random intercept and slope	$\log_e(M) = 1.533-1.038*\log_e(t_{max})$	1.02 − 1.97	-1.20 − -0.85
DureuilTmax	**$\log_e(M) = 1.543-1.065*\log_e(t_{max})$**	**1.38 − 1.71**	**-1.12 − -1.01**

Table 4.5: Performance of indirect natural mortality estimators. Shown is the performance of each tested estimator to predict the direct *M* estimate from either the adult or the juvenile database. Performance measures are given as the median relative error (%), the scaled mean absolute error (SMAE) and the scaled median absolute deviation (SMAD) error. The lowest value (best performance) is shown in bold.

Database	Estimator	Relative error	SMAE	SMAD
Adults	*DureuilTmax*	-0.60	**0.288**	**0.193**
	HoenigAll	10.18	0.354	0.221
	HoenigCetaceans	-10.87	0.342	0.252
	HoenigFish	4.73	0.319	0.206
	ThenTmax	49.14	0.721	0.491
	DureuilP	**0.00**	0.305	0.207
	HewittHoenigP	4.93	0.323	0.207
	P0.05	-25.15	0.326	0.312
	JensenTm	65.10	1.323	0.651
	JensenGrowth	65.20	2.458	0.660
	ThenGrowth	80.93	2.665	0.809
	PaulyGrowth	98.32	3.103	0.983
	DureuilLinf95	71.60	2.443	0.716
	DureuilLinf	-0.43	1.420	0.599
Juveniles	*LorLta*	**-0.38**	0.451	**0.212**
	LorLm	-10.40	**0.375**	0.338
	LorLmax	49.23	0.850	0.527
	LorW	-34.62	0.569	0.507
	PW	-44.95	0.513	0.527
	CW	-20.27	0.542	0.368
	Cha	71.40	1.112	0.714
	Gis	31.64	0.848	0.316

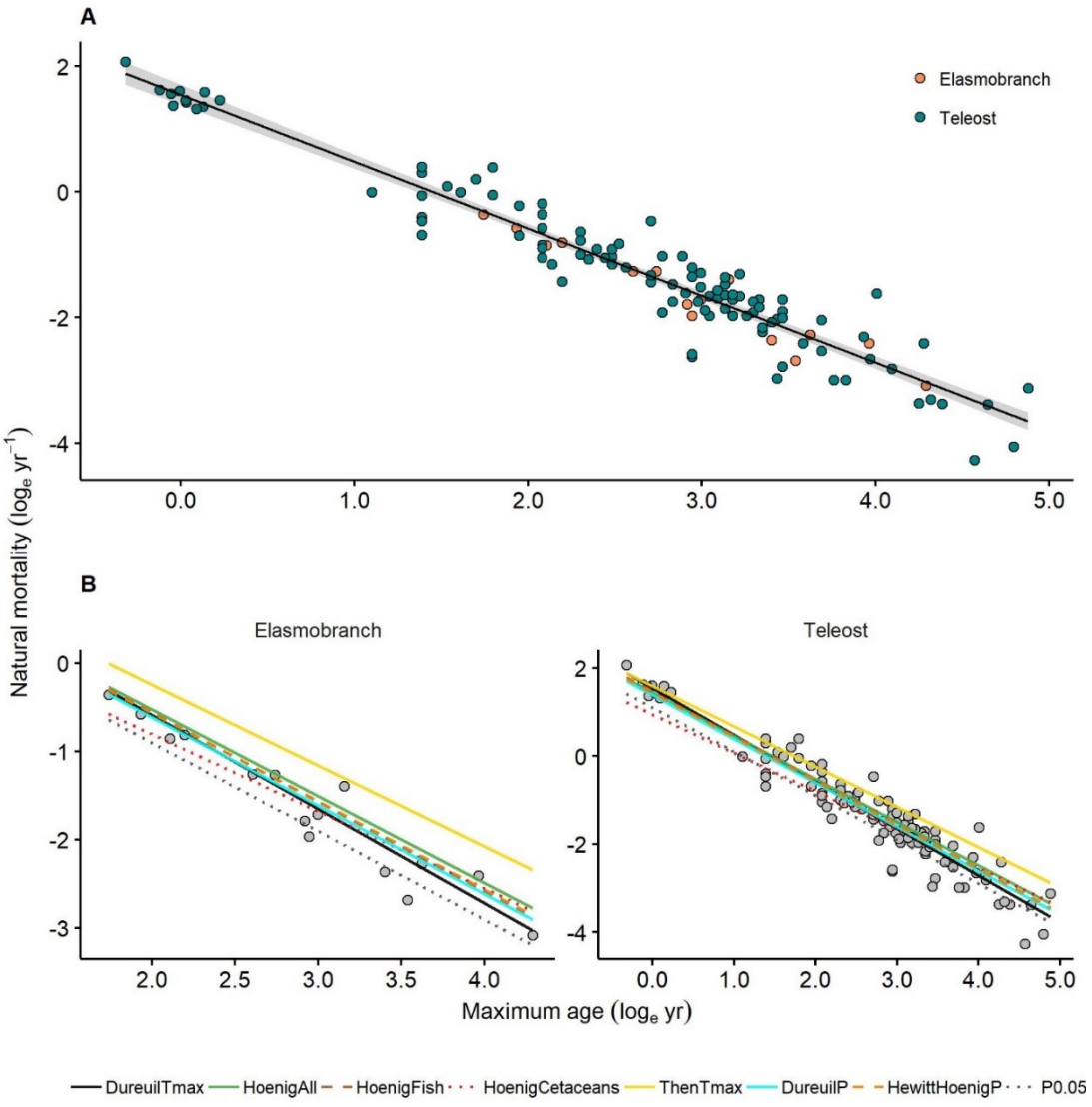

Fig. 4.1: Relationships of natural mortality and maximum age in marine fish. A) Predicted relationship (black line) of natural mortality (log_e yr^{-1}) and maximum age (log_e yr) for teleosts and elasmobranchs combined. The 95% confidence intervals are given by the shaded area. The black line represents the *DureuilTmax* estimator. **B)** Shown is the fit of predicted *M* estimates from various maximum age based indirect estimators (coloured lines) compared to the direct *M* estimates from the adult *M* database (grey dots) for elasmobranchs (left) and teleosts (right) independently. See table 4.1 for details on the different indirect estimators.

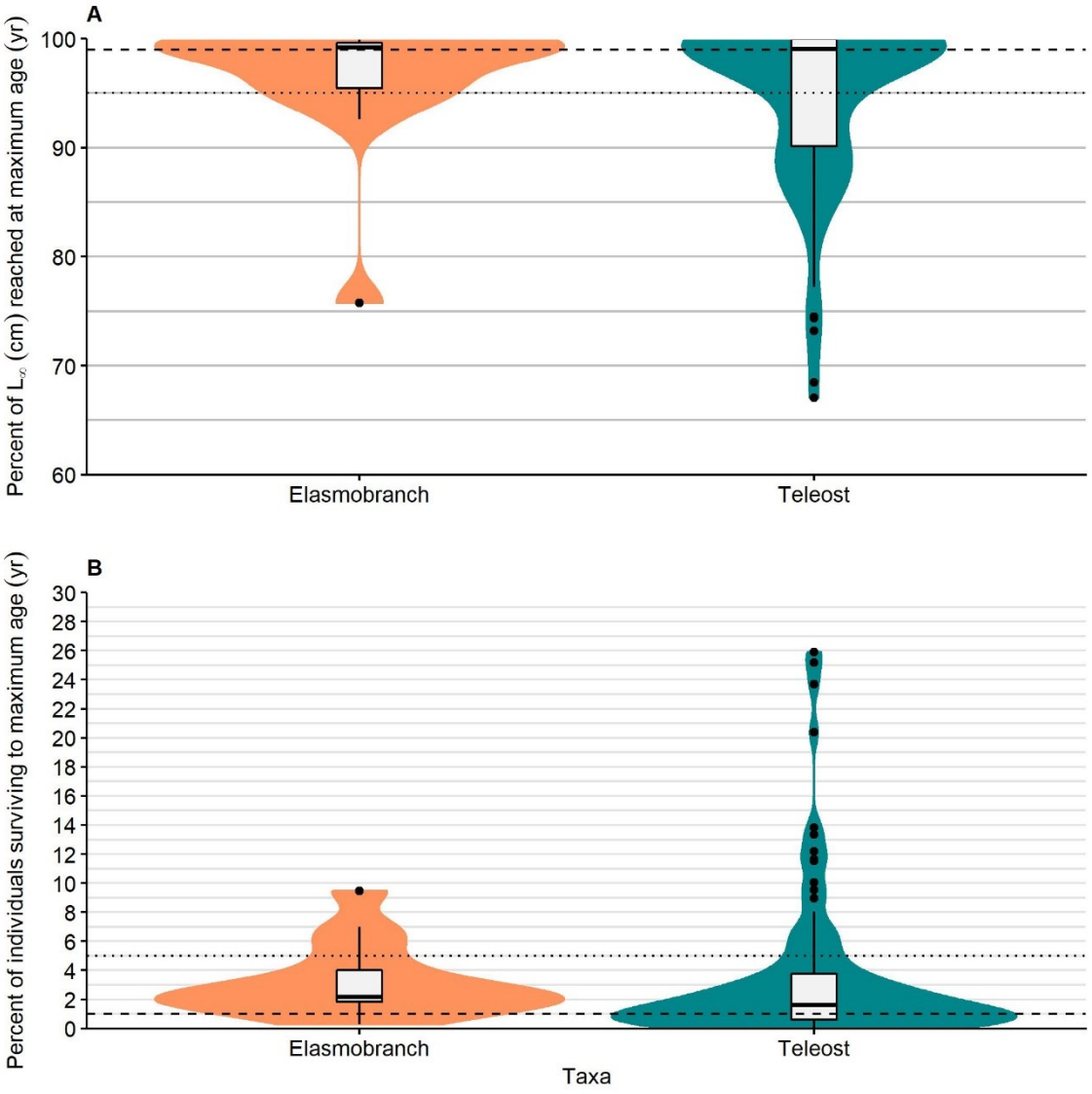

Fig. 4.2: Percentage of the asymptotic maximum length and individual survivors at maximum age. A) Percentage of the asymptotic maximum length, L_∞ (cm), reached at maximum age (years). The dashed line indicates 99% of L_∞ reached at maximum age and the dotted line indicates 95%. The medians were not significantly different for elasmobranchs and teleosts (Wilcox *p*-value = 0.8) and the combined median is 99.1%. **B)** Percentage of individuals surviving from birth to maximum age. The dashed line indicates 1% of individuals surviving from birth to maximum age and the dotted line indicates 5% survivors. The medians were not significantly different for elasmobranchs and teleosts (Wilcox *p*-value = 0.15) and the combined median is 1.83%. Kernel density estimates are shown for A) and B) around the box-whisker plots.

All estimators based on maximum age performed better than estimators based on growth, but the *DureuilLinf* estimator performed better than any other estimator that can be applied in the absence of observed maximum age.

4.4.2 Juvenile natural mortality

In total, 18 observations on directly estimated juvenile natural mortality rates were obtained for the juvenile *M* database (16 teleosts and 2 elasmobranchs). Observations included 5 taxonomic orders of 7 families, comprising of 8 different teleost and 2 different elasmobranch species. The juvenile direct natural mortality rates were estimated primarily from tagging data. Direct *M* observations ranged from 3.285 year^{-1} to 0.13 year^{-1}. The mean total length at the direct juvenile *M* ranged from 2.8 cm to 129.06 cm, the asymptotic maximum length ranged from 18.5 cm to 399 cm and length at maturity ranged from 11.45 cm to 232.5 cm. The von Bertalanffy growth coefficient, *k*, ranged from 0.43 year^{-1} to 0.057 year^{-1}. Observed maximum ages of species in the juvenile *M* database ranged from 4.5 years to 30 years. All 18 observations had corresponding life history information available required by any of the here tested indirect juvenile *M* estimators.

Based on the juvenile *M* database, the overall best performing estimator was *LorLta*, $M_L = M_r \frac{L_{ta}}{L}$, with M_r derived from *DureuilTmax* and the length at the age after which *M* is assumed constant, L_{ta}, as reference length (Fig. 4.3B; Table 4.5). The Lorenzen (2000) method with M_r derived from *DureuilTmax* but length at maturity, L_m, as reference length, *LorLm*, also performed well (Fig. 4.3B, Table 4.5; Fig. C12; Table C4). However, the *LorLta* estimator had better residual behaviour (Fig. C13). The weight-based estimators all tended to underestimate *M*, while the growth-based estimators tended to overestimate *M* (Fig. 4.3B, Table 4.5). The reference length, L_{ta}, was obtained from the age after which *M* is constant, t_a, using the von Bertalanffy growth function. Given that the proportion surviving to maximum age, *P*, is 0.018, then *x* is 0.499 and the age after which *M* is constant can be calculated from maximum age, $t_a = 0.499 * t_{max}$.

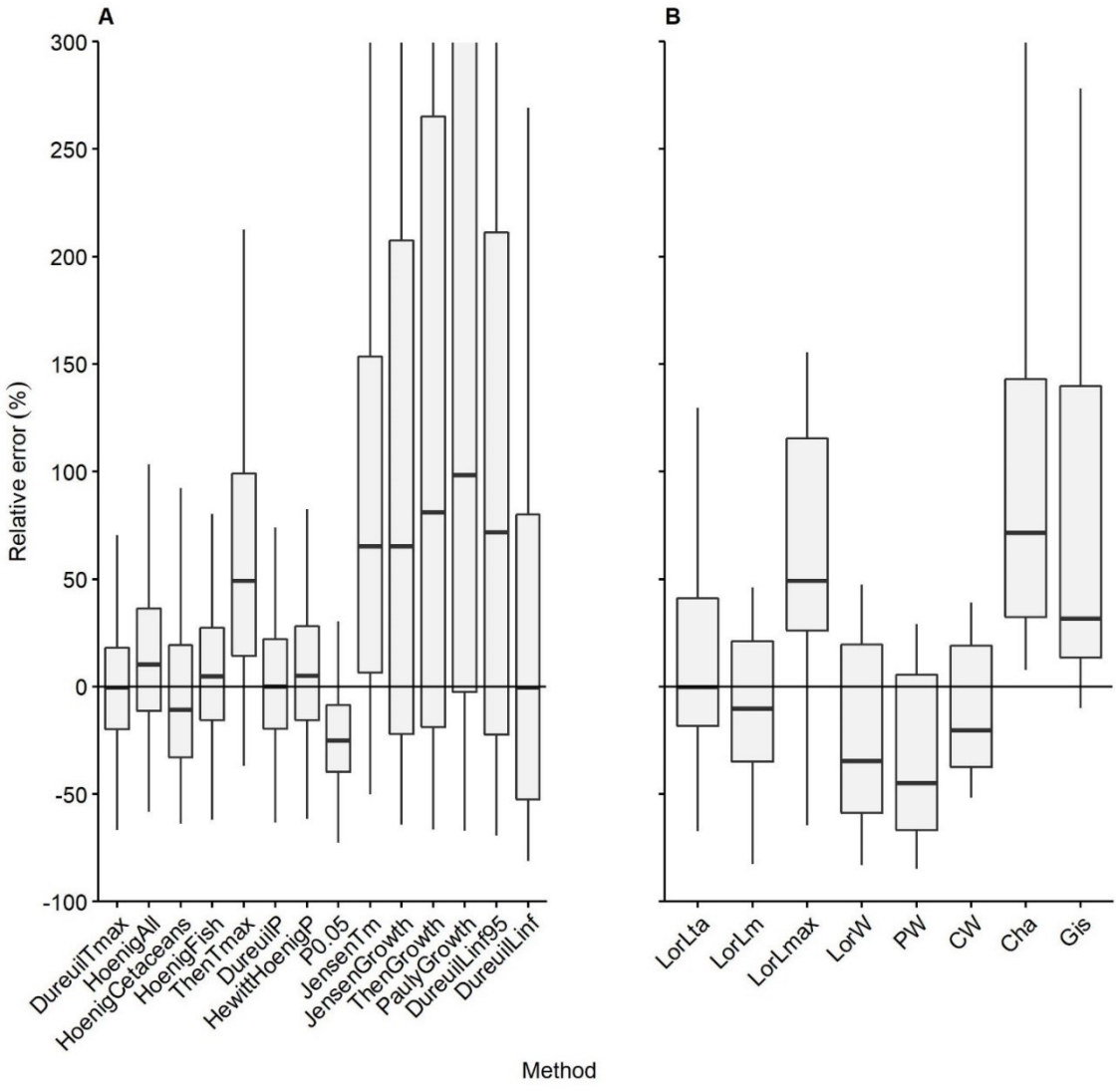

Fig. 4.3: Comparing indirect natural mortality estimators. Shown is the relative error (in percent) in predicting the direct natural mortality, *M* (year^{-1}), estimate for elasmobranchs and teleosts from the **A)** adult *M* database and **B)** juvenile *M* database from various indirect estimators. See table 4.1 for details on the indirect estimators.

4.5 Discussion

This study investigated approaches to indirectly estimate natural mortality for marine fish; elasmobranchs and teleosts. It was found that combined taxa estimators perform well among and across these two taxa. The best indirect adult *M* estimator, *DureuilTmax*, was based on updated data and ordinary linear regression with maximum age as the only covariate. The performance of this estimator was evaluated via an extensive analysis, including a sensitivity analysis applying various models, and a comparison with previously published estimators. Another new estimator also performed well, *DureuilP*, indicating that 1 – 2% (median = 1.8%) of individuals survive from birth to maximum age in unfished cohorts. In addition, it was shown that in the absence of observed maximum age, maximum age can be estimated using the von Bertalanffy growth function with the assumption that the length at maximum age is at 99.1% of the asymptotic maximum length. This approach, *DureuilLinf*, performed better than any other estimator that can be used in the absence of observed maximum age. Based on the constant adult *M* estimator, *DureuilTmax*, a subsequent unified approach to estimate juvenile *M* is suggested, which performed better than all other investigated age, size or weight dependent indirect *M* estimators. This estimator assumes that natural mortality is inversely proportional to body length (Lorenzen, 2000) and utilized a new reference length, the length after which natural mortality can be assumed constant.

Although the true natural mortality is unknown and indirect estimators can only be tested on how well they can reproduce the direct *M* estimates, the presented unified indirect estimator has shown to be promising with results highly comparable to direct methods.

Indirect adult natural mortality estimators based on maximum age achieved the best overall results in predicting the direct *M* estimate in the database. This is in accordance with previous studies (Punt et al., 2005; Kenchington, 2014; Then et al., 2015). It has also been shown that estimators including information in addition to t_{max} are not better in predicting *M* (Then et al., 2015) and, similarly, no improvement was observed here when taxa (elasmobranchs and teleosts) was utilized as an additional covariate.

While linear regression analysis appears straightforward to predict natural mortality from maximum age, Hoenig et al (2016) and Then et al (2015) also pointed out that the hierarchical nature of the data has to be taken into consideration, as this can violate assumptions of independence and random sampling. For example, when multiple observations for the same species from different populations are used, or observations are biased towards economically important groups. This was addressed by using a variety of

different approaches: a mixed effect model having taxonomic order as a random effect; evaluating estimator performance across taxonomic orders and based on randomly selected data; and by graphically evaluating autocorrelation in the model residuals. Overall the results of the sensitivity analysis suggest that ordinary linear regression is appropriate to predict natural mortality from maximum age based on the presented adult *M* database. Note, the results of the random effect model must be treated with caution because 7 of 15 included taxonomic orders had only one observation.

The exclusion of erroneous *M* estimates utilized in previous analyses likely explain much of the deviation between the here presented estimators and many previously published and empirically derived estimators. However, this explanation cannot hold for theoretical derived estimators. Jensen's (1996) estimators are based on the ecological theory that species select to maximize lifetime fecundity, using Beverton-Holt life history invariants with $M/k = 1.5$. However, the M/k ratio has been found to vary considerably among different species (Prince et al., 2015; Thorson et al., 2017), likely explaining why the two indirect *M* estimator proposed by Jensen (1996) did not perform well across taxa. In addition, the M/k ratio has been reported to differ between some teleost and elasmobranch species (Frisk et al., 2001), whereas no evidence was found here that the relationship between *M* and maximum age differs between these two taxa. The results suggest that for marine fish adult *M* is described by an exponential decay function with similar proportions of individuals surviving to maximum age. In the past, arbitrary values of 1% or 5% have been used for this proportion, while empirical data has suggested 1.5% (Hewitt & Hoenig, 2005). The empirical data presented here suggests a very similar result with approximately 1 – 2% of the individuals from birth surviving to maximum age. This finding is supported when examining the survivors from the age at 20% of the asymptotic maximum length and the age at maturity to maximum age (Fig. 4.4), where approximately 2% survive from the age at $0.2L_\infty$ to t_{max} and 5% from t_m to t_{max}.

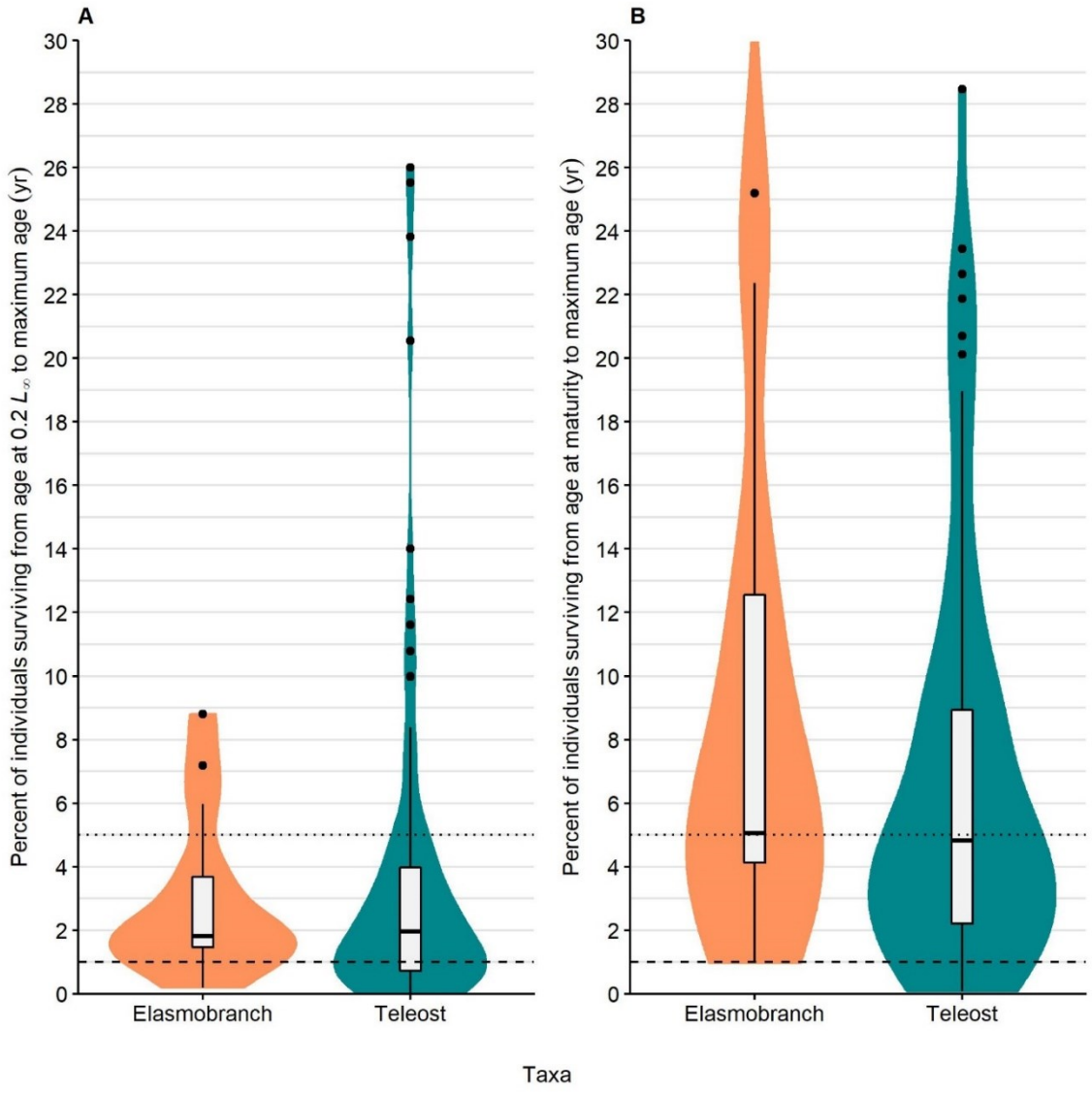

Fig. 4.4: Percentage of individual survivors from different ages at maximum age in teleosts and elasmobranchs. A) Percentage of individuals surviving from the age at 20% of the asymptotic maximum length, L_∞, to maximum age, t_{max} **B)** Percentage of individuals surviving from age at maturity, t_m, to maximum age. The dashed line indicates 1% of individuals surviving and the dotted line indicates 5% survivors. Kernel density estimates are shown for A) and B) around the box-whisker plots.

In the absence of observed maximum age, maximum age may be estimated. Approaches that estimate maximum age solely from maximum length (e.g. Ohsumi, 1979) are likely not universal, even within taxa. For example, the oldest known whale is the bowhead whale (*Balaena mysticetus*), reaching ages of over 200 years (George et al., 1999), however, it is not the largest whale species, and the spotted spiny dogfish (*Squalus suckleyi)* can reach ages over 80 years (Vega et al., 2009), but is not a particularly large shark. On the other hand, the von Bertalanffy model utilizes information on growth and has been used previously to estimate maximum ages. This requires an estimate for the percentage of the asymptotic maximum length reached at maximum age, which has been commonly suggested at 95% (Taylor, 1958; Ricker, 1979). Yet, the 95% were based on only a few cod stocks. The findings here indicate that this percentage is more generally 99.1% for marine fish. Note that this is almost identical to Fabens (1965) definition of $X = 0.9933$. This further suggests that maximum ages have potentially been underestimated in the past when using the 95% assumption.

Similar to the findings for adults, this study also suggested that juvenile natural mortality can be indirectly estimated utilizing the same estimator for elasmobranchs and teleosts. However, the results should be viewed with caution, given the small sample size and the uncertainty associated with the data. For example, the mean total length at the direct *M* estimate was only given for three observations, and for one of these three observations only fork length was given, and total length had to be estimated. In most cases the mean total length was estimated from age using the von Bertalanffy growth function, rather than being directly observed in the study. Nevertheless, the presented *LorLta* estimator performed generally well in predicting the direct *M* estimate in the juvenile *M* database, with overall more accurate predictions than any other previously published indirect age, size or weight dependent estimator. The *LorLta* estimator utilized a newly introduced reference length, the length after which *M* is assumed constant, L_{ta}. This length was generally larger than the length at maturity, L_m, with the median ratio of L_{ta} / L_m at 1.25 (range: 0.91 – 1.89), while the ratio with the asymptotic maximum length L_{ta} /L_∞ was at 0.72 (range: 0.48 – 0.92), for all 18 observations. This indicates that L_{ta} is typically larger than L_m and therefore L_{ta} might be closer associated with the length at which all individuals are mature, L_{m100}. The corresponding age at which *M* is constant, t_a, was found to occur at ~ 0.5*t_{max}, whereas the age at maturity, t_m, generally occurs at 0.16*t_{max} to 0.39*t_{max} (Beverton, 1992; Frisk et al., 2001), which also indicated t_a to be larger than t_m.

Although there is strong evidence that *M* declines with increased individual length

(Peterson & Wroblewski, 1984; Chen & Watanabe, 1989; Lorenzen, 1996, 2000; Gislason et al., 2010), a constant *M* for mature individuals might still be appropriate (Brodziak et al., 2011; Deroba & Schueller, 2013; Johnson et al., 2015). It has been previously suggested that *M* is constant from the length at maturity onwards, and that before maturity *M* follows the Lorenzen-curve, based on the assumption that an increase in mortality after reproduction is compensated by a decrease in mortality due to larger size (Brodziak et al., 2011). However, the stress of reproduction and other intrinsic factors, such as the accumulation of harmful mutations, may force *M* to increase at larger sizes or older ages (actuarial senescence). This phenomenon is likely more species-specific and currently not well predictable (Brodziak et al., 2011). Here, actuarial senescence was not examined. If senescence is likely to occur mortality estimates would be biased in two ways: 1) Direct mortality estimates in the *M* database would be too low for the actual observed maximum age, because it would be less likely to have found the oldest individual; 2) Indirect *M* estimators would overestimate *M* because maximum age would have been underestimated. Yet, evidence of senescence in wild fish is extremely limited (Nussey et al., 2013; Benoît et al., 2018). This might be particularly true for long-lived species, because the rate of senescence has been shown to decrease with increasing generation time (Jones et al., 2008). However, if the evidence for senescence is strong it might be included for older individuals using different approaches such as a logistic model (see Maunder, 2011 Abstract #11 in Brodziak et al., 2011). The only estimator that allowed for senescence to be considered in the current study was the estimator from Chen & Watanabe (1989). However, this method was inferior compared to *LorLta*, and has previously shown to be highly sensitive, often resulting in unreasonable estimates (Kenchington, 2014).

Apart from senescence, natural mortality is also likely to change over time, and these changes may even be more important than changes over age and size (Deroba & Schueller, 2013). A relatively simple approach to include changes in *M* over time for future indirect estimators could be to utilize information on body condition (Casini et al., 2016), because approaches on body measurements (Irschick & Hammerschlag, 2014), which are easier to obtain, have been shown to be related to the fitness of an individual (Gallagher et al., 2014). This information might therefore be more generally available than the information needed to estimate time-varying *M* within stock assessments. However, more research is needed to incorporate time-varying *M* in data-limited situations.

In conclusion, a relatively simple, reliable and general approach was presented to estimate adult and size-dependent (juvenile) natural mortality for marine fish in data-poor

situations. In its minimal form, the *DureuilLinf* estimator allows size dependent natural mortality to be estimated from growth information alone. The results of this study, combined with recent advances in estimating growth for difficult to age fish, such as elasmobranchs (Chapter 3), could therefore allow for the wide applicability of these estimators in data-poor situations. For example, the estimators could be used to indirectly estimate a natural mortality rate for stock assessment purposes, or as a sensitivity analysis for the comparison against directly estimated *M* rates, as well as to gain prior information in Bayesian analyses. The presented estimators may also be applicable for species other than marine fish, if there is reason to believe that mortality curves and proportions surviving to maximum age are similar across disparate taxa or species, such as marine fish, freshwater fish, cetaceans and invertebrates (Hoenig, 1983; Hewitt et al., 2007; McCoy, 2008; Maceina & Sammons, 2016). The application of indirect estimates should, however, consider some form of sensitivity analysis, given the importance of an accurate and precise *M* estimate and the difficulties in estimating *M*. For example, the von Bertalanffy growth function and information from similar species could be used to determine if the observed maximum age and growth are biologically reasonable. Some form of sensitivity analysis is highly relevant, as can be seen from the here reported tendency that many previously published indirect adult *M* estimators overestimate *M*. Overestimated natural mortality rates can increase the likelihood of unintentional overfishing: positive bias in *M* translates into higher assumed stock sizes (Cheilari & Rätz, 2009) and more optimistic reference points (Cheilari & Rätz, 2009; Maunder & Wong, 2011), but underestimated fishing mortalities (Cheilari & Rätz, 2009) and therefore overestimates the species' resilience to fishing. It is hoped that the new estimators presented here will enhance the estimation of natural mortality and thus fisheries assessments in data-poor situations, allowing for more species to be assessed and managed based on scientific information.

Chapter 5
Relationships between mortality, growth and reproduction in elasmobranchs

5.1 Abstract

The ratio of natural mortality, *M*, over the von Bertalanffy growth constant, *k*, is a crucial parameter in length-based stock assessments and the understanding of species' life history strategies. Hence, it is particularly relevant in data-poor and poor-data situations of threatened or targeted species, as is the case for many elasmobranchs (sharks, rays and skates). Although the *M*/*k* ratio has frequently been assumed invariant at 1.5, it has also been shown to be highly variable among species. Yet, this ratio can be calculated from the optimum length, L_{opt} (length at maximum cohort biomass), the von Bertalanffy asymptotic maximum length, L_∞, and the exponent of the length-weight relationship, *b*, $\frac{M}{k} = \frac{b}{(L^*_{opt}/L^*_\infty)} - b$. Given that *b* is readily available for many species, or can often be inferred, the ability to approximate the true ratio of L^*_{opt}/L^*_∞, would generally allow an estimation of *M*/*k*. While many previous studies have assumed L_{opt} to be equal to the length at maturity, L_m, when estimating *M*/*k*, life history theory would predict L_m to be smaller than L_{opt} for elasmobranchs. This study empirically investigated the predictability of L^*_{opt}/L^*_∞ from more available data in sharks, rays and skates, to facilitate the estimation of *M*/*k*. Therefore, observed data on *M*/*k* and *b* from 15 elasmobranch populations, compromising 12 species, were utilized together with information on L_m, L_∞ and observed maximum length, L_{max}. The empirical results agreed with the theory that elasmobranchs mature before L_{opt}, and furthermore suggest that the L^*_{opt}/L^*_∞ ratio can be approximated from L_m and L_∞ or L_m and L_{max}. However, in conflict with life history theory, the results indicated that maturity would occur after the length of maximum tissue production. Hence, elasmobranchs would either follow a different strategy to maximize fitness, or maximum length was underestimated and/or length at maturity overestimated in the utilized data. Given the small sample, future research is needed to address these questions. Nevertheless, the presented predictors of L^*_{opt}/L^*_∞ might be used with caution in the interim. Applications for data-poor stock assessment, maximum age estimation, and estimation of a minimum length, below which fishing mortality should be avoided, are discussed.

5.2 Introduction

In 1959, Beverton and Holt pioneered the studies of general relationships between natural death, growth and reproduction in marine fish (Beverton & Holt, 1959). Such relationships result from the allocation of finite energy available to maximize reproductive output (Roff, 1984; Charnov et al., 1993; Jensen, 1996) and appear to be relatively consistent across species or populations (Beverton & Holt, 1959; Beverton, 1992; Charnov et al., 1993). Of particular interest and relevance in both life history theory and stock assessment applications is the relationship between survival and growth, formally expressed as a ratio of natural mortality, M (year^{-1}), over the von Bertalanffy growth constant, k (year^{-1}). For example, it has been suggested that the M/k ratio determines the onset of maturity (Roff, 1984; Beverton, 1992; Jensen, 1996; Hordyk et al., 2015; Prince et al., 2015; Thorson et al., 2017), as well as the shape of the von Bertalanffy growth curve (Hordyk et al., 2015). Species with a low M/k ratio grow relatively quickly to their asymptotic maximum length and continue to live for a comparatively long time (Hordyk et al., 2015). Such species would be expected to mature later relative to their maximum length (Prince et al., 2015; Thorson et al., 2017). Species with a high M/k ratio will never grow close to their asymptotic maximum length (Hordyk et al., 2015; Prince et al., 2015) and would be expected to mature earlier relative to their maximum length (Prince et al., 2015; Thorson et al., 2017). In addition, the M/k ratio has been shown to determine the length distribution in an unfished population (Hordyk et al., 2015; Prince et al., 2015). Hence, it is a central parameter in length-based stock assessment methods (Pauly & Soriano, 1986; Pauly & Morgan, 1987; Gallucci et al., 1996; Hordyk et al., 2015; Froese et al., 2016, 2018, 2019; Huynh et al., 2018) and therefore important for data-poor threatened or targeted species.

The ratio between natural mortality and growth can be calculated from the exponent of the length-weight relationship, b, which is approximately 3 in most marine fish (Froese, 2006), and the relative length at maximum cohort biomass, expressed as the ratio between the length where cohort biomass is maximum (the optimum length) and the asymptotic maximum length (Beverton, 1992; Hordyk et al., 2015):

$$\frac{M}{k} = \frac{b}{(\frac{L^*opt}{L^*\infty})} - b. \quad (5.1)$$

Many studies have associated the M/k ratio with the ratio of length at maturity to asymptotic maximum length, also referred to as the reproductive load or relative length at maturity, L_m/L_∞ (Roff, 1984; Beverton, 1992; Jensen, 1996; Hordyk et al., 2015; Prince et

al., 2015; Thorson et al., 2017). This assumes that the relative length at maturity, L_m/L_∞, would equal the relative length at maximum cohort biomass, L^*_{opt}/L^*_∞, and therefore that the length at maturity coincides with the length where cohort biomass reaches its maximum. If maturation would be without costs, then species would mature as early as possible to maximize lifetime reproductive output (Roff, 1984). However, in species with indeterminate growth and a positive relationship of length and fecundity, reproductive output will increase to a maximum before decreasing, as a result of increasing numbers of offspring with length, but decreasing survival (Jensen, 1996). The onset of maturity is therefore thought to be determined through optimization of a growth and mortality trade-off (Roff, 1984; Jensen, 1996). When b equals 3, and the length at maturity occurs at maximum cohort biomass, L_{opt}, and also coincides with the length at maximum tissue production, L_i, then the M/k ratio is 1.5 (Jensen, 1996). In other words, if the M/k ratio equals 1.5, then maximum cohort biomass occurs at the same length as the maximum growth in body weight, b equals 3, and a general fitness advantage could be assumed if most offspring are produced at that point (Froese et al., 2016). This logic forms the basis of an assumed invariant M/k ratio of 1.5.

Empirically, however, several recent studies have shown that the M/k ratio may vary considerably across different fish species (e.g. Prince et al., 2015; Thorson et al., 2017), ranging from 0.06 to 21.2 overall (Then et al., 2015), but mostly constrained between 0.1 and 3.5 (Prince et al., 2015). Likewise, estimated M/k ratios have been reported significantly lower for some elasmobranch (sharks, rays and skates) species when compared with bony fish or reptiles (Frisk et al., 2001). An M/k ratio of 1.5 may therefore approximate a median across species rather than an invariant value (Prince et al., 2015), but the species-specific value tends to be somewhat predictable from timing of maturation within similar taxonomic groups, for example within a genus (Thorson et al., 2017). Therefore, the question that arises is if this variability can be predicted in data-poor elasmobranch populations where an estimate of the M/k ratio could be highly valuable for stock assessment and management purposes.

As mentioned before, many studies have used L_m equal to L_{opt} (Beverton, 1992; Hordyk et al., 2015; Prince et al., 2015; Thorson et al., 2017). However, this is only true for semelparous species, which are characterized by a single lifetime spawning event, where reproductive output of a cohort would be maximized when maturing, spawning and dying at L_{opt} (Froese & Pauly, 2013). Iteroparous species, on the other hand, are characterized by multiple lifetime spawning events. If these events can guarantee a

certain success rate, such as in elasmobranchs where young are large and survival is high, maturity would be expected at or before the point of maximum tissue production, and the maximum reproductive biomass would be expected to fall in the middle of the reproductive phase, thus $L_{opt} > L_m$ (Froese & Pauly, 2013). Consequently, a relationship different from L^*_{opt}/L^*_∞ equals L_m/L_∞ would be expected in elasmobranchs.

This study aimed to empirically investigate the predictability of L^*_{opt}/L^*_∞ from more available data in sharks, rays and skates, to subsequently allow the estimation of M/k. Therefore, observed data on M/k and b from 15 elasmobranch populations, comprising 12 species, were utilized together with information on L_m, L_∞ and observed maximum length, L_{max}. Uncertainties associated with the data, possible implications for data-poor assessment, and estimation of other life history parameters are discussed. This is the first study to examine the predictability of the M/k ratio for elasmobranchs based exclusively on observed and directly estimated information. Many elasmobranchs show higher than average risk of extinction (Dulvy et al., 2014; Fernandes et al., 2017), often have only limited information available (Dulvy et al., 2014), and have high uncertainty or bias in the estimation of basic life history parameters, such as age and growth (Harry, 2017; Natanson et al., 2018). The predictability of the M/k ratio is therefore particularly important to aid species assessments, which in turn form the basis of science-based management.

5.3 Materials and methods

Information on the following parameters was gathered: The constant adult instantaneous natural mortality rate, M (year^{-1}), von Bertalanffy growth parameters k (year^{-1}) and L_∞ (cm), observed maximum age, t_{max}, length and age where 50% of the individuals are mature, L_m (cm), t_m (year), and the parameters from the length, L, and weight, W, relationship, a and b, with $W = aL^b$, All of this information was extracted from the dataset utilized in Chapter 4, “A unified natural mortality estimator for marine fish”. As detailed in Chapter 4, quality control criteria were also applied beforehand, such as only considering directly estimated M values as opposed to indirectly estimated values from pre-specified empirical relationships. In addition, records on the observed maximum length, L_{max}, were obtained from the published literature. In total, 15 data points were collected from 12 different elasmobranch species (4 males, 3 females, 8 combined sexes) (Table 5.1).

The observed relative length at maximum cohort biomass, expressed as the ratio between optimum length and the asymptotic maximum length, was calculated following Beverton (1992):

$$\frac{L^*opt}{L^*\infty} = \frac{b}{\left(b+\frac{M}{k}\right)}, \quad (5.2)$$

where b is the exponent of the length-weight relationship (Froese, 2006) and M/k is the observed (directly estimated) M/k ratio. Note, that if M/k = 1.5 and b = 3, a common value for marine fish (Froese, 2006), then $L_{opt} = 0.67L_\infty$, and L_{opt} would be equal to the length at maximum growth in weight, L_i, i.e. the length that corresponds to the inflection point of the weight-based von Bertalanffy growth function, where tissue production reaches its maximum (Froese et al., 2008). Linear regression was utilized to investigate if the observed ratio, L^*_{opt}/L^*_∞, can be predicted from available information on L_m and L_∞:

$$\frac{L^*opt}{L^*\infty} = \beta_0 + \beta_1 \frac{L_m}{L_\infty}, \quad (5.3)$$

where the intercept with the y-axis, β_0, and the slope, β_1, are assumed constant. Given the difficulties in obtaining unbiased growth parameters for elasmobranchs and the associated uncertainties in L_∞ (Chapters 2; 3), the suitability of the ratio between L_m and maximum observed length, L_{max}, as a predictor was also investigated:

$$\frac{L^*opt}{L^*\infty} = \beta_0 + \beta_1 \frac{L_m}{L_{max}}. \quad (5.4)$$

Model fits were compared using the coefficient of determination, R^2, and the results were discussed with respect to their compliance with ecological theory and with respect to the quality of the underlying data.

Table 5.1: Life history information of the investigated elasmobranchs. Sex (female, F, male, M, combined, C), the von Bertalanffy growth constant, k, asymptotic maximum length, L_∞ and length at birth, L_0, the length at which 50% of the individuals are mature, L_m, the exponent of the length-weight relationship, b, and the observed maximum age, t_{max}, the age corresponding to L_m, t_m, and the sex-specific observed maximum length, L_{max}, are shown. The age at maturity, t_m, was either directly observed (*) or calculated from L_m and the von Bertalanffy growth function. If sexes were combined the mean L_{max} of males and females was used. All rates are given in year^{-1}, ages in years, and length in cm total length. References for L_{max} are given, for all further details and references see Chapter 4.

Scientific name	Common name	Sex	k	L_∞	L_m	b	t_{max}	t_m	L_{max}
Carcharhinus limbatus	Blacktip shark	F	0.187	169.8	134.6	2.87	18.5	6.3*	201.9 [1]
		M	0.214	155.9	119.6	2.87	23.5	4.8*	189.2 [1]
Carcharhinus plumbeus	Sandbar shark	C	0.040	274.8	155.5	2.97	30.0	15.4	278.0 [2]
Rhizoprionodon taylori	Australian sharpnose shark	F	1.013	73.3	57.5	3.13	6.9	1.1	78.4 [3]
		M	1.337	65.2	56.0	3.13	5.7	1.1	69.1 [3]
Sphyrna tiburo	Bonnethead	F	0.307	105.8	82.2	3.59	13.6	3.0*	110.0 [4]
		M	0.560	84.7	72.1	3.59	8.2	2.0*	93.0 [4]
Galeorhinus galeus	School shark	C	0.166	161.3	132.9	3.18	52.7	9.2	173.0 [5]
Mustelus antarcticus	Gummy shark	C	0.188	170.3	111.6	3.09	15.5	4.4	166.7 [6]
Heterodontus portusjacksoni	Port Jackson shark	C	0.077	116.1	83.6	3.15	34.4	12.5	114.5 [7]
Lamna nasus	Porbeagle	C	0.116	280.0	200.0	2.96	20.0	8.3	297.4 [8]
Urolophus paucimaculatus	White spotted stingaree	C	0.330	50.1	32.5	3.21	9.0	2.0	50.0 [9]
Leucoraja ocellata	Winter skate	C	0.150	94.1	76.5	3.32	19.0	12.4*	107.5 [10]
Squalus acanthias	Spiny dogfish	C	0.125	95.0	73.0	3.22	37.5	8.5	103.5 [11]
Squalus suckleyi	Pacific spiny dogfish	M	0.067	91.9	72.0	3.09	73.0	21.3	107.0 [12]

[1]Castro (2011); [2]Braccini & Taylor (2016); [3]Simpfendorfer, (1993); [4]Lombardi-Carlson (2007); [5]Moulton et al (1992); [6]Walker (2007); [7]Tovar-Ávila et al (2009); [8]Francis et al (2008); [9]Edwards (1980); [10]Stone (2017); [11]Hammond & Ellis (2005); [12]Ketchen (1972)

5.4 Results

Empirically determined *M*/*k* ratios for sampled elasmobranchs ranged from 0.52 to 2.36 (median = 0.9), and the majority of species had *M*/*k* ratios markedly different from 1.5 (Table 5.1). Maximum ages ranged from 5.7 years to 73 years. The asymptotic maximum lengths ranged from 50 cm to 280 cm and the von Bertalanffy growth coefficient, *k,* ranged from 0.04 year^{-1} to 1.34 year^{-1}. The length at maturity ranged from 32.5 cm to 200 cm. Age at maturity ranged from 1.1 to 21.3 years and was generally obtained from length at maturity via the von Bertalanffy growth function. The optimum length ranged from 35.2 cm to 183.5 cm. The exponent of the weight-length relationship, *b*, ranged from 2.87 to 3.59 with a median at 3.13.

A marginally better model fit was obtained when predicting the observed relative length at maximum cohort biomass, L^*_{opt}/L^*_{∞}, from the ratio of estimated length at maturity and asymptotic maximum length, L_m/L_{∞}, than from L_m and observed maximum length, L_m/L_{max} (Fig. 5.1). The average relationships were given by:

$$\frac{L^*opt}{L^*\infty} = 0.0058 + 0.932 * \frac{L_m}{L_\infty} \quad (5.5)$$

($p < 1*10^{-5}$, $R^2 = 0.78$, with 95% confidence intervals for the intercept between -0.17 – 0.28 and for the slope between 0.64 – 1.23), and:

$$\frac{L^*opt}{L^*\infty} = -0.047 + 1.154 * \frac{L_m}{L_{max}} \quad (5.6)$$

($p < 3*10^{-5}$, $R^2 = 0.75$, with 95% confidence intervals for the intercept between -0.33 – 0.24 and for the slope between 0.75 – 1.56). For both relationships, the predicted *M*/*k* values agreed well with the observed *M*/*k* values, even if *b* was assumed unknown and set to 3 (Fig. 5.2). Overall, the cohort trajectories suggest that species matured before L_{opt}, i.e. before maximum cohort biomass, whereas species with an *M*/*k* ratio of 1.5 would tend to mature after L_{opt}. Furthermore, the results indicated that most species matured after the point of maximum tissue production (Fig. 5.3). The length or age at maximum tissue production, L_i or t_i, and the length or age at maturity, L_m or t_m, are closer to each other when *M*/*k* was estimated from length at maturity and observed maximum length.

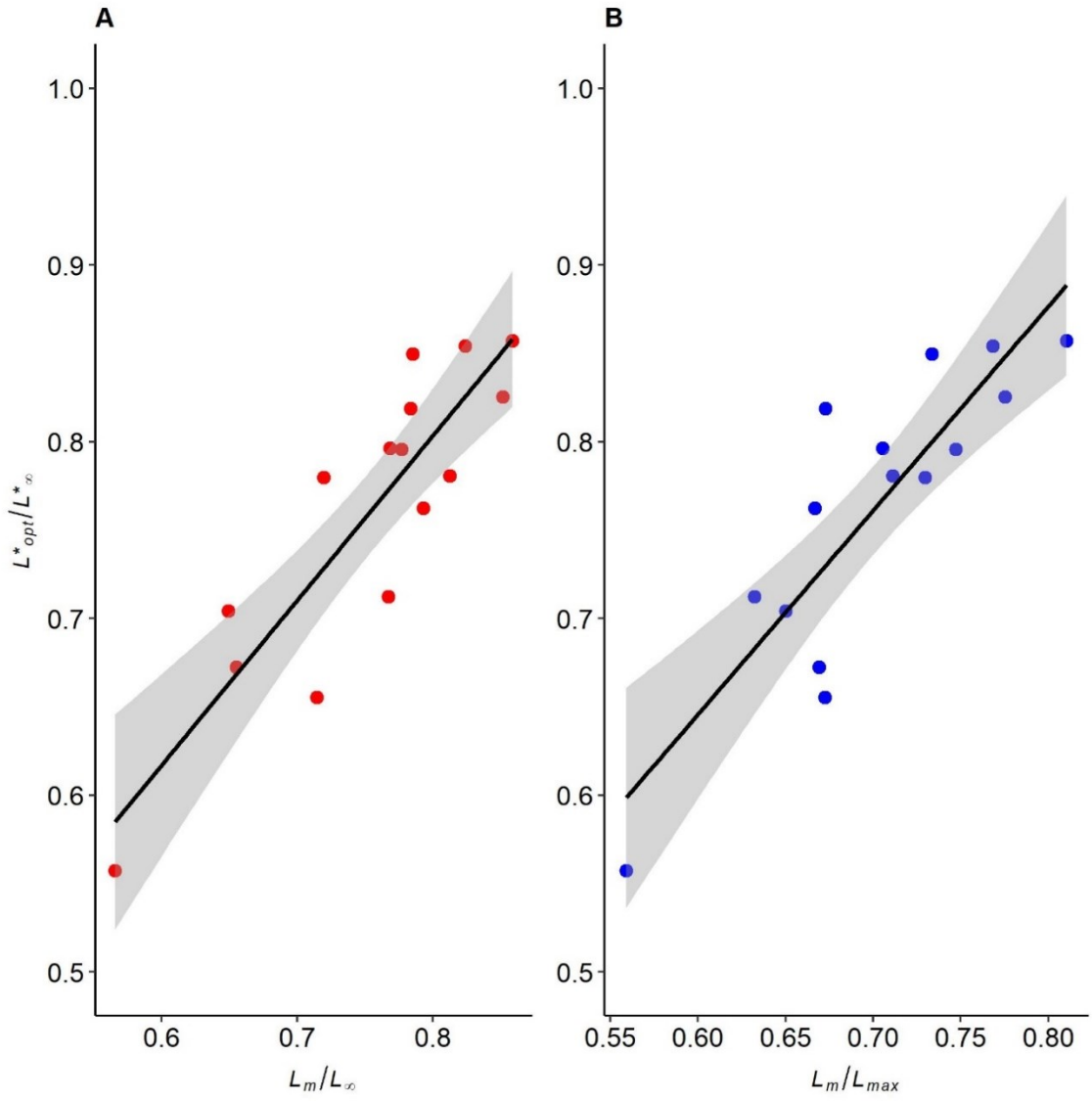

Fig. 5.1: Relative length at maximum cohort biomass versus relative length at maturity for the investigated elasmobranchs. Observed relative length at maximum cohort biomass expressed as the ratio between length at maximum cohort biomass and asymptotic maximum length, L^*_{opt}/L^*_∞, versus the relative length at maturity, determined by the ratio of **A)** length at maturity over asymptotic maximum length (red) and **B)** length at maturity over observed maximum length (blue). A linear regression model was fitted (black line) with 95% confidence intervals (shaded grey).

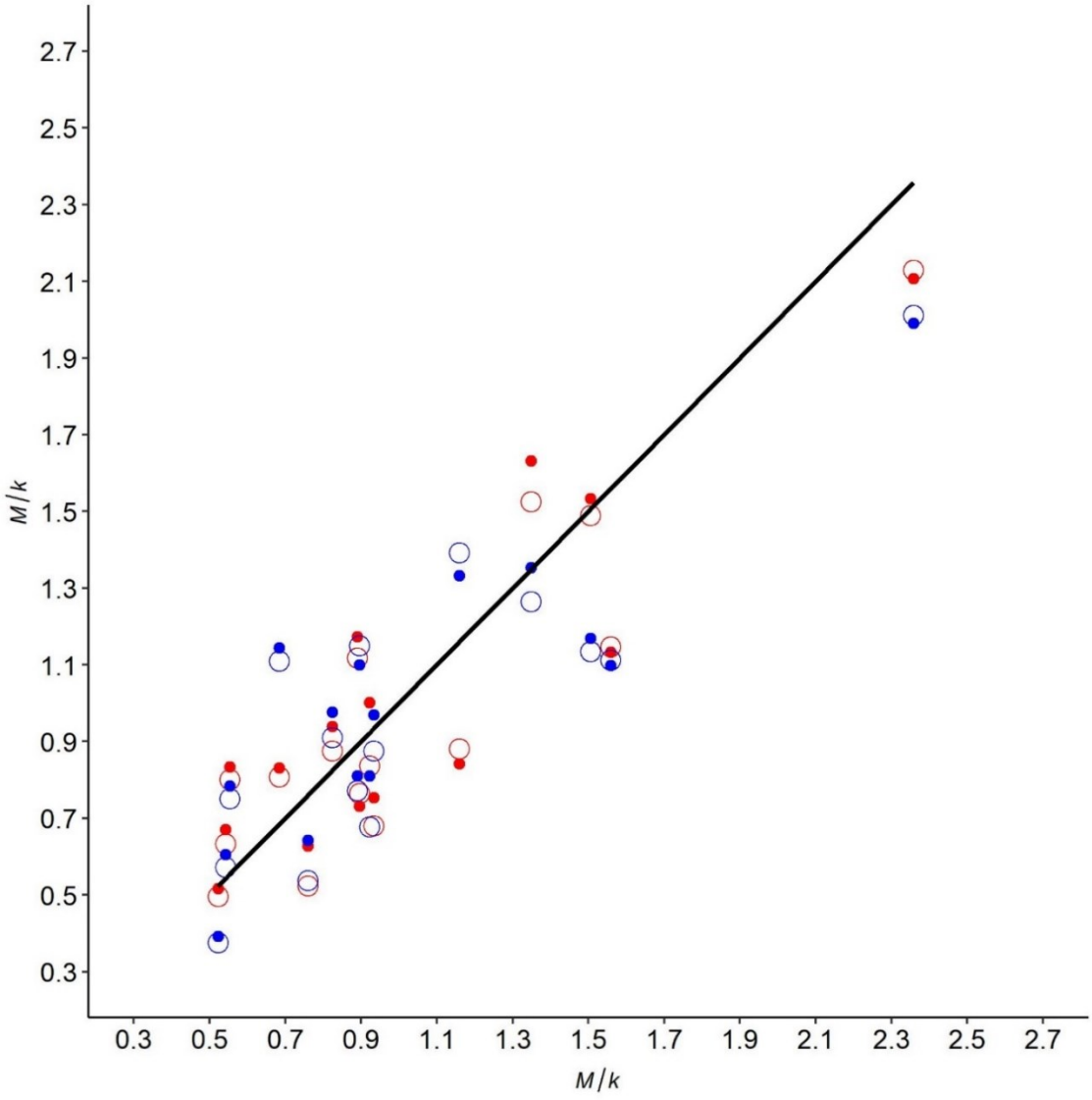

Fig. 5.2: Predictability of the *M*/*k* ratio in the studied elasmobranchs. Estimates for the ratio of natural mortality, *M* (year^{-1}), over the von Bertalanffy growth constant, *k* (year^{-1}), from length at maturity and asymptotic maximum length (red), equation (5.5), and from length at maturity and observed maximum length (blue), equation (5.6). Open circles had the length-weight exponent *b* = 3. The 1:1 line shown in black.

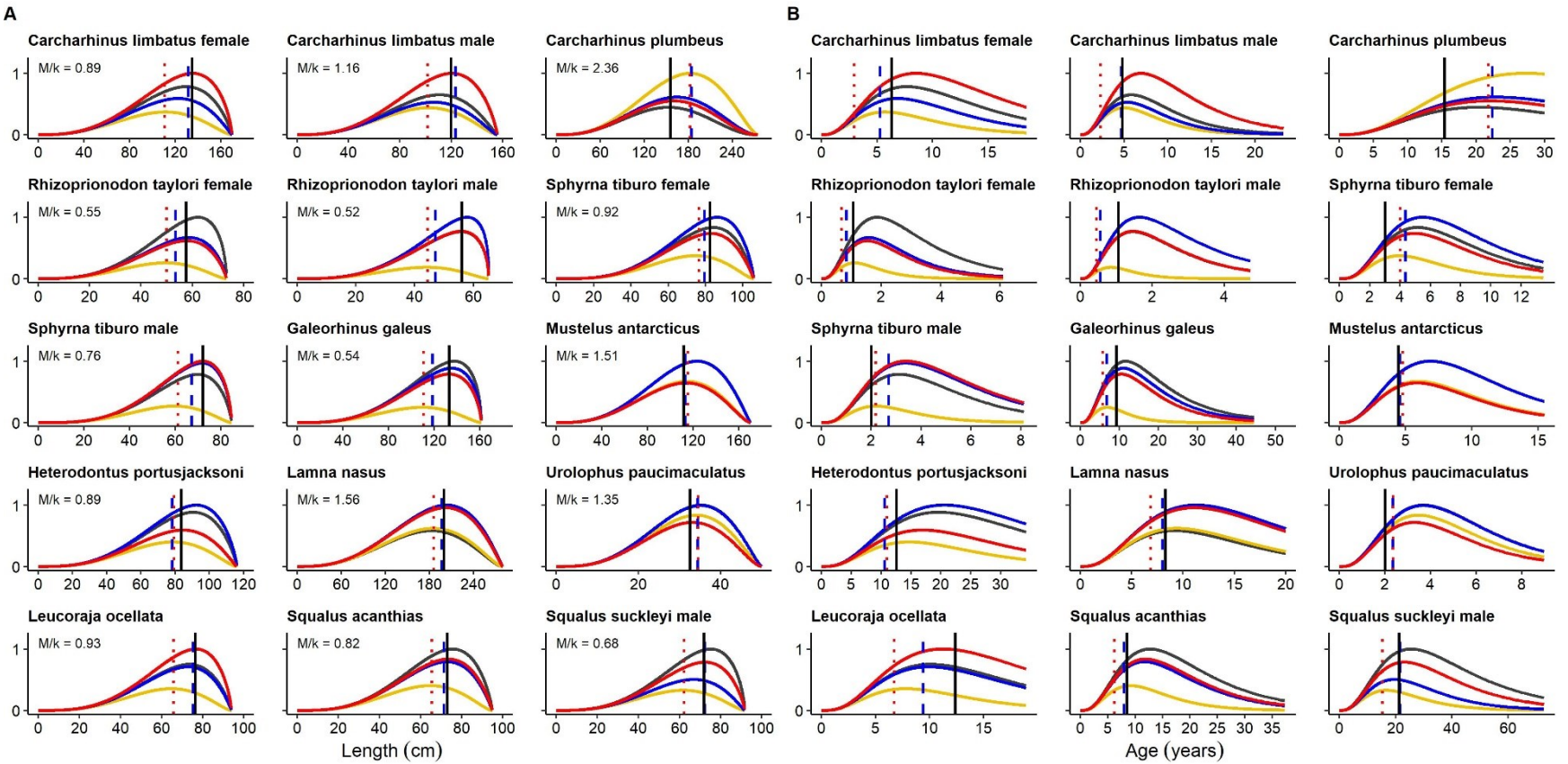

Fig. 5.3: Cohort trajectories of the investigated elasmobranchs. Normalized cohort biomass (cohort biomass/maximum cohort biomass) over **A)** length (cm) and **B)** age (years) with the observed ratio of the natural mortality, *M* (year^{-1}), and the von Bertalanffy growth constant, *k* (year^{-1}), (dark grey), an *M*/*k* ratio of 1.5 (yellow), the *M*/*k* ratio estimated from length at maturity and asymptotic maximum length, L_∞, equation 5.5 (red) and the *M*/*k* ratio estimated from length at maturity and observed maximum length, L_{max}, equation 5.6 (blue). The point where tissue production is maximum was obtained via $L_i = L_\infty \left(1 - \frac{1}{b}\right)$ (red dotted vertical line) or $L_i = L_{max} \left(1 - \frac{1}{b}\right)$ (blue dashed vertical line), where *b* is the exponent of the length-weight relationship. The length at which 50% of the individuals mature is shown by the black solid vertical line. Cohort biomass at length, *L*, was estimated from $100 * (\frac{(L_\infty - L)}{L_\infty})^{\frac{M}{k}} * W$, with weight, *W,* and the respective *M*/*k* ratio. Ages were obtained from the von Bertalanffy growth function.

5.5 Discussion

This study investigated the predictability of the ratio between length at maximum cohort biomass and asymptotic maximum length in elasmobranchs, in order to enable the estimation of another ratio, the ratio of natural mortality, *M*, and the von Bertalanffy growth constant, *k*. This ratio is an important parameter in data-poor stock assessment and life history theory. Reliable estimates of the *M*/*k* ratio could aid in predicting the unfished size structure of a cohort (Hordyk et al., 2015; Prince et al., 2015), and be utilized as priors in length-based stock assessments (Froese et al., 2018, 2019) or serve as fisheries reference points. The findings here suggest that the ratio between length at maximum cohort biomass and asymptotic maximum, L^*_{opt}/L^*_{∞}, can be predicted with some precision from length at maturity and maximum length information, yet caution should be taken due to the limited database upon which these generalizations were founded. In the following the ecological significance, compliance with life history theory, limitations and potential applications in data-poor assessments of the results are discussed.

It was found that in elasmobranchs the length at maximum cohort biomass, L_{opt}, is generally larger than the length at maturity, L_m. In previous studies the optimum length and the length at maturity have often been treated as equal (Roff, 1984; Beverton, 1992; Jensen, 1996; Hordyk et al., 2015; Prince et al., 2015; Thorson et al., 2017). Yet, others have described their relationship as unequal. For example, Froese & Binohlan (2000) found that larger species have L_{opt} values larger than L_m, using information predominantly on teleosts. Indeed, L_{opt} can only be assumed to equal L_m in semelparous fish (Froese & Pauly, 2013), where maturing earlier than L_{opt} would invest energy in reproduction instead of body growth before fecundity is highest, and maturing later would increase the likelihood of dying without reproducing (Roff, 1984; Jensen, 1996; Froese & Pauly, 2013).

The findings that elasmobranchs mature before L_{opt} further indicate that larger females have disproportionally more offspring, because if all individuals are mature before L_{opt}, lifetime reproductive output is maximized when the exponents of the length-weight and fecundity-length relationships are similar. In other words, with similar exponents the maximum cohort fecundity coincides with maximum cohort biomass (Froese et al., 2016; Figs. E1; E2). However, this is only true if all individuals are mature at this point, i.e. $L_{m100} \leq L_{opt}$. Fecundity increasing with maternal length as a power function with an exponent similar to the exponent of the length-weight relationship is supported by other studies, showing that larger females have disproportionally more offspring (Froese & Luna, 2004; Barneche et al., 2018). Therefore, the exponent of the fecundity-length relationship can

be expected to be similar to the exponent of the length-weight relationship, with an average of 3 (Froese, 2006). A slightly lower exponent would suggest that larger females also produce slightly larger pups. In elasmobranchs it is generally assumed that the relationship between the numbers of offspring (fecundity) and maternal length is positive, likely because larger females increase more in girth and can accommodate more offspring in their body cavity (Conrath, 2005).

The optimum length, i.e. the position of the peak in cohort biomass along the x-axis, can also be seen as a proxy for generation time, and the height of the peak in cohort biomass as a proxy for lifetime reproductive output (Froese et al., 2016; Figs. E1A; E2A). Note, in cases where not all individuals are mature at L_{opt} the maximum cohort fecundity would be at a length larger than L_{opt}, yet the peak in cohort biomass would still hold information on lifetime reproductive output or generation time relative to another cohort (Figs. E1B; E2B). Therefore, the relative change in lifetime reproductive output and generation time can be directly compared in two different cohorts with different M/k ratios: If mortality is low relative to growth then the M/k ratio is smaller than 1.5 and the peak at cohort biomass would be higher, but at a later age or length, i.e. increasing cohort fitness in terms of lifetime reproductive output, but decreasing cohort fitness in terms of generation time. The opposite would occur for M/k ratios larger than 1.5, and there is no obvious optimum between this trade-off (Froese et al., 2016). It seems that many of the elasmobranch species investigated here have a larger generation time than would be expected if M/k equals 1.5. This is evident by the position of the peak cohort biomass along the x-axis when M/k = 1.5 compared to the observed M/k (Fig. 5.3B). The peak of the latter is generally far from maximum age, and therefore elasmobranchs may decrease their fitness in terms of generation time to increase their fitness in terms of lifetime reproductive output, as evident by the height of the peak in cohort biomass (Fig. 5.3B). For most species this peak in cohort biomass is higher with the observed M/k ratio, than with the theoretical value of 1.5. Elasmobranch species with M/k ratios > 1.5 might be generation time limited, i.e. they cannot increase their generation time much more in order to increase lifetime reproductive output. A good example is the sandbar shark (*Carcharhinus plumbeus*) in Figure 5.3B, where a peak in cohort biomass of M/k = 1.5 would be close to maximum age. Elasmobranch species with M/k ratios < 1.5 might be reproductive output limited, i.e. they cannot have less offspring in order to decrease generation time, and mature late relative to their maximum length. One explanation for this could be that sharks, rays and skates give birth to live young or lay egg cases, both

of which are significantly larger than bony fish eggs. Therefore, females may need to attain a certain minimum length before its biologically possible to mature. A high *M*/*k* ratio indicates a high natural mortality rate relative to growth, and species would be expected to mature earlier relative to their maximum length (Prince et al., 2015). In addition, larger elasmobranch species tend to have larger and more offspring (Cortes, 2000). Consequently, only relatively large elasmobranchs might be able to afford a high *M*/*k* ratio, with maturity occurring relatively early compared to their maximum size. The association of higher *M/k* ratios with larger elasmobranchs is also supported by the increase of the *M*/*k* ratio with maximum length (Fig. 5.4). This is contradictory to many bony fish where the *M*/*k* ratio generally decreases with maximum length (Prince et al., 2015). However, a high *M*/*k* ratio and a small maximum length might be an unfeasible life history combination for elasmobranchs, prevented by the relatively large size of their offspring, i.e., elasmobranchs have low fecundity and therefore need large offspring with low mortality rates (Frisk et al., 2001), but the exact reasons for these observed patterns are unknown and warrants future investigation.

Another observed pattern, that many elasmobranchs appear to mature after the length at maximum tissue production, L_i (Fig. 5.3), is more difficult to explain from an ecological standpoint, because this should theoretically minimize fitness (Figs. E1; E2), unless elasmobranchs follow a different strategy. For example, a very large L_m could biologically be needed to produce large young with higher survival. While the very late maturity would decrease fitness, the high survival of the young may increase fitness. However, not only larger offspring, but also other factors associated with higher energetic costs during reproduction, such as migrating to pupping grounds, could hold possible explanations for L_m being larger than L_i, because individuals may utilize the produced tissue to enhance their own condition. The same could be true for elasmobranch species that stop feeding during pregnancies (Lucifora et al., 2002; Hammerschlag et al., 2018).

Yet, evidence for L_m being smaller than L_i is also present in elasmobranchs. This can been seen when utilizing the growth parameters obtained from mark-recapture information via the Bayesian version of Fabens (1965) method with informative priors in Chapter 3, together with literature values for the length at which individuals in a cohort start to mature, and where 50% of the individuals are mature, L_m, for these stocks. Given that these growth parameters do not suffer from the difficulties in aging elasmobranchs (Harry, 2017; Natanson et al., 2018), a clearer picture may be obtained. Indeed, the results indicate that L_m is generally smaller or close to L_i, whereas the length at first maturity is

always smaller than the length at maximum tissue production, L_i, except for *Raja microocellata* (Table 5.2). However, only four mark-recapture observations were available for this species, and when utilizing the suggested L_∞ from over 2,500 aged individuals of 137 cm (Ryland & Ajayi, 1984), L_i becomes 95 cm and therefore larger than L_m.

Hence, the observations of L_m being larger than the length at maximum tissue production, L_i, might rather be an artefact due to bias in the utilized data. Bias in the observed relative length at maximum cohort biomass, an overestimated length at maturity, or an underestimated asymptotic maximum length, could all lead to $L_m > L_i$, and are discussed in the following.

First, relative length at maximum cohort biomass utilized here could have been biased. It has been argued that the reproductive output is only maximized if maturity occurs at the length with maximum tissue production, L_i, which occurs at $0.67L_\infty$ if b equals 3 (Jensen, 1985; 1996), and thus $\frac{M}{k} = \frac{3}{0.67} - 3 = 1.5$. This M/k ratio was markedly different from the observed M/k ratios in most of the investigated elasmobranchs. Likewise, the relative length at maximum cohort biomass was markedly different from 0.67. Values differing from 0.67 have been claimed to be an artefact of L_∞ not being representative for the expected size at maximum age (Nadon & Ault, 2016). Yet, no major difference was found here when utilizing either the L_m/L_{max} or L_m/L_∞ ratio, with both being different from 0.67 in many cases (Fig. 5.1). In addition, the values reported here are within the common range of 0.4 to 0.9 following the general patterns with smaller values for larger species (Froese & Binohlan, 2000). More importantly, a constant value for the relative length at maximum cohort biomass at 0.67 would suggest $L_m = L_{opt}$ and this was neither supported by the results reported here, nor by ecological theory (Froese & Pauly, 2013). For species with relatively constant reproductive success, it would rather be expected that L_m is smaller than L_i, and hence $L_m \neq 0.67L_\infty$, to have full reproductive potential in the middle of the reproductive phase (Froese & Pauly, 2013). The relative length at maximum cohort biomass utilized here was calculated from the observed M/k ratio and the exponent of the length-weight relationship, b, which themselves are only estimates. However, the reported values for b were close to the expected value of 3 (Froese, 2006) and this study utilized only natural mortality values that were obtained from direct methods (Chapter 4). These direct natural mortality estimates were also similar to those theoretically expected if 1% to 2% of the initial individuals in a cohort would survive to maximum age (Fig. E3). Moreover, for most populations investigated here approaches to validate the annual formation of rings in the vertebrae have been applied in aging studies. The only exception was the

tope shark (*Galeorhinus galues*) where growth was estimated from length increment data (Moulton et al., 1992) which was preferred due to difficulties in aging large tope (Walker et al., 2001). This indicates that the growth parameters utilized here were also largely unbiased and together with the above listed arguments suggests that the values for the observed relative lengths at maximum cohort biomass were plausible.

Second, the length at maturity utilized here could have been overestimated. To investigate this, alternative studies on reproduction for the 12 elasmobranch species investigated here were consulted. For most of the species, maturity values smaller than the length at maximum tissue production, L_i, have been reported elsewhere (Table 5.3). These findings could indicate that L_m has indeed been overestimated for some of the populations studied here, which is potentially associated with difficulties in determining maturity of these species, for example due to a resting phase or early sperm production (Conrath, 2005).

Third, the asymptotic maximum length utilized here could have been underestimated. The length at maximum tissue production, L_i, is directly linked to L_∞, i.e., the larger the L_∞ the larger the L_i. When utilizing the observed maximum length instead of L_∞ to estimate the length at maximum tissue production, L_i, the gap between L_m and L_i was narrower, which could suggest underestimation of L_∞ (Fig. 5.3). However, the expected asymptotic maximum length based on the relationship between L_∞ and the observed maximum length from 551 marine fish (Froese and Binohlan, 2000), was relatively similar to the here utilized asymptotic maximum length for most populations, and not significantly different (Fig. 5. 5). This, together with the fact that most growth parameters came from populations where approaches have been applied to validate annual ring formation, might suggest that the asymptotic maximum lengths utilized in the present study were largely unbiased.

Yet, given the small sample size in the present study, future studies based on high quality growth and maturity information are needed to confirm that $L_m < L_i$ in elasmobranchs.

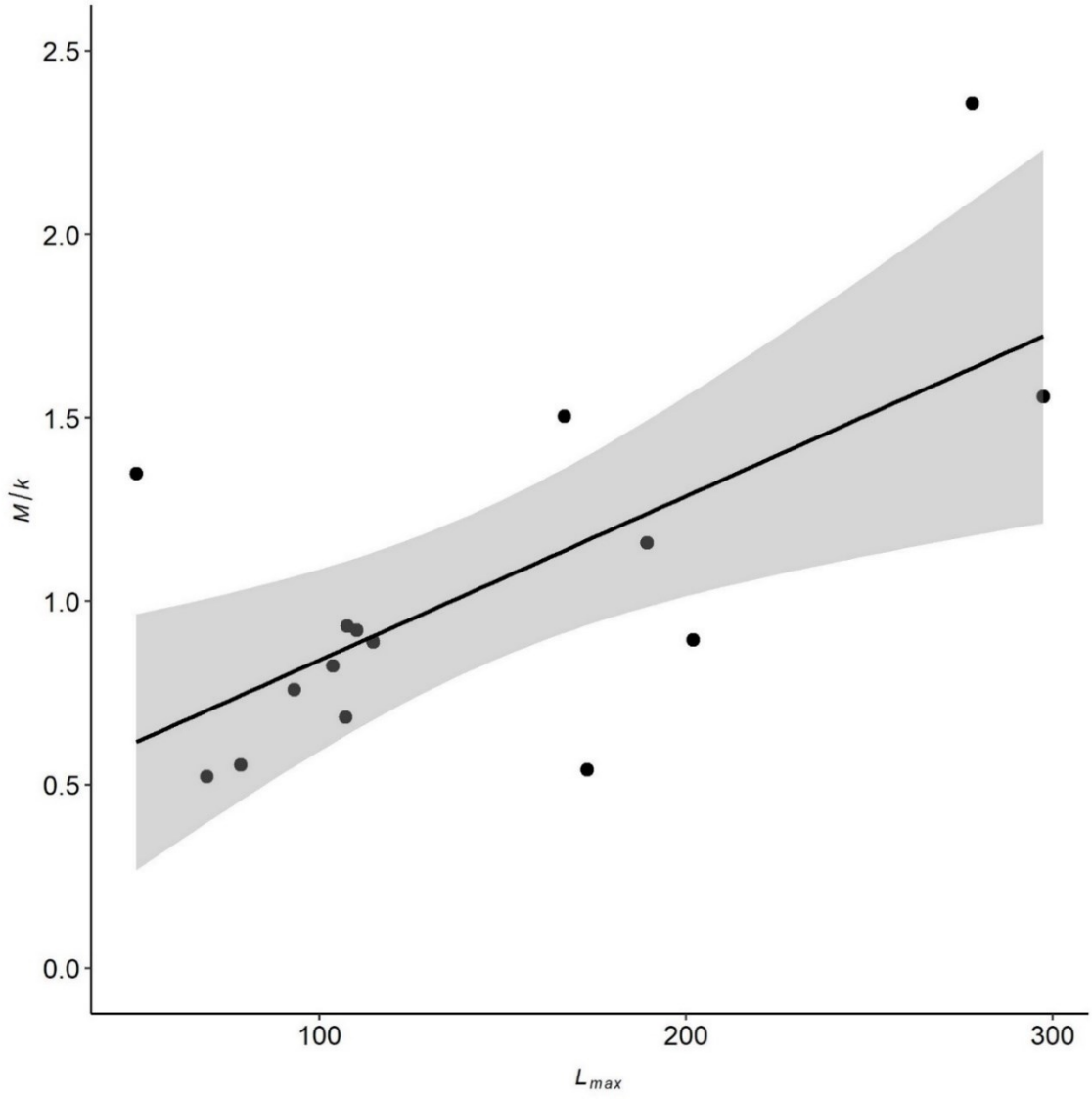

Fig. 5.4: The *M*/*k* ratio versus observed maximum length of the investigated elasmobranchs. Observed ratios of natural mortality, *M* (year^{-1}), over the von Bertalanffy growth constant, *k* (year^{-1}), versus the observed maximum length, L_{max} (cm). A linear trend line is shown (black) with 95% confidence intervals (shaded grey).

Table 5.2: Comparison of growth and maturity information for 11 North Atlantic elasmobranchs. Shown are the von Bertalanffy growth parameters L_∞ (cm) and k (year^{-1}), obtained from mark-recapture tagging data via a Bayesian implementation of the Fabens (1965) method with informative priors (Chapter 3). The associated exponent of the length-weight relationship, b, the length at first maturity (cm) and length where 50% of the individuals in the cohort are mature, L_m, were obtained from literature. The length at maximum tissue production, L_i, was calculated via $L_i = L_\infty(1 - \frac{1}{b})$ (Jensen, 1985).

Species	Location	L_∞	b	*First maturity*	L_m	L_i	Source
Amblyraja radiata	North Sea	69.7	3.0	31	32	46	Mccully et al (2012)
Dipturus batis	North Sea and Celtic Sea	240.4	3.2	120	130	165	McCully et al (2012)
Isurus oxyrinchus	North Atlantic	352.4	3.1	230	254	240	Stevens (2008); Natanson et al (2006)
Lamna nasus	Western North Atlantic	335.2	3.0	175	200	222	Aasen (1961), Kohler et al (1996)
Leucoraja naevus	Celtic Sea	73.1	3.1	50	59	50	McCully et al (2012)
Prionace glauca	North Atlantic	348.7	3.1	201	219	237	Pratt (1979); Kohler et al (1996)
Raja brachyura	North Sea and Celtic Sea	119.6	3.3	58	81	83	McCully et al (2012)
Raja clavata	North Sea and Celtic Sea	106.2	3.2	47	72	73	McCully et al (2012)
Raja microocellata	North Sea and Celtic Sea	92.7	3.2	70	73	64	McCully et al (2012)
Raja montagui	North Sea and Celtic Sea	73.6	3.1	45	57	50	McCully et al (2012)
Squalus acanthias	Northeast Atlantic	97.9	3.1	60	71	66	Dureuil (2013)

Table 5.3: Relative length at maximum cohort biomass, growth and alternative maturity information for the investigated elasmobranchs. Given are Sex (female, F, male, M, combined, C), the observed ratio of optimum length over the asymptotic maximum length, L^*_{opt}/L^*_{∞}, the exponent of the length-weight relationship, b, the literature von Bertalanffy asymptotic maximum length, L_{∞} (cm), the observed maximum length, L_{max} (cm), the length at maximum tissue production calculated after Jensen (1985) and obtained from either L_{∞}, $L_{iL\infty}$,or L_{max}, L_{iLmax}, and alternative values for the length at maturity, L_{mature} (cm). The length at maturity is generally shown as length at 50% maturity from alternative studies or areas, but the same populations, or from different populations of the same species (*), as minimum estimates over various methods or time periods (**), or as smallest mature individual (***).

Scientific name	Sex	L^*_{opt}/L^*_{∞}	b	L_{∞}	L_{max}	$L_{iL\infty}$	L_{iLmax}	L_{mature}	Source
Carcharhinus limbatus	F	0.76	2.87	169.8	201.9	110.6	131.6	120.0	Ebert & Stehmann (2013)
	M	0.71	2.87	155.9	189.2	101.6	123.3	116.5	Carlson et al (2006)
Carcharhinus plumbeus	C	0.56	2.97	274.8	278.0	182.3	184.4	155.5	Table 1
Rhizoprionodon taylori	F	0.85	3.13	73.3	78.4	49.8	53.3	45.0	Stevens & McLoughlin (1991)
	M	0.86	3.13	65.2	69.1	44.4	47.0	43.0	Stevens & McLoughlin (1991)
Sphyrna tiburo	F	0.80	3.59	105.8	110.0	76.3	79.4	77.0	Lombardi-Carlson (2007)
	M	0.83	3.59	84.7	93.0	61.1	67.1	65.5	Lombardi-Carlson (2007)
Galeorhinus galeus	C	0.85	3.18	161.3	173.0	110.5	118.5	110**	McCord (2005)
Mustelus antarcticus	C	0.67	3.09	170.3	166.7	115.2	112.8	96.4*	Walker (2007)
Heterodontus portusjacksoni	C	0.78	3.15	116.1	114.5	79.2	78.1	75*	Powter & Gladstone (2008)
Lamna nasus	C	0.66	2.96	280.0	297.4	185.5	197.0	175***	Aasen (1961)
Urolophus paucimaculatus	C	0.70	3.21	50.1	50.0	34.5	34.4	32.5	Table 1
Leucoraja ocellata	C	0.78	3.32	94.1	107.5	65.8	75.1	65***	McPhie & Campana (2009)
Squalus acanthias	C	0.80	3.22	95.0	103.5	65.5	71.3	59.5	Nammack et al (1985)
Squalus suckleyi	M	0.82	3.09	91.9	107.0	62.2	72.4	62***	Bonham et al (1949)

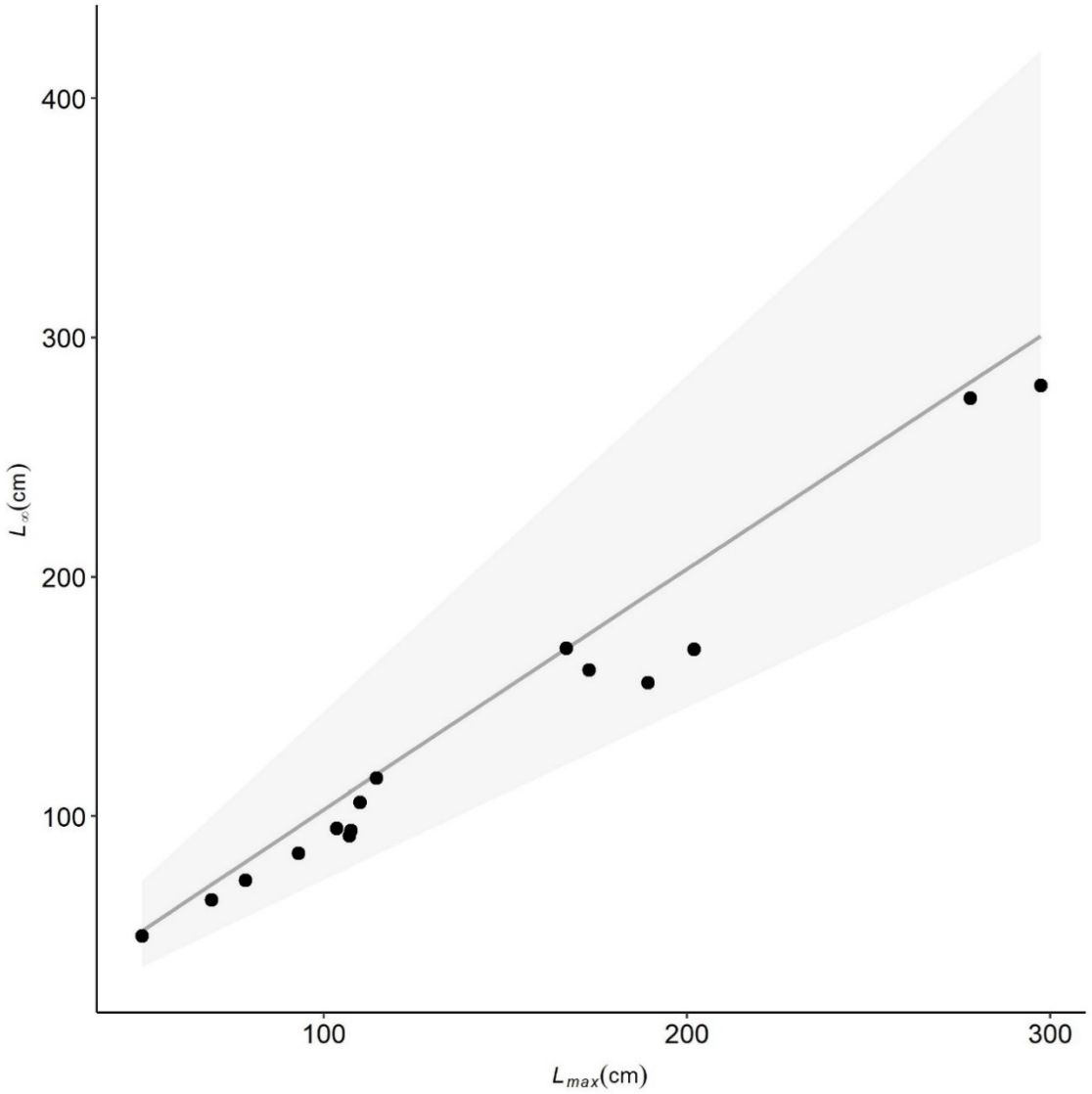

Fig. 5.5: Expected versus observed asymptotic maximum length of the investigated elasmobranchs. Observed asymptotic maximum length, L_∞ (cm), versus the observed maximum length, L_{max} (cm). The grey line shows the expected L_∞ based its relationship to L_{max} for 551 marine fish (Froese & Binohlan, 2000), with 95% confidence intervals (shaded grey).

The importance of answering the above addressed questions can be seen by the many practical applications of the *M*/*k* ratio. For example, the length at maximum age is directly linked to *M*/*k* (Hordyk et al., 2015). In Chapter 4, it was shown that maximum age can generally be estimated from L_∞ and *k* via $t_{max} = \frac{1}{k} * log_e\left(\frac{(L_\infty - L_0)}{(L_{tmax} * L_\infty)}\right)$, where L_0 is the length at birth and L_{tmax} is the length reached at maximum age, with $L_{tmax} = xL_\infty$, and x = 0.991. If the *M*/*k* ratio equals 1.5 then $L_{tmax} = 0.95L_\infty$, a value for x suggested by others (Taylor, 1958), but not empirically supported for elasmobranchs (Chapter 4). The variability in the *M*/*k* ratio observed here and elsewhere means that the approach with a constant L_{tmax} can only be considered a median solution across species. However, if an estimate of *M*/*k* is present, and assuming that the percentage of the initial individuals surviving to maximum age, *P*, is between 1 – 2% (Chapter 4), an improved estimate of maximum age for elasmobranchs might be derived from an estimated L_{tmax} via the formula provided by Hordyk et al (2015):

$$L_{tmax} = 1 - P^{\left(\left(\frac{t}{tmax}\right) * \left(\frac{k}{M}\right)\right)} * L_\infty \approx 1 - 0.015^{\left(1/\left(\frac{M}{k}\right)\right)} * L_\infty. \quad (5.7)$$

Furthermore, the findings here suggest that some elasmobranchs have relatively high L_m/L_∞ ratios (Fig. 5.1), which would be indicative that juvenile harvesting is generally posing a greater risk of population depletion in elasmobranchs than removal of the adults (Gallucci et al., 2006). Yet, as argued above, the sample here is rather incomplete and not representative for large species. Nevertheless, growing until reaching maturity is important to ensure biologically functional population structures and to avoid decreasing population productivity (Froese et al., 2016; Kindsvater et al., 2016). The minimum length below which fishing mortality (including bycatch) should be avoided, so that biomass is high and age structures are similar to unfished populations, is called the optimum length at first capture, L_{copt}, and can be estimated from the *M*/*k* ratio (Froese et al., 2016) via:

$$L_{copt} = 3.2L_\infty/(1.4 * \left(3 + \frac{M}{k}\right)), \quad (5.8)$$

assuming that a fishing mortality, *F*, of 0.4*M* would be sustainable in elasmobranchs (Zhou et al., 2012).

Moreover, the *M*/*k* ratio can also be used as input in data-poor stock assessment approaches, such as in a recently developed length-based Bayesian biomass method (LBB) (Froese et al., 2018, 2019) or in other length-based approaches (Pauly & Soriano, 1986; Pauly & Morgan, 1987; Gallucci et al., 1996; Hordyk et al., 2015; Huynh et al., 2018).

To conclude, the findings here suggest that the *M*/*k* ratio might be approximated from length at maturity, L_m, and L_∞ or L_{max}, equations (5.5 and 5.6). If *b* is unknown weight may

be assumed proportional to length with an exponent of $b = 3$ (Froese, 2006). However, the results should be treated with much caution, because the limited information utilized here may not display a representative sample for all elasmobranchs. According to the findings of this study, the M/k ratio would increase with maximum length. Given the median maximum length of 110 cm in the present data, it is therefore likely that many elasmobranch species would have higher M/k ratios than reported here. Indeed, higher M/k ratios have been reported for elasmobranch species elsewhere (Pierce et al., 2015), but largely on the basis of indirectly estimated natural mortality rates. If the M/k ratio would be, on average, higher in elasmobranchs compared to bony fish, differences in growth may exist, assuming that natural mortality rates are similar between those taxa (Chapter 4). Future studies may use the enhanced estimators (Chapter 3, 4) to obtain the M/k ratio for more species, in order to address the here raised open questions.

Chapter 6
Elevated trawling inside protected areas undermines conservation outcomes in a global fishing hotspot

6.1 Abstract

Marine protected areas (MPAs) are increasingly used as a primary tool to conserve biodiversity. This is particularly relevant in heavily exploited fisheries hotspots such as Europe, where MPAs now cover 29% of territorial waters, with unknown effects on fishing pressure and conservation outcomes. Here we investigate industrial trawl fishing and sensitive indicator species in and around 727 MPAs designated by the European Union. We find that 59% of MPAs are commercially trawled and average trawling intensity across MPAs is at least 1.4-fold higher compared to non-protected areas. Abundance of sensitive species (sharks, rays and skates) decreased by 69% in heavily trawled areas. The widespread industrial exploitation of MPAs undermines global biodiversity conservation targets elevating recent concerns about growing human pressures on protected areas worldwide.

6.2 Introduction

In light of mounting anthropogenic pressures, spatial protection of sensitive habitats and species has emerged as a leading strategy to halt ongoing biodiversity loss, both on land and in the sea (Worm, 2017). However, it has been shown recently that about one third of terrestrial protected areas experience intense human pressure, potentially undermining global conservation targets and sustainable development goals (Jones et al., 2018). Here we ask to which extent this conflict may also occur in the ocean, using newly available satellite sensors that allow fine-scale real-time quantification of industrial fishing effort from space (Kroodsma et al., 2018). We focus on Europe, which is both a global hotspot of industrial fishing (Kroodsma et al., 2018), and features extensive marine protected area (MPA) networks covering 29% of European Union (EU) territorial waters (European Union, 2016).

According to International Union for the Conservation of Nature (IUCN) guidelines, MPAs should be managed primarily for biodiversity conservation objectives (Day et al., 2012), and exclude environmentally damaging industrial activities in any of their six protected-area categories (WCC-2016-Rec-102-EN, 2016); see Table F1. With respect to

Dureuil, M., Boerder, K., Burnett, K. A., Froese, R., & Worm, B. (2018). Elevated trawling inside protected areas undermines conservation outcomes in a global fishing hot spot. Science, 362(6421), 1403-1407. https://science.sciencemag.org/content/362/6421/1403

commercial fisheries in MPAs, recent IUCN guidelines clarify that “any fishing gear used should be demonstrated to not significantly impact other species or other ecological values” (IUCN, 2018). In the EU a variety of different MPA types exist; while they may or may not adhere to non-binding IUCN criteria (Table F1), all feature biodiversity protection as a cross-cutting objective (Table F2), and contribute towards international conservation targets (Reker et al., 2015). Yet, many MPA types do not address commercial fisheries, which are often regulated under the EU Common Fisheries Policy (Table F2).

By far the most common industrial fishing method in Europe is trawling (Kroodsma et al., 2018), targeting mainly bottom-associated fishes, often with a high rate of unwanted bycatch (Fig. F1). This fishing technique has been identified as a threat to many endangered species in Europe, including most elasmobranchs (sharks, rays and skates) (www.redlist.org), and has well-documented impacts on seafloor biodiversity (Thrush & Dayton, 2002), sensitive habitats and indicator species (Cook et al., 2013). Here we directly quantify the extent of commercial trawling in the EU with respect to MPAs. We investigate associated changes in biodiversity using elasmobranchs as indicator species, because they are particularly vulnerable to industrial exploitation and bycatch (Dulvy et al., 2014; Fernandes et al., 2017), have one of the highest extinction risk among marine fishes in Europe (Nieto et al., 2015; Fernandes et al., 2017), and are generally not targeted by EU MPAs (Table F2).

6.3 Materials and methods

Commercial trawling effort in the EU was quantified from Automatic Identification System (AIS) vessel tracking data at grid cells of 0.01°x0.01° resolution for the year 2017, using a neural network algorithm with 98% precision when run on test data (Kroodsma et al., 2018). AIS is legally required for all EU industrial fishing vessels larger than 15m, accounting for 94% of commercial trawling effort in our data. AIS data may miss some fraction of smaller artisanal boats, rendering our estimates of trawling effort conservative. All 727 MPAs included in our study were classified as 100% marine (no terrestrial components), were designated before 2017, and are registered in the World Database on Protected Areas, thus counting towards international biodiversity conservation targets.

6.4 Results and discussion

We found that trawling effort concentrated along coastlines of continental Europe and the United Kingdom (Fig. 6.1A), a pattern that is consistent with other data sources

(ICES, 2016, 2017a; Eigaard et al., 2017). Aggregate commercial effort exceeded one million hours of trawling in 2017, with more than 225,000 hours occurring inside MPAs (Table 6.1). Trawling intensity (hr km^{-2}) across the entire MPA network was 38% higher inside MPAs compared to unprotected areas (Fig. 6.1A; Table 6.1) and 46% higher inside MPAs when comparing trawling intensity per trawled area (Table 6.1). This suggests that MPAs do not reduce fishing pressure under current management.

Elevated trawling intensity inside MPAs was especially pronounced in large-scale EU-wide MPA types, whereas untrawled MPAs were often small and designated by individual countries (Figs. 6.1C; 6.1D; F2). Of all 727 MPAs, 489 were located in territorial waters (inside 12 nautical miles, 67%).

The MPAs with highest commercial trawling effort were typically located along the continental coastline (Fig. F3), were recently designated, and in IUCN categories II or V (Fig. F4). No trawling effort was detected in 295 of the 727 MPAs considered in this study, implying that at least 59% of MPAs experienced commercial trawling. Of these 295 MPAs 171 were located in territorial waters. MPAs with no commercial trawling were generally smaller, older and had some IUCN category assigned; yet only 40% had management plans compared to 60% of commercially trawled MPAs (Table F3).

We addressed the cited IUCN criterion regarding fishing impacts on other species and ecological values (IUCN, 2018) by assessing elasmobranchs inside and outside of MPAs, and over time. Randomized scientific trawl surveys by the International Council for the Exploration of the Sea (ICES) were utilized to estimate relative abundance for 20 elasmobranchs species (Table F4) from 1997-2016. Only surveys with gear types and depth appropriate to catch these species were considered. Data were normalized to avoid any one species dominating aggregate indices.

Elasmobranchs were generally rare across the study area, particularly in heavily trawled areas (Fig. 6.1B). The primary aggregations west and south of the British Isles are in agreement with previously described hotspots (Ellis et al., 2005), and British MPAs also had the highest abundance of elasmobranchs (Figs. 6.1E; F5). Elasmobranchs were caught in 141 (79 %) of the 178 MPAs scientifically surveyed by ICES. Remarkably, total elasmobranch catch per research haul was 2.3-fold higher outside MPAs than inside (Fig. 6.1B; Table 6.1) and a normalized multispecies abundance index was 24% higher outside of MPAs (Table 6.1). This conservation paradox was especially pronounced for endangered and critically endangered species, which were all ≥5-fold more abundant outside MPAs (Fig. 6.2). Size, age, and management attributes of MPAs are all thought to drive conservation

outcomes (Edgar et al., 2014). Yet under current fishing pressure, only MPA size showed a positive trend with relative elasmobranch abundance in our study area (Fig. F6). No pattern emerged between elasmobranch abundance and the age of the MPA, whether it was classified according to the IUCN categories, or had a management plan (Fig. F7). Of the 178 MPAs scientifically surveyed only 24 (or 13%) had no commercial trawling present, and in 10 of those MPAs elasmobranchs have been reported. These untrawled MPAs had indeed higher average elasmobranch abundance compared to commercially trawled MPAs (Fig. F8). Overall, elasmobranch abundance decreased with increasing trawling intensity both inside (Fig. F9) and outside MPAs (Fig. F10).

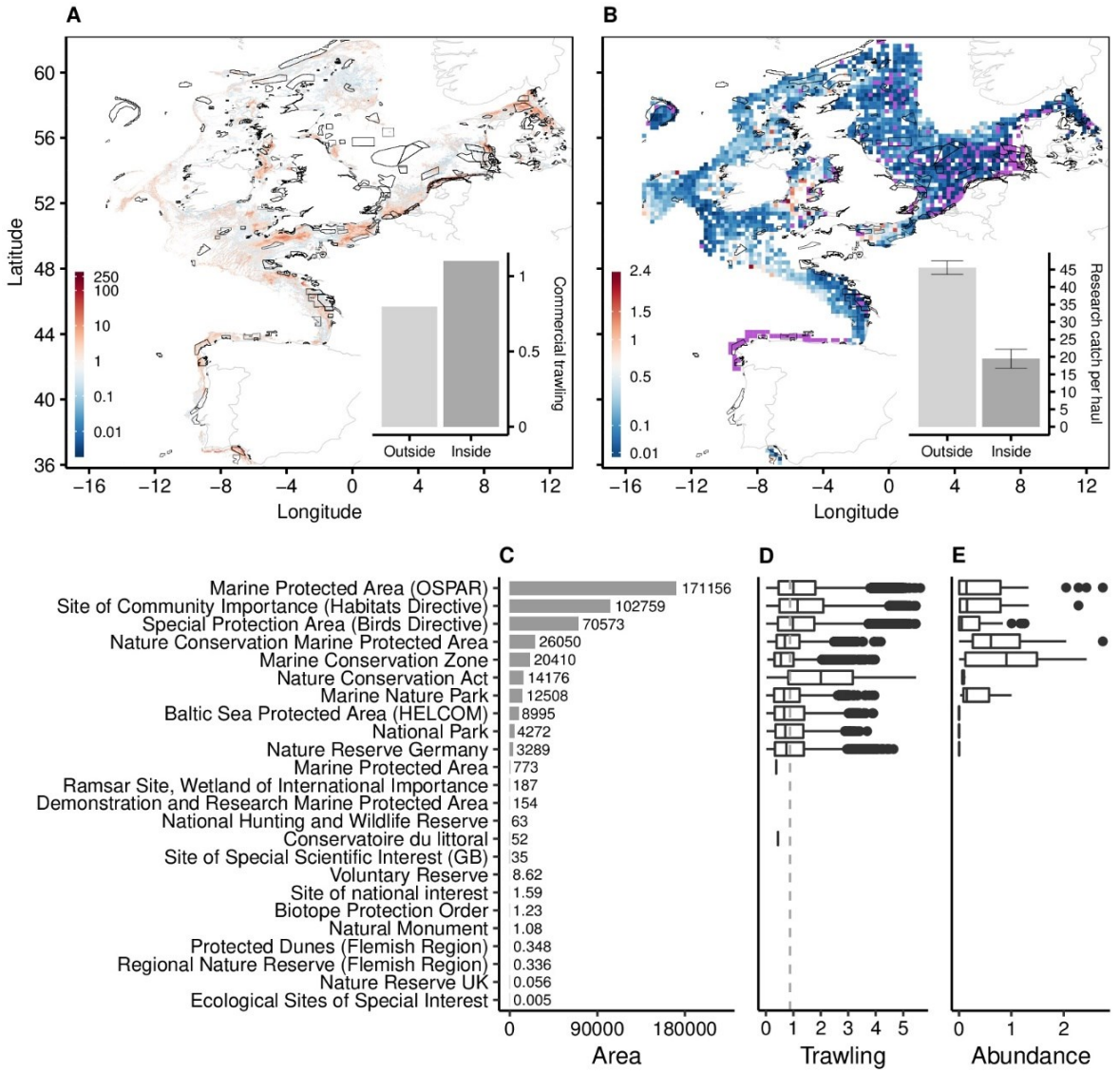

Fig. 6.1: Spatial distribution of marine protected areas, commercial trawling and elasmobranchs in the European Union. A) Commercial trawl fishing hours per 0.01 x 0.01 grid cell in 2017 (log_{10} color scale). Existing marine protected areas (MPAs) as of 2016 are outlined with black borders. (Inset) Aggregate commercial trawling intensity (hours per square kilometer) across MPAs versus unprotected areas. **B**) Elasmobranchs scientific survey abundance expressed as normalized multispecies catch per unit effort per 0.25° × 0.25° grid cell (square-root transformed color scale). Grid cells in purple were surveyed, but no elasmobranchs were present. (Inset) The total elasmobranch research catch per haul inside versus outside MPAs, with 95% confidence limits. **C)** MPA area (square kilometers), **D)** commercial trawling intensity per trawled area (log_e hours per square kilometer trawled) and **E)** elasmobranch abundance index for each MPA type. The grey dotted line in D) indicates the median commercial trawling intensity in nonprotected areas for reference. No data in E) indicates MPA types that were not scientifically surveyed.

Table 6.1: Commercial trawling effort and elasmobranch catch from research surveys inside and outside of MPAs. Commercial trawling is given in hours for the year 2017. Grid cells encompass 0.01° longitude by 0.01° latitude. Research catch from scientific surveys is given for the years 1997 – 2016 in total number of elasmobranch specimens per 60 min haul duration. The abundance index is given as normalized total multi-species catch per unit effort (msCPUE). Area (km^2) and commercial trawling hours for MPAs were calculated by subtracting the non-protected area or hours from the total study area or hours, to avoid multiple counts for MPA types whose areas overlap.

	Outside MPAs	Inside MPAs	Total study area
Commercial trawling hours	848,703	227,718	1,076,421
Area (km^2)	1,063,533	206,674	1,270,207
Number of 0.01°cells commercially trawled	335,167	57,085	392,252
Commercially trawled area (km^2)	252,886	43,812	296,698
Commercial trawling (hr km^{-2})	0.80	1.10	0.85
Commercial trawling (hr 0.01°$cell^{-1}$)	2.53	3.99	2.74
Commercial trawling (hr km^{-2} trawled area)	3.56	5.20	3.63
Research catch (number of elasmobranchs)	1,142,533	94,419	1,236,952
Research effort (number of hauls)	25,092	4,850	29,942
Total research catch per haul	45.53	19.47	41.31
Abundance index (msCPUE)	15.76	12.70	28.46

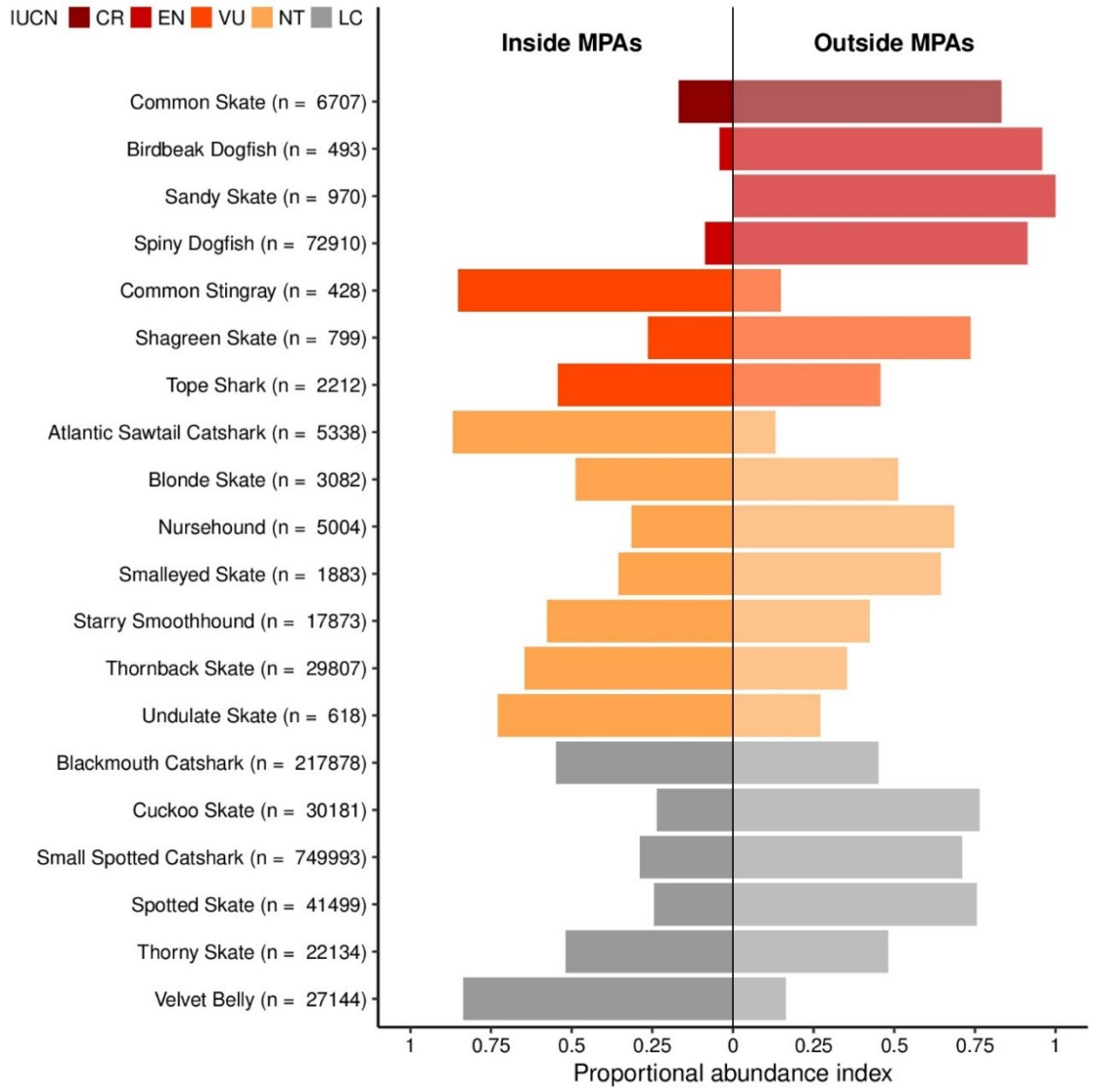

Fig. 6.2: Abundance of threatened species in relation to marine protected areas. Proportional scientific survey catch per unit effort is given for each elasmobranch species inside versus outside marine protected areas (MPAs). The sample size for each species is given in brackets. Colors represent the International Union for Conservation of Nature (IUCN) Red List status per species (CR = critically endangered, EN = endangered, VU = vulnerable, NT = near threatened, LC = least concern).

After controlling for spatial autocorrelation and potentially confounding effects of habitat and climate we found that commercial trawling was the strongest predictor of elasmobranch relative abundance across the study area ($p<0.001$; Fig. 6.3A; Table F5) with an average decrease of 69% across the observed gradient of trawling intensity (0 - 6.4 hr km^{-2}). Analyzing this relationship over time, we detected no trend in relative elasmobranch abundance in areas with high trawling intensity, but higher and increasing abundance in areas with low trawling intensity (Fig. 6.3B). These results further support the notion that elevated trawling effort in MPAs negatively impacts sensitive species and ecological values, and is thus conflicting with IUCN criteria.

To summarize, these data demonstrate that simply designating areas as MPAs has little benefit for those species that require protection the most. The fact that most major EU MPA types exhibit high trawling intensity (Figs. 6.1D; F2) and do not address industrial fishing (Table F2) leaves protected zones vulnerable to fishing effort aggregation and associated biodiversity impacts documented here. Our finding that 59% of studied MPAs are fished industrially exceeds recently documented shortfalls on land where 33% of protected areas are exposed to undue human pressures (Jones et al., 2018). A sectoral approach whereas marine conservation measures are implemented by EU member states, but fisheries are managed by a Common Fisheries Policy may drive this apparent disconnect. Finally, the lack of transparent international MPA standards may further exacerbate this; we found that of 727 EU MPAs studied here >50% do not report a management plan, >90% are not classified according to IUCN criteria, and >99% have no information on no-take areas according to the World Database on Protected Areas. We suggest that better reporting and independent vetting of MPA standards is needed to assess the true value of the world's increasing MPA coverage.

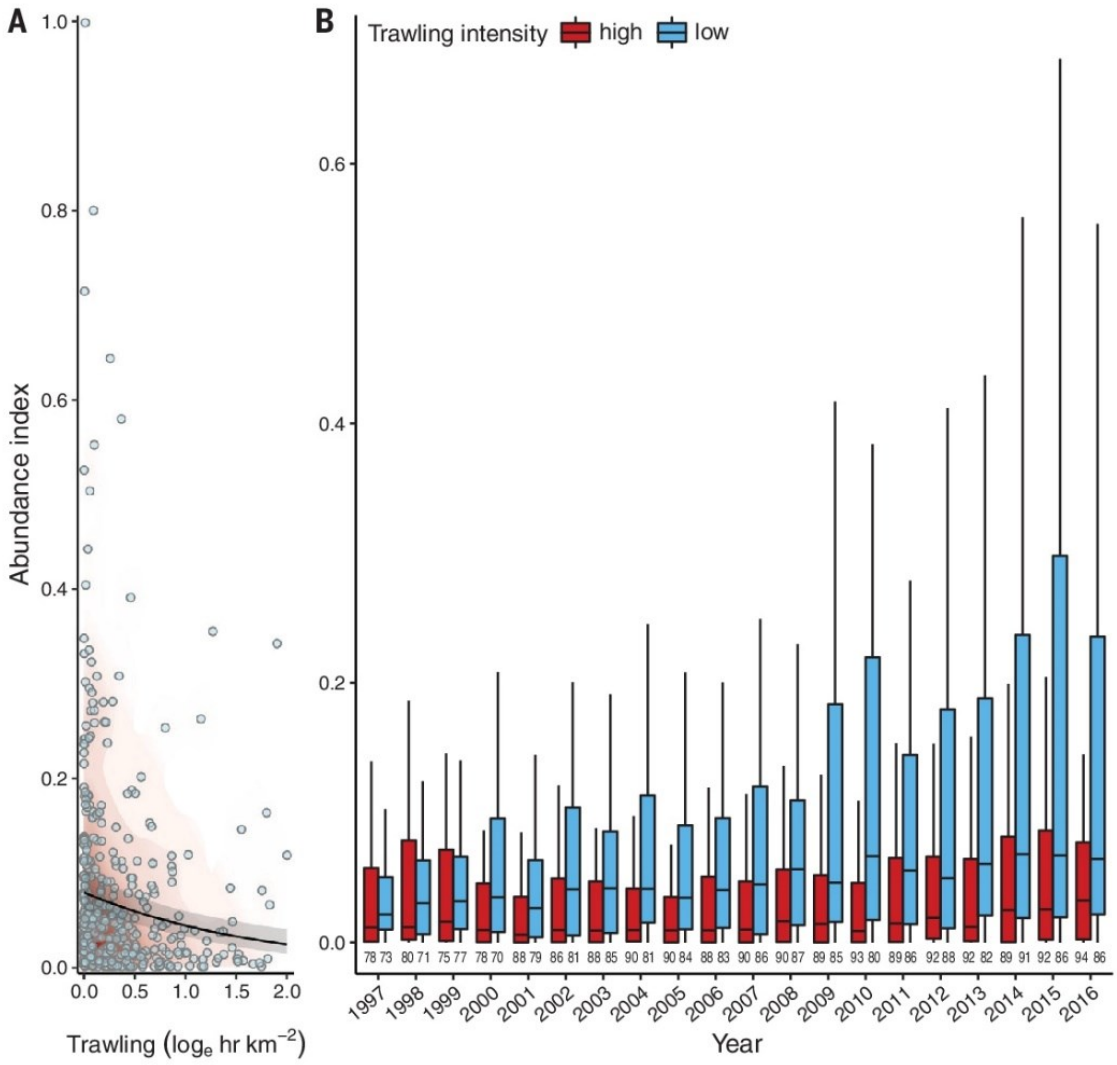

Fig. 6.3: Relationship between elasmobranch abundance and commercial trawling. A) Elasmobranch abundance index (scaled multispecies catch per unit effort) versus commercial trawling intensity (log_e +1 hr km^{-2}) for all 392 International Council for the Exploration of the Sea (ICES) statistical management areas scientifically surveyed over the study area. The black line shows the predicted relationship of relative abundance and commercial trawling intensity for the average temperature and depth across management areas with 95% confidence limits in grey (Table F5). Red shading visualizes the density distribution of data points. **B**) The temporal trend of elasmobranch multispecies catch per unit effort is shown in ICES statistical management areas, with high (upper quartile, ≥0.616 hr km^{-2}) versus low (lower quartile, ≤0.037 hr km^{-2}) commercial trawling intensity. Sample size of ICES statistical areas for each year is indicated below.

Our results suggest that much of the EU's spatially impressive MPA network is being impacted more heavily by industrial fishing than non-protected areas, and as such provides a false sense of security about positive conservation actions being taken. This is not an isolated occurrence, as data from terrestrial protected areas (Jones et al., 2018), and marine case studies from elsewhere suggest (Cramp et al., 2018; Magris & Pressey, 2018). Hence, internationally agreed-upon conservation targets under the Convention on Biological Diversity might be undermined by increasing human pressure, both on land and in the sea. Considerable work remains to be done to improve MPA policy, to develop and enforce minimum standards for MPA designation and classification, and to make MPA regulations and management stronger and more transparent. This would help to ensure that international targets for increased protected area coverage translate into tangible benefits for biodiversity conservation and the recovery of threatened marine wildlife.

Chapter 7
Conclusions

7.1 Main conclusions

The overarching goal of this thesis was to evaluate vital components that are integral to the assessment, management, and conservation of elasmobranchs (sharks, rays and skates). Improvements and modifications of existing methodologies were presented in order to increase reliability and effectiveness for data-poor tools in stock assessments and spatial protection measures. The addressed vital components were mainly concerned with the species' life history (Chapters 2 – 5) and habitat protection (Chapter 6), which are important elements in many fisheries, management and conservation approaches.

Elasmobranchs comprise of some of the least understood but most threatened species on this planet (Dulvy et al., 2014), yet conventional methods to estimate growth and mortality have been found of limited value for these species, particularly in data-poor situations (Dureuil & Worm, 2015; Harry, 2017; Natanson et al., 2018; Chapter 2, 3, 4, 5). Likewise, it was shown that spatial protection measures, at least under current marine protected area (MPA) management in Europe are not likely to aid in the conservation of threatened elasmobranchs (Chapter 6). Given the unsustainable pressure of direct exploitation and incidental bycatch for many sharks, skates and rays (Stevens et al., 2000; Dulvy et al., 2014; Worm et al., 2013), their fast depletions (Baum et al., 2003) coupled with long recovery times (Ward-Paige et al., 2012), effective science-based management strategies are urgently needed to prevent local extirpations and foster recovery. Additionally, such strategies must build on new scientific assessments and conservation approaches suitable for data-poor situations, given the limited information available for many elasmobranchs. Unfortunately, a lot of research has concentrated on a form of data-poor approaches that still require substantial information such as catch data (Prince & Hordyk, 2018). This is because information on catch is essential in many stock assessment applications. However, catch data is highly uncertain for elasmobranchs with official landings often underreported as many species are caught as bycatch and discarded at sea (Stevens et al., 2000; Worm et al., 2013). Yet, a stock assessment combines both fisheries and biological processes, the latter describing the population dynamics throughout the life history of a species. Furthermore, there are new approaches to stock assessment that are independent of catch data, and other tools that can be utilized in data-poor situations to conserve and manage a species. Hence, elasmobranch research in this field should focus

on a) obtaining reliable estimates of vital life history parameters from limited observations to inform assessments and gain greater insights into species ecology and vulnerability; b) developing data-poor stock assessment methods that do not depend on reliable catch data; and c) investigate alternative data-poor management tools that are not based on reliable catch information. This thesis was concerned with a) and c), while b) is developed elsewhere (e.g. Froese et al., 2018, 2019, in review).

In Chapter 2 it was shown that it is possible to obtain biologically reasonable growth estimates for sharks from limited mark-recapture information. This was the first comparative study on different methods used to estimate von Bertalanffy growth parameters from tagging information for a shark species, considering previously unutilized methods and applying a combination of empirical and simulated data to find the most suitable approach. However, the finding that a fixed asymptotic maximum length improved parameter estimates suggests that prior information is needed in order to obtain reasonable estimates of growth parameters.

In Chapter 3, a Bayesian implementation of Fabens original method to estimate von Bertalanffy growth parameters from mark-recapture data was applied, which allowed the inclusion of prior information. This approach was rigorously tested on simulated data and on empirical information from 15 different elasmobranch stocks, then compared to a set of other promising methods. It was found that only the Bayesian implementation of the Fabens method performed reasonably well in all scenarios and for all stocks, even in cases with very few tagged individuals. Prior information was obtained from observed maximum length, which is available for many species, and it is suggested that this approach can be used as an alternative to conventional length-at-age methods in elasmobranch growth studies.

Chapter 4 was concerned with another vital population parameter, the natural mortality rate. It was shown that bony fish and elasmobranchs follow the same relationship between natural mortality and observed maximum age. Furthermore, it was confirmed that juvenile natural morality rate can be estimated under the assumption that natural mortality is inversely proportional to body length. On this basis, a new indirect natural mortality estimator was suggested that requires prior information on maximum age and allows for the estimation of juvenile natural mortality rates by utilizing a newly introduced length; the length after which natural morality can be assumed constant. The calculation of this length requires an estimate of the proportion surviving to maximum age, which was found to lie between 1% and 2%. In addition, the percentage of the asymptotic maximum length at maximum age was found to be at 99.1%, which can be utilized to obtain estimates of maximum age from

growth information. More generally, the results also indicated that many of the conventional methods give highly biased parameter estimates.

Chapter 5 investigated relationships between natural mortality, growth and reproduction, in order to facilitate the predictability of the ratio between natural mortality, *M*, over the von Bertalanffy growth constant, *k*. This is a vital parameter in length-based assessments and the understanding of a species life history strategy, and therefore particularly relevant in data-poor situations. The findings underpinned that the *M*/*k* ratio is variable across species but predictable from length at maturity and maximum length. This was suggested as an interim approach, as the results indicated that either the length at maturity and/or the asymptotic maximum length is commonly misestimated in elasmobranchs, or that there is a lack of understanding in life history theory with regards to these species. Still, applications for data-poor assessment, maximum age estimation, and estimation of a minimum length, below which human induced mortality should be avoided, were discussed.

In Chapter 6, marine protected areas were investigated to determine their current ability to assist in the spatial conservation of data-poor, and threatened species. specifically, 727 MPAs in the European Union were evaluated with regards to the abundance of elasmobranchs and the magnitude of industrial trawl fishing. The results showed that 59% of MPAs were commercially trawled with an average trawling intensity at least 1.4-fold higher across MPAs than compared to non-protected areas. Contrary, elasmobranchs were generally rare in MPAs, and elasmobranch abundance decreased by 69% in heavily trawled areas. This conservation paradox was even more pronounced for the most threatened elasmobranch species. The results therefore suggest that increasing protected area coverage is not enough to safeguard sharks, skates and rays, but that stronger and more transparent MPA protection standards are needed, in order to limit harmful industrial activities in protected areas in Europe and elsewhere. Such approaches should also be combined with improved data-poor assessments in order to adequately conserve these species.

To conclude, the findings reported in this thesis can help to improve stock assessments, gain greater insights into species ecology and vulnerability to exploitation, and inform the development of more effective spatial conservation measures.

7.2 Implications for elasmobranch ecology and conservation

This thesis has presented data-poor solutions to obtain vital life history parameters more reliably and has revealed current limitations in protected area management for elasmobranchs. In the following, implications of these findings for the ecology, conservation and management of elasmobranchs are discussed.

Harry (2017) pointed out that consequences from erred life history parameters can be rather complex: greater maximum ages would suggest lower natural mortality rates and thus lower productivity and resilience to exploitation, but longer lifespans can also lead to greater net reproductive rates which would suggest faster population doubling times and hence greater productivity. Ergo, the effect of overestimated or underestimated life history parameters on fitness measures of a species is not straightforward. For example, the net reproductive rate (the number of offspring over a female's lifetime), the generation time (the average age of a mother in a population) and the intrinsic rate of population increase are important fitness measures of a cohort. When estimating these three fitness measures following Simpfendorfer (2005) for four different elasmobranch species, the large but convoluted effect of biased life history parameters can be seen (Fig. 7.1). The intrinsic rate of population increase is more severely underestimated than overestimated, while the net reproductive rate is more severely overestimated than underestimated, when other life history parameters are biased. The generation time is largely unaffected. If maturity would occur earlier, the intrinsic rate of population increase and the net reproductive rate would be both be higher. Therefore, the current information on elasmobranchs life history and the relationships among ecological traits might be biased as well, given that it is not unlikely that misestimated life history information has been utilized for elasmobranch species in the past. Furthermore, biased life history information increases the risk of mismanagement of a species. Overestimated natural mortality rates can increase the likelihood of unintentional overfishing: positive bias in natural mortality translates into overestimated stock sizes (Cheilari & Rätz, 2009) and more optimistic reference points (Cheilari & Rätz, 2009; Maunder & Wong, 2011), but underestimated fishing mortalities (Cheilari & Rätz, 2009). This becomes more apparent when reminded that the fishing mortality equals the total mortality minus the natural mortality.

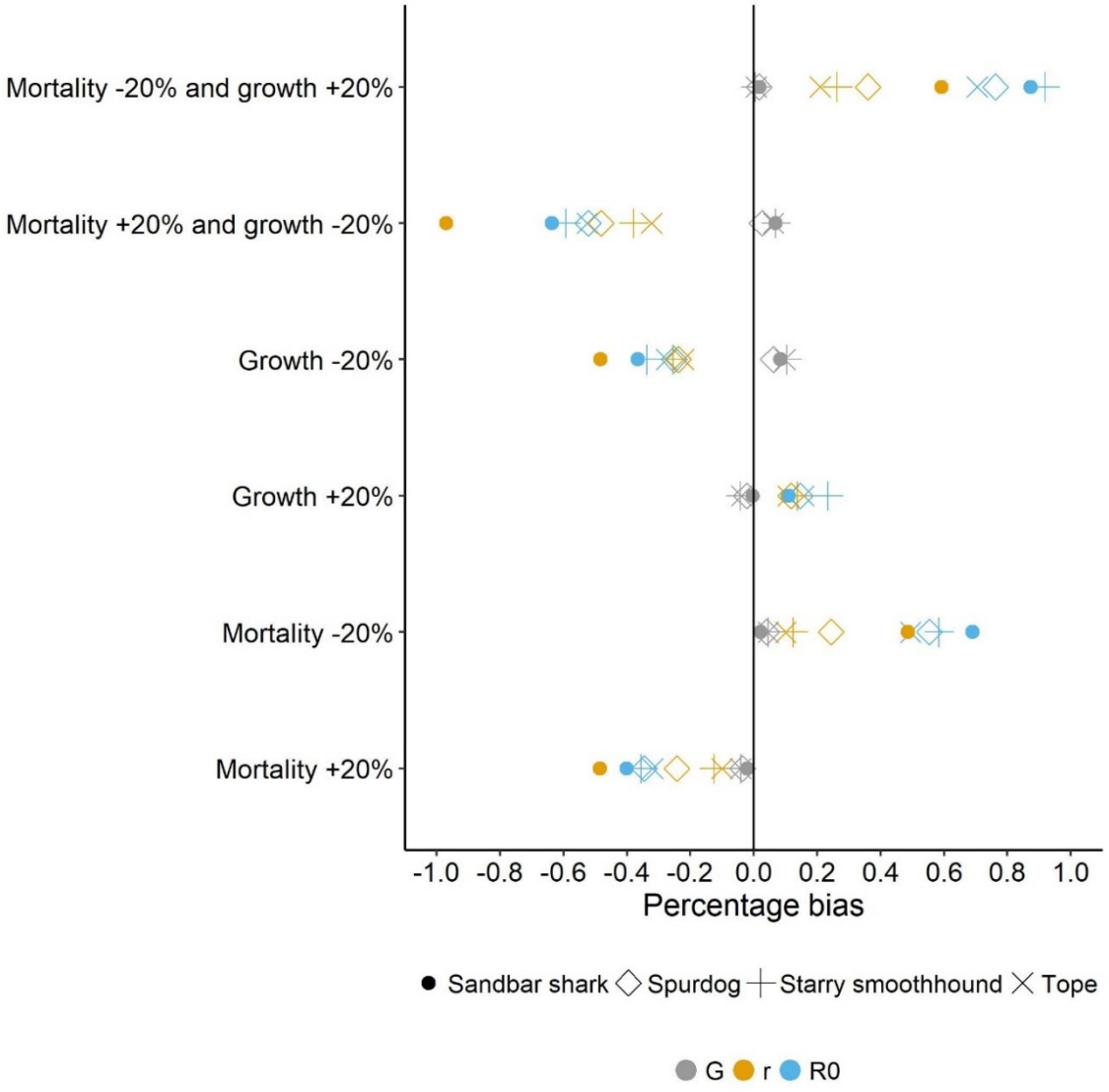

Fig. 7.1 Effect of biased life history parameters on elasmobranch fitness estimates. Shown are three fitness measures, net reproductive rate, *R0* (the number of offspring over a female's lifetime), generation time, *G* (the average age of a mother in a population), and intrinsic rate of population increase, *r*. The fitness measures were estimated from the Euler-Lotka equation following Simpfendorfer (2005). Life history information for sandbar shark (*Carcharhinus plumbeus*) was taken from McAuley et al (2007) and from Dureuil (2013) for spurdog (*Squalus acanthias*), starry smoothhound (*Mustelus asterias*) and tope (*Galeorhinus galeus*). An error of ± 20% was introduced in the natural mortality rate, *M*, and/or the von Bertalanffy growth constant *k*.

In cases where information is absent to estimate natural mortality and growth separately, their ratio might be estimated. The findings of this thesis suggest that this ratio is predictable in elasmobranchs, and thus can have important applications for the assessment of data-poor species. For example, this ratio can be used as an input parameter in novel length-based stock assessment methods (Froese et al., 2018, 2019). In this thesis, such an assessment was conducted for the Eastern Scotian Shelf and Newfoundland winter skate (*Leucoraja ocellate*), utilizing only length frequency information and information about the *M*/*k* ratio. It was found that the stock size (biomass) is overestimated with an invariant *M*/*k* ratio of 1.5, yet biomass estimates are very close to a full surplus production stock assessment model when the observed *M*/*k* of 0.9 was used (Fig. 7.2). Notably, surplus production models utilized information on observed catch data and biomass indices, yet reliable catch information is generally absent in many elasmobranch species, whereas a length-based Bayesian biomass estimation (LBB) utilized more commonly available length-frequency data. Although this is just one example, and in other instances an *M*/*k* ratio of 1.5 might be suitable, the Eastern Scotian Shelf and Newfoundland winter skate population is highly endangered (DFO, 2017), and therefore this shows the enormous potential and importance of such approaches for data-poor and threatened species. Moreover, estimates of the *M*/*k* ratio could be used in even more data-limited situations. It has been hypothesized that decreased juvenile survival has, in general the highest negative effect on elasmobranch populations (Gallucci et al., 2006). Here it was demonstrated how the *M*/*k* ratio could be utilized to estimate a minimum length below which a species should not experience human induced mortalities, a new reference point introduced by Froese et al (2016).

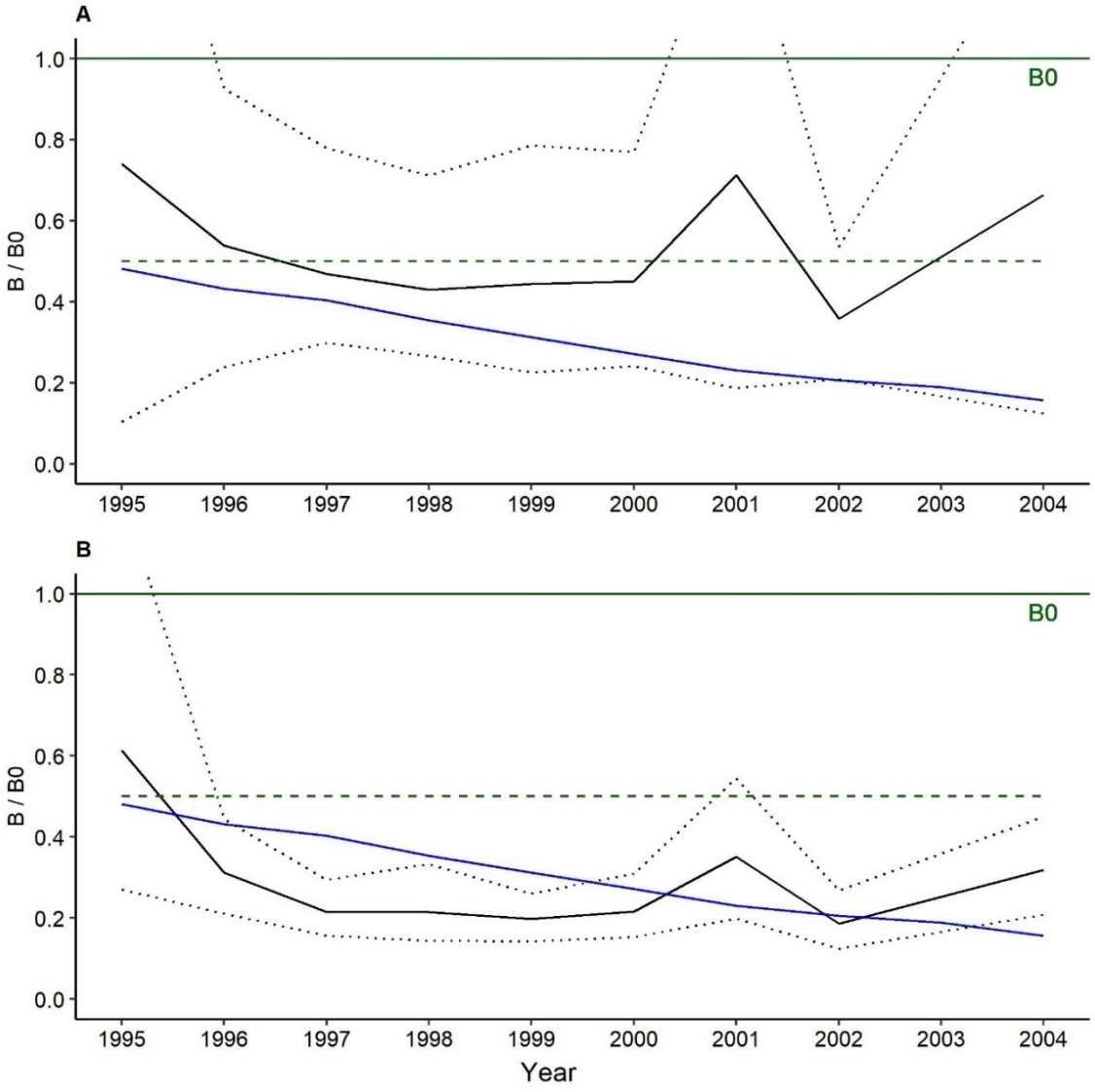

Fig. 7.2 Comparison of a data-poor and a full stock assessment for winter skate. Assessment results in biomass, *B*, over unfished biomass, *B0*, from a length-based Bayesian biomass estimation method (LBB) (Froese et al., 2018) from length frequency information (black line) and **A)** an assumed ratio of natural mortality, *M*, to the von Bertalanffy growth constant, *k*, of 1.5 or **B)** an the observed *M*/*k* ratio of 0.9. The black dotted lines indicate 95% confidence limits of LBB, the blue line shows the results of a full surplus production stock assessment (DFO, 2017). The green dotted line indicates the stock size that would enable maximum sustainable yield, *MSY*.

Yet, improved stock assessment approaches might only be of limited conservation and management success when applied isolated. In order to actually restrict fishing or bycatch mortality for data-poor species, additional approaches are needed. Spatial protection by marine protected areas can be applied as a complementary strategy where entire habitats are protected rather than a single species. There are numerous studies that have confirmed positive effects of MPAs on elasmobranchs (Garla et al., 2006; Claudet et al., 2010; Bond et al., 2012; Knip et al., 2012a; Le Port et al., 2012; Bond et al., 2017; Da Silva et al., 2013; Edgar et al., 2014; Espinoza et al., 2014; Escalle et al., 2015; Graham et al., 2016; Ward-Paige & Worm, 2017; White et al., 2017; Davidson & Dulvy, 2017; Speed et al., 2018; Boerder et al., 2019; Germanov et al., 2019; Carlisle et al., 2019). For example, well enforced, no-take, old, large and isolated MPAs on average report 20 times the shark biomass compared to fished areas (Edgar et al., 2014). However, it was shown here that many MPAs do lack strong protection standards that would be important to implement in order to benefit elasmobranch conservation. Foremost, MPAs should follow the International Union for Conservation of Nature (IUCN) guidelines and exclude industrial and harmful fishing practices.

To summarize, based on the findings reported here more elasmobranch populations could receive improved science-based management, even in very data limited scenarios, creating additional hope for one of the most endangered group of marine animals on this planet.

7.3 Future research directions

This thesis has generated some interesting and open questions that need to be addressed to further advance the conservation of elasmobranchs. Future research directions with regards to this thesis are discussed in the following. It is important to note that these directions do not reflect a complete inventory of available and suitable conservation tools for elasmobranchs. For instance, important measures such as bycatch mitigations or shark sanctuaries were not considered in this thesis, yet it is believed that the following would display important next steps.

This thesis showed that biologically reasonable information on elasmobranchs life history can be obtained from limited data, such as the von Bertalanffy growth parameters. In this specific case, an alternative is therefore provided to the many species where age and growth cannot be accurately determined (Harry, 2017; Natanson et al., 2018). It also adds to the non-lethal sampling toolbox for elasmobranchs, because vertebrae age readings

require dead specimens, whereas for mark-recapture studies the survival of the specimen is crucial to obtain the data. Furthermore, alternative tagging approaches such as photo identification can easily be paired with laser photogrammetry (Dureuil et al., 2015) to gather information needed to estimate growth from novel non-fishing censusing methods such as Baited Remote Underwater Video Systems (BRUVS). Next steps should also include further methodological development to investigate if approaches that account for individual variability in growth are applicable to the limited information available for most elasmobranchs, or if these are too complex. Likewise, alternatives to the classical von Bertalanffy growth model, such as the Gompertz or logistic growth model, should be formulated in a Bayesian mark-recapture framework to allow multimodal approaches (Smart et al., 2016). However, due to the importance of the von Bertalanffy constant, *k,* in many data-poor applications, biphasic models where, for example, growth is assumed linear for juveniles but to follow von Bertalanffy in adults (Lester et al., 2004), might be the most promising candidates that need to be investigated in a mark-recapture fashion for elasmobranchs. Based on these steps, an important ecological question could be addressed; do elasmobranchs grow significantly different from bony fish and are there different growth patterns among different elasmobranchs species? More generally, improved quality of life history parameter estimates will benefit the investigation of elasmobranchs and teleosts, or other taxa, and show fundamental differences in life history theory. In addition, a combination of different approaches should be applied to further increase the reliability of life history parameter estimates in data-poor situations. For example, estimates of the length at maturity could be verified by a comparison with length-weight information, because the increase in weight over length changes with the onset of maturation (Finucci et al., 2019).

Another field of future research direction to aid the conservation and management of elasmobranchs would be to investigate which data-poor stock assessment method performs best, given the input information available. This goes hand in hand with tailoring these assessment approaches more towards the data-poor and poor-data availability for elasmobranchs, including new techniques to minimize the effect of errors in the input data, for example resulting from biased length frequencies or catch per unit effort indices. This will lead to a greater number of elasmobranch species with more reliable assessments, hence allowing for a more rigorous investigation of which conservation measures have the most positive effect, and therefore foster the future development of more effective conservation strategies.

Finally, a more complete conservation strategy could be developed by a better integration of population assessments, fisheries management measures and spatial conservation approaches. Therein, the development of data-poor tools to assess suitability and critical elasmobranch habitat will become an important challenge. A crucial step within here will be a better understanding of the movement ecology of elasmobranchs, and more specifically the identification of species with similar habitat preferences. Advances in this field can have important applications, including identification of suitable habitat for restoration, reintroduction, monitoring, and/or the mitigation of bycatch. Furthermore, such approaches might be critical for ecologically distinct and globally endangered (EDGE) species, such as giant guitarfishes, which now belong to the most threatened elasmobranchs (Kyne et al., 2019). Given that these species are taxonomically and ecologically distinct, their life history might also be different, and the fact that they are threatened indicates that they are generally rare and likely data-poor. Hence, life history information might be more difficultly obtained and may not be borrowed from similar species. Yet, given the species status, suitable conservation strategies would need to be developed quickly to avoid further depletion and local extinction.

By answering these questions data-poor conservation and management of elasmobranchs will become an even more powerful and reliable tool, enabling science-based conservation strategies for many currently unmanaged species, including many small-bodied and deep-water sharks, as well as a skates and rays.

Appendix A
Supporting information for Chapter 2

Electronic supplement

The electronic supplement for Chapter 2 “Estimating growth from tagging data: an application to north-east Atlantic tope shark *Galeorhinus galeus*” gives further details on the outlier identification method, the detailed results of each simulation run from the selection procedure, and the full R code used to run the simulation analysis (selection procedure). The supplementary information can be downloaded from the publisher site: https://onlinelibrary.wiley.com/doi/abs/10.1111/jfb.12830

Appendix B

Supporting information for Chapter 3

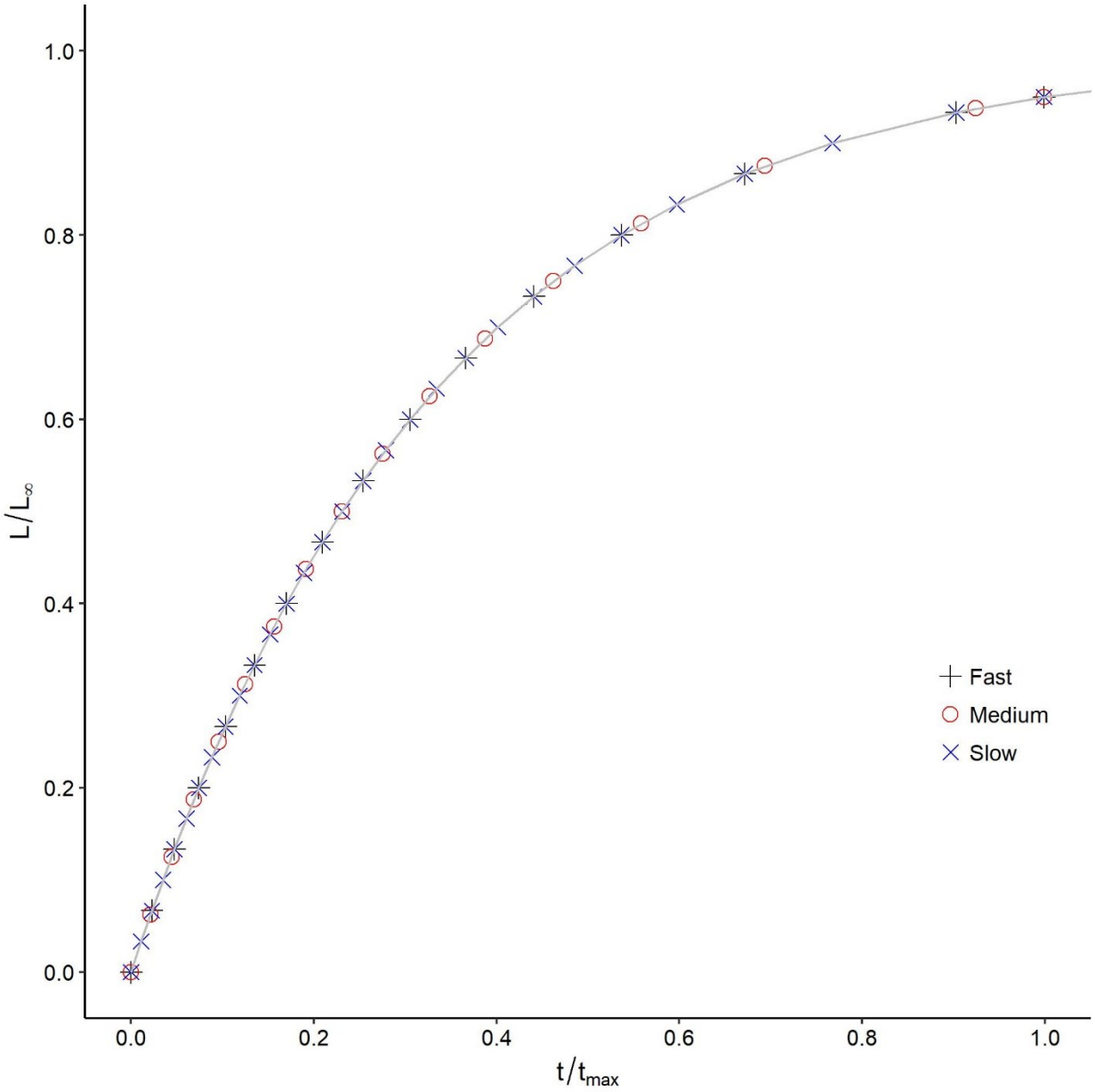

Fig. B1: Comparison of different hypothetical species with different von Bertalanffy growth trajectories. Standardized von Bertalanffy growth curves of species with different growth trajectories are shown. The asymptotic maximum length, L_∞, was set at 15 cm, 80 cm and 300 cm and the growth constant, k, was set at 0.9 year^{-1}, 0.4 year^{-1} and 0.05 year^{-1}, representing slow, medium and fast growth, respectively. The maximum age, t_{max}, was set at 3/k. The overlap of the data points shows that species with different growth trajectories have the same growth curves if they grow after the von Bertalanffy growth model.

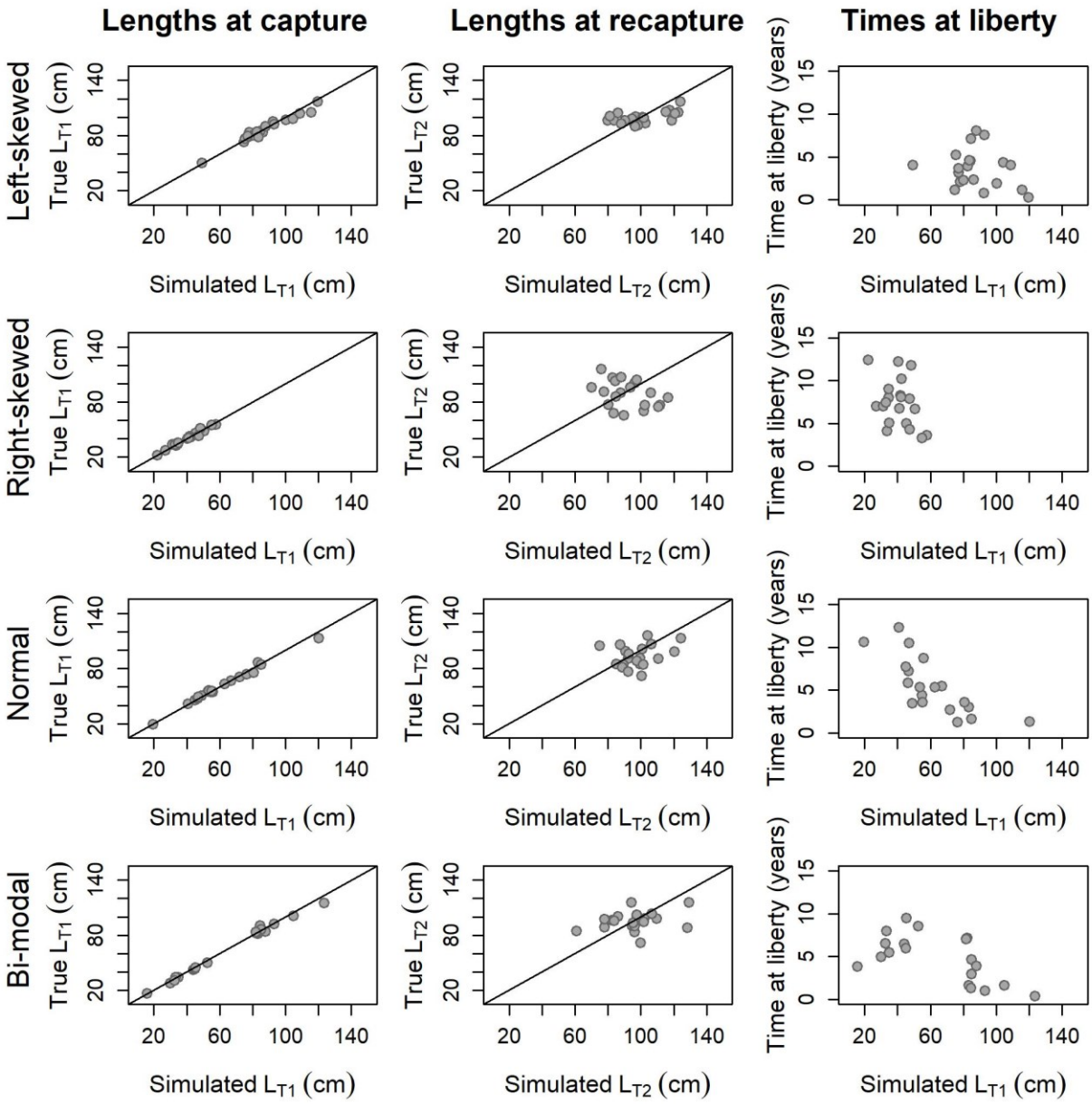

Fig. B2: Simulation design to mimic mark-recapture tagging data with long times at liberty. Shown are the lengths at capture (L_{T1}, left column), lengths at recapture (L_{T2}, middle column) and times at liberty (right column) under different length at capture distributions (rows). The black lines indicate the 1:1 line between the true lengths versus the simulated lengths where growth variability and measurement error were introduced. The negative correlation implemented between lengths at capture and the times at liberty is presented in the third column. All scenarios shown here were simulated with a sample size of 20 individuals and on average long times at liberty.

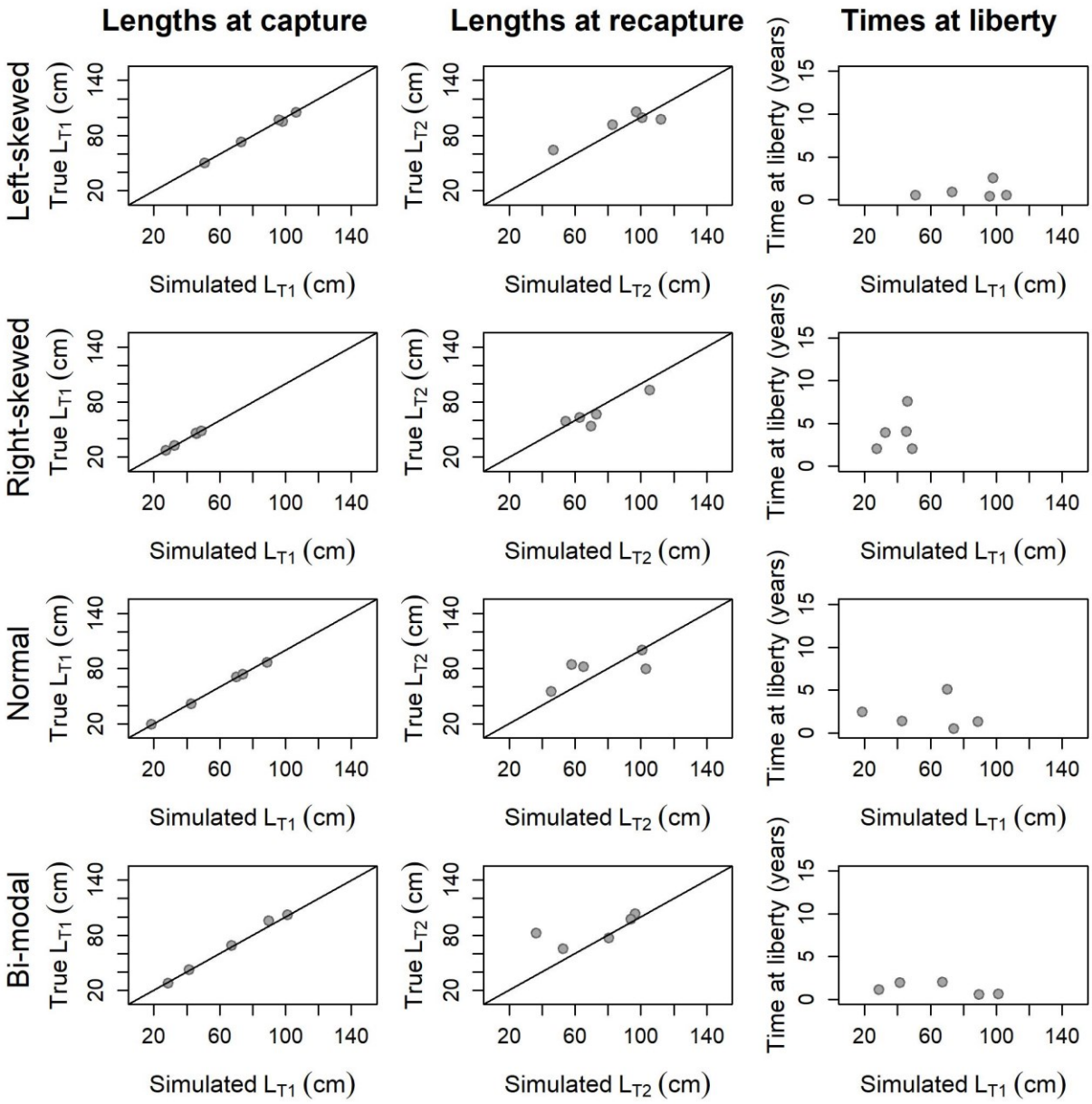

Fig. B3: Simulation design to mimic mark-recapture tagging data with small sample size and short times at liberty. Shown are the lengths at capture (L_{T1}, left column), lengths at recapture (L_{T2}, middle column) and times at liberty (right column) under different length at capture distributions (rows). The black lines indicate the 1:1 line between the true lengths versus the simulated lengths where growth variability and measurement error were introduced. The negative correlation implemented between lengths at capture and the times at liberty is presented in the third column. All scenarios shown here were simulated with a sample size of 5 individuals and on average short times at liberty.

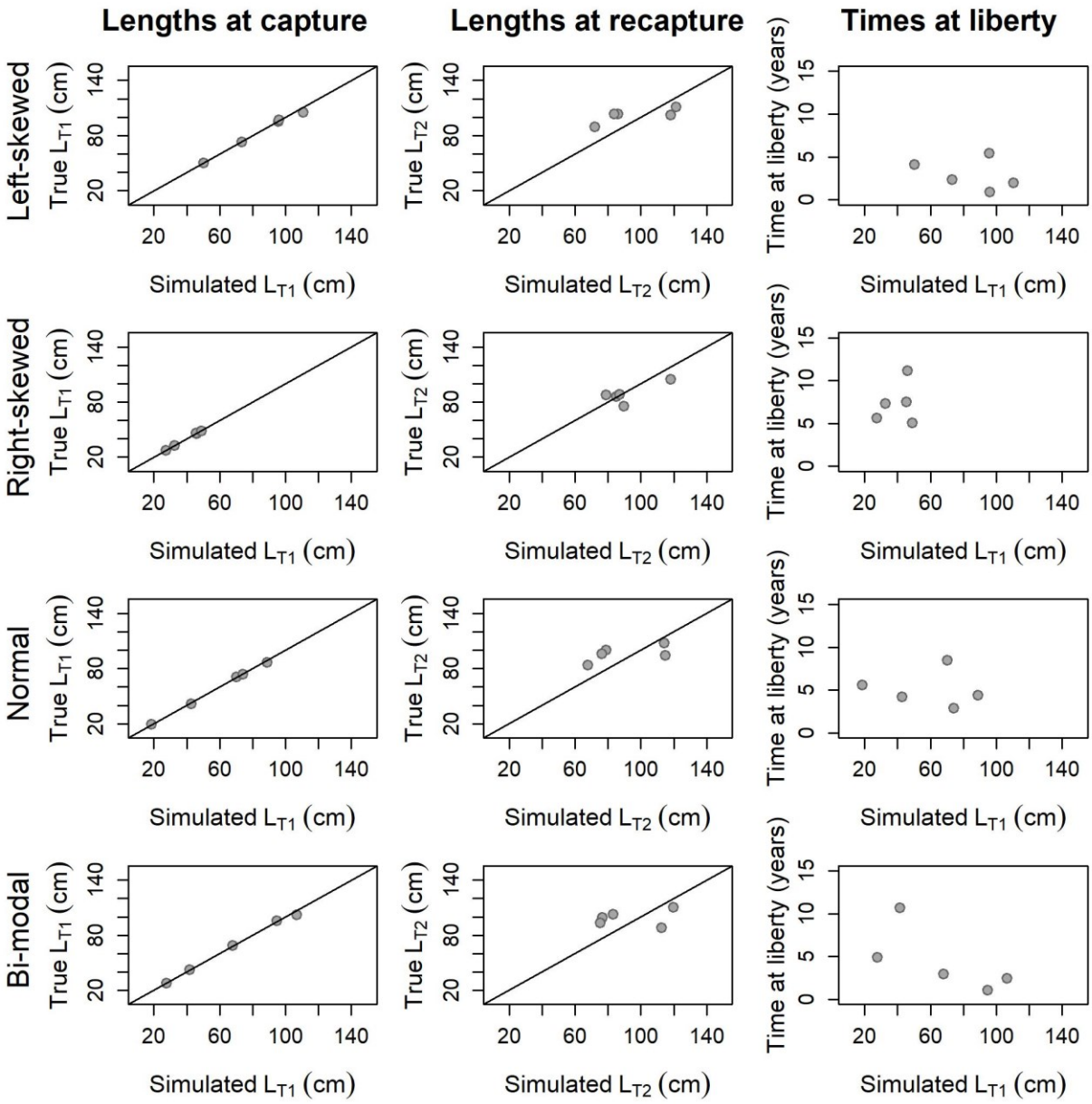

Fig. B4: Simulation design to mimic mark-recapture tagging data with small sample size and long times at liberty. Shown are the lengths at capture (L_{T1}, left column), lengths at recapture (L_{T2}, middle column) and times at liberty (right column) under different length at capture distributions (rows). The black lines indicate the 1:1 line between the true lengths versus the simulated lengths where growth variability and measurement error were introduced. The negative correlation implemented between lengths at capture and the times at liberty is presented in the third column. All scenarios shown here were simulated with a sample size of 5 individuals and on average long times at liberty.

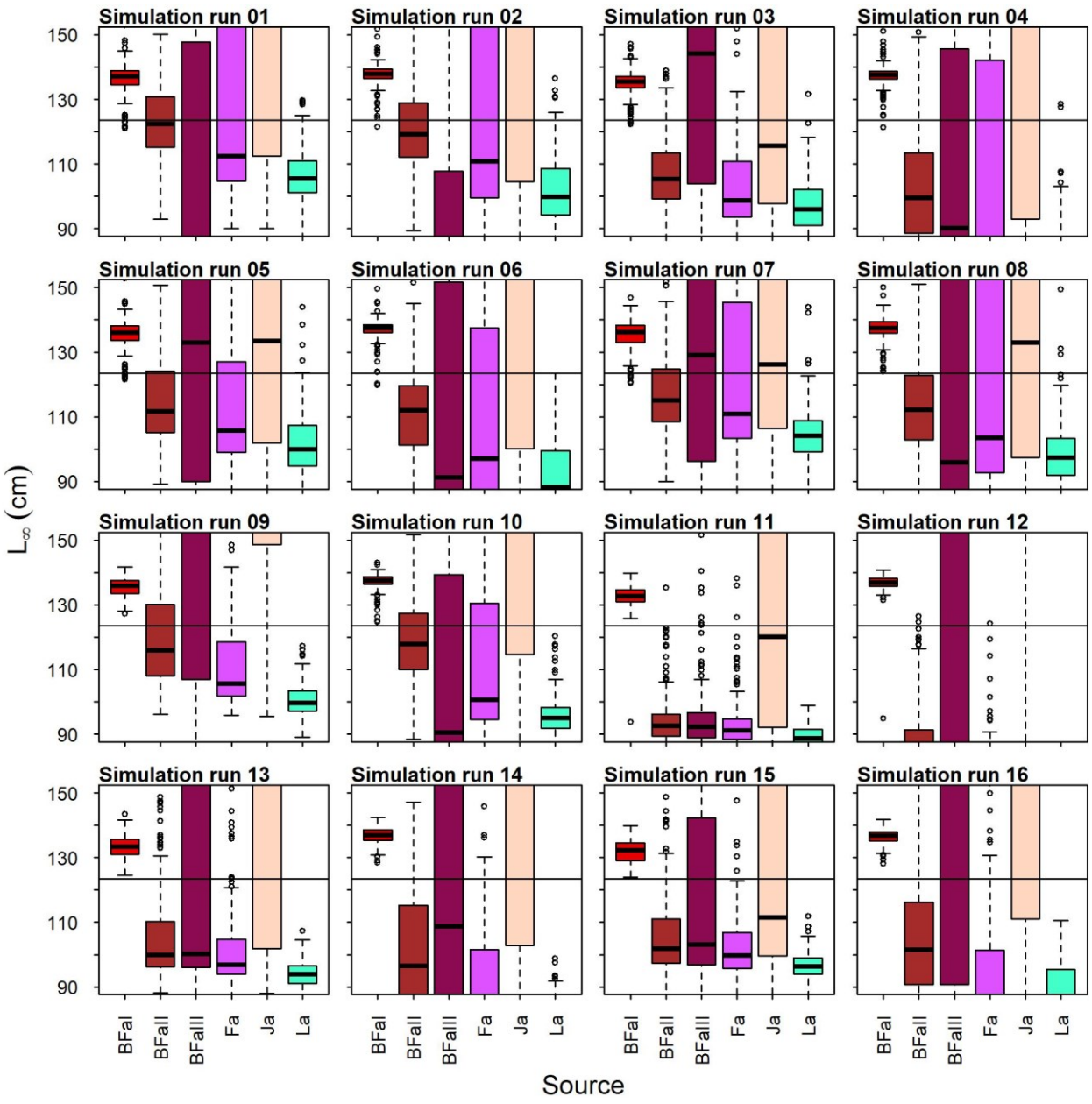

Fig. B5: Detailed simulation analysis results for the asymptotic maximum size. The asymptotic maximum lengths (L_∞, cm) estimated from each simulation run compared with the true L_∞ at 123.5 cm (black horizontal lines) for different methods that estimate growth from mark-recapture tagging data. Each run had 200 replications. Details of the different controlled scenarios for each simulation run in length at capture distributions, sample size and overall times at liberty are given in Table 3.1.

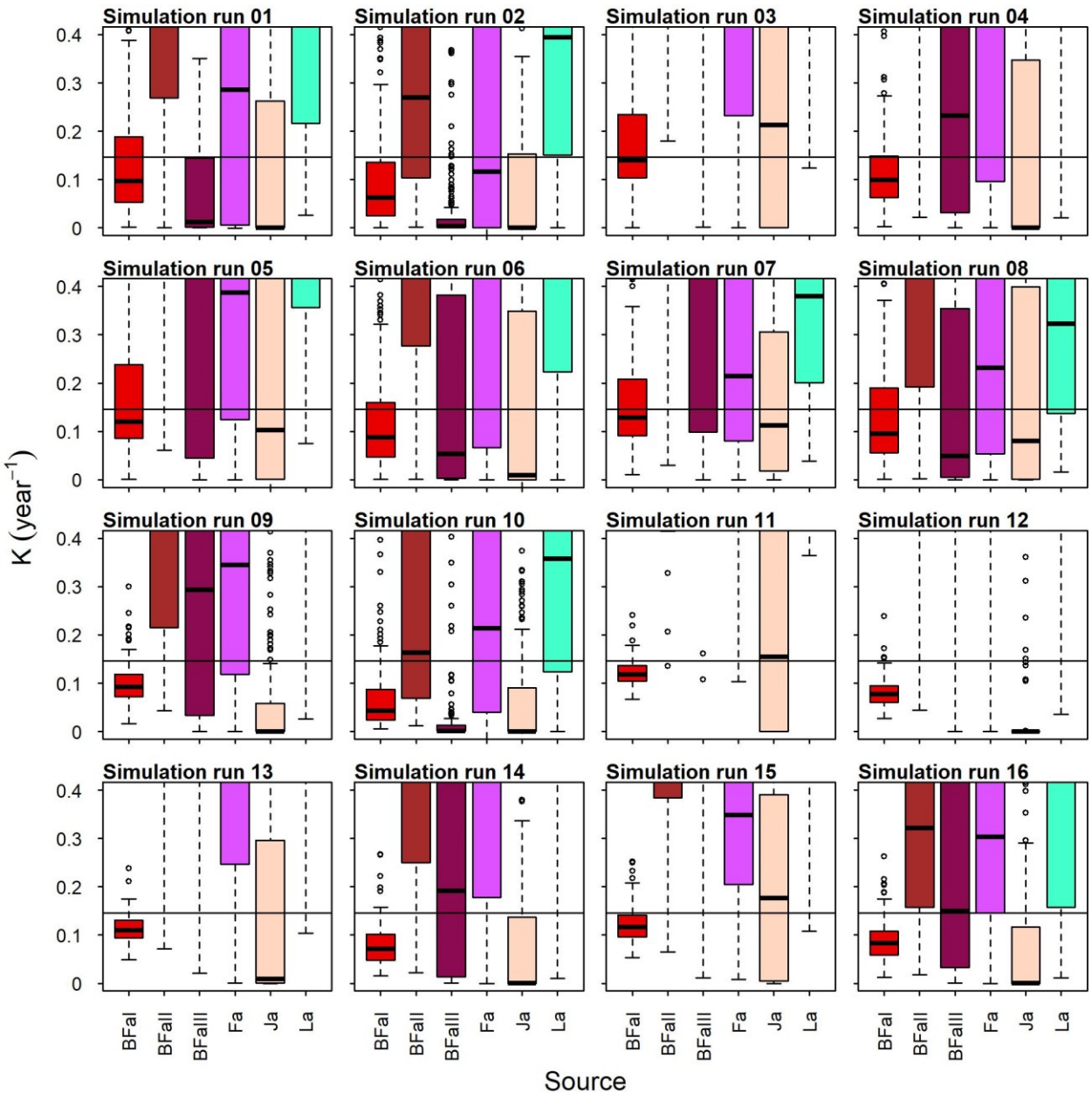

Fig. B6: Detailed simulation analysis results for the von Bertalanffy growth constant. The von Bertalanffy growth constant (k, year^{-1}) estimated from each simulation run compared with the true k at 0.146 year^{-1} (black horizontal lines) for different methods that estimate growth from mark-recapture tagging data. Each run had 200 replications. Details of the different controlled scenarios for each simulation run in length at capture distributions, sample size and overall times at liberty are given in Table 3.1.

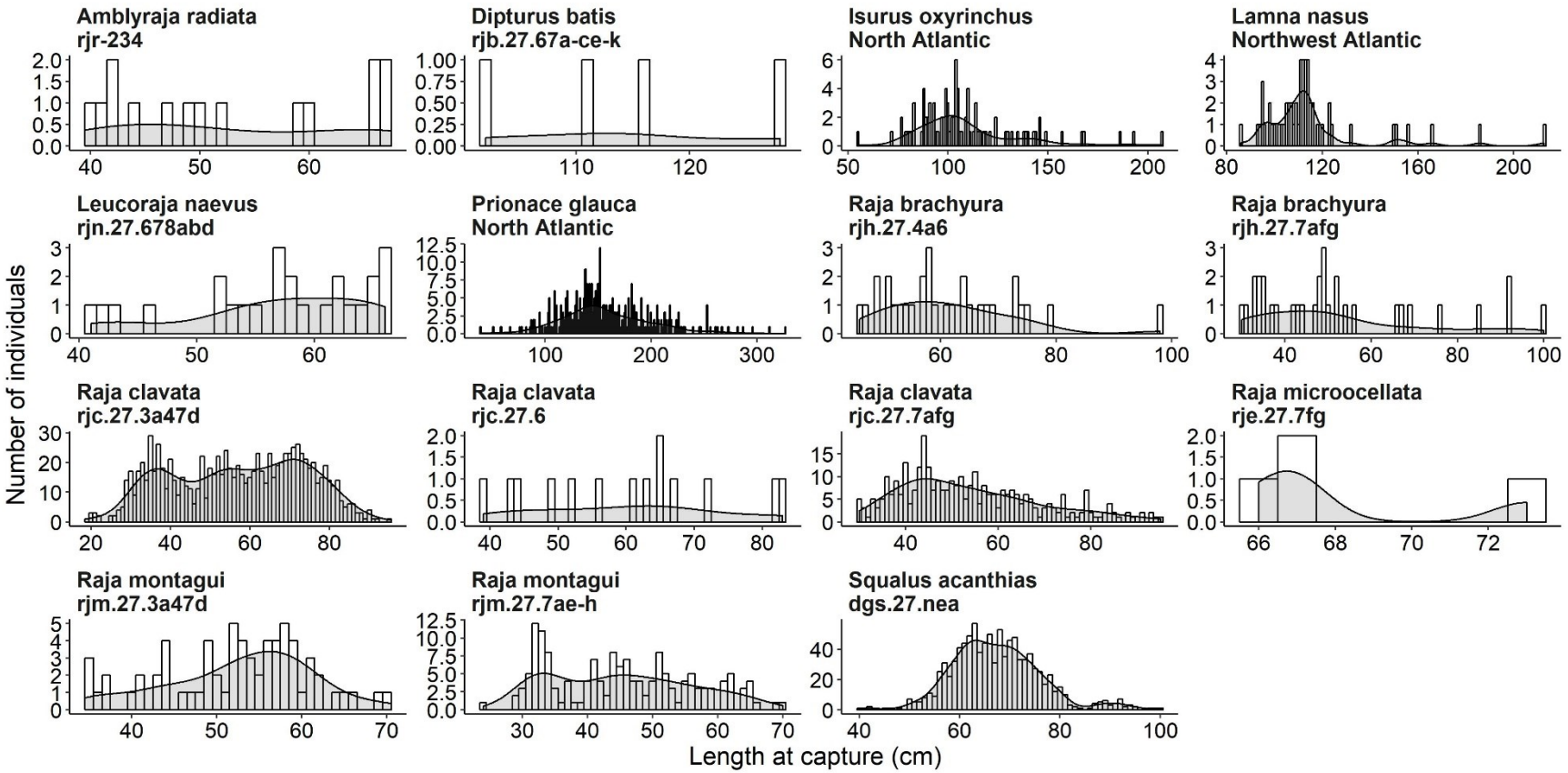

Fig. B7: Length at capture distributions for the investigated elasmobranch species. Shown is the total length at capture (cm) distribution (1 cm bins) from mark-recapture tagging data of 15 different elasmobranch stocks from 11 different species investigated in this study. Elasmobranch species names and stock ID's are given above each panel.

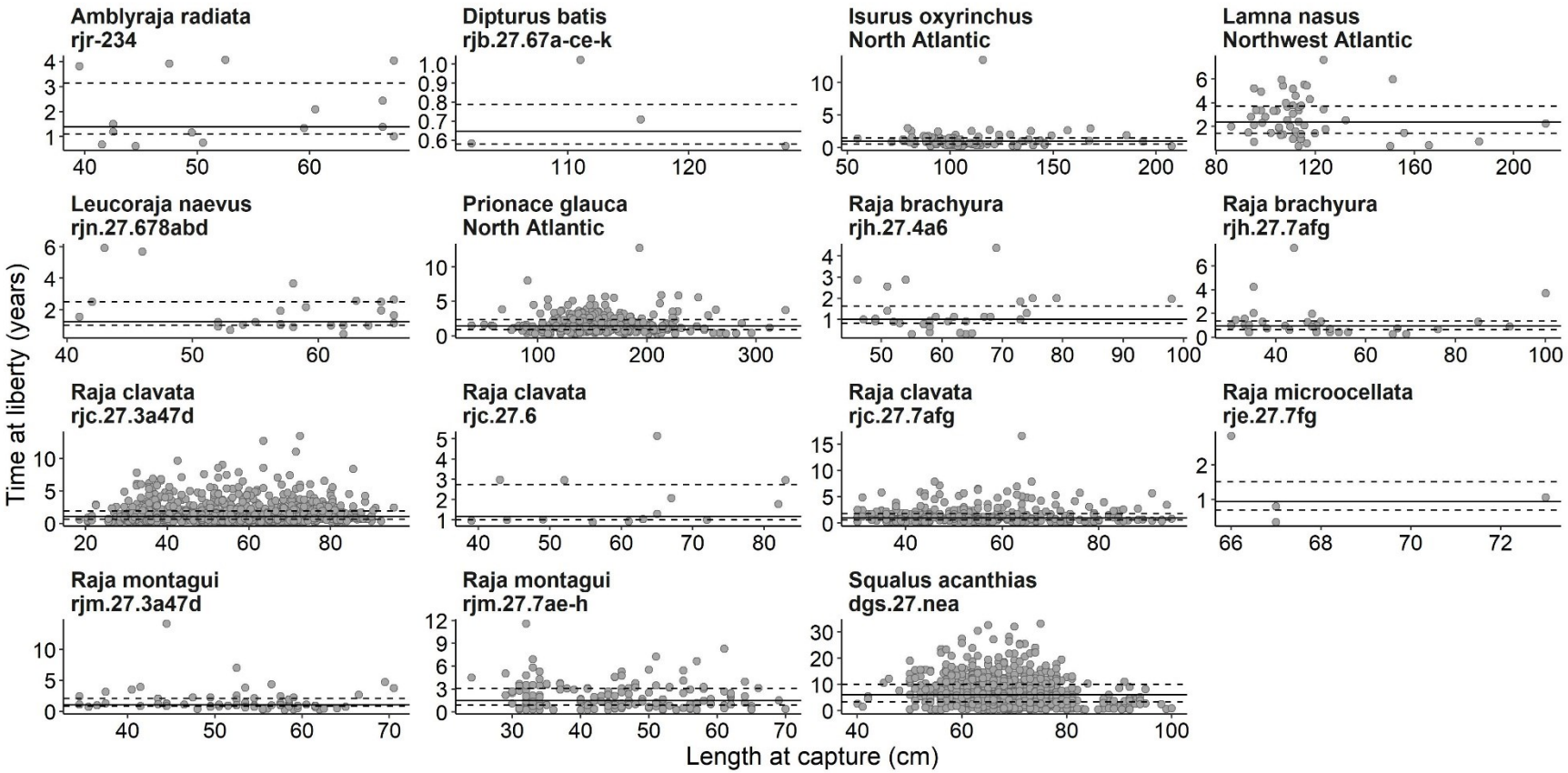

Fig. B8: Times at liberty versus length at capture distributions for the investigated elasmobranch species. Shown is the total length at capture (cm) and the corresponding time at liberty (years) from mark-recapture tagging data of 15 different elasmobranch stocks from 11 different species investigated in this study. The black horizontal lines indicate the median (solid line) and the 25th and 75th percentile (dashed lines) times at liberty. Elasmobranch species names and stock ID's are given above each panel.

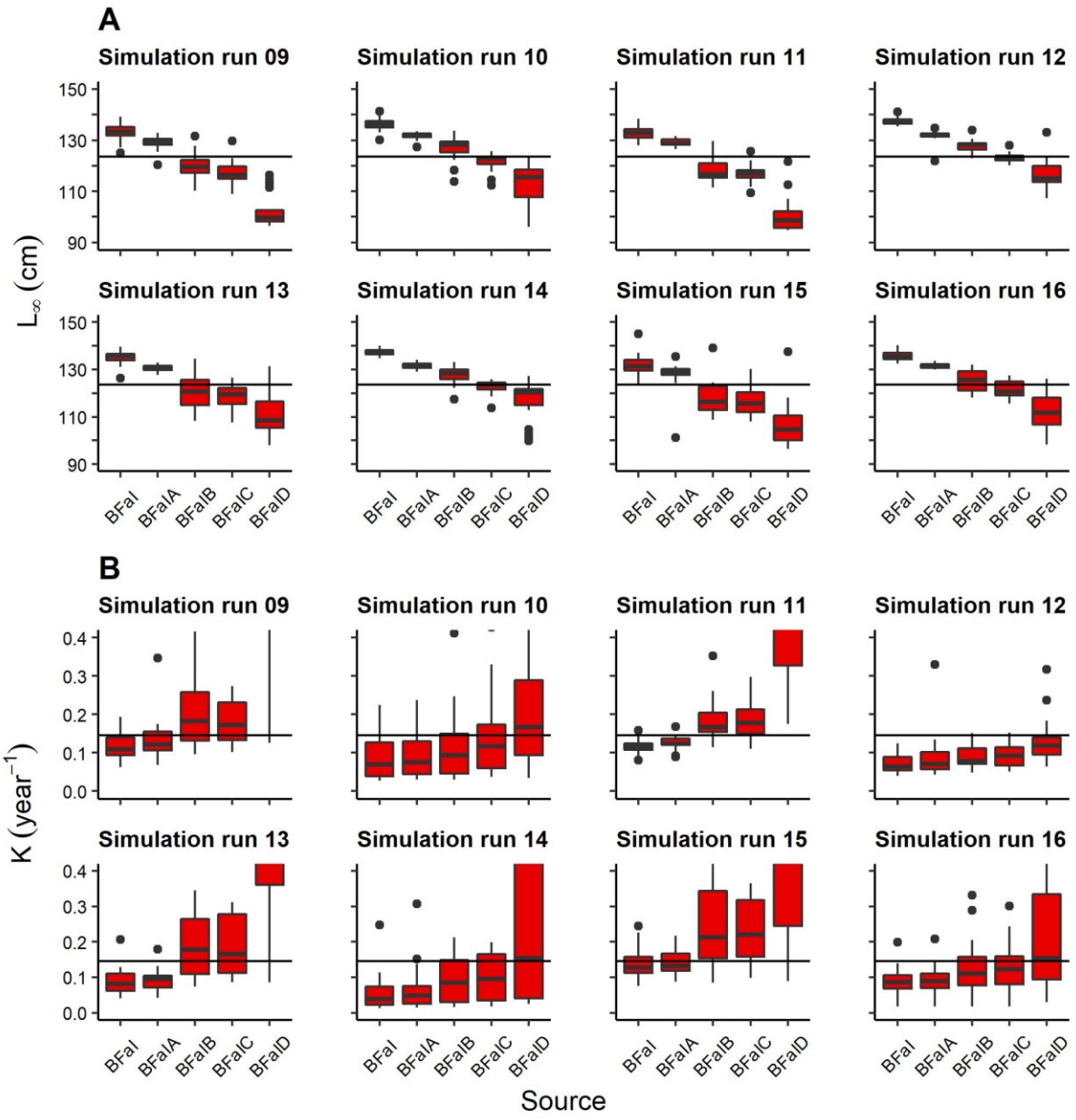

Fig. B9: Effect of different informative prior scenarios when estimating von Bertalanffy growth from mark-recapture tagging data. A) True asymptotic maximum lengths, L_∞, at 123.5 cm and **B)** true growth constant k at 0.146 year^{-1} (black horizontal lines) compared to growth parameters estimated with a Bayesian implementation of Fabens (1965) with informative priors (BFa). The approaches differ in the defined uniform prior bounds around L_∞, obtained from observed maximum length, L_{max}, with $0.9L_{max}$ and $1.2L_{max}$ (BFaI), with $0.9L_{max}$ and $1.1L_{max}$ (BFaIA), with $0.8L_{max}$ and $1.2L_{max}$ (BFaIB), with $0.8L_{max}$ and $1.1L_{max}$ (BFaIC), and with $0.7L_{max}$ and $1.2L_{max}$ (BFaID). All approaches were tested under different controlled scenarios for length at capture distributions, overall short or long times at liberty and a sample size of 20 individuals (simulation runs 09 – 16), with 20 replicates per run. For details see table 3.1.

Table B1: Deterministic results. Shown is the performance for each of the investigated methods under ideal simulated data. Here, each individual grew after the same von Bertalanffy growth function without any growth variability or measurement error. In total, 20 datasets were simulated with a sample size of 5 individuals, a normal distribution for length at capture and overall shorter times at liberty. Based on this, methods should find the true growth parameters used as inputs in the simulation study of 123.5 cm for the asymptotic maximum length, L_∞, and 0.146 year-1 for the growth constant, k. Methods exceeding the relative error of 5% for either L_∞ at 117.33 cm – 129.66 cm or k at 0.139 year^{-1} – 0.153 year^{-1} more than once (bold) were excluded from further simulation analyses (i.e. the methods Zh, Gh, Fr). Runs in which the method failed are indicated with NA. The Bayesian methods BFa and Zh were run with vague priors as defined in the methods section.

BFa		Zh		Gh		Fa		Fr		Ja		La	
L_∞	k	L_∞	k	L_∞	k	L_∞	k	L_∞	k	L_∞	k	L_∞	k
123.50	0.146	123.50	0.146	124.87	**0.136**	123.50	0.146	**NA**	**NA**	123.50	0.146	123.50	0.146
123.50	0.146	**0.00**	**0.000**	119.00	**0.160**	123.50	0.146	125.51	**0.137**	123.50	0.146	123.50	0.146
123.50	0.146	**0.76**	**0.000**	120.44	0.146	123.50	0.146	**155.47**	**0.082**	123.50	0.146	123.50	0.146
123.50	0.146	**0.00**	**0.000**	127.06	**0.126**	123.50	0.146	**133.38**	**0.109**	123.50	0.146	123.50	0.146
123.50	0.146	**0.00**	**0.000**	122.37	0.148	123.50	0.146	**NA**	**NA**	123.50	0.146	123.50	0.146
123.50	0.146	123.50	0.146	123.49	0.145	123.50	0.146	**NA**	**NA**	123.50	0.146	123.50	0.146
123.50	0.146	123.51	0.146	123.44	0.144	123.50	0.146	123.50	0.146	123.50	0.146	123.50	0.146
123.50	0.146	**0.01**	**0.000**	125.21	0.139	123.50	0.146	123.50	0.146	123.50	0.146	123.50	0.146
123.50	0.146	123.50	0.146	123.29	0.141	123.50	0.146	124.54	0.142	123.50	0.146	123.50	0.146
123.50	0.146	**0.00**	**0.000**	124.63	**0.138**	123.50	0.146	**NA**	**NA**	123.50	0.146	123.50	0.146
123.50	0.146	**0.00**	**0.000**	123.20	0.145	123.50	0.146	123.50	0.146	123.50	0.146	123.50	0.146
123.50	0.146	123.50	0.146	123.53	0.144	123.50	0.146	123.50	0.146	123.50	0.146	123.50	0.146
123.50	0.146	123.50	0.146	119.47	**0.154**	123.50	0.146	118.71	**0.115**	123.50	0.146	123.50	0.146
123.50	0.146	**NA**	**NA**	123.82	0.140	123.50	0.146	123.66	0.145	123.50	0.146	123.50	0.146
123.50	0.146	**0.00**	**0.000**	124.37	0.140	123.50	0.146	**NA**	**NA**	123.50	0.146	123.50	0.146
123.50	0.146	**NA**	**NA**	123.63	0.144	123.50	0.146	123.50	0.146	123.50	0.146	123.50	0.146
123.50	0.146	**0.00**	**0.000**	124.07	0.140	123.50	0.146	123.50	0.146	123.50	0.146	123.50	0.146
123.50	0.146	123.50	0.146	120.36	0.151	123.50	0.146	123.50	0.146	123.50	0.146	123.50	0.146
123.50	0.146	123.50	0.146	124.09	0.141	123.50	0.146	**NA**	**NA**	123.50	0.146	123.50	0.146
123.50	0.146	**0.00**	**0.000**	128.43	**0.122**	123.50	0.146	123.50	0.146	123.50	0.146	123.50	0.146

Table B2: Prior information for elasmobranch species. Shown are the maximum total lengths, L_{max} (cm), and the derived prior information for the von Bertalanffy growth parameters (L_∞, cm and k, year^{-1}) for all elasmobranch species utilized in the evaluation analysis. The lower and upper asymptotic total lengths, L_∞ (cm), and the lower and upper growth constants, k (year^{-1}), of the von Bertalanffy growth function were used as uniform bounds in the informative prior scenario (with lower $L_\infty = 0.9L_{max}$ and upper $L_\infty = 1.2L_{max}$) for the Bayesian methods BFaI and ZhI. Details on how the prior information were obtained are given in the Method section. All values for L_{max} were taken from Ebert & Stehmann (2013).

Scientific name	L_{max}	*lower* L_∞	*upper* L_∞	*lower k*	*upper k*
Amblyraja radiata	61	54.9	73.2	0.039	1.593
Dipturus batis	230	207	276	0.003	0.117
Isurus oxyrinchus	342.5	308.25	411	0.000	0.514
Lamna nasus	355	319.5	426	0.000	0.479
Leucoraja naevus	71.5	64.35	85.8	0.028	1.165
Prionace glauca	383	344.7	459.6	0.000	0.412
Raja brachyura	120	108	144	0.010	0.421
Raja clavata	117.5	105.75	141	0.011	0.438
Raja microocellata	91	81.9	109.2	0.018	0.725
Raja montagui	80	72	96	0.023	0.934
Squalus acanthias	108.5	97.65	130.2	0.001	7.890

Appendix C

Supporting information for Chapter 4

Table C1: Taxon-specific performance of indirect adult natural mortality estimators. Shown is the performance of each tested estimator to predict the direct natural mortality, *M* (year^{-1}), estimate in the adult *M* database, for either elasmobranchs or teleosts. Performance measures are given as the median relative error (%), the scaled average absolute error (SMAE) and the scaled median absolute deviation (SMAD) error. The lowest value (best performance) is shown in bold.

Taxon	Estimator	Relative error	SMAE	SMAD
Elasmobranch	*DureuilTmax*	5.82	**0.186**	**0.107**
	DureuilP	4.26	0.202	0.142
	P0.05	-21.97	0.216	0.224
	HoenigCetaceans	-4.46	0.224	0.173
	HoenigFish	9.28	0.239	0.161
	HewittHoenigP	9.40	0.242	0.167
	HoenigAll	16.64	0.292	0.234
	DureuilLinf	**1.68**	0.355	0.320
	ThenGrowth	46.52	0.624	0.465
	JensenTm	85.39	0.720	0.854
	ThenTmax	66.82	0.776	0.668
	JensenGrowth	67.63	0.783	0.676
	DureuilLinf95	77.19	0.896	0.772
	PaulyGrowth	93.54	0.932	0.935
Teleost	*DureuilTmax*	-2.18	**0.303**	**0.201**
	DureuilP	-2.82	0.320	0.220
	HoenigFish	**1.68**	0.331	0.211
	HewittHoenigP	1.96	0.335	0.220
	P0.05	-27.27	0.342	0.325
	HoenigCetaceans	-13.18	0.359	0.270
	HoenigAll	4.30	0.363	0.220
	ThenTmax	46.38	0.714	0.464
	JensenTm	58.76	1.450	0.588
	DureuilLinf	-2.55	1.575	0.661
	DureuilLinf95	71.45	2.669	0.714
	JensenGrowth	62.77	2.702	0.643
	ThenGrowth	90.10	2.962	0.901
	PaulyGrowth	106.11	3.420	1.061

Table C2: Performance of indirect adult natural mortality estimators across taxonomic orders. Shown is the performance of each tested estimator to predict the direct natural mortality, M (year^{-1}), estimate in the adult M database across the 15 different orders considered in this study. Estimators were ranked from 1 to 15 for each order based on either the scaled average absolute error (SMAE) or the scaled median absolute deviation (SMAD) error. The lowest value (best performance across orders) is shown in bold. The mean and median rank of either SMAE or SMAD across all 15 orders is also provided. Note, if one estimator would perform best for each of the 15 orders the sum rank would be 15, and the mean and median rank would be 1.

Estimator	SMAD			SMAE		
	sum rank	mean rank	median rank	sum rank	mean rank	median rank
DureuilTmax	**72**	**4.8**	**5**	**72**	**4.8**	5
HoenigAll	96	6.4	6	100	6.7	6
HoenigCetaceans	88	5.9	6	88	5.9	6
HoenigFish	82	5.5	6	88	5.9	6
ThenTmax	134	8.9	9	130	8.7	9
DureuilP	83	5.5	**5**	77	5.1	**4**
HewittHoenigP	83	5.5	6	89	5.9	6
P0.05	106	7.1	7	102	6.8	7
JensenTm	126	9.0	10	128	9.1	10
JensenGrowth	135	9.0	11	139	9.3	11
ThenGrowth	143	9.5	11	143	9.5	11
PaulyGrowth	158	10.5	12	155	10.3	12
DureuilLinf95	137	9.1	10	135	9.0	10
DureuilLinf	118	7.9	9	115	7.7	9

Table C3: Performance of indirect adult natural mortality estimators based on common information across estimators. Shown is the performance of each tested estimator to predict the direct natural mortality, *M* (year^{-1}), estimate in the adult *M* database, based on a common database. Here, only direct *M* estimates were included in the database for which also all other life history information required by any of the estimators were available. The resulting database had 86 observations. Performance measures are given as the median relative error (%), the scaled mean absolute error (SMAE) and the scaled median absolute deviation (SMAD) error. The lowest value (best performance) is shown in bold.

Estimator	Relative error	SMAE	SMAD
DureuilTmax	0.46	**0.263**	0.220
HoenigAll	10.13	0.329	0.226
HoenigCetaceans	-15.41	0.337	0.293
HoenigFish	4.73	0.295	**0.213**
ThenTmax	46.75	0.660	0.468
DureuilP	**0.00**	0.282	0.221
HewittHoenigP	4.93	0.299	0.220
P0.05	-25.15	0.311	0.303
JensenTm	65.10	1.323	0.651
JensenGrowth	27.02	1.240	0.568
ThenGrowth	30.02	1.486	0.472
PaulyGrowth	65.80	1.555	0.672
DureuilLinf95	28.73	1.214	0.591
DureuilLinf	-22.58	0.731	0.563

Table C4: Taxon-specific performance of indirect juvenile natural mortality estimators. Shown is the performance of each tested estimator to predict the direct natural mortality, *M* (year^{-1}), estimate in the juvenile *M* database, for either elasmobranchs or teleosts. Performance measures are given as the median relative error (%), the scaled mean absolute error (SMAE) and the scaled median absolute deviation (SMAD) error. The lowest value (best performance) is shown in bold.

Taxon	Estimator	Relative error	SMAE	SMAD
Elasmobranch	*LorLta*	5.34	0.154	0.154
	LorLm	**1.13**	**0.153**	**0.153**
	LorLmax	50.50	0.505	0.505
	LorW	-26.07	0.261	0.261
	PW	-32.09	0.321	0.321
	CW	-12.76	0.229	0.229
	Cha	71.40	0.714	0.714
	Gis	30.71	0.307	0.307
Teleost	*LorLta*	**-0.38**	0.488	**0.267**
	LorLm	-10.40	**0.403**	0.348
	LorLmax	43.76	0.893	0.579
	LorW	-41.19	0.608	0.556
	PW	-50.48	0.537	0.586
	CW	-20.27	0.582	0.386
	Cha	57.68	1.162	0.577
	Gis	34.53	0.916	0.345

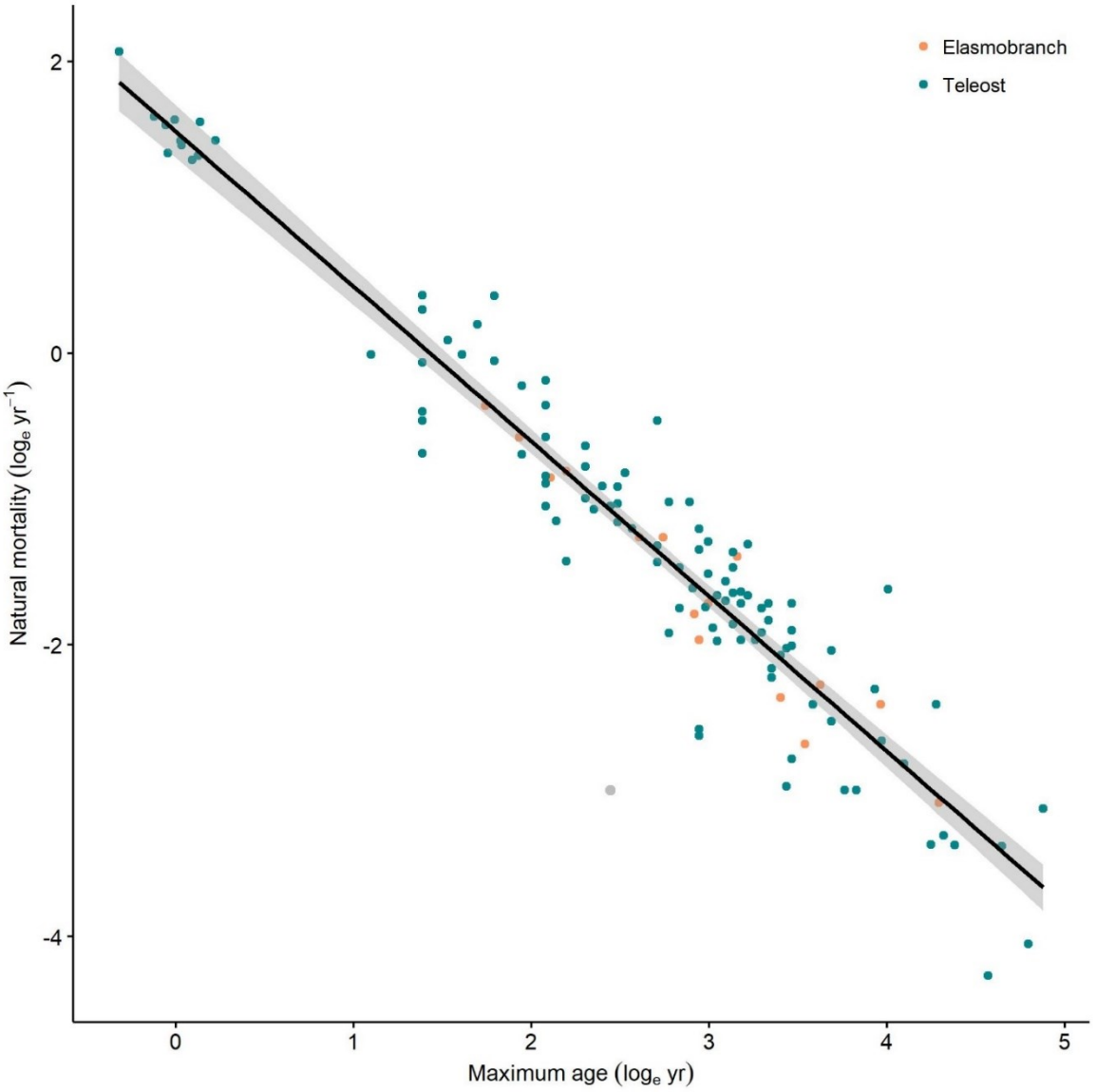

Fig. C1: Raw data visualization of natural mortality versus maximum age. Predicted relationship (black line) of natural mortality (log_e yr^{-1}) and maximum age (log_e yr) for teleosts and elasmobranchs combined. 95% confidence intervals are given by the shaded area. The grey dot indicates one observation that was considered as an outlier and removed from the analysis. This observation was also > 10 times the mean Cook's distance and identified as an outlier using a Bonferroni outlier test (Bonferroni $p < 0.05$).

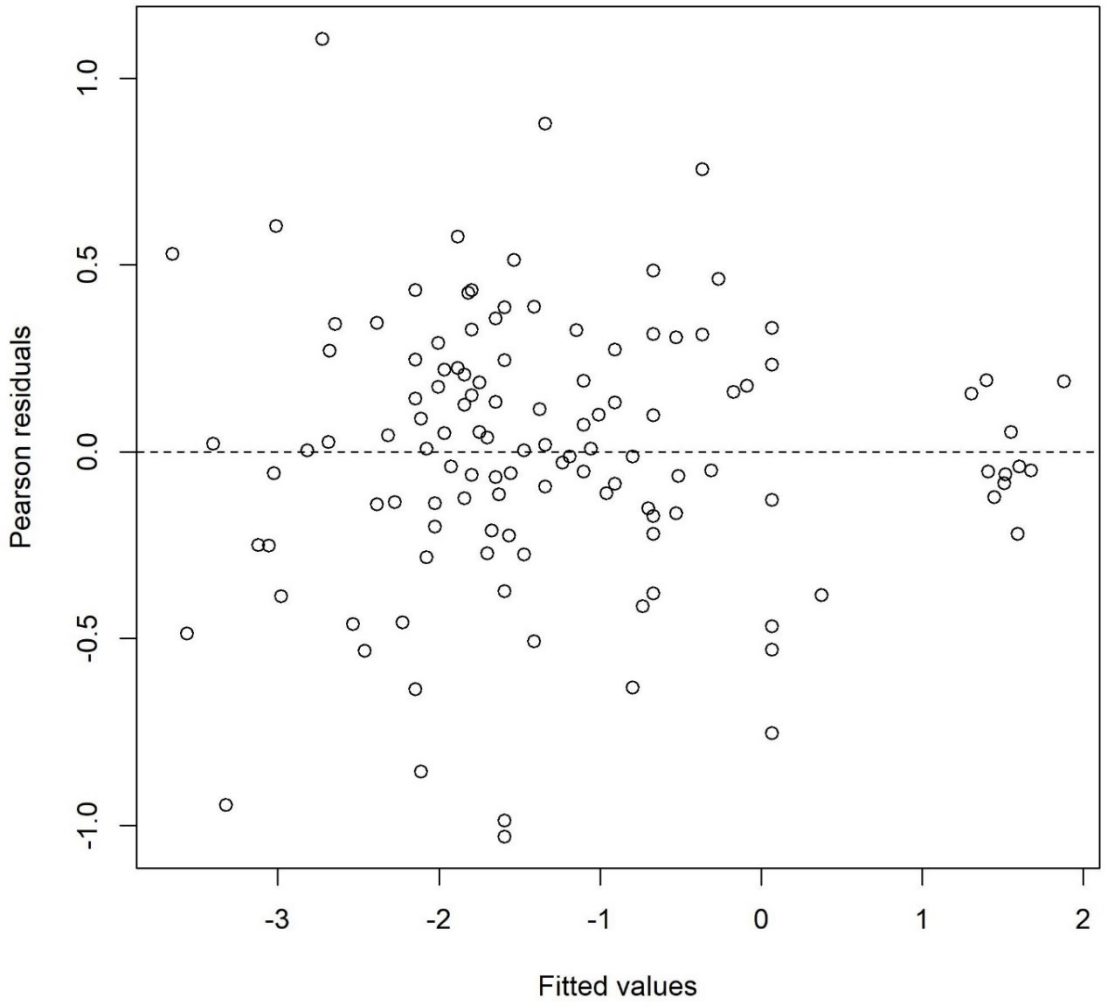

Fig. C2: Residual versus fitted values for the *DureuilTmax* estimator. Shown are the residuals versus the fitted values from a linear regression model predicting the relationship of natural mortality ($\log_e$ yr^{-1}) and maximum age ($\log_e$ yr) for teleosts and elasmobranchs combined (*DureuilTmax*), to assess homogeneity of variances.

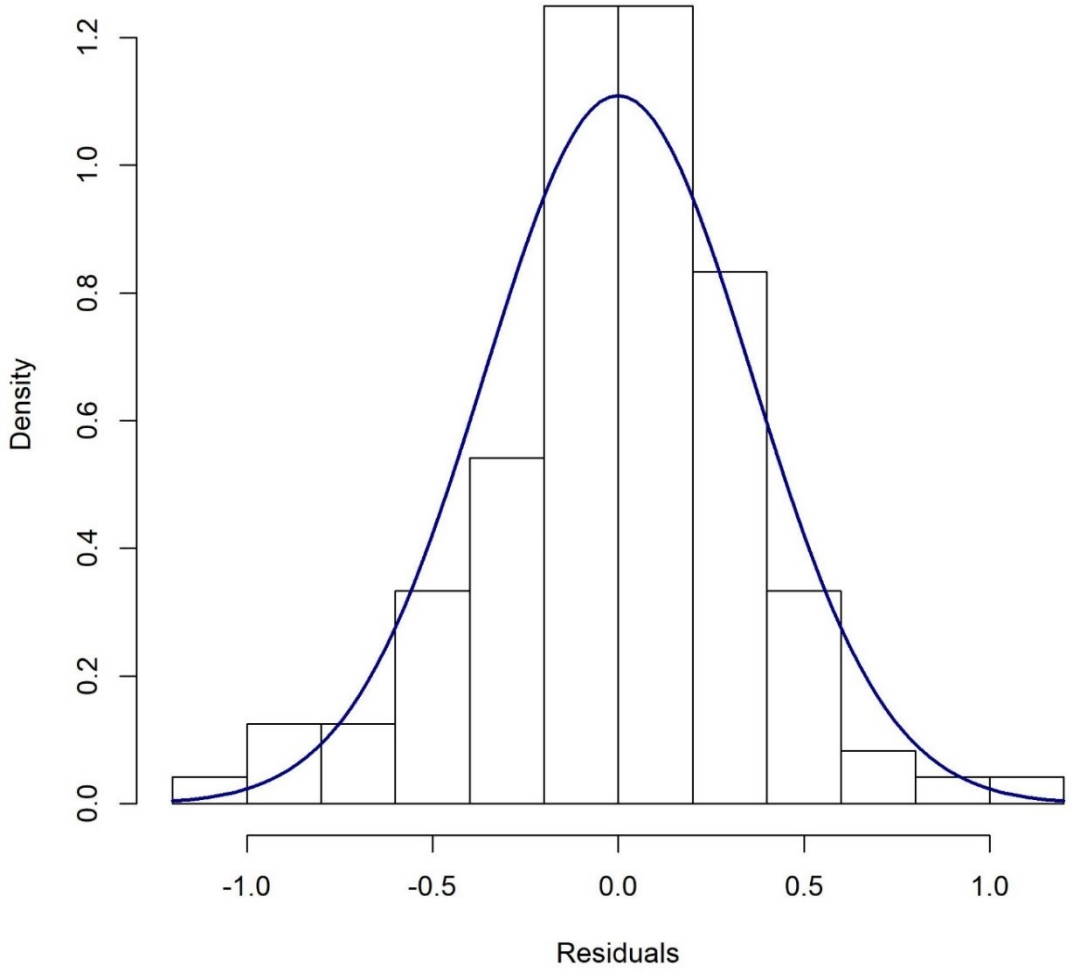

Fig. C3: Histogram of the *DureuilTmax* estimator residuals. Shown is a normal density curve (blue line) and the residual distribution from a linear regression model predicting the relationship of natural mortality ($\log_e$ yr^{-1}) and maximum age ($\log_e$ yr) for teleosts and elasmobranchs combined (*DureuilTmax*), to assess normality of errors.

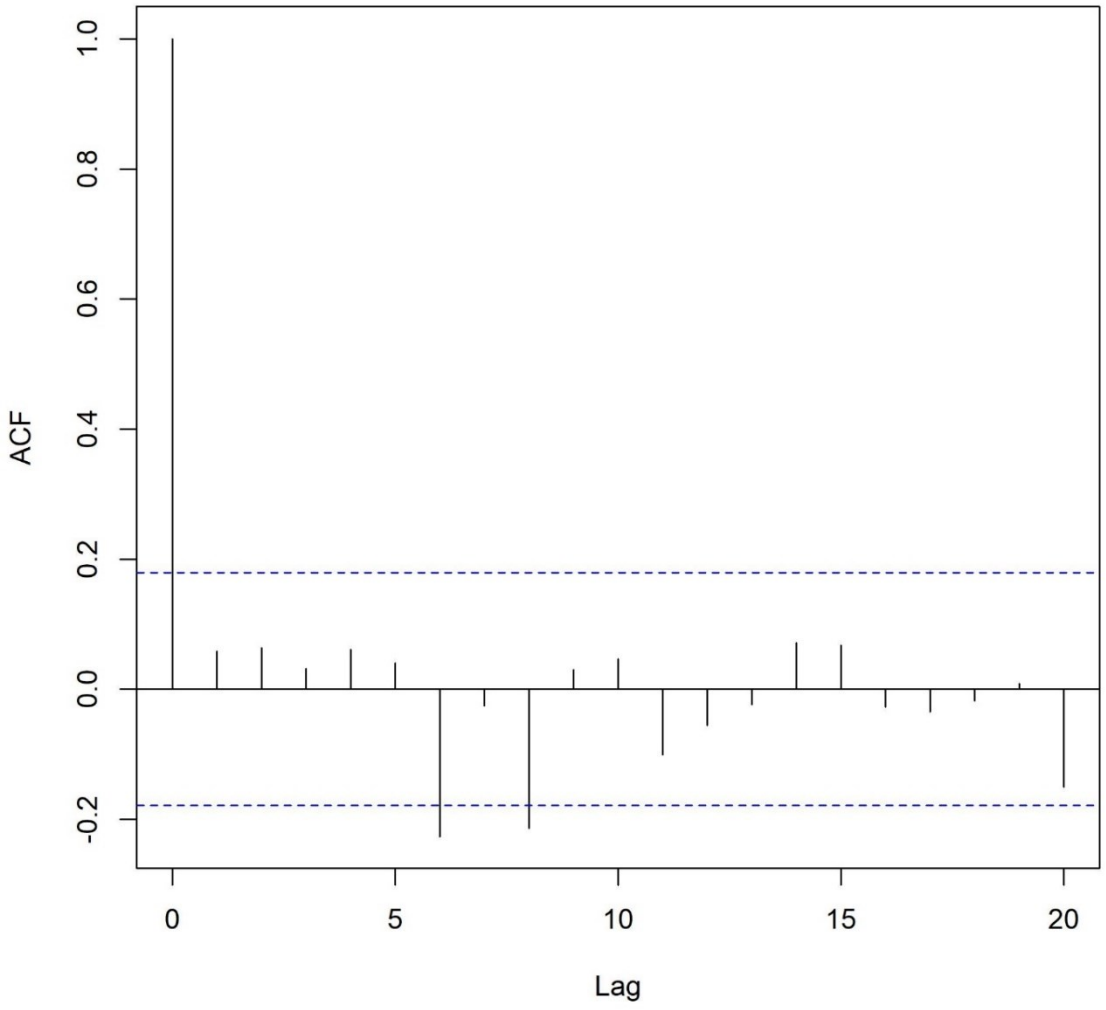

Fig. C4: Autocorrelation plot of the *DureuilTmax* estimator. Shown is the amount of autocorrelation in the linear regression model predicting the relationship of natural mortality ($\log_e yr^{-1}$) and maximum age ($\log_e$ yr) for teleosts and elasmobranchs combined (*DureuilTmax*). Autocorrelation between observations (e.g. male and female observations from the same species and population) would be present if the second line would cross the blue dashed lines.

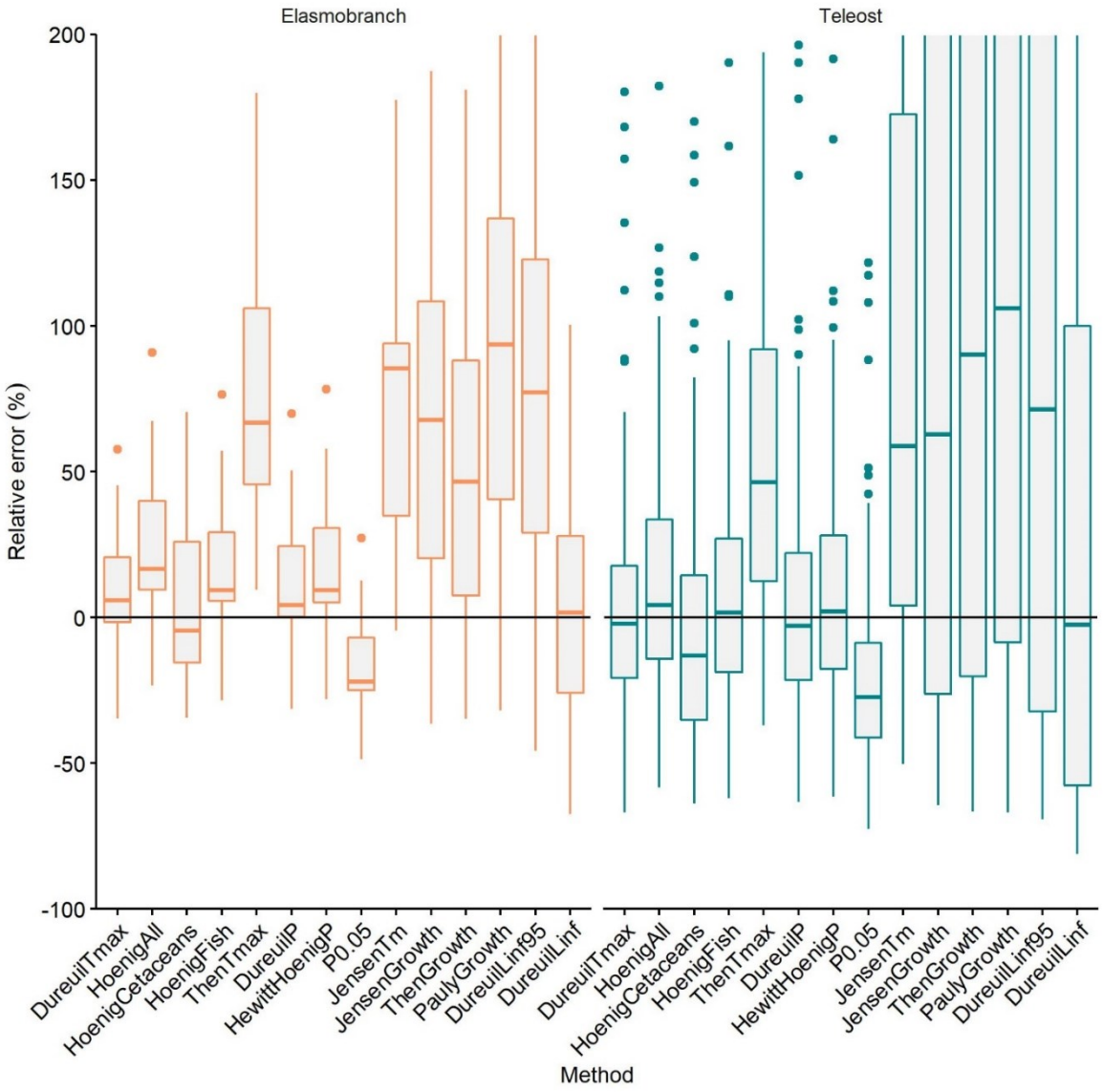

Fig. C5: Comparing indirect adult natural mortality estimators for each taxon. Shown is the relative error in percent in predicting the direct natural mortality, *M* (year^{-1}), estimate from the adult *M* database for each taxon (elasmobranch or teleost) from various indirect estimators. See table 4.1 for details on the indirect estimators.

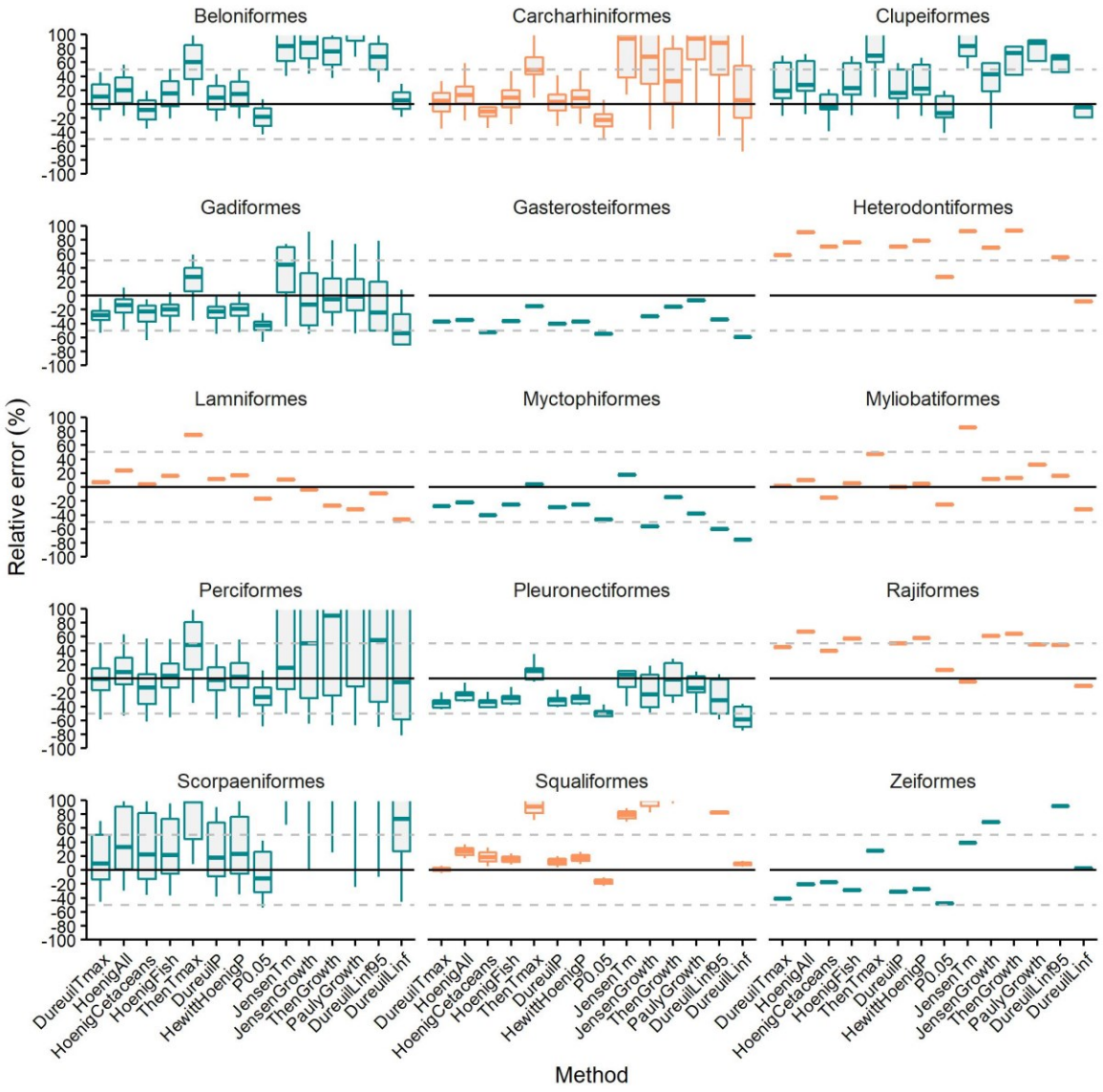

Fig. C6: Comparing indirect adult natural mortality estimators across taxonomic orders. Shown is the relative error in percent in predicting the direct natural mortality, *M* (year^{-1}), estimate from the adult *M* database for each order from various indirect estimators. See table 4.1 for details on the indirect estimators. Orders belonging to elasmobranchs are shown in orange, orders belonging to teleosts in blue.

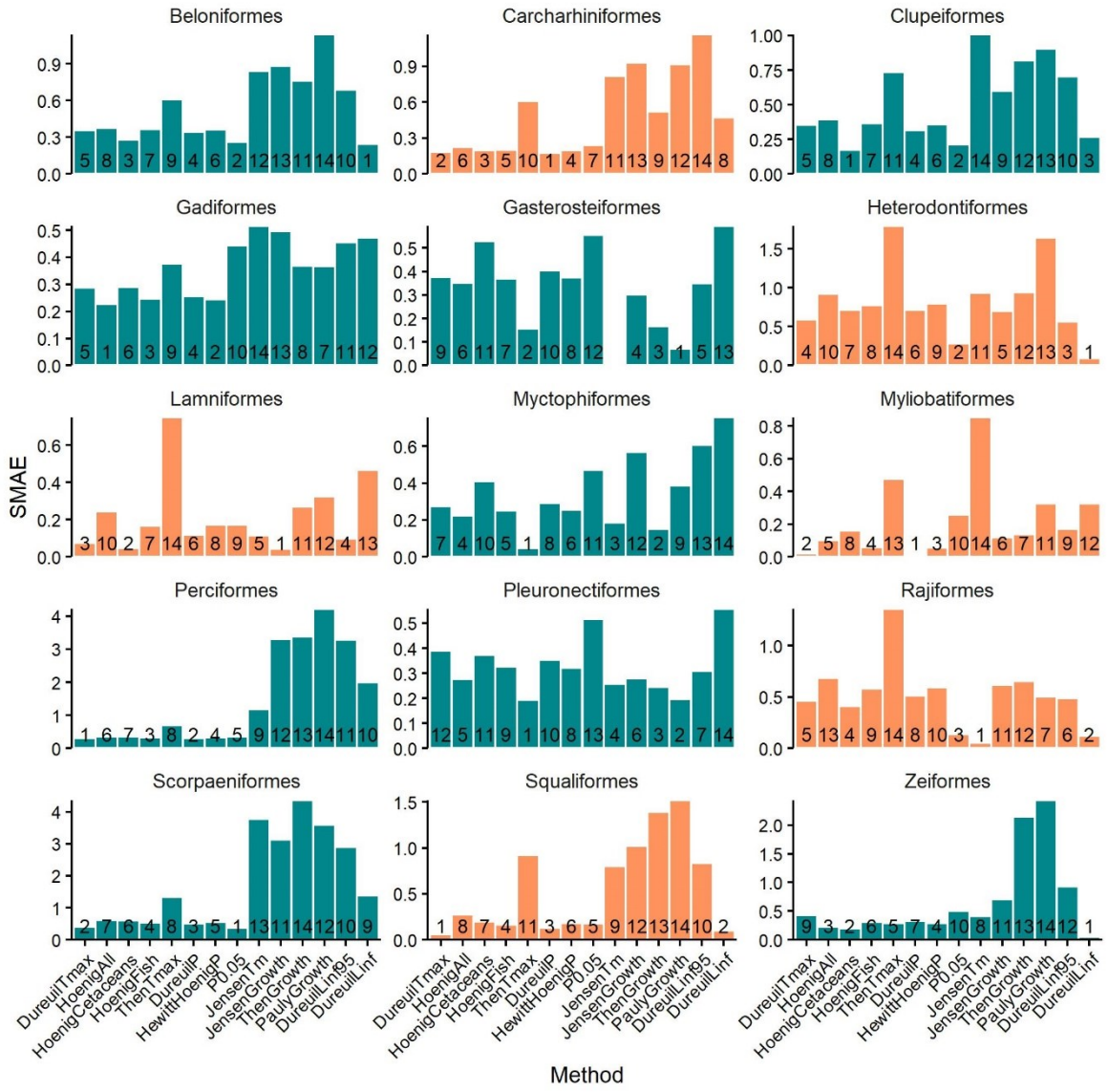

Fig. C7: Performance of indirect adult natural mortality estimators across taxonomic orders. Shown is the scaled mean absolute error (SMAE), a measure for accuracy and precision, for various indirect natural mortality, *M* (year^{-1}), estimators. A lower SMAE indicates better performance of the estimator in predicting the direct *M* estimate from the adult *M* database. See table 4.1 for details on the indirect estimators. Orders belonging to elasmobranchs are shown in orange, orders belonging to teleosts in blue. The numbers belonging to each bar show the rank of the estimator for the respective order. The estimators with the lowest SMAE have rank 1.

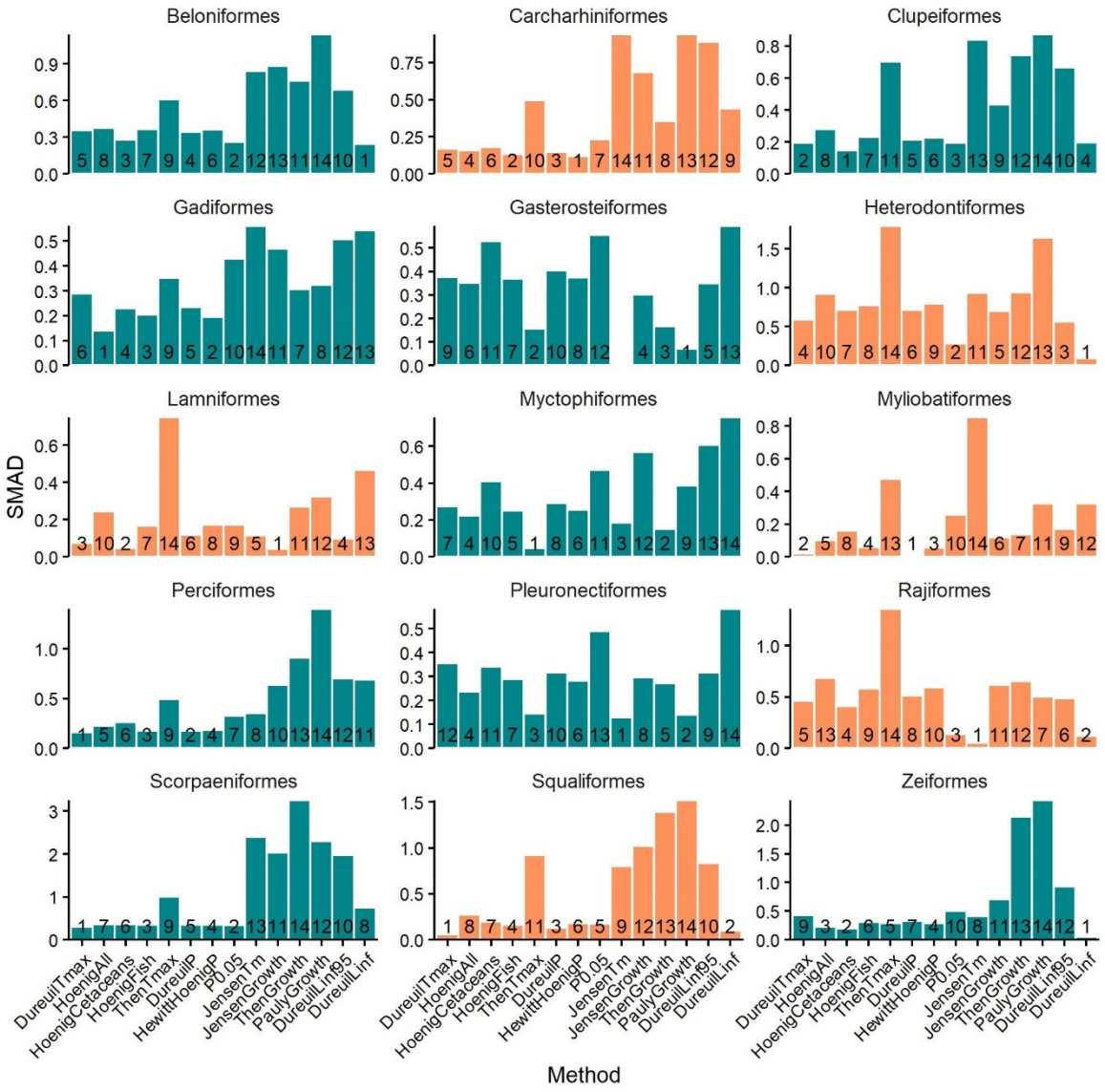

Fig. C8: Performance of indirect adult natural mortality estimators across taxonomic orders. Shown is the scaled median absolute deviation (SMAD), a measure for accuracy and precision, for various indirect natural mortality, *M* (year^{-1}), estimators. A lower SMAD indicates better performance of the estimator in predicting the direct *M* estimate from the adult *M* database. See table 4.1 for details on the indirect estimators. Orders belonging to elasmobranchs are shown in orange, orders belonging to teleosts in blue. The numbers belonging to each bar show the rank of the estimator for the respective order. The estimators with the lowest SMAD have rank 1.

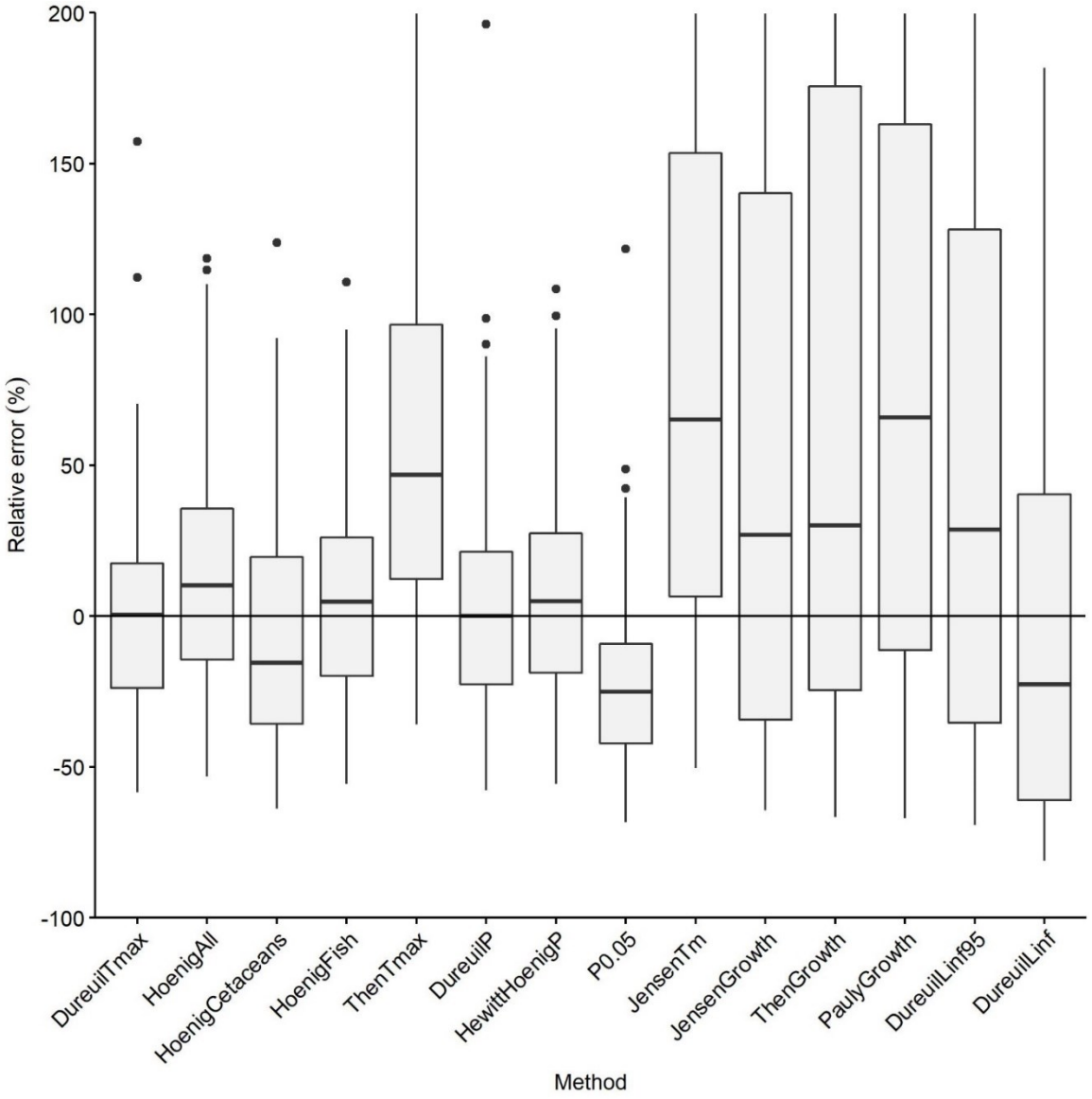

Fig. C9: Comparing indirect adult natural mortality estimators based on common information across estimators. Shown is the relative error in percent in predicting the direct natural mortality, *M* (year^{-1}), estimate from a common adult *M* database for elasmobranchs and teleosts from various indirect estimators. Here, only direct *M* estimates were included in the database for which all other life history information required by any of the estimators were also available. The resulting database had 86 observations. See table 4.1 for details on the indirect estimators.

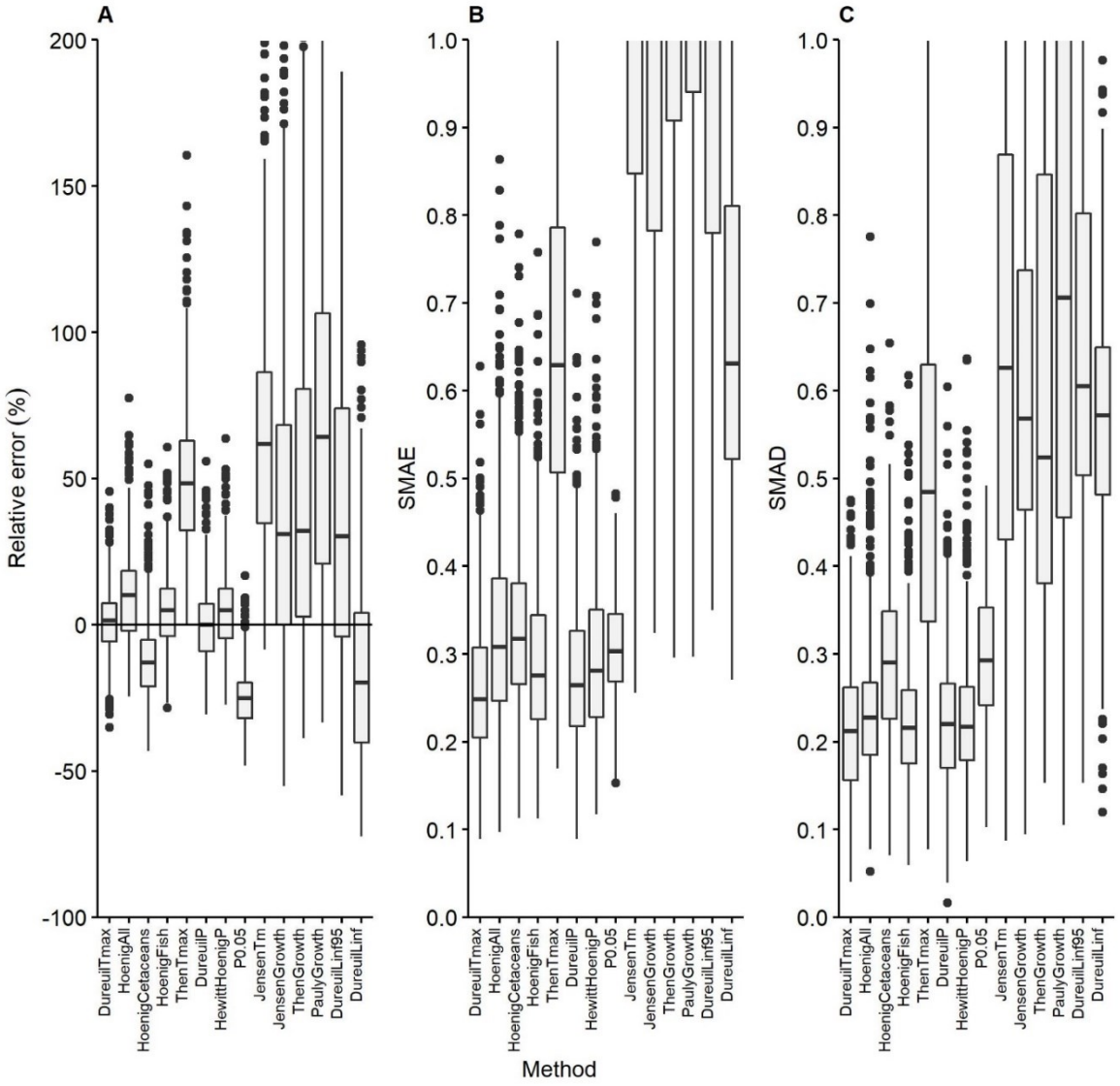

Fig. C10: Performance of indirect adult natural mortality estimators based on random information. A) Shown is the relative error in percent in predicting direct natural mortality, *M* (year^{-1}), **B)** the scaled mean absolute error (SMAE), and **C)** the scaled median absolute deviation (SMAD) for a random selection of 10 direct *M* estimates from the common adult *M* database, i.e. only direct *M* estimates were included for which also all other life history information required by any of the estimators were available. From the resulting database with 86 observations, 10 observations were then selected randomly, all estimators were applied, and the relative error, SMAE and SMAD, were calculated. This was repeated 1000 times. See table 4.1 for details on the indirect estimators.

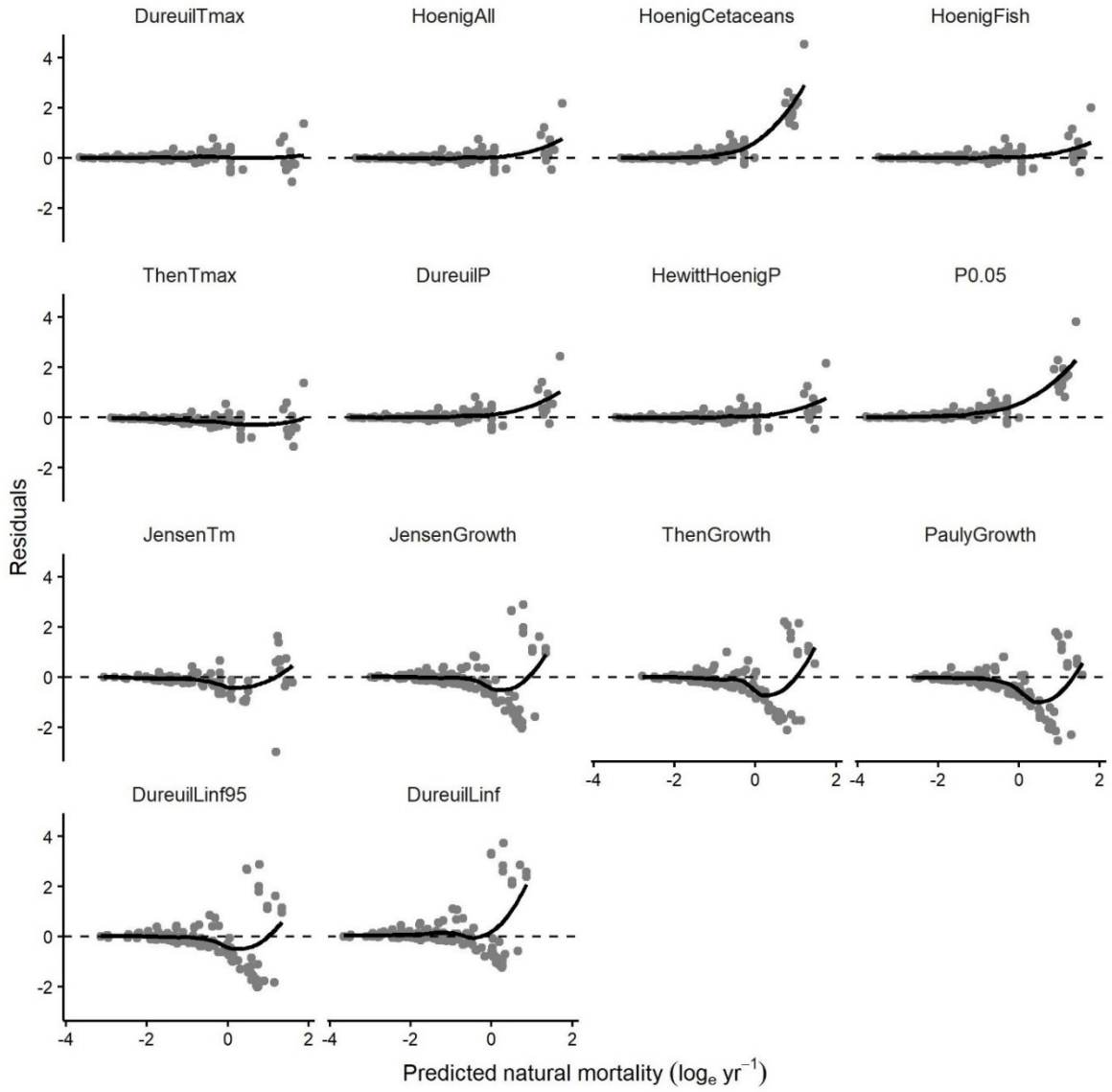

Fig. C11: Residual analysis across indirect adult natural mortality estimators. Shown are the residuals (direct natural mortality rate, *M* (year^{-1}), from the adult *M* database minus predicted *M* from the respective indirect estimator) versus the predicted *M* (log$_e$ year^{-1}) from various indirect estimators. The predicted *M* was log$_e$ transformed for visualization purposes. The black line indicates a loess fit. See table 4.1 for details on the indirect estimators.

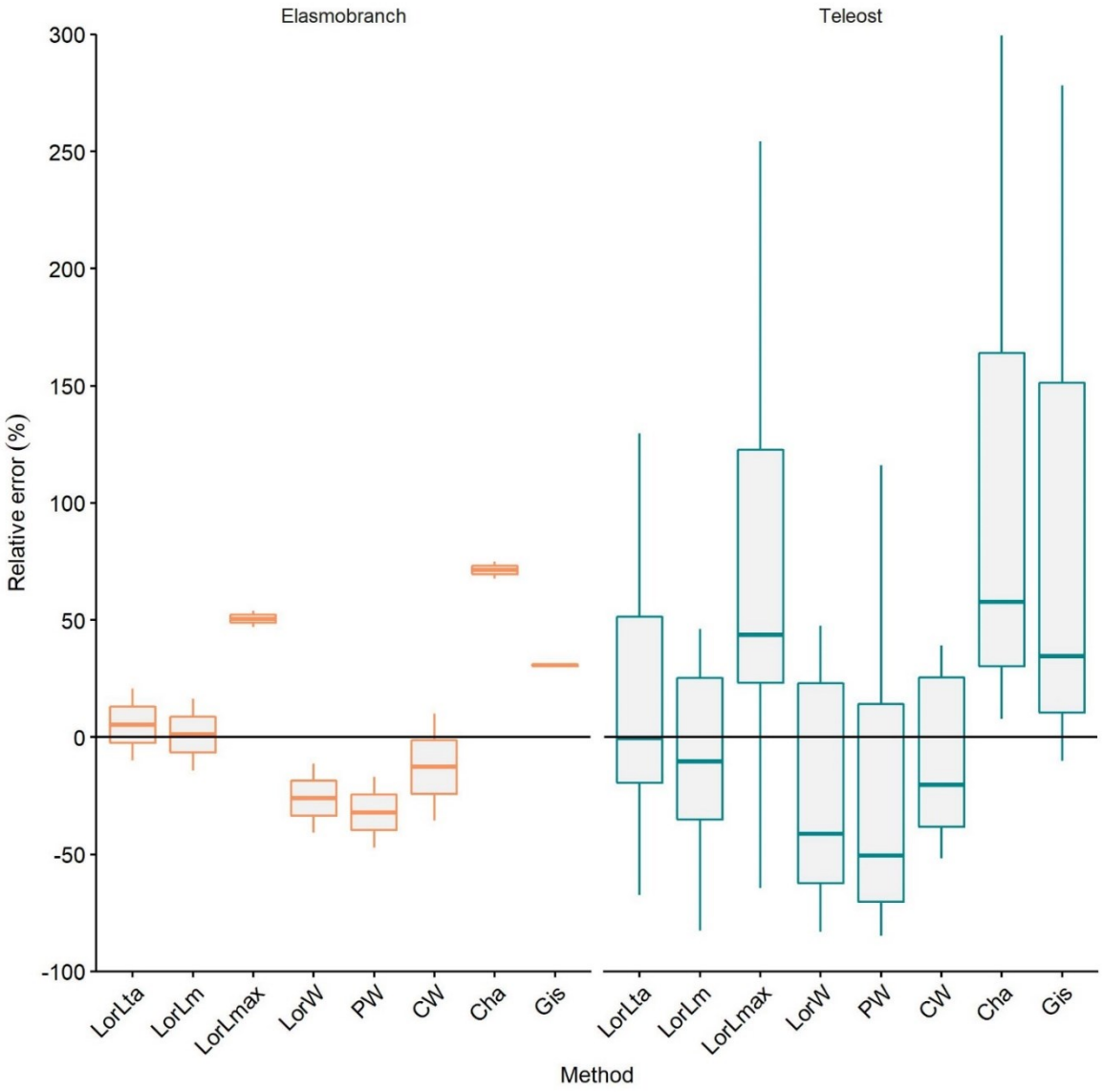

Fig. C12: Comparing indirect juvenile natural mortality estimators for each taxon. Shown is the relative error (in percent) in predicting the direct natural mortality *M* (year^{-1}) estimate from the juvenile *M* database for each taxon (elasmobranch or teleost) from various indirect estimators. See table 4.2 for details on the indirect estimators.

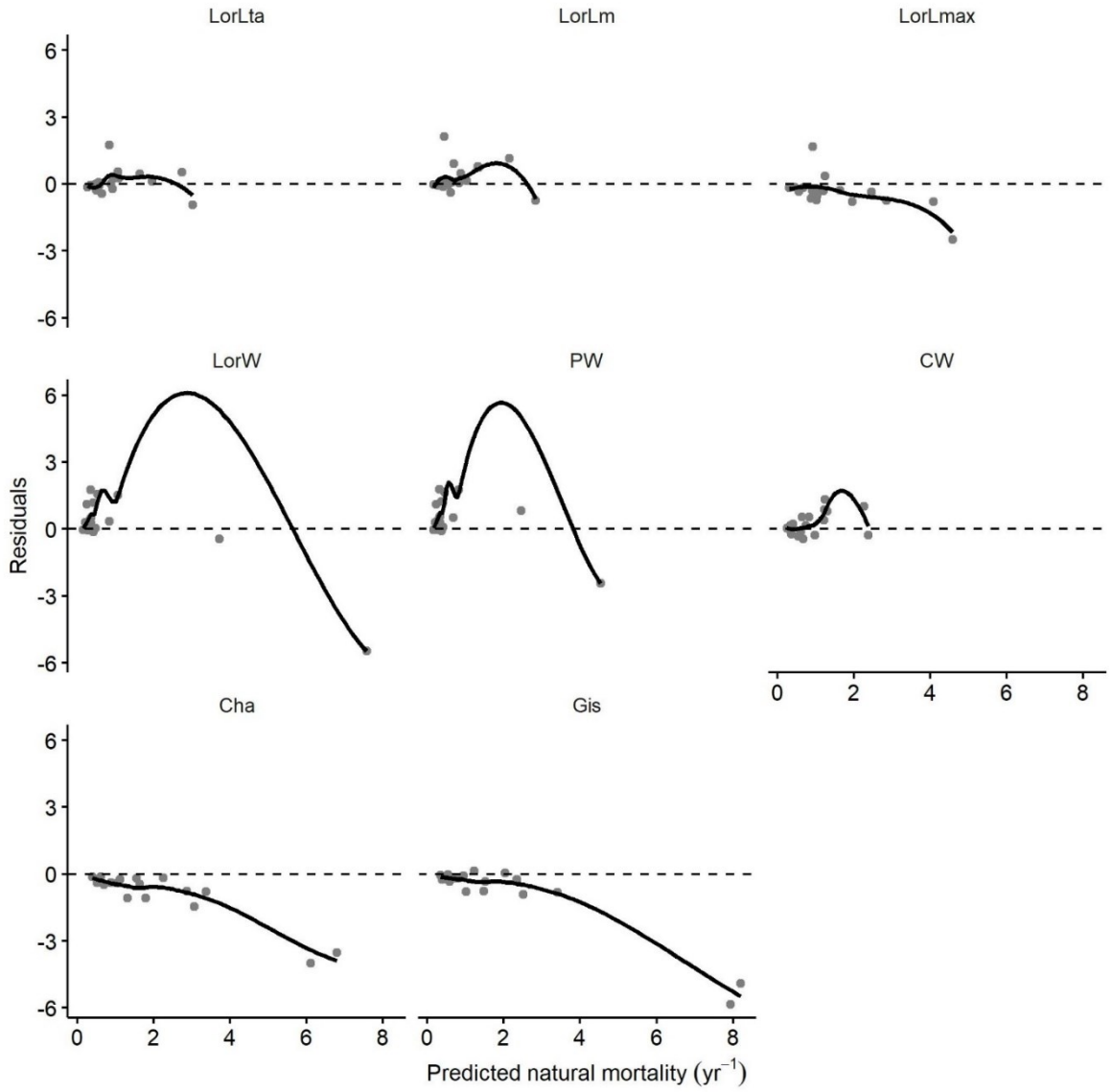

Fig. C13: Residual analysis across indirect juvenile natural mortality estimators. Shown are the residuals (direct natural mortality rate, *M* (year^{-1}), from the juvenile *M* database minus predicted *M* from the respective indirect estimator) versus the predicted *M* from various indirect estimators. The black line indicates a loess fit. See table 4.2 for details on the indirect estimators.

Appendix D
Supporting information for Chapter 4

Electronic supplement

The electronic supplement for Chapter 4 “A unified natural mortality estimator for marine fish” contains the references utilized in the adult natural mortality database (Table D1), the juvenile natural mortality database (Table D2) and a list of excluded studies with exclusion criteria provided (Table D3). The electronic supplement is available from DalSpace (http://dalspace.library.dal.ca).

Appendix E

Supporting information for Chapter 5

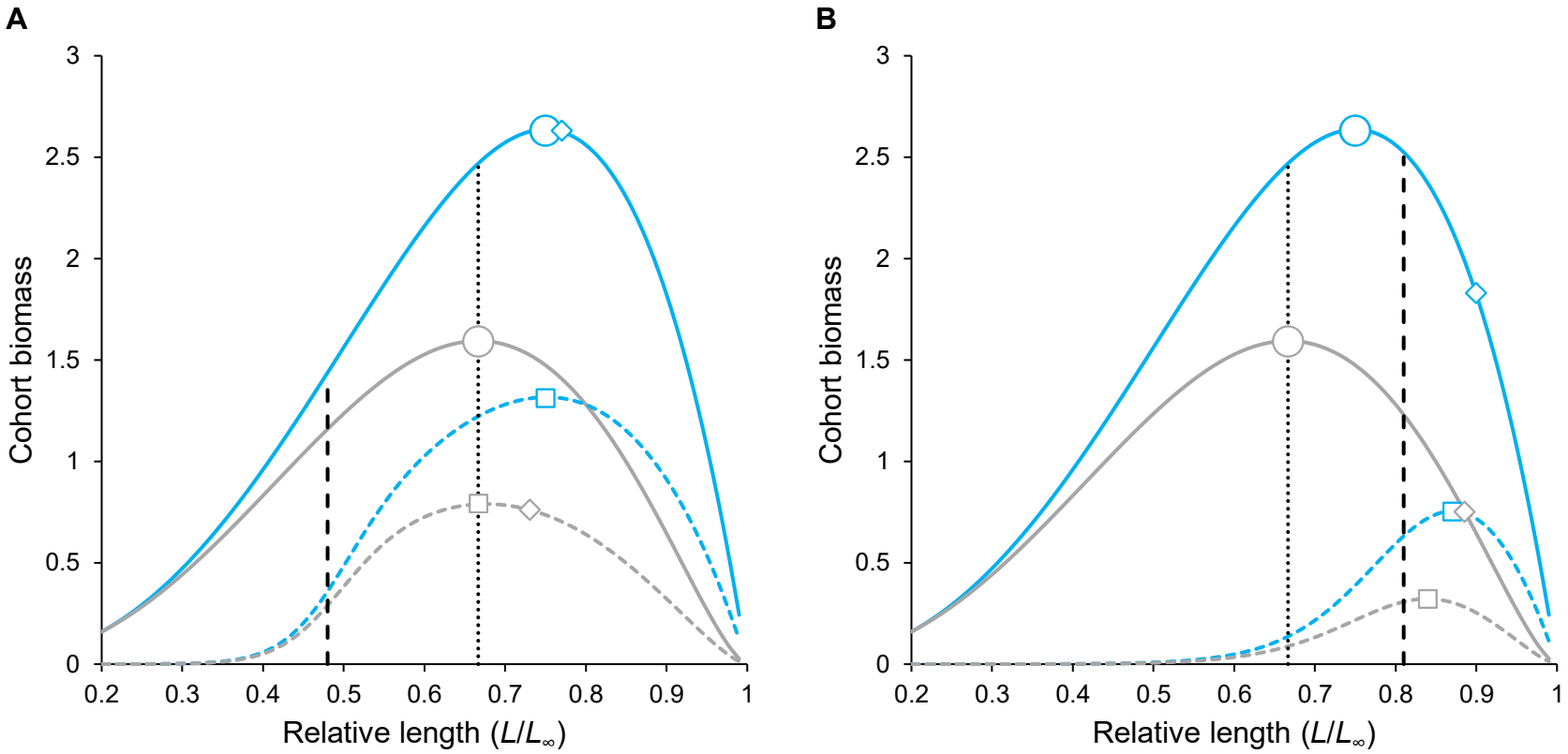

Fig. E1: Illustrative biomass trajectories over cohort age under different *M*/*k* ratios Biomass trajectory with *M*/*k* = 1 (blue) and *M*/*k* = 1.5 (grey) over relative length (length/asymptotic maximum length, L/L_∞) of a hypothetical cohort with **A)** length at maturity (dashed vertical line) below the length at maximum tissue production (dotted vertical line) and below the optimum length, i.e. the length at maximum cohort biomass (circles), and **B)** length at maturity above the length at maximum tissue production and above the optimum length. The peak in reproductive output (dashed curves) is shown as squares and the length corresponding to generation time as diamonds. Cohort biomass (solid curves) at length, *L*, was estimated from $(\frac{(L_\infty - L)}{L_\infty})^{\frac{M}{k}} * aL^3$, with *a* being a constant, and *3* being the exponent of the length-weight relationship, and the respective *M*/*k* ratio. The number of offspring at length was also assumed to be a power function with the exponent *3*. The length at maximum tissue production was calculated via $L_{ti} = L_\infty(1 - \frac{1}{3})$ (Jensen, 1985).

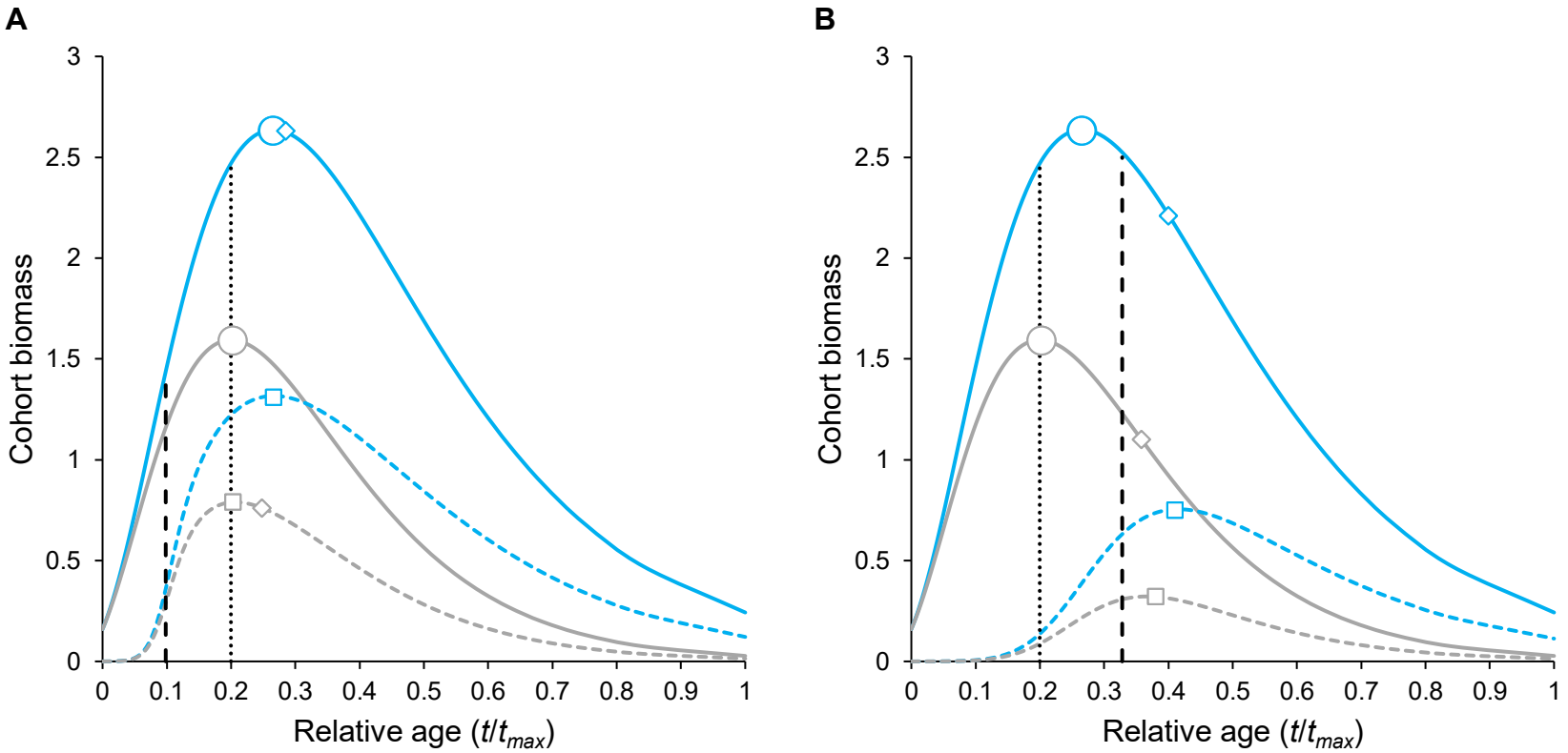

Fig. E2: Illustrative biomass trajectories over cohort length under different *M*/*k* ratios. Biomass trajectory with *M*/*k* = 1 (blue) and *M*/*k* = 1.5 (grey) over relative age (age/maximum age, t/t_{∞}) of a hypothetical cohort with **A)** age at maturity (dashed vertical line) below the age at maximum tissue production (dotted vertical line) and below the optimum age, i.e. the age at maximum cohort biomass (circles), and **B)** age at maturity above the age at maximum tissue production and above the optimum age. The peak in reproductive output (dashed curves) is shown as squares and the generation time as diamonds. Cohort biomass (solid curves) at length, *L*, was estimated from $(\frac{(L_{\infty}-L)}{L_{\infty}})^{\frac{M}{k}} * aL^3$, with *a* being a constant, and *3* being the exponent of the length-weight relationship, and the respective *M*/*k* ratio. The number of offspring at length was also assumed to be a power function with the exponent *3*. The length at maximum tissue production was calculated via $L_{ti} = L_{\infty}(1-\frac{1}{3})$ (Jensen, 1985) The corresponding ages were obtained from the von Bertalanffy growth function.

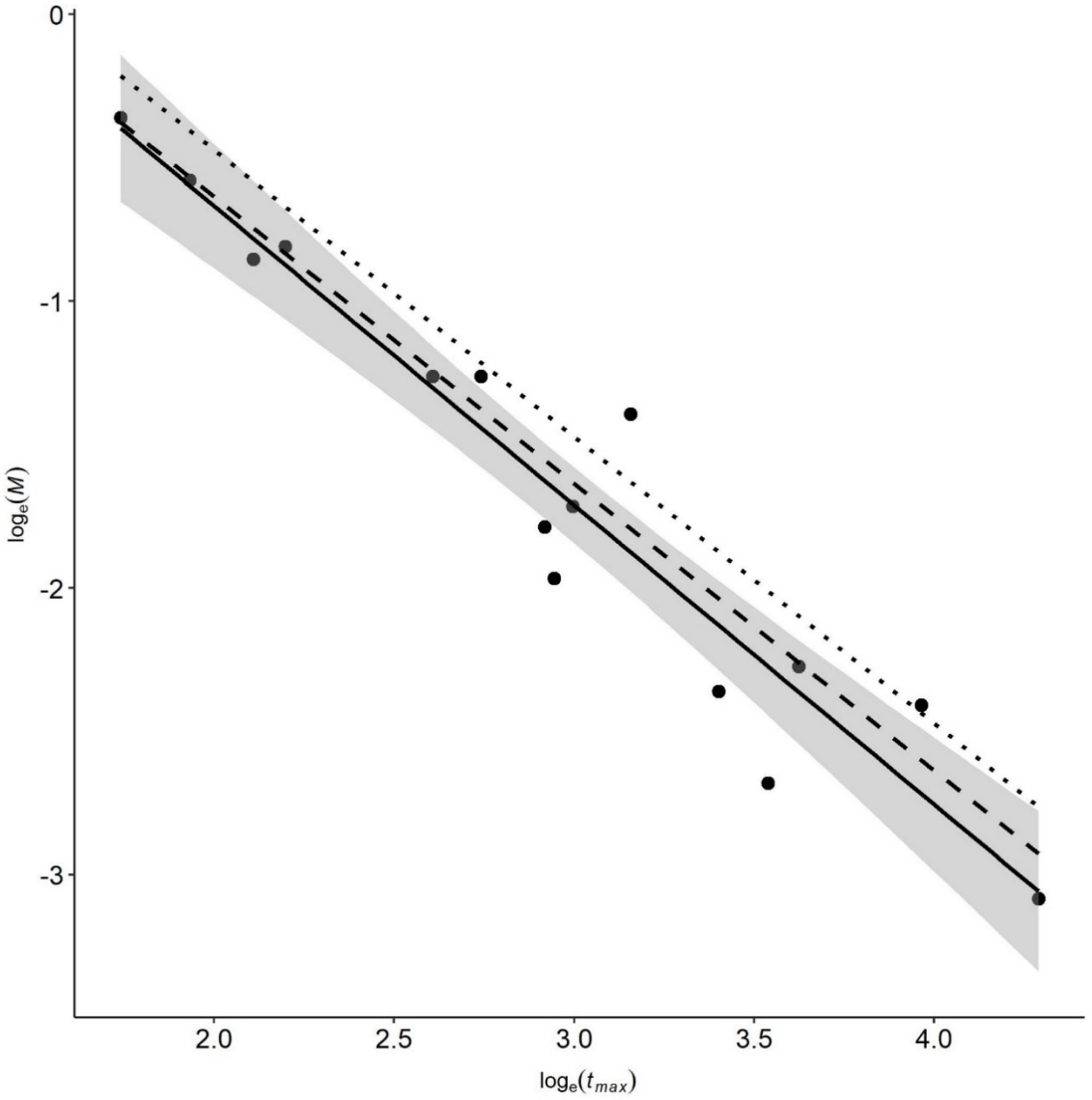

Fig. E3: Comparison of observed versus theoretically expected natural mortality in the studied elasmobranchs. The observed natural mortality rates, M ($\log_e$ year^{-1}), from direct methods versus observed maximum age, t_{max} ($\log_e$ year). Linear trend line in black with 95% confidence intervals in shaded grey. The dotted lines correspond to the natural mortality rate expected under the observed t_{max} with 1% surviving from birth to maximum age, the dashed line corresponds to 2% survivors.

Appendix F
Supporting information for Chapter 6

Supporting materials and methods

Study area

The study area comprises European Union (EU) territorial waters and exclusive economic zones (EEZ) excluding the Mediterranean Sea between 16°W, 13°E and 62°N and 36°N to a water depth of 800 meter. The study area was chosen based on catches of elasmobranch species in the International Council for the Exploration of the Sea (ICES) scientific surveys (Fig. E11) and the trawling ban on depth below 800 m introduced in the EU in 2017 (EU, 2016). GIS shapefiles of EEZs EU member countries were obtained from www.marineregions.org, the 800-m depth contour was derived from using the getNOAA.bathy function from the R package *marmap* (Pante & Simon-Bouhet, 2013).

Scientific survey data

Scientific research trawl surveys are independent from commercial fisheries and collect consistent and standardized data that can be used to derive relative abundance indices and spatial distributions of species (SISP 1-IBTS VIII, 2012). Here, raw data on elasmobranch distribution and abundance were derived from international bottom trawl research surveys compiled by ICES in the Northeast Atlantic and available from DATRAS (https://datras.ices.dk/). Only hauls marked as valid and survey data over the last 20 years (1997-2016) were considered in this study, as elasmobranchs can change their distribution patterns over longer time periods (Sguotti et al., 2016).

Species were identified by their valid AphiaID in the survey data. In total twenty species were used to reconstruct relative abundance patterns (Table F4). The two smoothhound species present in the data, *Mustelus mustelus* and *M. asterias*, were both considered to be starry smoothhound, *M. asterias*, as suggested by others (Farrell, 2010). Furthermore, only hauls 0-800 m and within the depth range of the elasmobranch species were included in the analysis. The maximum depth for a species was obtained from either the survey data or literature. The minimum depth was taken from the survey data or literature (Table F4). Next, we identified survey gears that sample a species in comparable manner. ICES surveys are following standardized procedures, but different survey gear types might be used to target different species. Elasmobranchs are not targeted and

different gears might result in different catches, for example, if a gear type cannot sample small juveniles due to larger mesh sizes or if a gear type catches more individuals due to a larger net. In this study, only comparable gear types based on their catchability and size selectivity were included. Selectivity was defined as the size range a specific gear type can catch and catchability was defined as the efficiency of the gear to catch a specific elasmobranch species. Comparable gear types were selected for each elasmobranch species based on a comprehensive analysis of size distribution of all fish species caught in ICES surveys (see Figs. F12 – F31). Here, ICES survey data were extracted for fish species only, i.e. classes Actinopterygii, Elasmobranchii, Holocephali or Myxini. The order Clupeiformes (herring-likes) were excluded because of different measurement units (SISP 1-IBTS VIII, 2012). The 99 percentile was used as maximum length for each fish species to account for measurement errors. Only species with similar size ranges compared to the respective elasmobranch species were included. To establish a size range for each elasmobranch species we estimated a minimum and maximum size, both with a lower and higher value, as identified in the data and from literature. First, we defined an elasmobranch species' lower maximum size as the smaller of either the smallest reported maximum size from the literature or the largest specimen present in the survey data. We then defined an elasmobranch species upper maximum size as the larger of either the smallest reported maximum size from literature or the largest specimen present in the survey data. All fish species that attained at least a maximum size of 90% the elasmobranch species lower maximum size and were not larger than the elasmobranch species upper maximum size were included in the size selectivity analysis. Likewise, we defined the lower minimum size as the smaller of either the maximum reported size at birth or the smallest elasmobranch specimen caught. Fish species smaller than the minimum size of the respective elasmobranch species were excluded. All length measurements were binned into 5 cm length classes. Then, the total number of individuals caught per length class and gear type was normalized to a maximum value of 1 for each fish species. This was done to remove the influence of highly abundant species. The normalized relative abundance indices were then summed up across fish species and again standardized to a maximum value of 1 for visualization purposes. Finally, comparable gear types that showed similar pattern in selectivity and catchability (i.e. the size range caught and the number of individuals caught per size range) were selected for each elasmobranch species individually, see (Figs. F12 – F31). This procedure made sure that only comparable survey gear types were included for each species.

Commercial trawl data

The spatial distribution of commercial trawl fishing effort in the study area for the year 2017 was obtained from processed Automatic Identification System (AIS) data provided by Global Fishing Watch (http://globalfishingwatch.org/). AIS is an electronic safety device to remotely track movements of vessels carrying an AIS transponder. The AIS signal is received via ground stations and/or satellites and can be automatically processed to identify behavior based on spatial movement patterns (de Souza et al., 2016; Kroodsma et al., 2018). Fishing effort from AIS data is identified and calculated as hours of fishing effort per area based on machine learning methods as described in (Kroodsma et al., 2018). Using convoluted neural networks, fishing vessel types are first identified according to the fishing gear used and fishing activity is then classified based on a set of vessel movement characteristics such as speed and turning angles. Within the bounding box, excluding the Mediterranean Sea, 2689 trawlers were active in 2017 as classified by Global Fishing Watch's neural network version 7, i.e. vessels using towed gears and with an active license at December 31st 2017 as listed in the European Fleet Register. Of those, 339 were smaller than 15 m, with the smallest being 9.3 m and the largest 144.6 m (mean = 26.1 m). The detection of vessels larger than 15 m is considered close to 100% given strict EU regulations on AIS use for these vessels (EU, 2002).

Marine protected area data

Marine protected area (MPA) shapefiles were extracted from the World Database of Protected Areas (www.protectedplanet.net) and tailored to the study area, i.e. only the part of the MPA that overlapped within the study area was considered. Furthermore, only MPAs classified as 100% marine protected areas, i.e. excluding all MPAs that had also terrestrial parts, with a declaration year of 2016 or earlier and with designated status were included in the analysis. One MPA with no information on status year (Coastal National Park in Jersey) was removed. Two Spanish national MPAs listed as Natura 2000 sites were categorized as Site of Community Importance (Habitat directive) following information on http://www.mpatlas.org. MPAs listed as Nature Reserves were divided into German and UK Nature Reserves. MPAs were differentiated by their World Database of Protected Areas identification number which is the unique identifier of a protected area. However, in the EU MPAs can be designated under several frameworks, such as the Convention for the Protection of the Marine Environment of the North-East Atlantic

(OSPAR) or the EU Habitats Directive through Natura 2000, and consequently the same area can be managed under multiple, varying management plans and regimes. Hence, the protected area identifier is only unique to the designation type not the geography which can result in the same MPA being covered by multiple designation types. To illustrate this, the Noordzeekustzone in the Dutch Wadden Sea is designated under OSPAR, Habitats Directive, Birds Directive and the national Nature Conservation Act and therefore contains four MPA types with four different identification numbers covering the same area. Whether a management plan was present or not was decided based on the MPAs in the dataset having a link to a management plan or being categorized as "Management plan is implanted and available". MPAs categorized as "not reported" or "Management plan is not implemented and not available" were assumed to not have a management plan.

Data analysis

Standardized research survey catch per unit effort time series were calculated as a normalized index of relative elasmobranch abundance from the ICES survey data. First, all elasmobranch catches in research surveys were standardized to 60 min of hauling. Then, the numbers caught per species *i* standardized to 60 min of hauling N_h and the number of hauls *H* were summed up per area *A*. Whether a haul was counted inside an area was based on the mean between the start and end haul longitude and latitude. If the end coordinates were not given, the start coordinates were used. The per species catch per unit effort was then obtained by dividing the total number of individuals caught by the number of hauls in the area for each species:

$$CPUE_{i,A} = \frac{\sum_{i,A} N_h}{\sum_{i,A} H}. \quad \text{(F1)}$$

In order to identify areas that have the highest relative abundance across species, a standardized multi-species catch per unit effort was calculated, here referred to as abundance index. First, the per species catch per unit effort was normalized to a maximum value of 1 for each species. This was done to eliminate the influence of highly abundant species. Then the abundance index per investigated area was calculated by summing up the catch per unit effort normalized to a maximum value of 1 across species.

Commercial trawl effort was given as the sum of trawling hours per 0.01 by 0.01 degree grid cell for the year 2017. Trawling inside versus outside the investigated areas were computed by overlaying the area and the trawl data on a 0.01 by 0.01 degree grid scale. For comparison, trawling effort was standardized per investigated area. This was done by dividing the sum of total effort (hours) with either the number of grid cells subject

to trawling (commercial trawling hours per grid cell (hr 0.01°cell^{-1}), the area in square kilometers of the trawled grid cells (commercial trawling hours per trawled area (hr km^{-2} trawled area), or the total area in squared kilometers, i.e. considering also those parts of an area that were not subject to trawling (commercial trawling hours per area (hr km^{-2}). Note, if the investigated area was either a grid cell or an ICES statistical management area (rectangles of 1 degree longitude x 0.5 degrees latitude), the simplifying assumption that all grid cells and statistical areas have the same size was made, although coastal grids and rectangles can be smaller. Therefore, the estimates for coastal areas can be conservative as the same trawling effort would be divided by a larger area.

To investigate if there is a significant relationship between relative elasmobranch abundance across species (abundance index) and trawling intensity (commercial trawling per area) a generalized linear model with a beta-distributed dependent variable (beta regression) was applied (Cribari-Neto & Zeileis, 2010). Beta regression can be used for ratios between 0 and 1, such as the abundance index, but excluding 0 and 1. Therefore, the abundance index was standardized again to a maximum abundance index of 1 and transformed via (abundance index*(N-1)+0.5)/N, where N is the sample size (Smithson & Verkuilen, 2006). Additional covariates and a spatial autocorrelation term were included in the model to test whether the effect and significance of the main covariate, commercial trawling per area (km^{-2}), remains after accounting for confounding factors and potential spatial dependence. The baseline model had commercial trawling hours per area, sea bottom temperature in degree Celsius (SBT), mean depth in meter, the km^2 of the statistical management area protected and dominant substrate type in a statistical management area as covariates. Substrate type had 8 factor levels (coarse sediment, fine mud, mixed sediment, mud to muddy sand, rocky or other hard substrata, sand, sandy mud to muddy sand, unknown). Rocky seafloor habitats, which may experience lower trawling intensity in Europe (Eigaard et al., 2017), were present in 8.4% of MPAs without trawling effort, which was slightly higher than the 6.2% across all MPAs and 2.1% across EU waters. Temperature, depth and substrate were used because they have been shown to be important predictors of elasmobranch distribution in Europe (Sguotti et al., 2016). The climate covariates were obtained from AquaMaps (www.aquamaps.org). Classification of substrate type was taken from The European Nature Information System. Information contained here has been derived from data that is made available under the European Marine Observation Data Network (EMODnet) Seabed Habitats project (www.emodnet-seabedhabitats.eu), funded by the European Commission's Directorate-

General for Maritime Affairs and Fisheries. Model selection was done using the Akaike information criterion (AIC). First, variable dispersion (commercial trawling hours per area | commercial trawling hours per area), commercial trawling per area $\log_e$ plus 1 transformed and all other continuous covariates $\log_e$ transformed and a Gaussian spatial correlation term (gau; Gaussian decay in correlation with distance) were tested on the baseline model (Table F6). Transformation of the covariates ($\log_e$) were tested due to potentially very influential observations from a few highly trawled areas. Based on the model with the lowest AIC and no spatial autocorrelation (Moran's I test for spatial autocorrelation p-value > 0.05), covariate selection was done by removing the least significant covariate till the AIC was not decreasing anymore and all covariates were significant (Table F5). Models were fitted using the *glmmTMB* package in R (Mollie et al., 2017). A sensitivity analysis was done by investigating if resolution on a finer scale (grids of 0.1 degree longitude x 0.1 degrees latitude) results in similar trends between the relative elasmobranch abundance index and commercial trawling per area (Fig. F32).

To investigate if there are different trends over time in the abundance index of high versus low trawled areas, the abundance index and commercial trawling per area were calculated for ICES statistical management area. Then, for each survey year (1997-2016), areas with high and low trawling intensity were determined. Low-trawling areas were defined as the 25 percentile of trawling effort per area from 2017. High-trawling areas were defined as the 75 percentile of trawling effort per area from 2017. This approach assumes that the relative distribution of trawl effort is approximately constant over time; this assumption was supported by comparing the distribution of trawl effort from 2017 with previously published maps estimating trawl intensity in Europe dating back to 2009 (ICES, 2016, 2017a; Eigaard et al., 2017). Boxplots were then used to investigate trends in relative elasmobranch abundance over time in both low and high trawled areas.

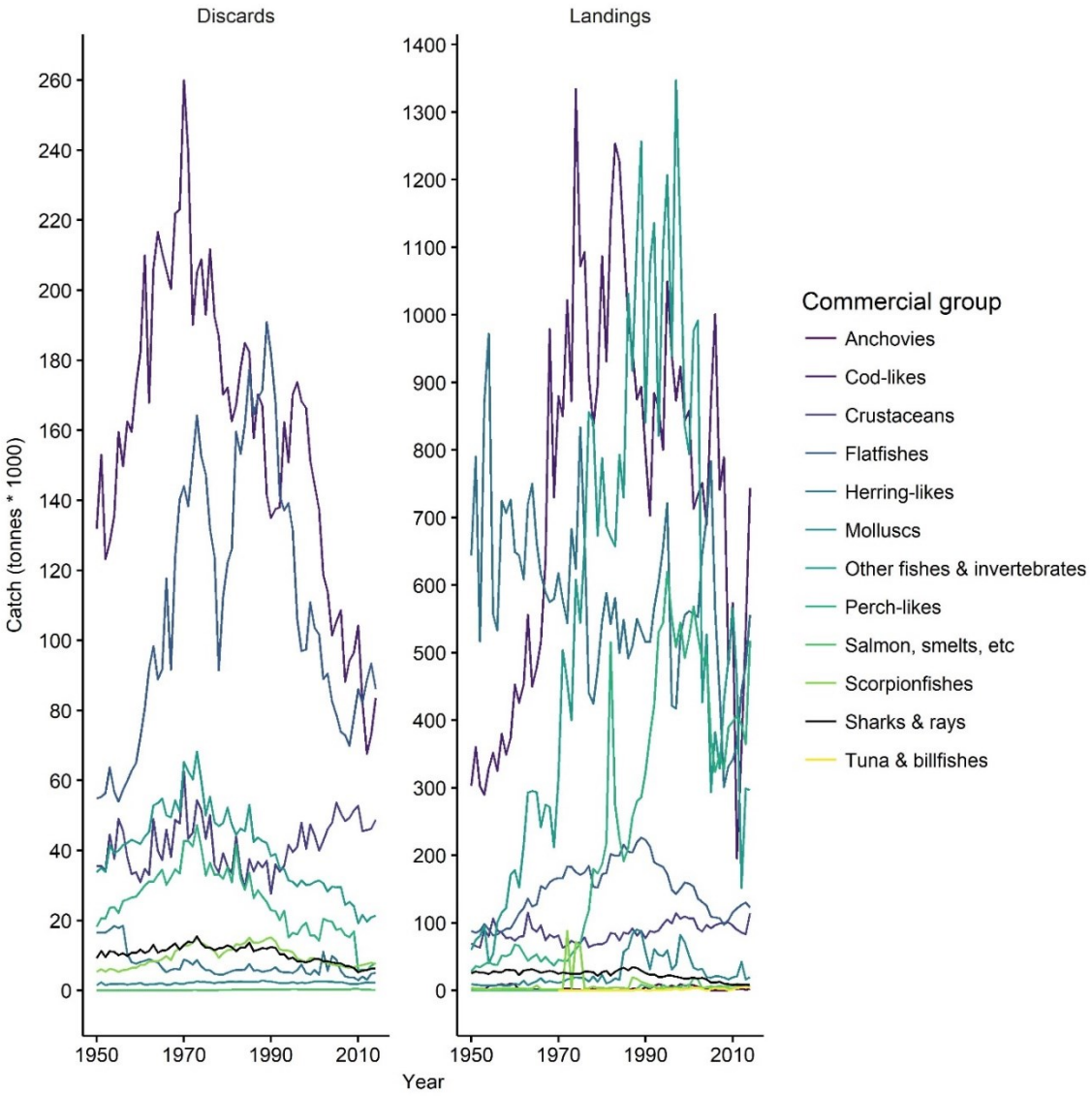

Fig. F1: Trawling discards and landings by commercial species groups in the European Union. Shown is the estimated discards on the left and landings on the right in 1000 tonnes for major commercial species from 1950 to 2014, using the Sea Around Us database (www.seaaroundus.org). Only the landings and discards estimated for bottom or pelagic trawlers were utilized and the area encompassed the large marine ecosystems (LMEs) within the study area, i.e. the Celtic-Biscay Shelf, Iberian Coastal and North Sea LMEs.

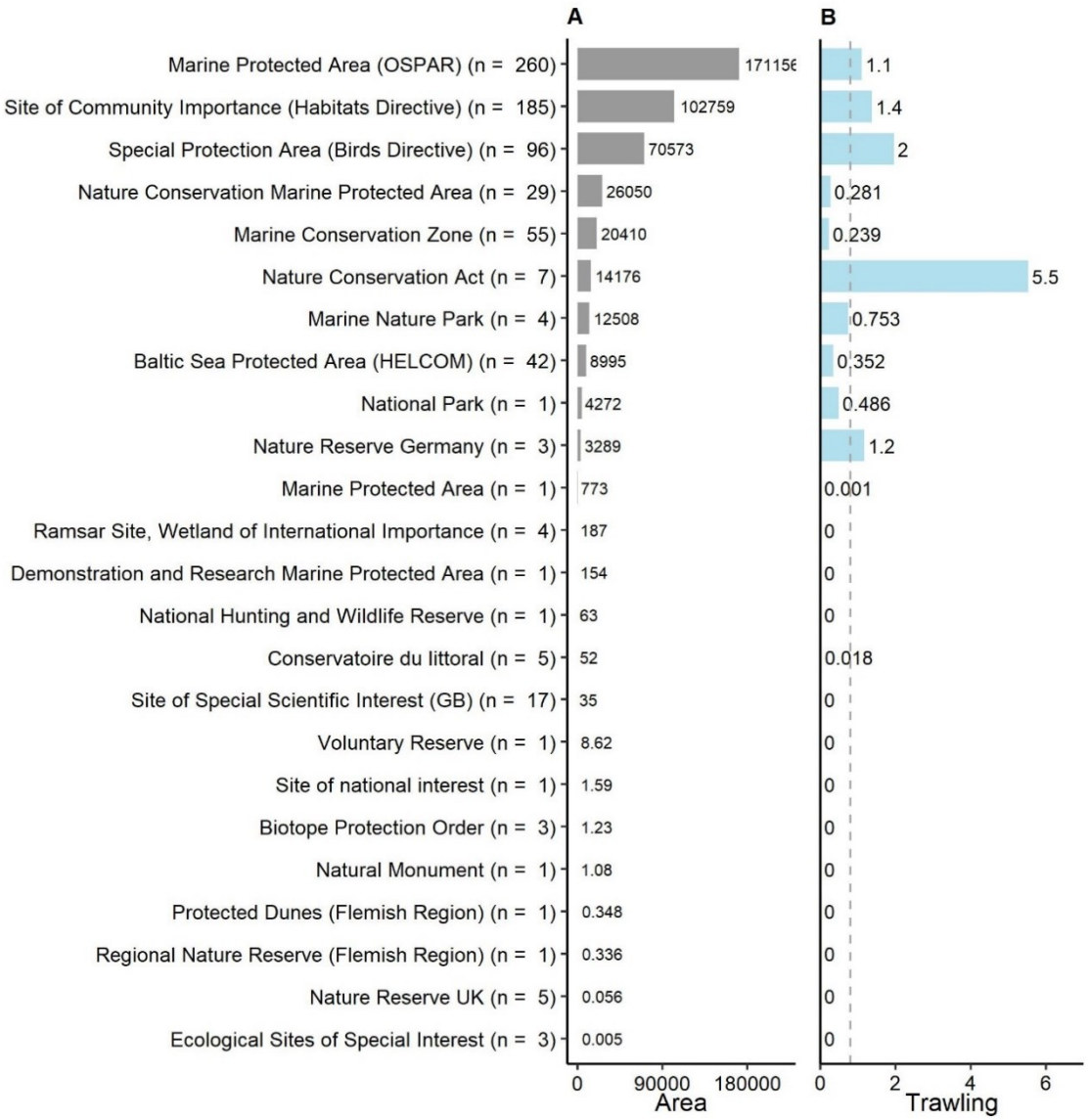

Fig. F2: Commercial trawling intensity and marine protected area coverage per designation type. Shown are all marine protected area (MPA) designation types (nationally and internationally) that were considered in this study. The number of MPAs present in the respective designation type is given in the brackets. **A)** The area covered by each designation type. **B)** Commercial trawling intensity per area (hr km^{-2}) for each designation type. The grey dotted line indicates the average commercial trawling intensity in non-protected areas for reference.

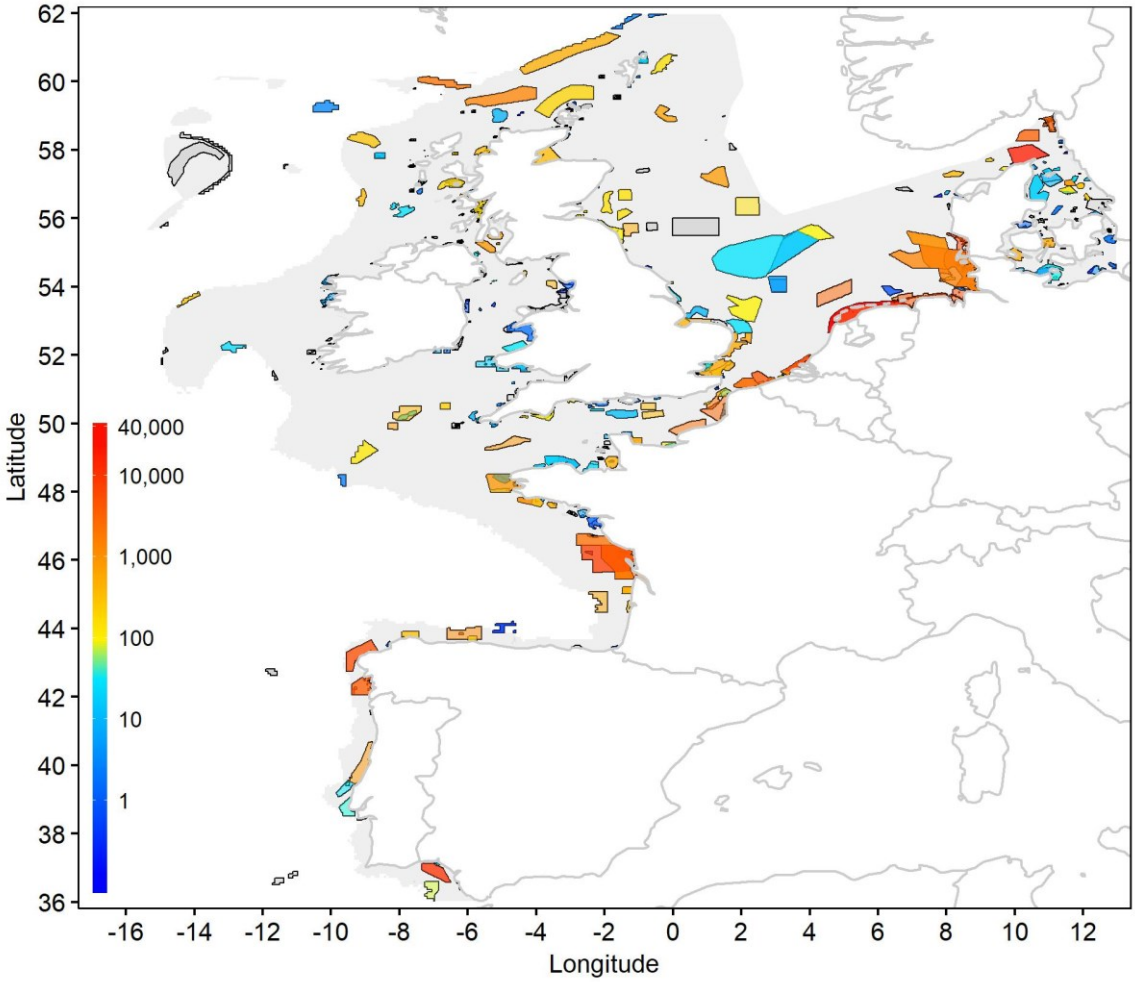

Fig. F3: Commercial trawling intensity inside European Union marine protected areas. The semi-transparent colors represent the hours of trawling per marine protected area (MPA). The overall study area is shown in grey. Protected areas filled with grey had zero trawling effort. Note that different MPA types can occupy the same area and therefore MPA designations with no commercial trawling can be overlaid by MPAs with trawling occupying the same area.

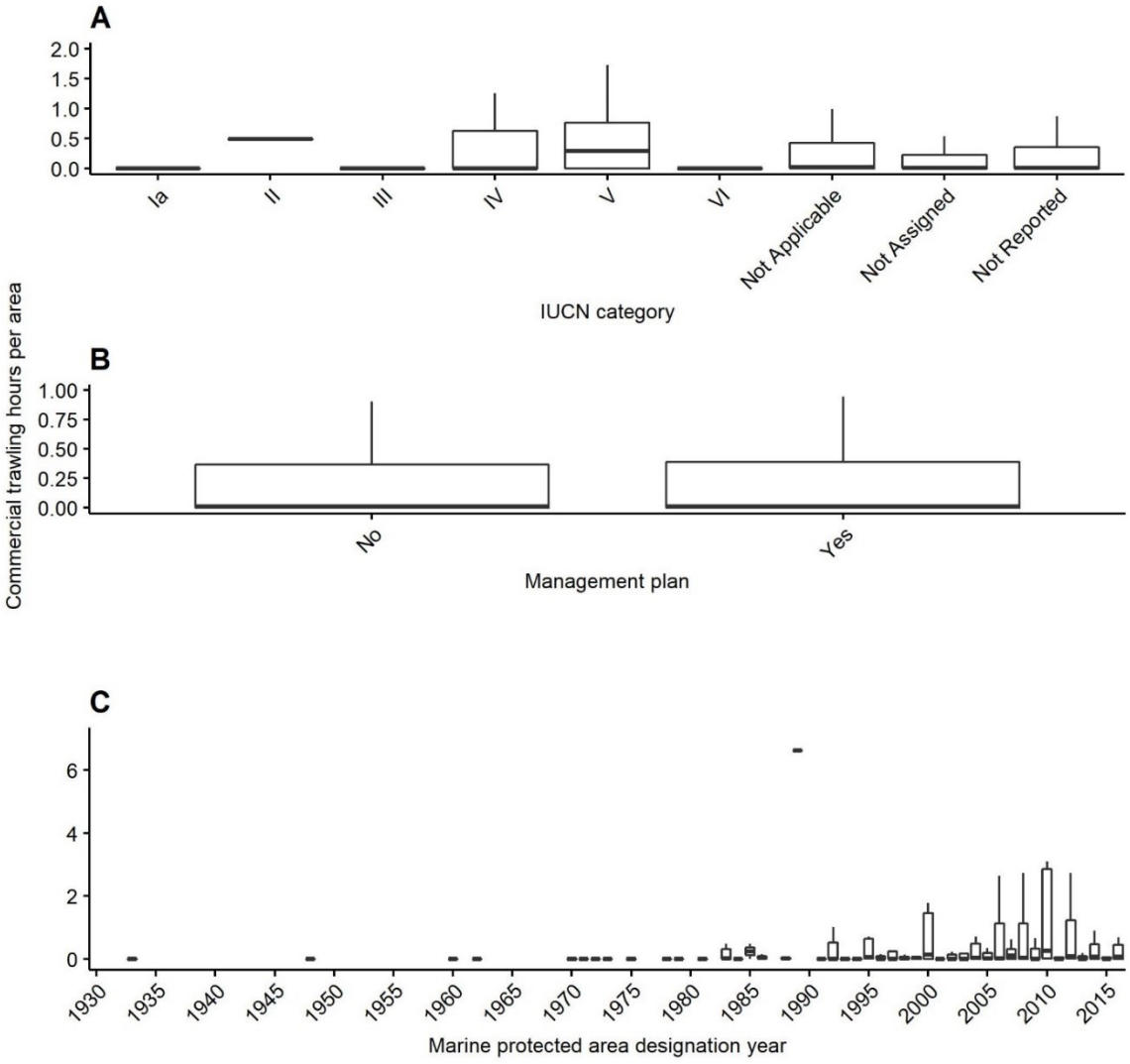

Fig. F4: Commercial trawling intensity versus marine protected areas characteristics. Shown is the commercial trawling effort expressed as hours per total area in square kilometers for marine protected areas (MPAs) with **A)** different International Union for Conservation of Nature (IUCN) protected area categories, **B)** with a management plan present or absent and **C)** with different years of MPA designation. Data were extracted from the World Database of Protected Areas (WDPA) for all 727 different MPAs considered in this study. Note that >50% of MPAs had no management plan available and >90% did not report IUCN protected area categories. None of the MPAs with an IUCN category assigned had a management plan available.

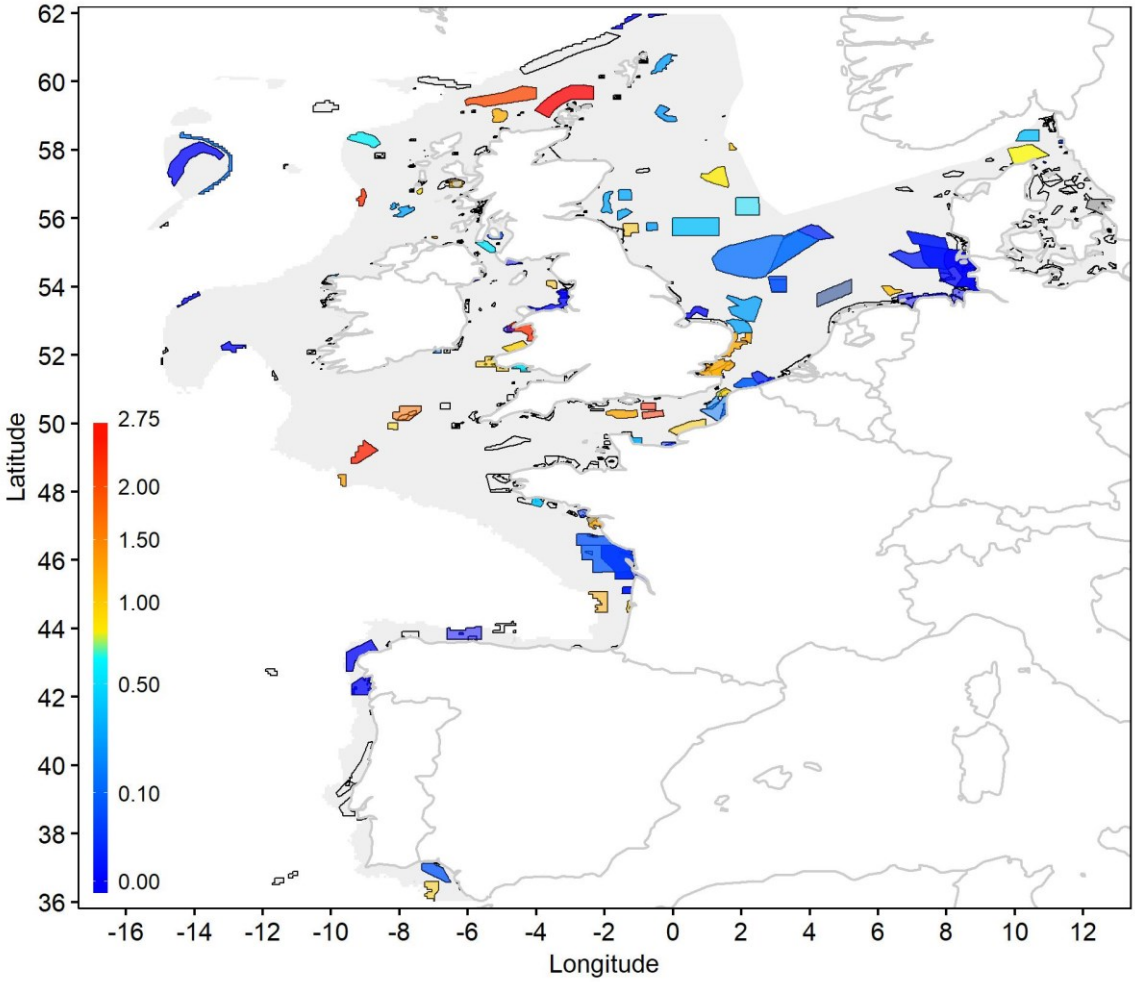

Fig. F5: Relative elasmobranch abundance inside European Union marine protected areas. Given is abundance index (multi-species catch per unit effort) obtained from scientific research trawls in semi-transparent colors. The study area is shown in grey. Marine protected areas (MPAs) filled with grey but no color were not surveyed or the survey was not considered after data standardization. Note that different MPAs can occupy the same area fully or partially.

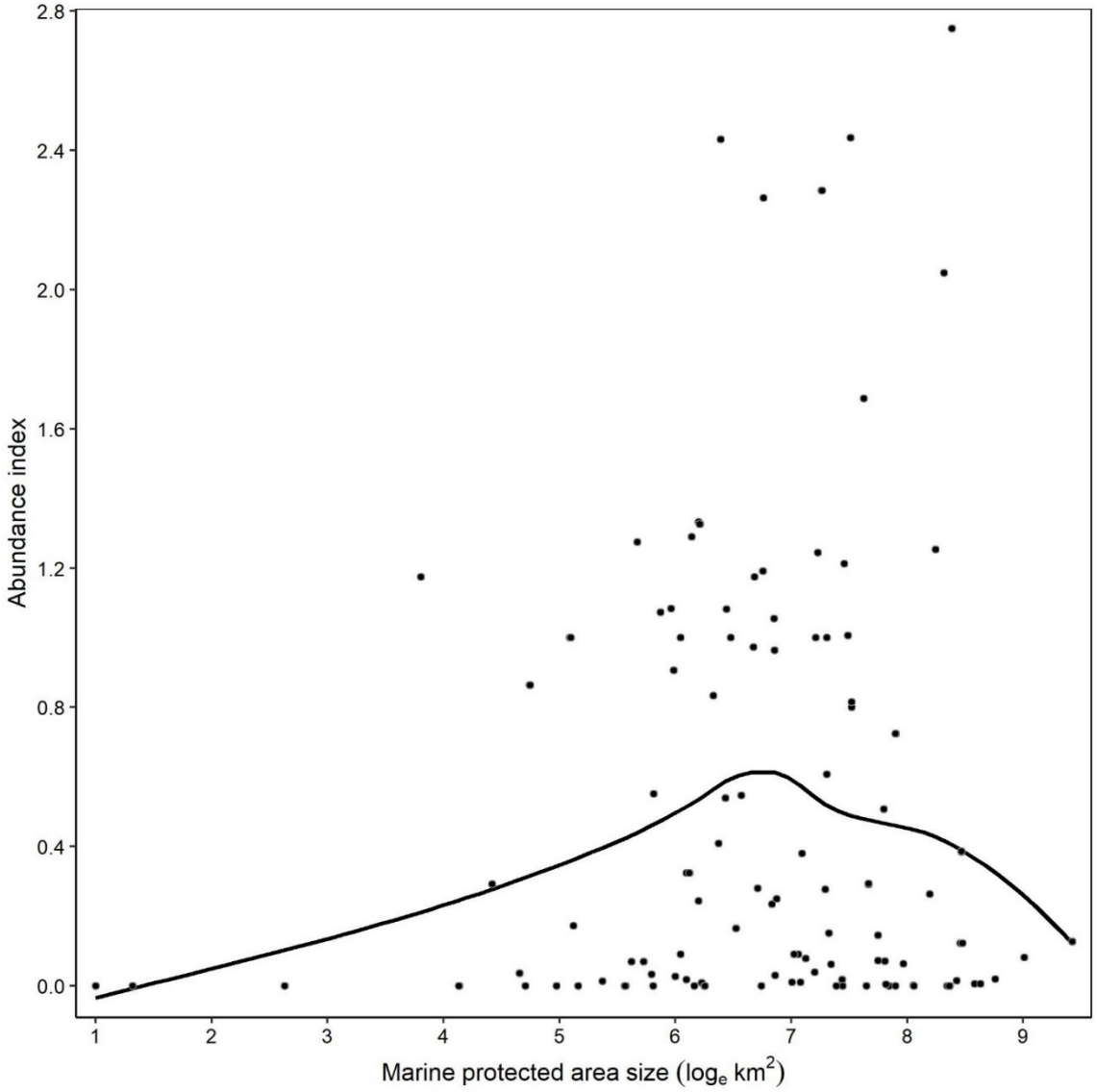

Fig. F6: Relationship between elasmobranch abundance and marine protected area size. Abundance index (multi-species catch per unit effort) versus $\log_e$ transformed marine protected area (MPA) size in square kilometers. The black line shows a loess smoothing fit.

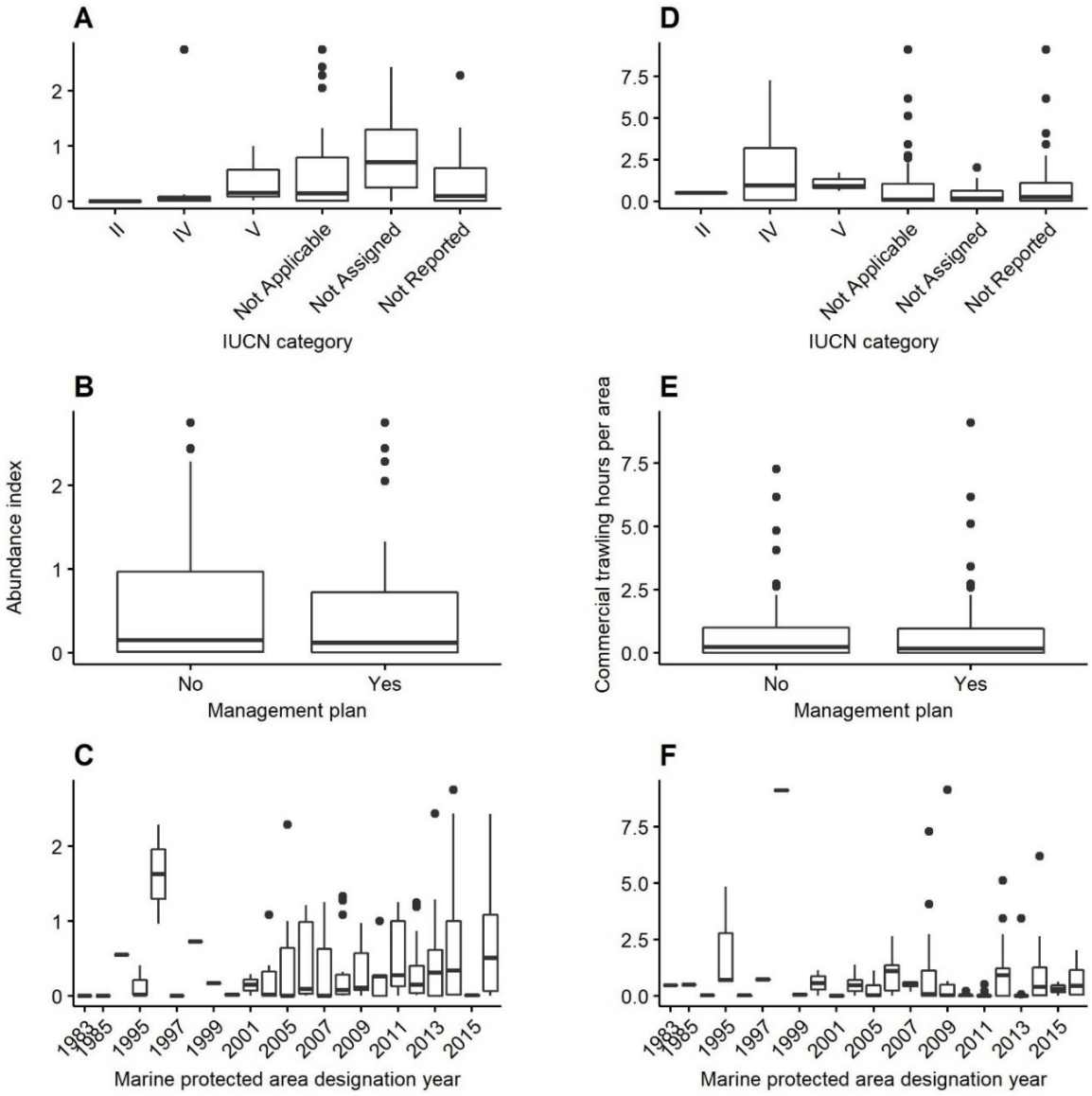

Fig. F7: Elasmobranch abundance and commercial trawling intensity versus marine protected areas characteristics. Shown is the elasmobranch abundance index (multi-species catch per unit effort) obtained from scientific research trawls for marine protected areas (MPAs) with **A)** different International Union for Conservation of Nature (IUCN) protected area categories, **B)** with a management plan present or absent and **C)** with different years of MPA designation. The commercial trawling hours per total area in square kilometers for the same MPAs in which elasmobranchs were sampled is given for **D)** IUCN MPA categories, **E)** management plan availability and **F)** year of MPA designation. MPA characteristics were assigned according to the World Database of Protected Areas.

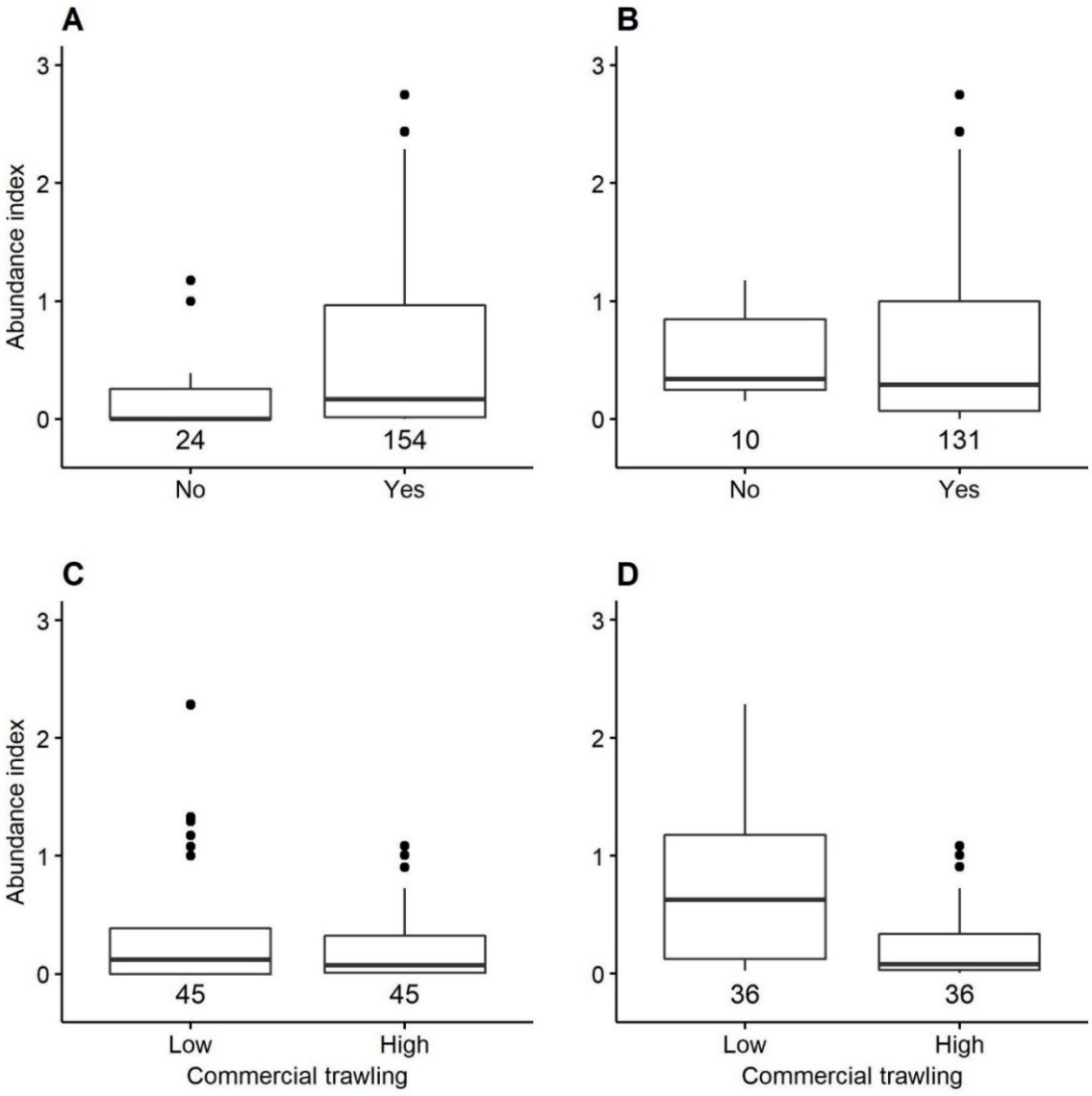

Fig. F8: Relative elasmobranch abundance in commercially trawled versus non-trawled marine protected areas. Marine protected areas (MPAs) with different commercial trawling intensity (no trawling, trawling present, low trawling intensity and high trawling intensity all measured as hr km^{-2}) are compared to **A)** and **C)** the elasmobranch abundance index (multi-species catch per unit effort normalized across species) in all MPAs where the International Council for the Exploration of the Sea (ICES) scientific surveys were conducted and elasmobranch species could have been caught, and **B)** and **D)** all MPAs where ICES scientific surveys were conducted and elasmobranch species have been caught. Low and high trawled MPAs were defined as lower quartile (≤0.009 in **C)** and ≤0.0015 in **D)**) and upper quartile (≥1.06 in **C)** and ≥1.11 **D)**) respectively. The sample size is given below the boxplots.

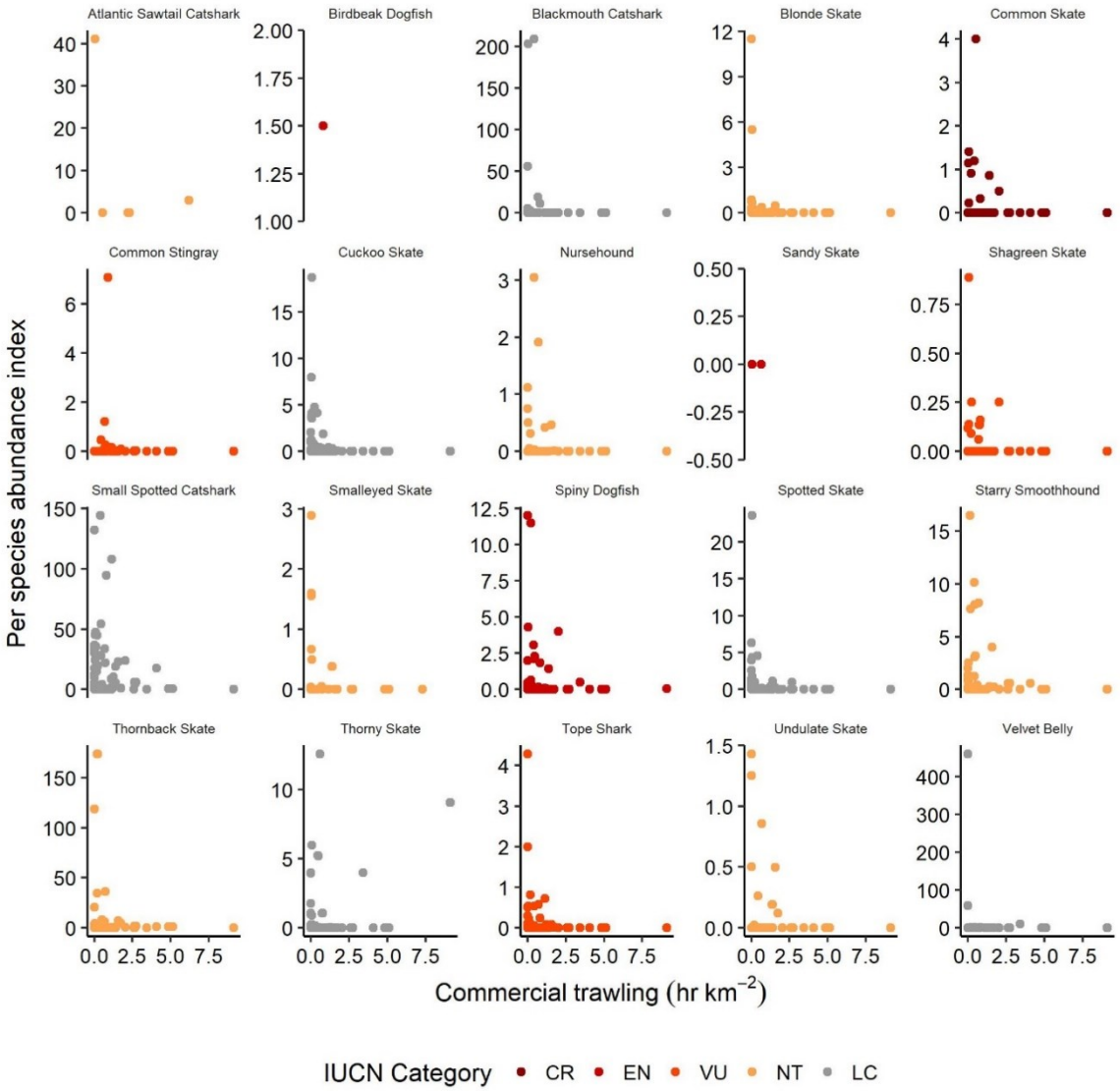

Fig. F9: Relationship between relative elasmobranch abundance and commercial trawl intensity inside European Union marine protected areas. Shown is the per species abundance index (catch per unit effort) versus the commercial trawling hours per total area in square kilometers for each marine protected area (MPA) that was scientifically surveyed. Colors represent a species' International Union for Conservation of Nature (IUCN) redlist status for Europe (CR = critically endangered, EN = endangered, VU = vulnerable, NT = near threatened, LC = least concern). Note that different MPA designation types can occupy the same area fully or partly and these points would therefore overlap.

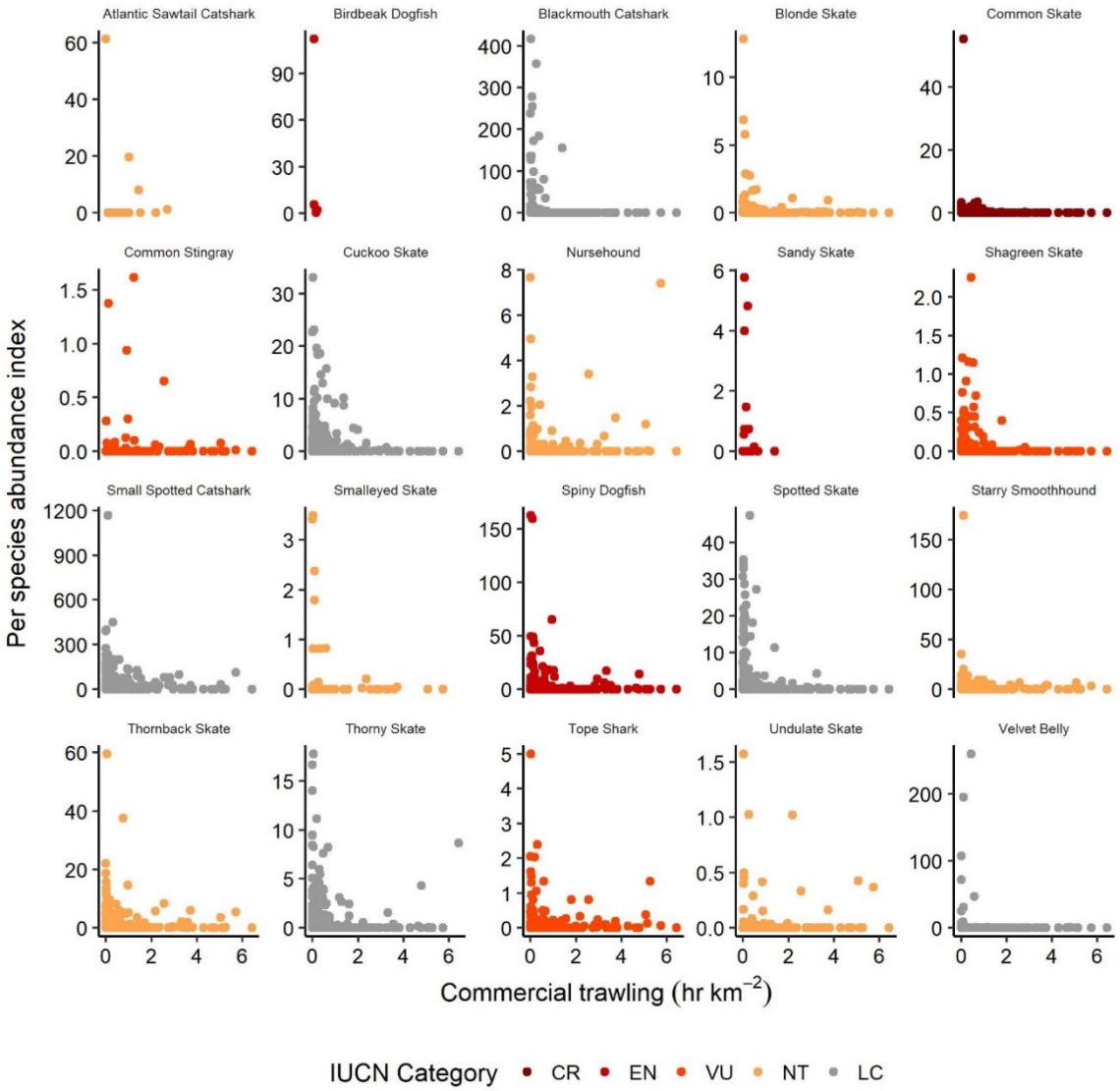

Fig. F10: Relationship between relative elasmobranch abundance and commercial trawl intensity for the whole study area. Shown is the per species abundance index (catch per unit effort) versus the commercial trawling hours per total area in square kilometers for the International Council for the Exploration of the Sea (ICES) statistical management areas (rectangles of 1 degree longitude x 0.5 degrees latitude). Colors represent a species' International Union for Conservation of Nature (IUCN) redlist status for Europe (CR = critically endangered, EN = endangered, VU = vulnerable, NT = near threatened, LC = least concern).

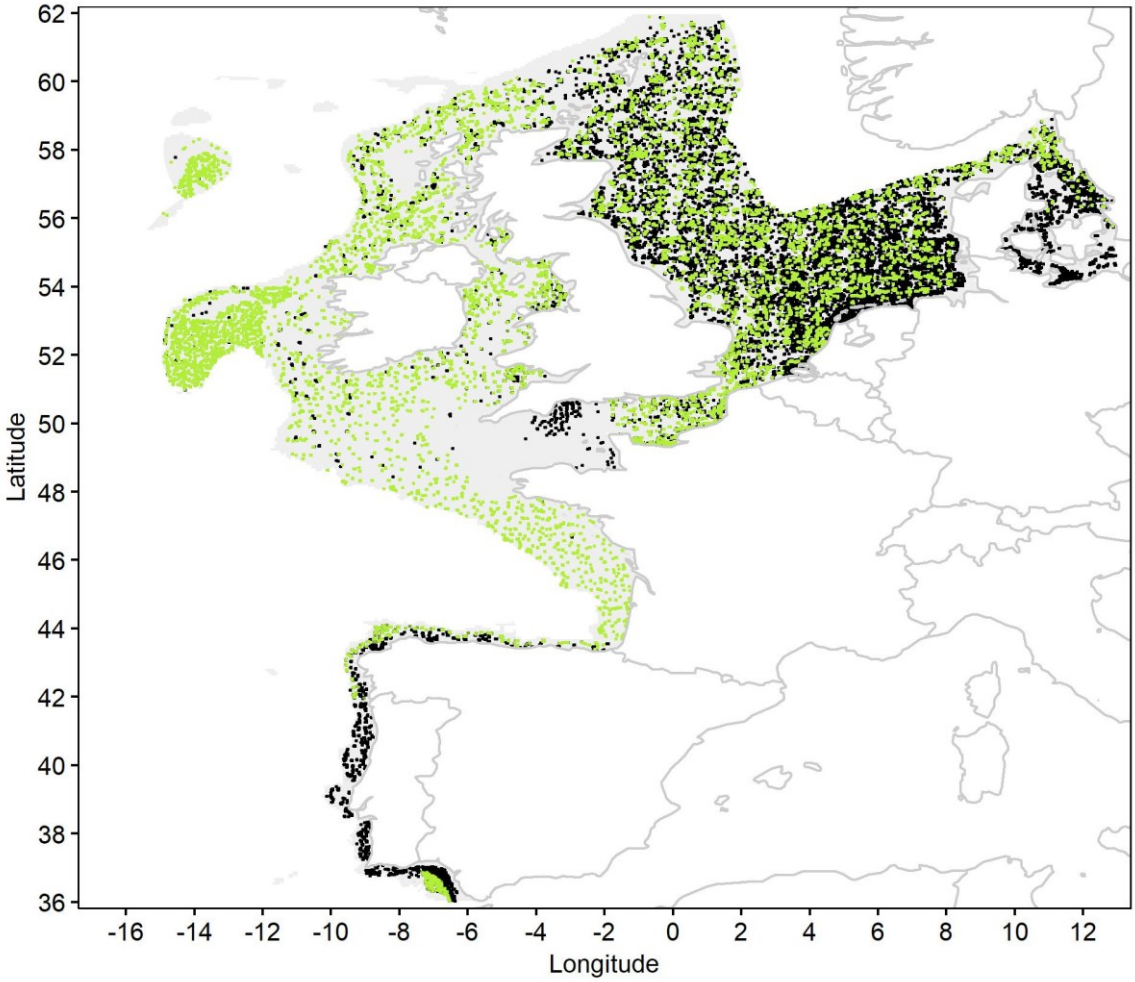

Fig. F11: Scientific research survey coverage in the study area. Green dots indicate the International Council for the Exploration of the Sea (ICES) scientific surveys considered in the analysis after standardization. Black dots indicate surveys that were not considered in this study due to incomparable gear types.

*

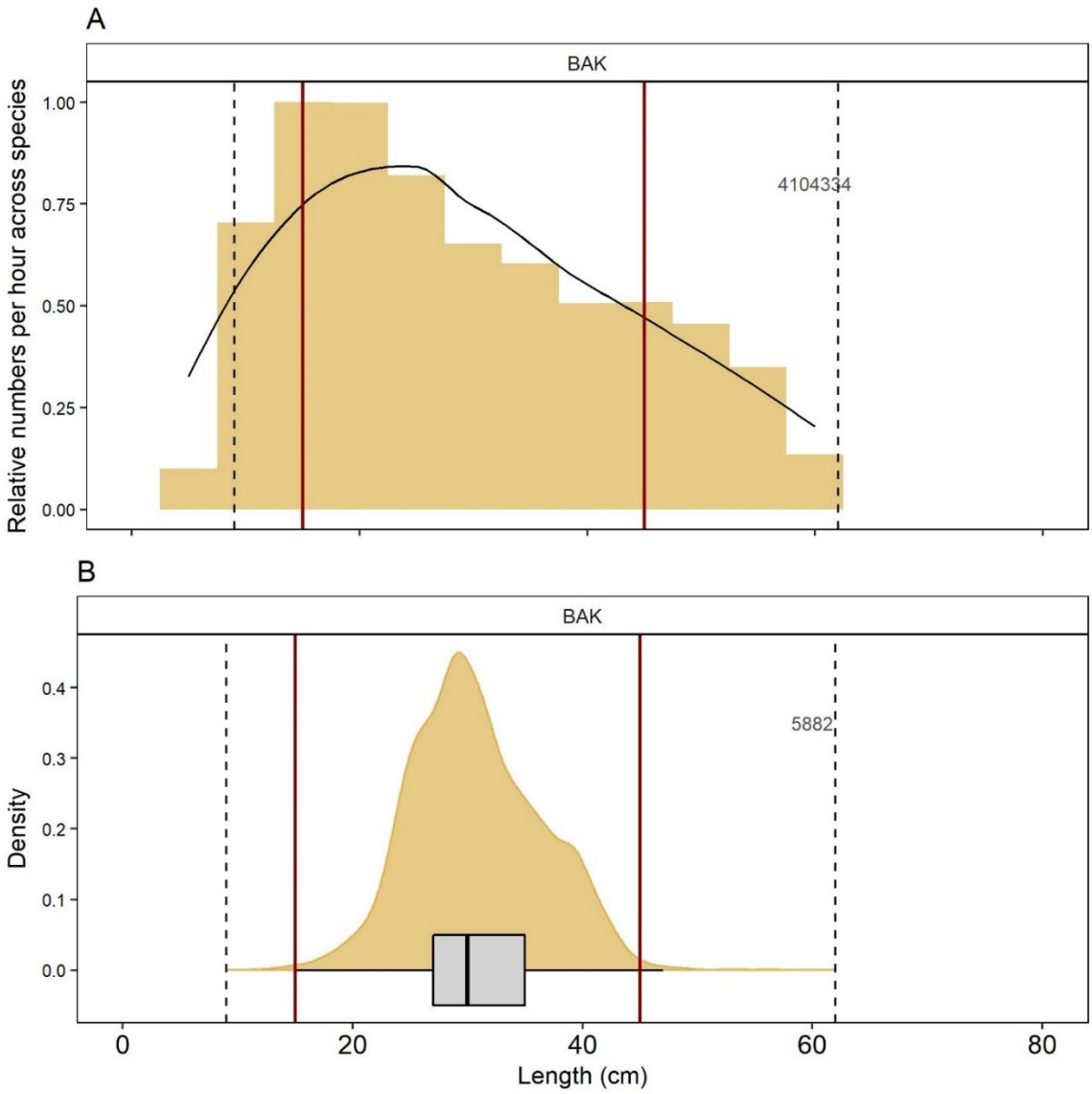

Fig. F12: Gear selectivity analysis for the Atlantic Sawtail Catshark. a) Shows the relative numbers caught by this gear type for all fish species in scientific surveys as a histogram with a bin width of 5 cm length intervals and a smoother line (black). b) Shows the numbers caught by this gear for the Atlantic Sawtail Catshark as flat violin plot. The vertical dotted lines are the minimum and maximum size caught of this elasmobranch species in the scientific surveys, the vertical red lines indicate maximum size at birth and the smallest maximum size reported in literature. The numbers in the plots show the sample size.

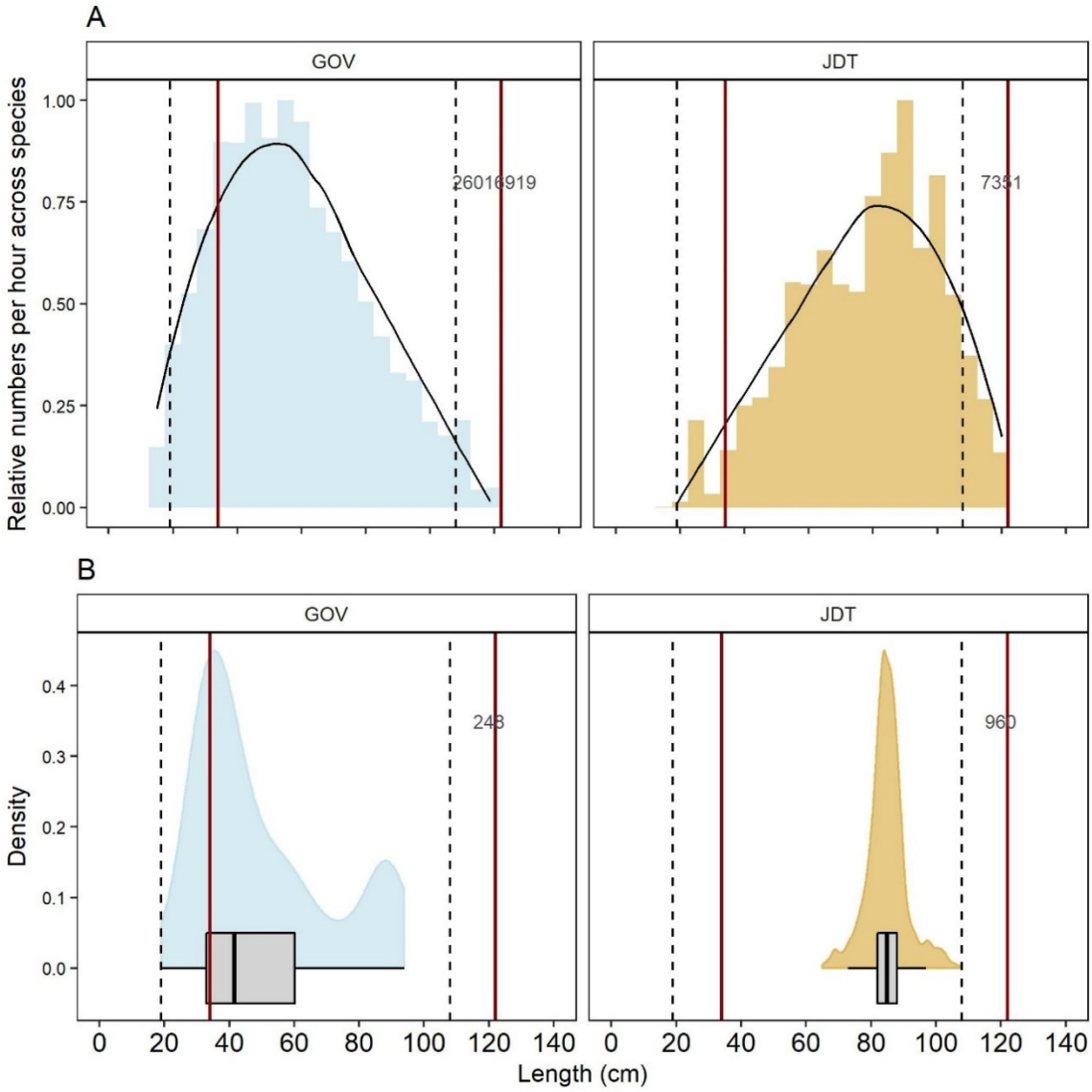

Fig. F13: Gear selectivity analysis for the Birdbeak Dogfish. a) Shows the relative numbers caught by gear type for all fish species in scientific surveys as a histogram with a bin width of 5 cm length intervals and a smoother line (black). Based on a) comparable gears were selected (gear types with golden bars). b) Shows the numbers caught by gear type for the Birdbeak Dogfish as flat violin plots. The vertical dotted lines are the minimum and maximum size caught of this elasmobranch species in the scientific surveys, the vertical red lines indicate maximum size at birth and the smallest maximum size reported in literature. The numbers in the plots show the sample size per gear type.

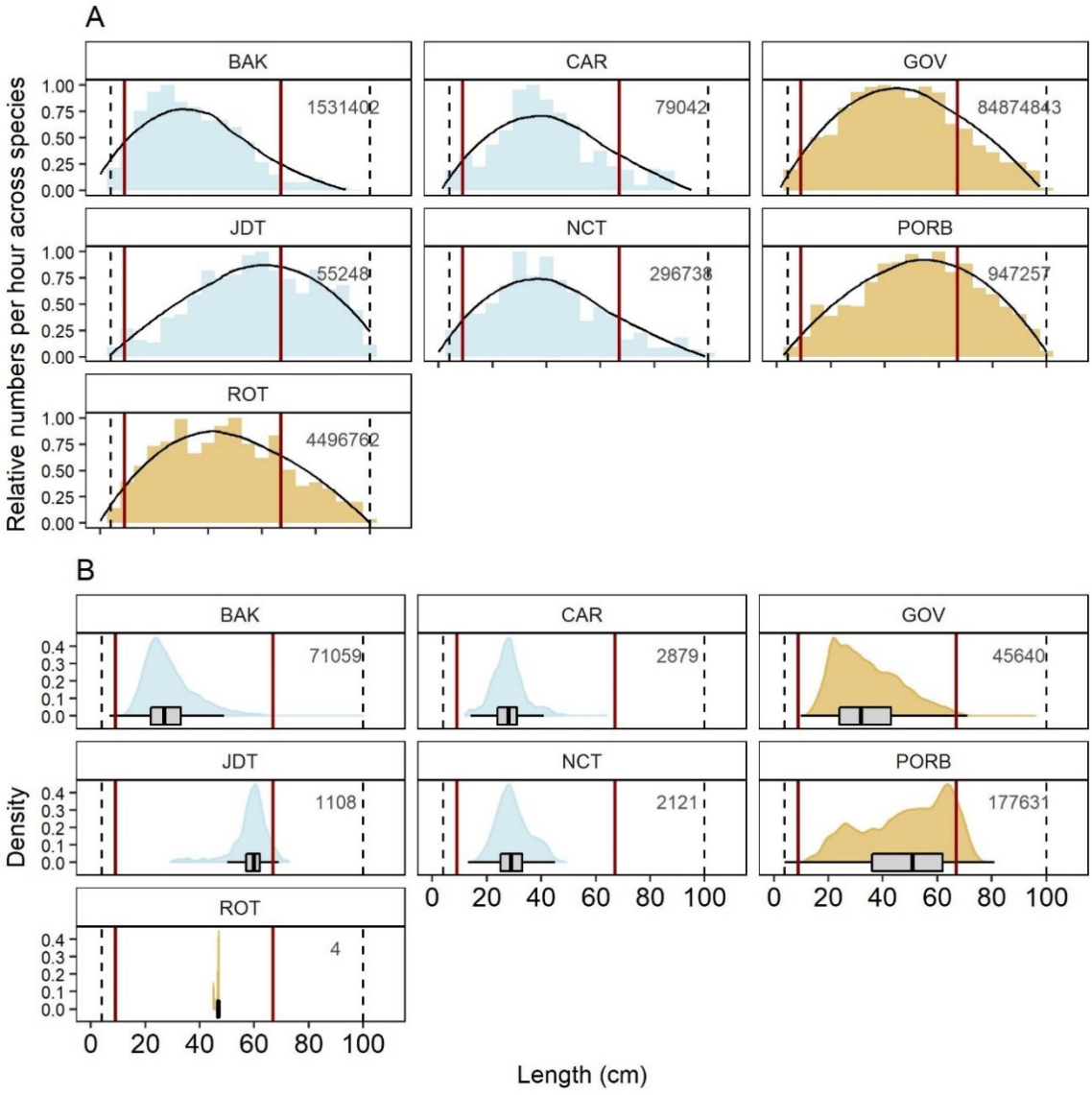

Fig. F14: Gear selectivity analysis for the Blackmouth Catshark. a) Shows the relative numbers caught by gear type for all fish species in scientific surveys as a histogram with a bin width of 5 cm length intervals and a smoother line (black). Based on a) comparable gears were selected (gear types with golden bars). b) Shows the numbers caught by gear type for the Blackmouth Catshark as flat violin plots. The vertical dotted lines are the minimum and maximum size caught of this elasmobranch species in the scientific surveys, the vertical red lines indicate maximum size at birth and the smallest maximum size reported in literature. The numbers in the plots show the sample size per gear type.

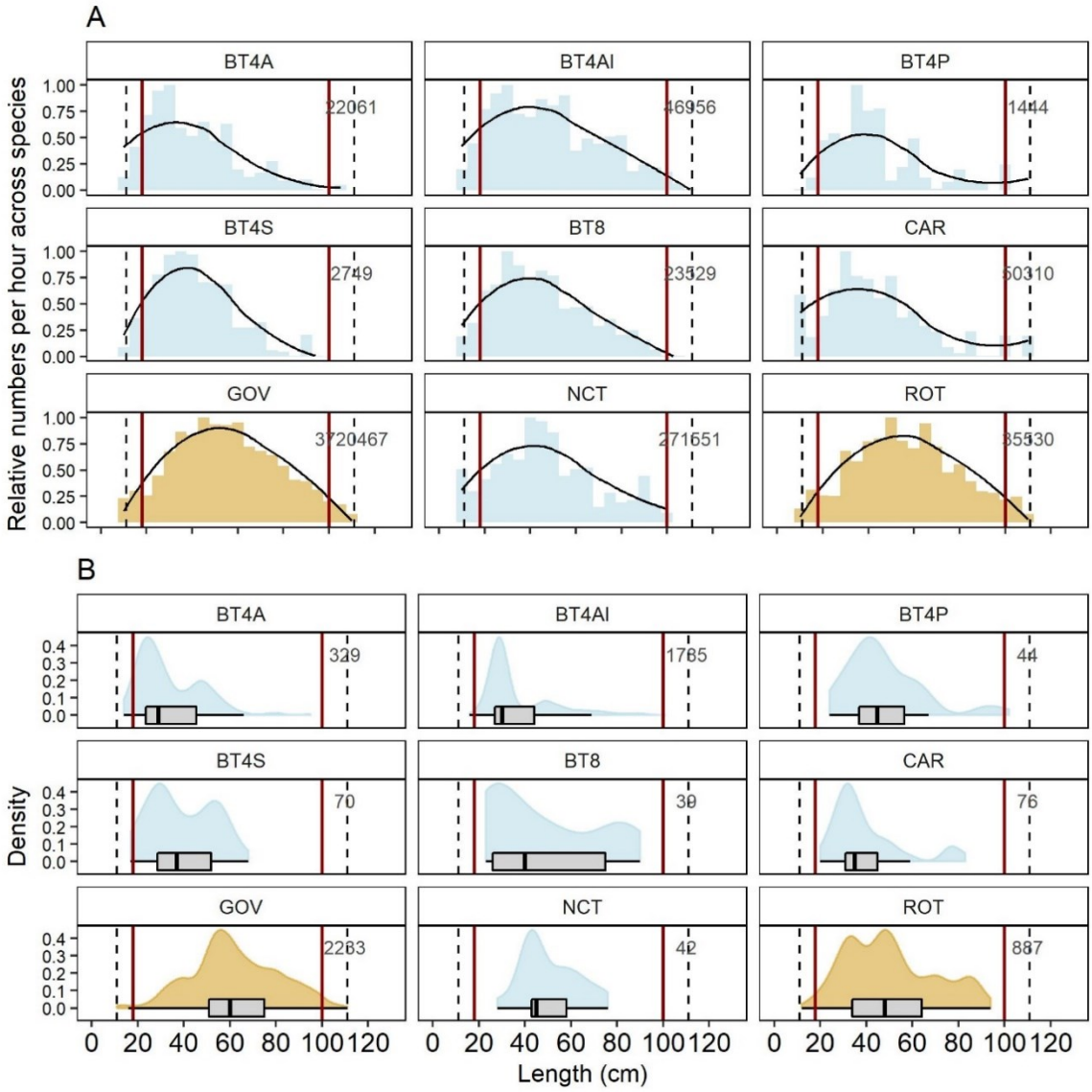

Fig. F15: Gear selectivity analysis for the Blonde Skate. a) Shows the relative numbers caught by gear type for all fish species in scientific surveys as a histogram with a bin width of 5 cm length intervals and a smoother line (black). Based on a) comparable gears were selected (gear types with golden bars). b) Shows the numbers caught by gear type for the Blonde Skate as flat violin plots. The vertical dotted lines are the minimum and maximum size caught of this elasmobranch species in the scientific surveys, the vertical red lines indicate maximum size at birth and the smallest maximum size reported in literature. The numbers in the plots show the sample size per gear type.

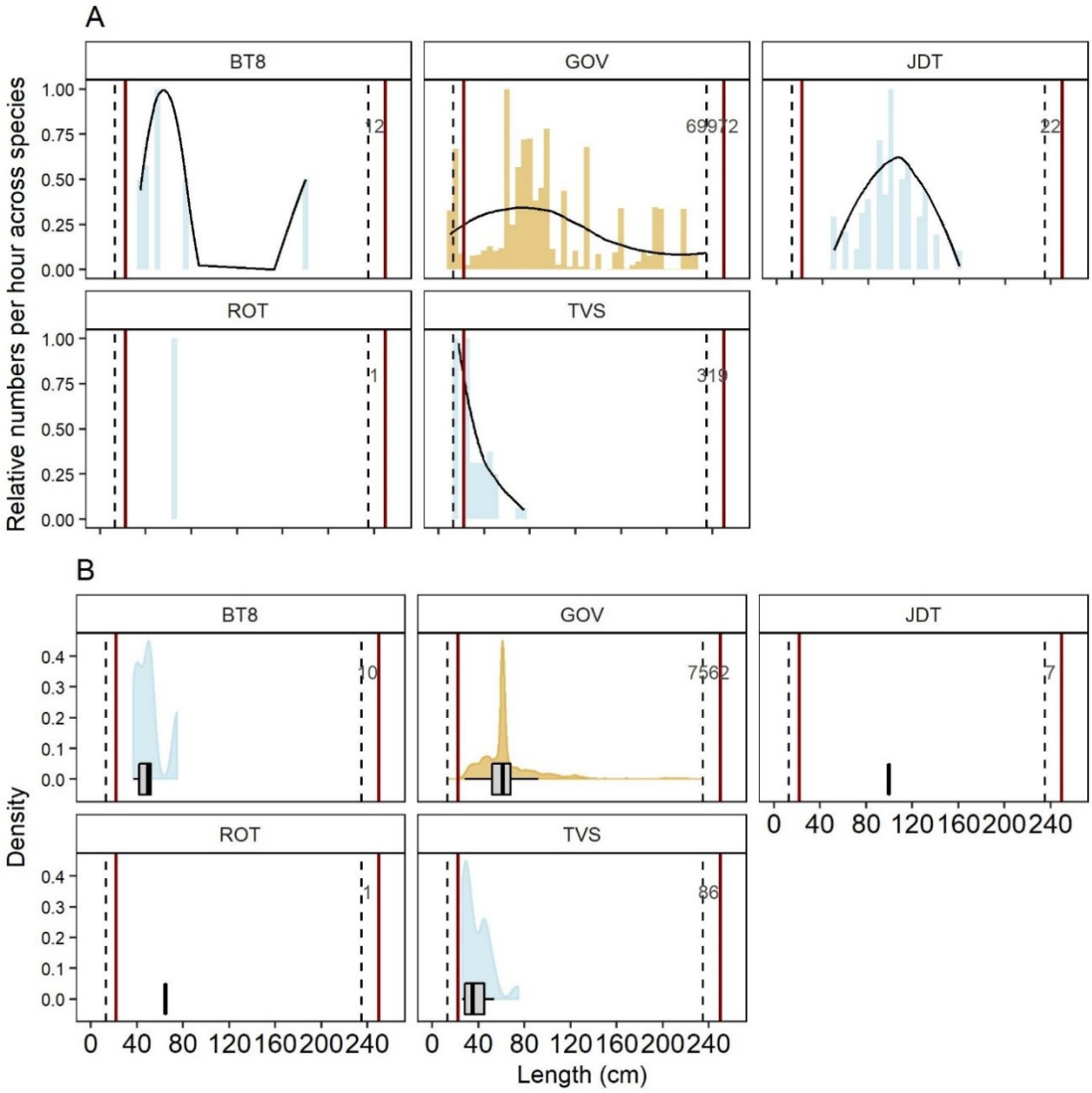

Fig. F16: Gear selectivity analysis for the Common Skate. a) Shows the relative numbers caught by gear type for all fish species in scientific surveys as a histogram with a bin width of 5 cm length intervals and a smoother line (black). Based on a) comparable gears were selected (gear types with golden bars). b) Shows the numbers caught by gear type for the Common Skate as flat violin plots. The vertical dotted lines are the minimum and maximum size caught of this elasmobranch species in the scientific surveys, the vertical red lines indicate maximum size at birth and the smallest maximum size reported in literature. The numbers in the plots show the sample size per gear type.

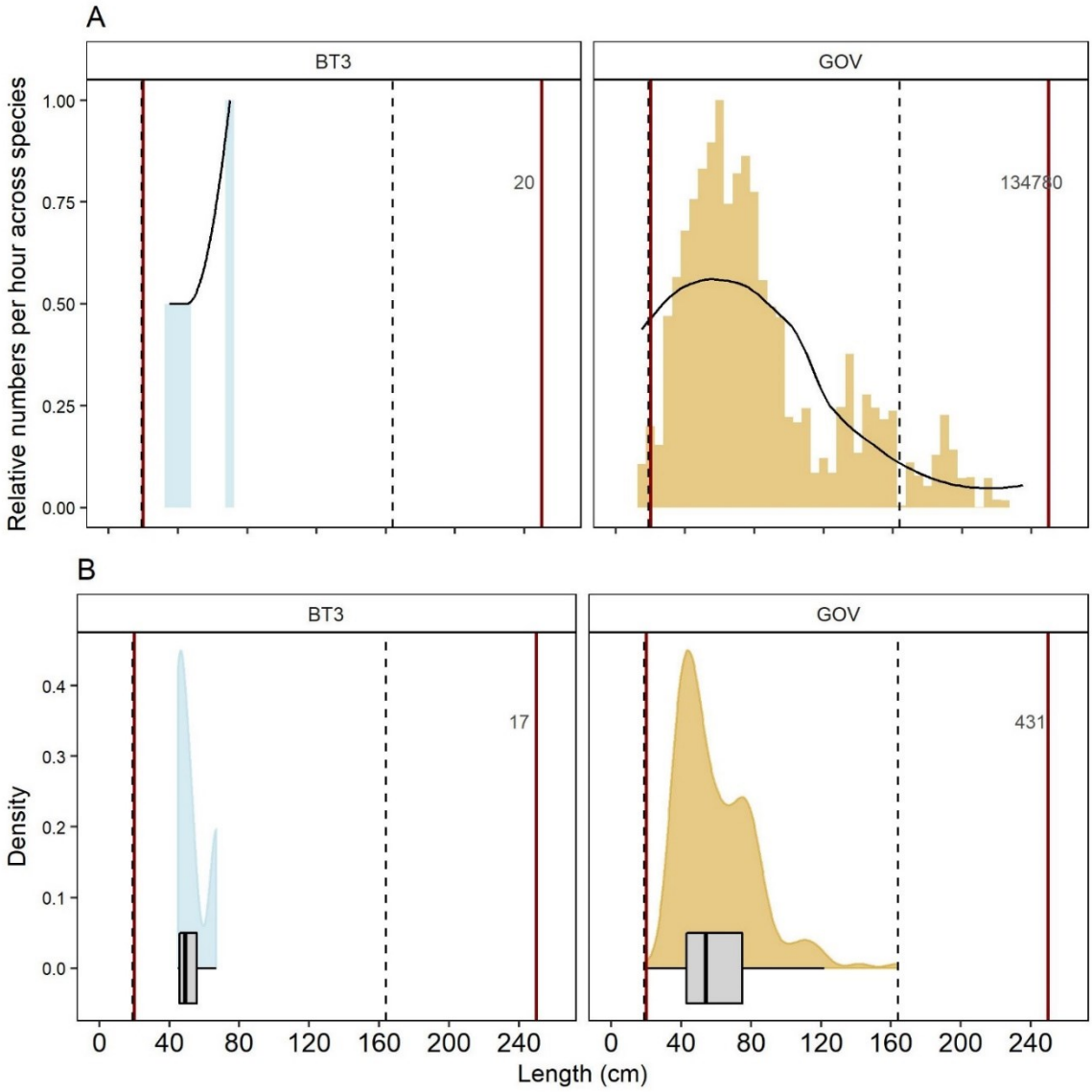

Fig. F17: Gear selectivity analysis for the Common Stingray. a) Shows the relative numbers caught by gear type for all fish species in scientific surveys as a histogram with a bin width of 5 cm length intervals and a smoother line (black). Based on a) comparable gears were selected (gear types with golden bars). b) Shows the numbers caught by gear type for the Common Stingray as flat violin plots. The vertical dotted lines are the minimum and maximum size caught of this elasmobranch species in the scientific surveys, the vertical red lines indicate maximum size at birth and the smallest maximum size reported in literature. The numbers in the plots show the sample size per gear type.

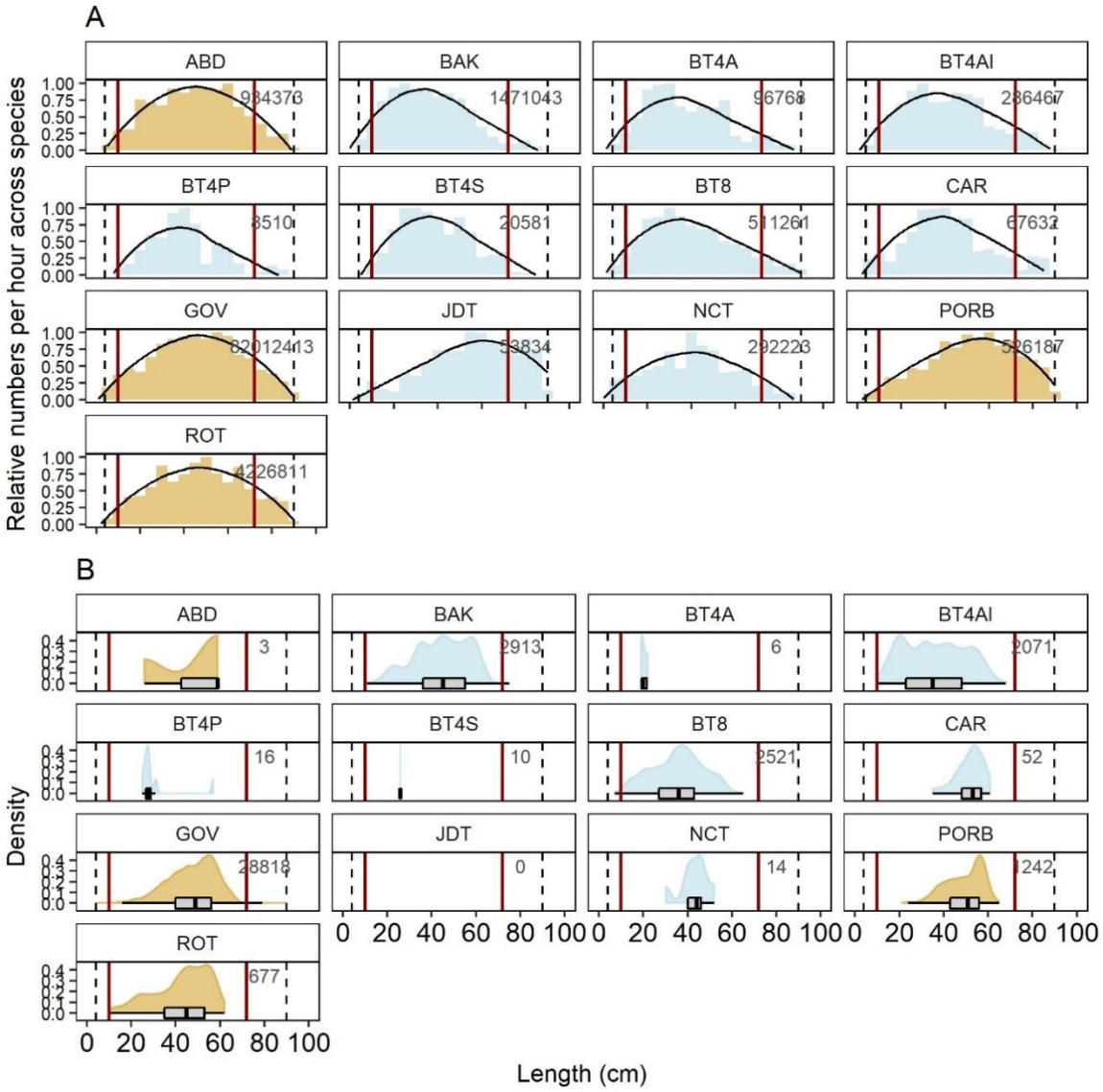

Fig. F18: Gear selectivity analysis for the Cuckoo Skate. a) Shows the relative numbers caught by gear type for all fish species in scientific surveys as a histogram with a bin width of 5 cm length intervals and a smoother line (black). Based on a) comparable gears were selected (gear types with golden bars). b) Shows the numbers caught by gear type for the Cuckoo Skate as flat violin plots. The vertical dotted lines are the minimum and maximum size caught of this elasmobranch species in the scientific surveys, the vertical red lines indicate maximum size at birth and the smallest maximum size reported in literature. The numbers in the plots show the sample size per gear type.

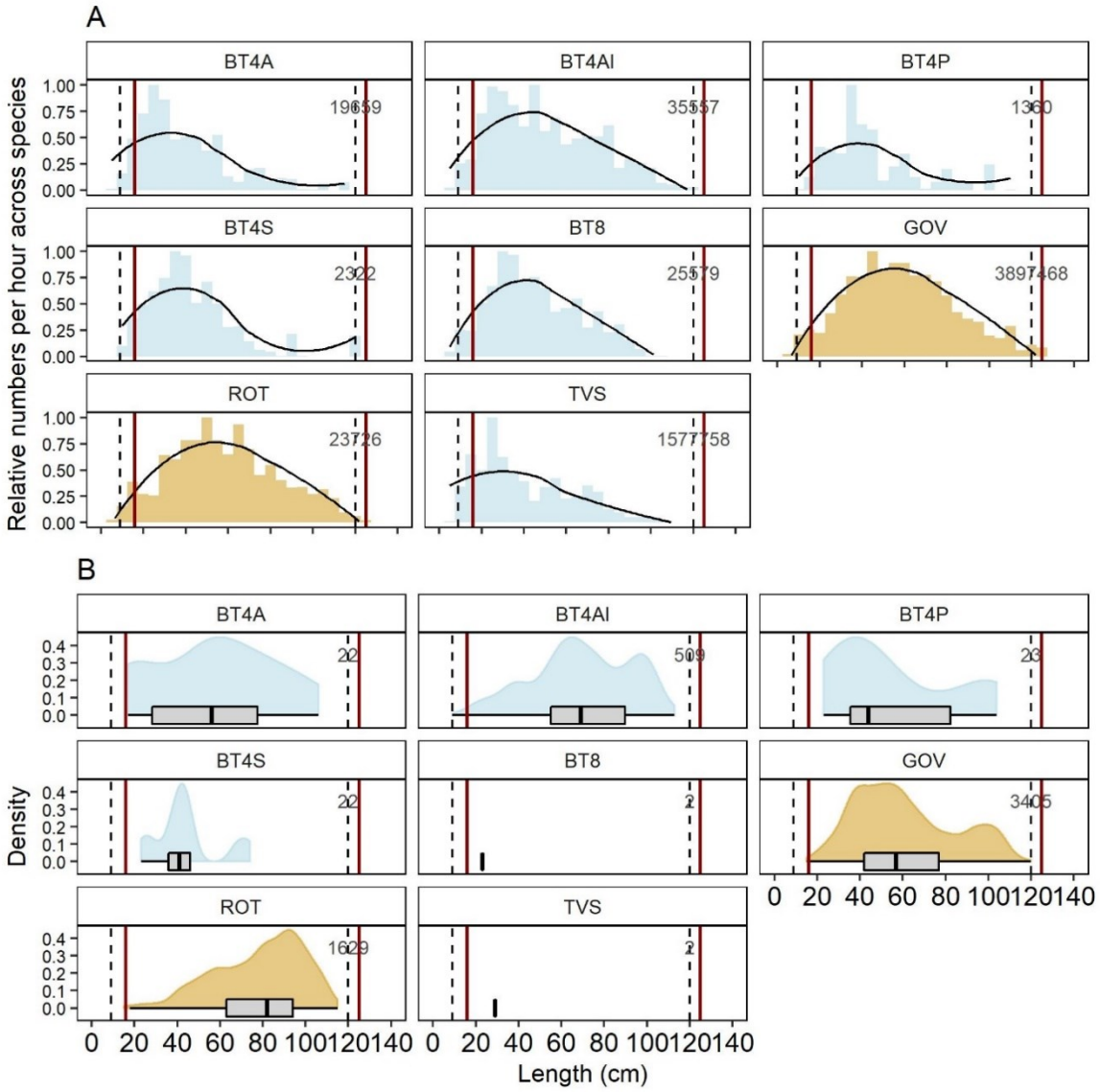

Fig. F19: Gear selectivity analysis for the Nursehound. a) Shows the relative numbers caught by gear type for all fish species in scientific surveys as a histogram with a bin width of 5 cm length intervals and a smoother line (black). Based on a) comparable gears were selected (gear types with golden bars). b) Shows the numbers caught by gear type for the Nursehound as flat violin plots. The vertical dotted lines are the minimum and maximum size caught of this elasmobranch species in the scientific surveys, the vertical red lines indicate maximum size at birth and the smallest maximum size reported in literature. The numbers in the plots show the sample size per gear type.

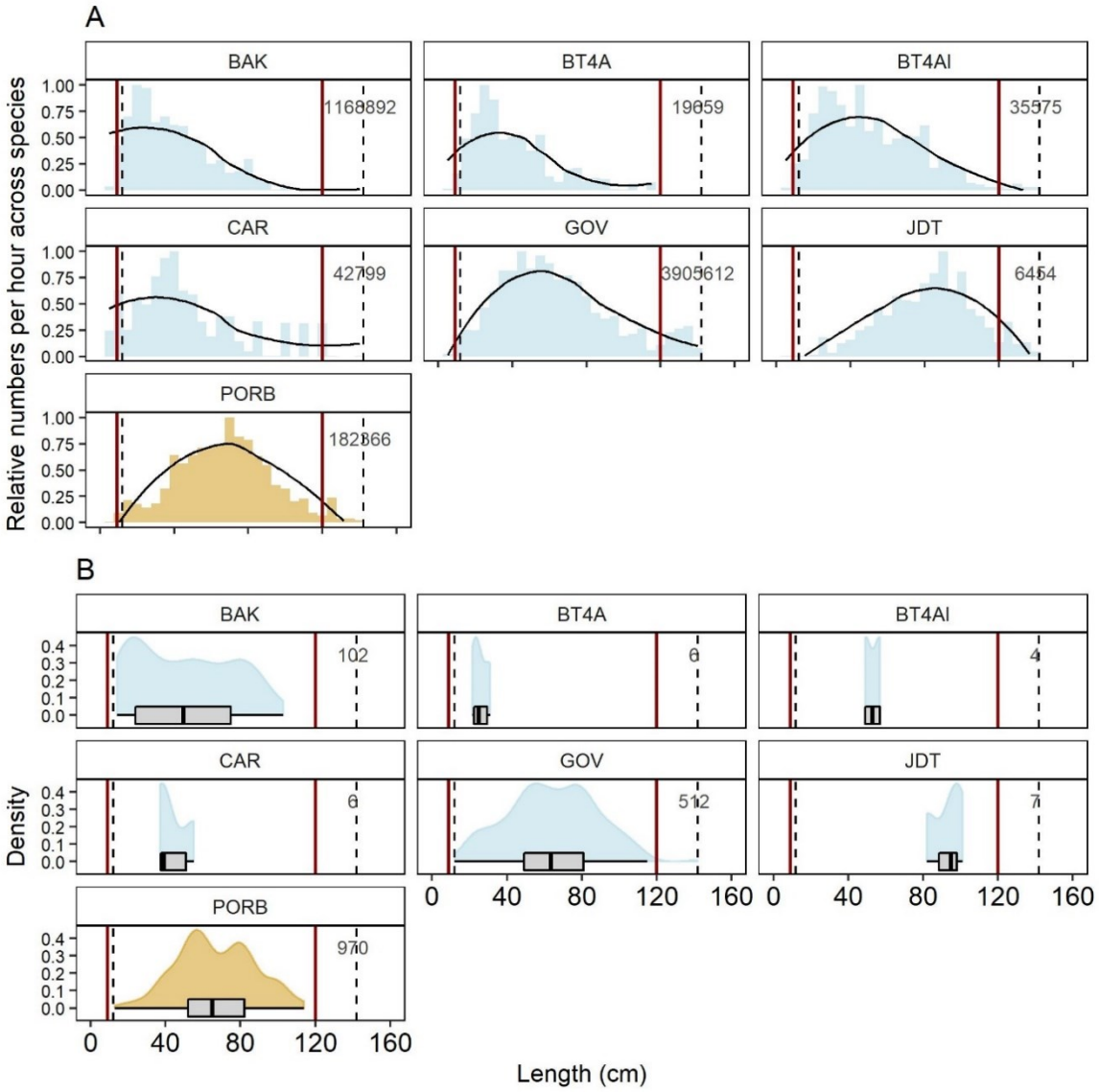

Fig. F20: Gear selectivity analysis for the Sandy Skate. a) Shows the relative numbers caught by gear type for all fish species in scientific surveys as a histogram with a bin width of 5 cm length intervals and a smoother line (black). Based on a) comparable gears were selected (gear types with golden bars). b) Shows the numbers caught by gear type for the Sandy Skate as flat violin plots. The vertical dotted lines are the minimum and maximum size caught of this elasmobranch species in the scientific surveys, the vertical red lines indicate maximum size at birth and the smallest maximum size reported in literature. The numbers in the plots show the sample size per gear type.

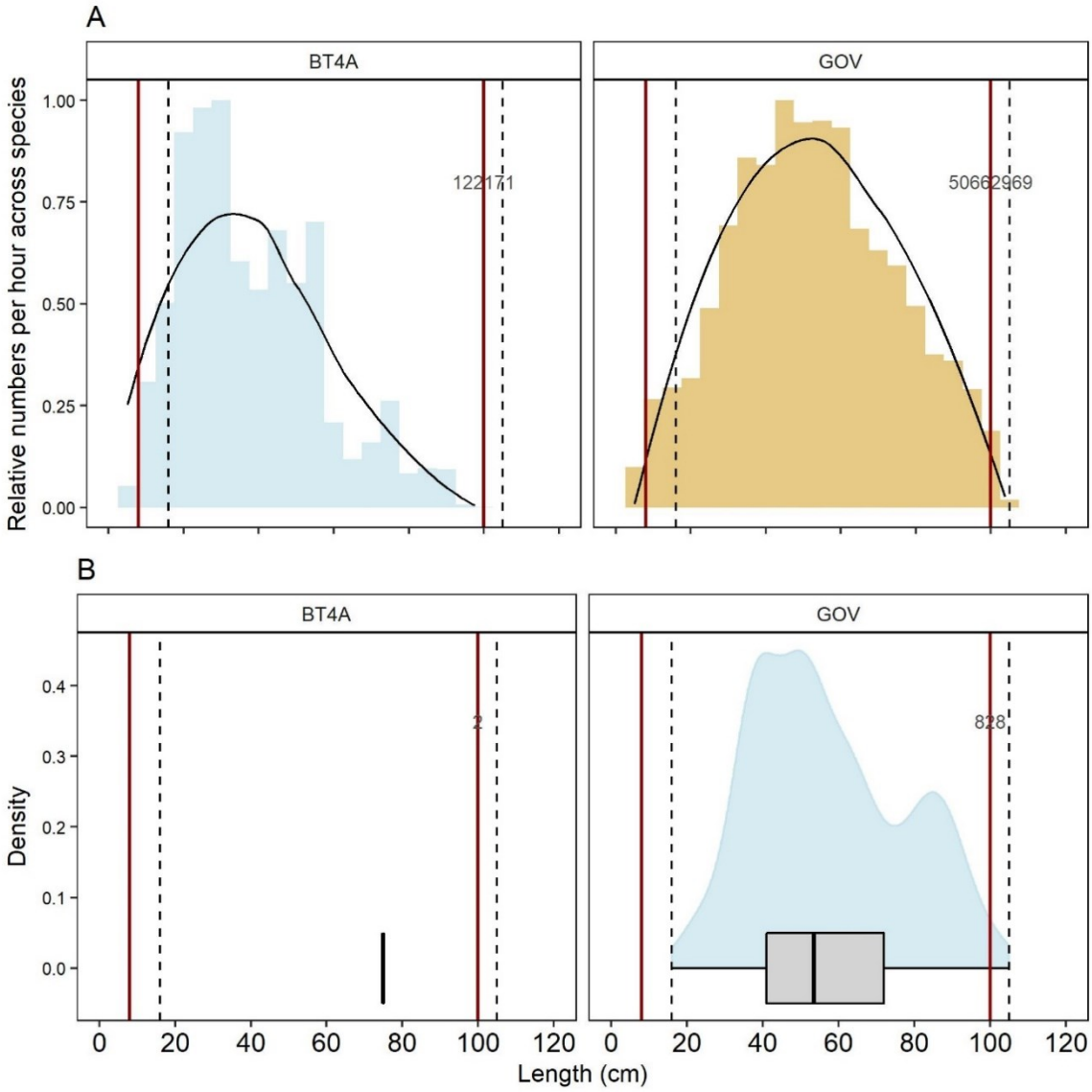

Fig. F21: Gear selectivity analysis for the Shagreen Skate. a) Shows the relative numbers caught by gear type for all fish species in scientific surveys as a histogram with a bin width of 5 cm length intervals and a smoother line (black). Based on a) comparable gears were selected (gear types with golden bars). b) Shows the numbers caught by gear type for the Shagreen Skate as flat violin plots. The vertical dotted lines are the minimum and maximum size caught of this elasmobranch species in the scientific surveys, the vertical red lines indicate maximum size at birth and the smallest maximum size reported in literature. The numbers in the plots show the sample size per gear type.

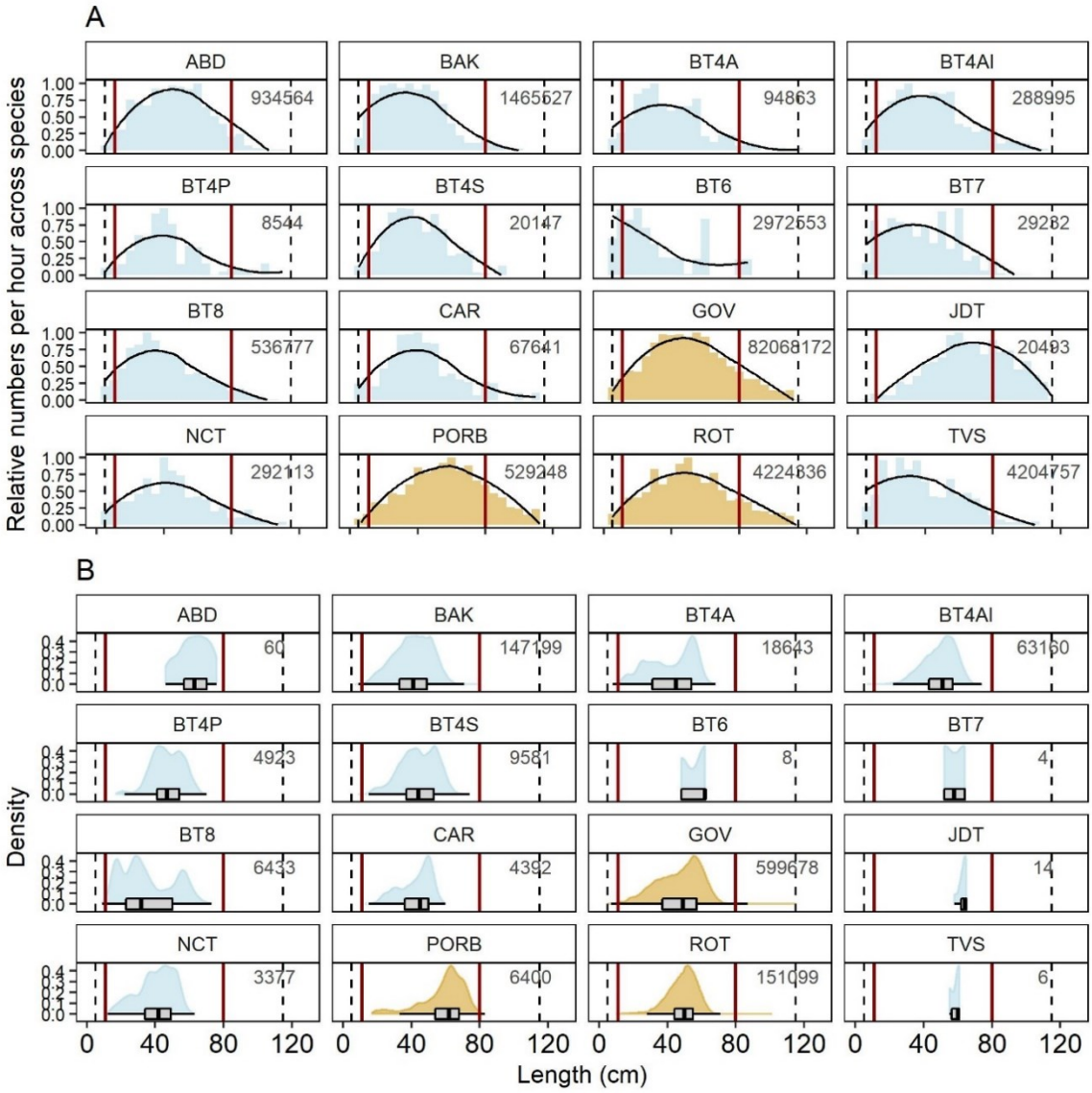

Fig. F22: Gear selectivity analysis for the Small Spotted Catshark. a) Shows the relative numbers caught by gear type for all fish species in scientific surveys as a histogram with a bin width of 5 cm length intervals and a smoother line (black). Based on a) comparable gears were selected (gear types with golden bars). b) Shows the numbers caught by gear type for the Small Spotted Catshark as flat violin plots. The vertical dotted lines are the minimum and maximum size caught of this elasmobranch species in the scientific surveys, the vertical red lines indicate maximum size at birth and the smallest maximum size reported in literature. The numbers in the plots show the sample size per gear type.

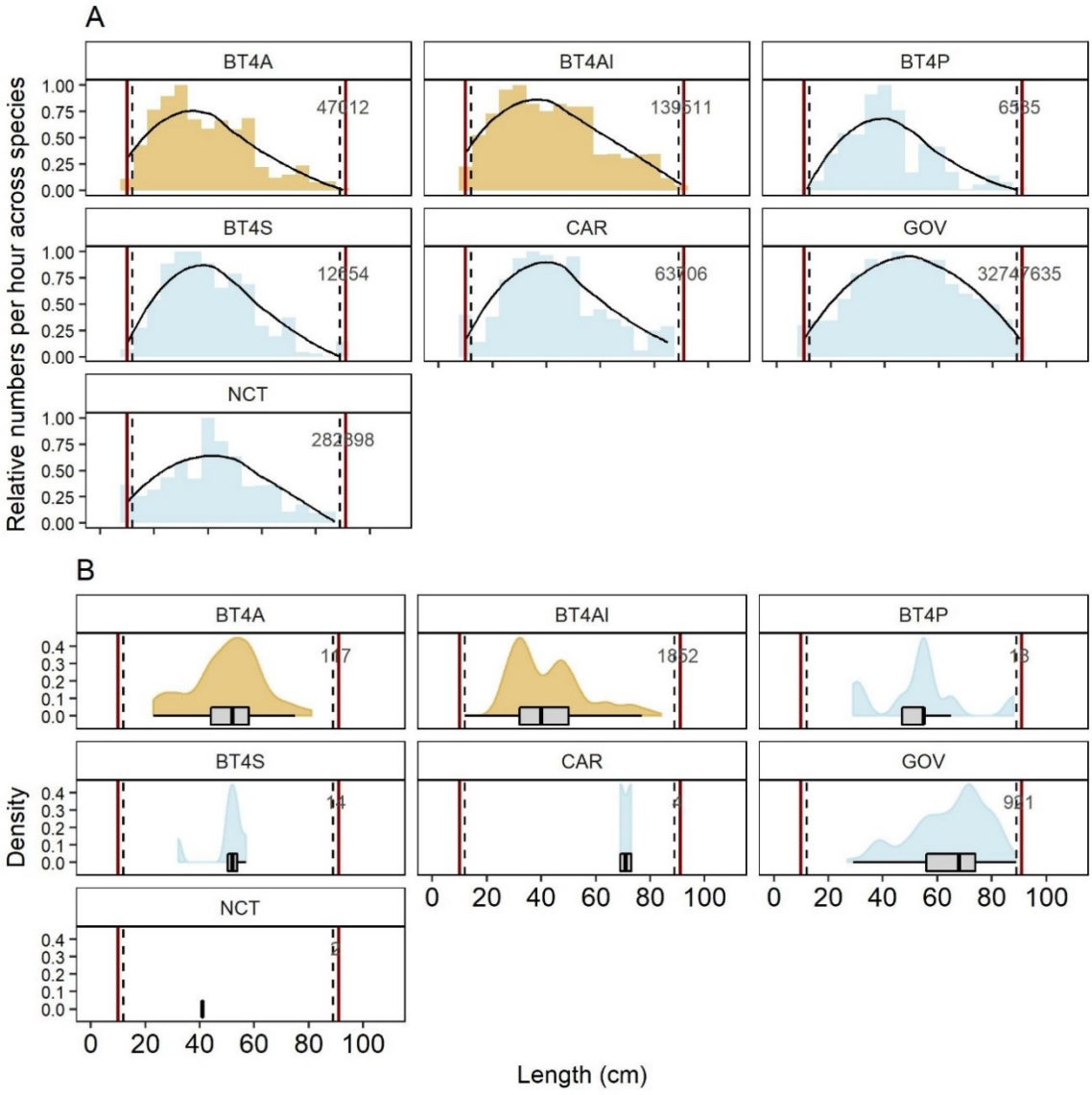

Fig. F23: Gear selectivity analysis for the Smalleyed Skate. a) Shows the relative numbers caught by gear type for all fish species in scientific surveys as a histogram with a bin width of 5 cm length intervals and a smoother line (black). Based on a) comparable gears were selected (gear types with golden bars). b) Shows the numbers caught by gear type for the Smalleyed Skate as flat violin plots. The vertical dotted lines are the minimum and maximum size caught of this elasmobranch species in the scientific surveys, the vertical red lines indicate maximum size at birth and the smallest maximum size reported in literature. The numbers in the plots show the sample size per gear type.

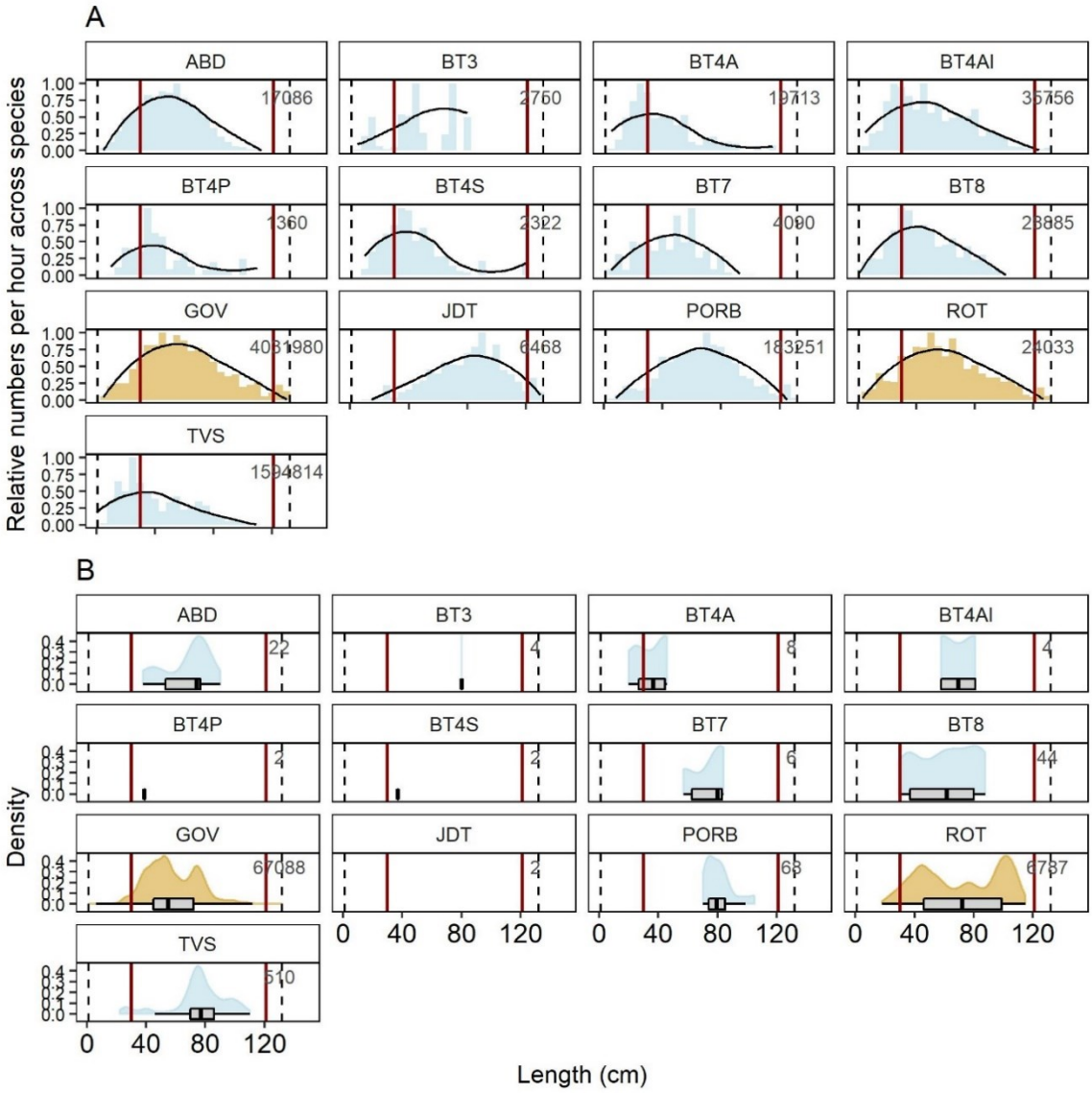

Fig. F24: Gear selectivity analysis for the Spiny Dogfish. a) Shows the relative numbers caught by gear type for all fish species in scientific surveys as a histogram with a bin width of 5 cm length intervals and a smoother line (black). Based on a) comparable gears were selected (gear types with golden bars). b) Shows the numbers caught by gear type for the Spiny Dogfish as flat violin plots. The vertical dotted lines are the minimum and maximum size caught of this elasmobranch species in the scientific surveys, the vertical red lines indicate maximum size at birth and the smallest maximum size reported in literature. The numbers in the plots show the sample size per gear type.

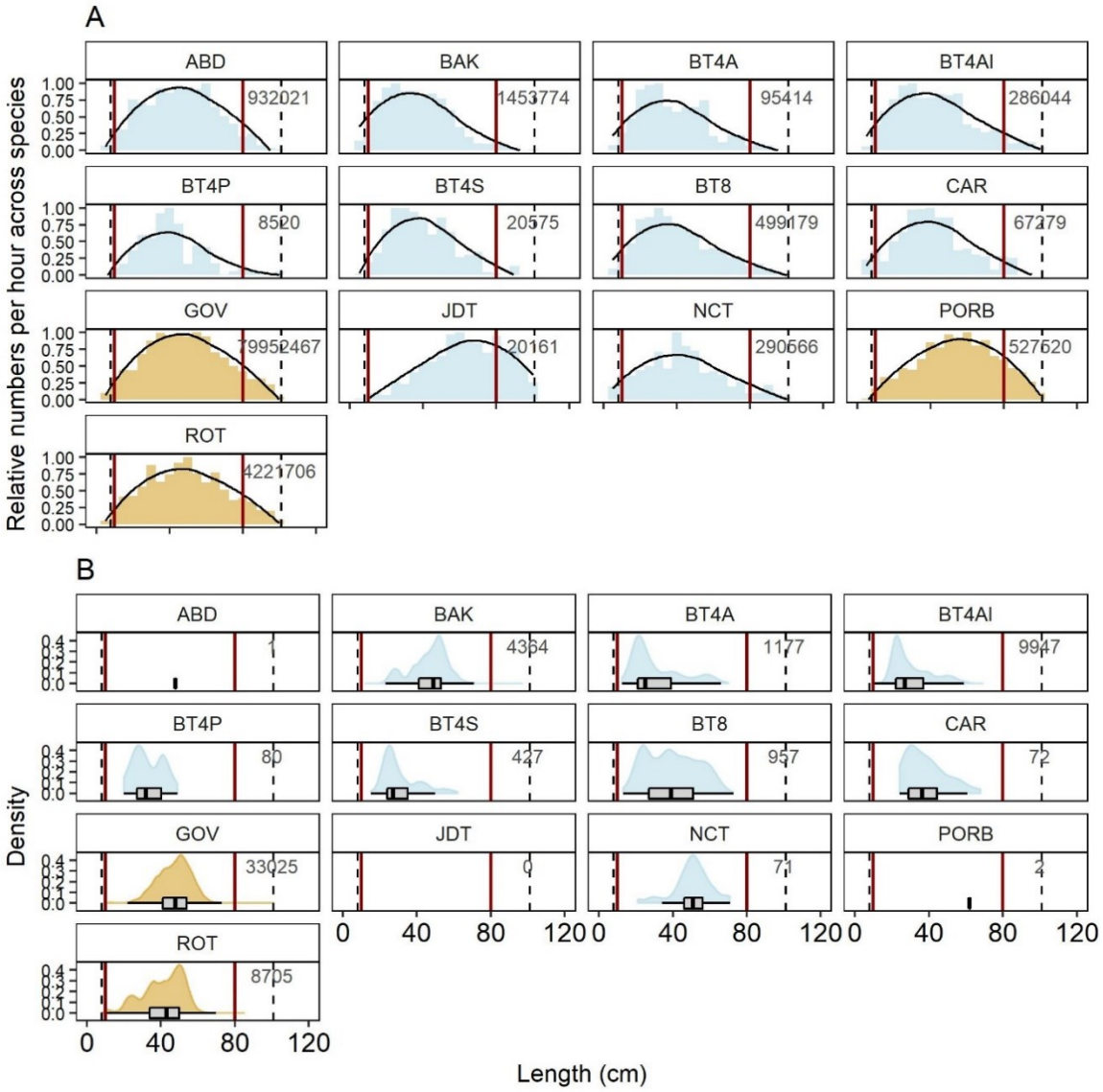

Fig. F25: Gear selectivity analysis for the Spotted Skate. a) Shows the relative numbers caught by gear type for all fish species in scientific surveys as a histogram with a bin width of 5 cm length intervals and a smoother line (black). Based on a) comparable gears were selected (gear types with golden bars). b) Shows the numbers caught by gear type for the Spotted Skate as flat violin plots. The vertical dotted lines are the minimum and maximum size caught of this elasmobranch species in the scientific surveys, the vertical red lines indicate maximum size at birth and the smallest maximum size reported in literature. The numbers in the plots show the sample size per gear type.

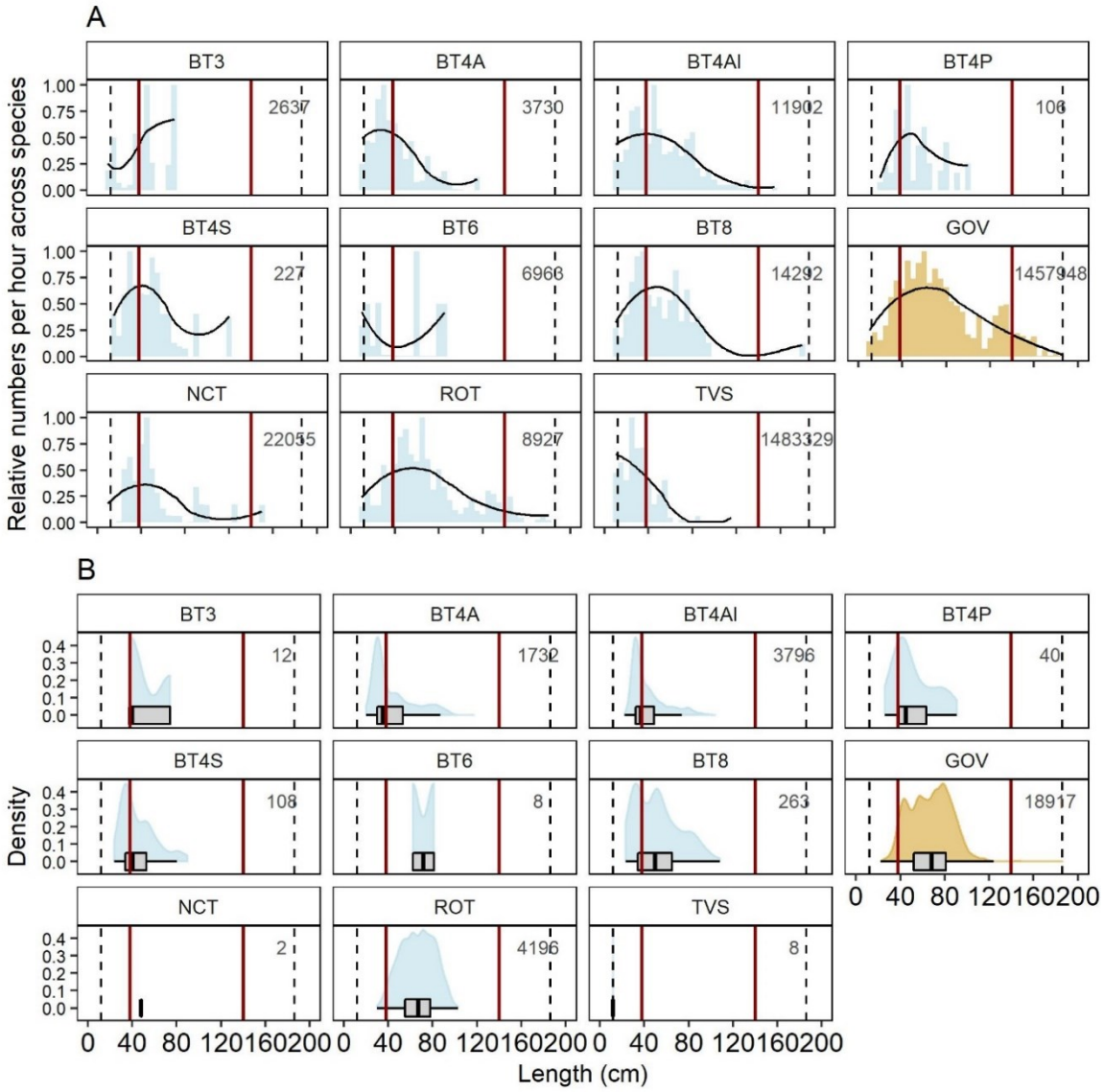

Fig. F26: Gear selectivity analysis for the Starry Smoothhound. a) Shows the relative numbers caught by gear type for all fish species in scientific surveys as a histogram with a bin width of 5 cm length intervals and a smoother line (black). Based on a) comparable gears were selected (gear types with golden bars). b) Shows the numbers caught by gear type for the Starry Smoothhound as flat violin plots. The vertical dotted lines are the minimum and maximum size caught of this elasmobranch species in the scientific surveys, the vertical red lines indicate maximum size at birth and the smallest maximum size reported in literature. The numbers in the plots show the sample size per gear type.

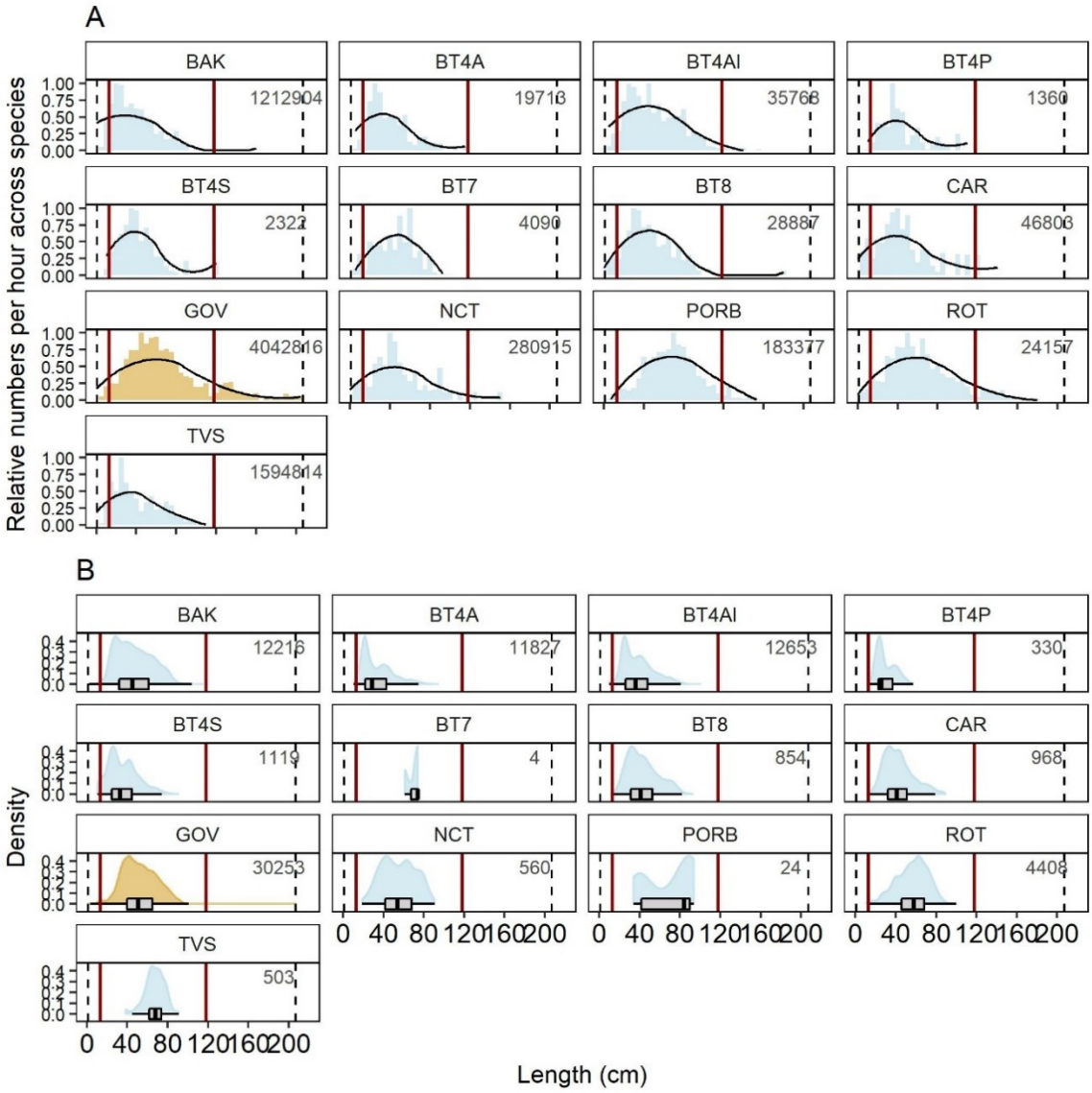

Fig. F27: Gear selectivity analysis for the Thornback Skate. a) Shows the relative numbers caught by gear type for all fish species in scientific surveys as a histogram with a bin width of 5 cm length intervals and a smoother line (black). Based on a) comparable gears were selected (gear types with golden bars). b) Shows the numbers caught by gear type for the Thornback Skate as flat violin plots. The vertical dotted lines are the minimum and maximum size caught of this elasmobranch species in the scientific surveys, the vertical red lines indicate maximum size at birth and the smallest maximum size reported in literature. The numbers in the plots show the sample size per gear type.

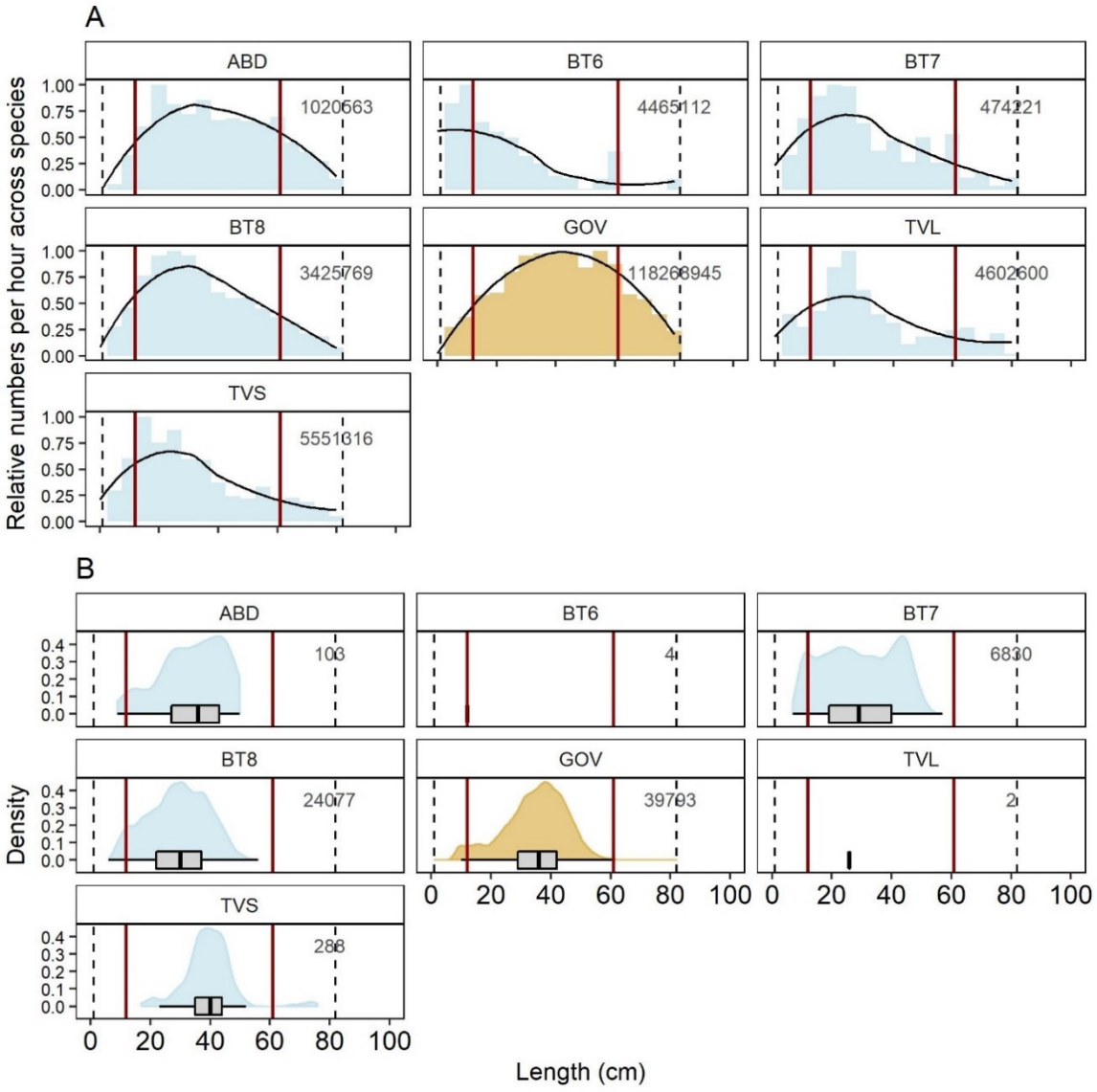

Fig. F28: Gear selectivity analysis for the Thorny Skate. a) Shows the relative numbers caught by gear type for all fish species in scientific surveys as a histogram with a bin width of 5 cm length intervals and a smoother line (black). Based on a) comparable gears were selected (gear types with golden bars). b) Shows the numbers caught by gear type for the Thorny Skate as flat violin plots. The vertical dotted lines are the minimum and maximum size caught of this elasmobranch species in the scientific surveys, the vertical red lines indicate maximum size at birth and the smallest maximum size reported in literature. The numbers in the plots show the sample size per gear type.

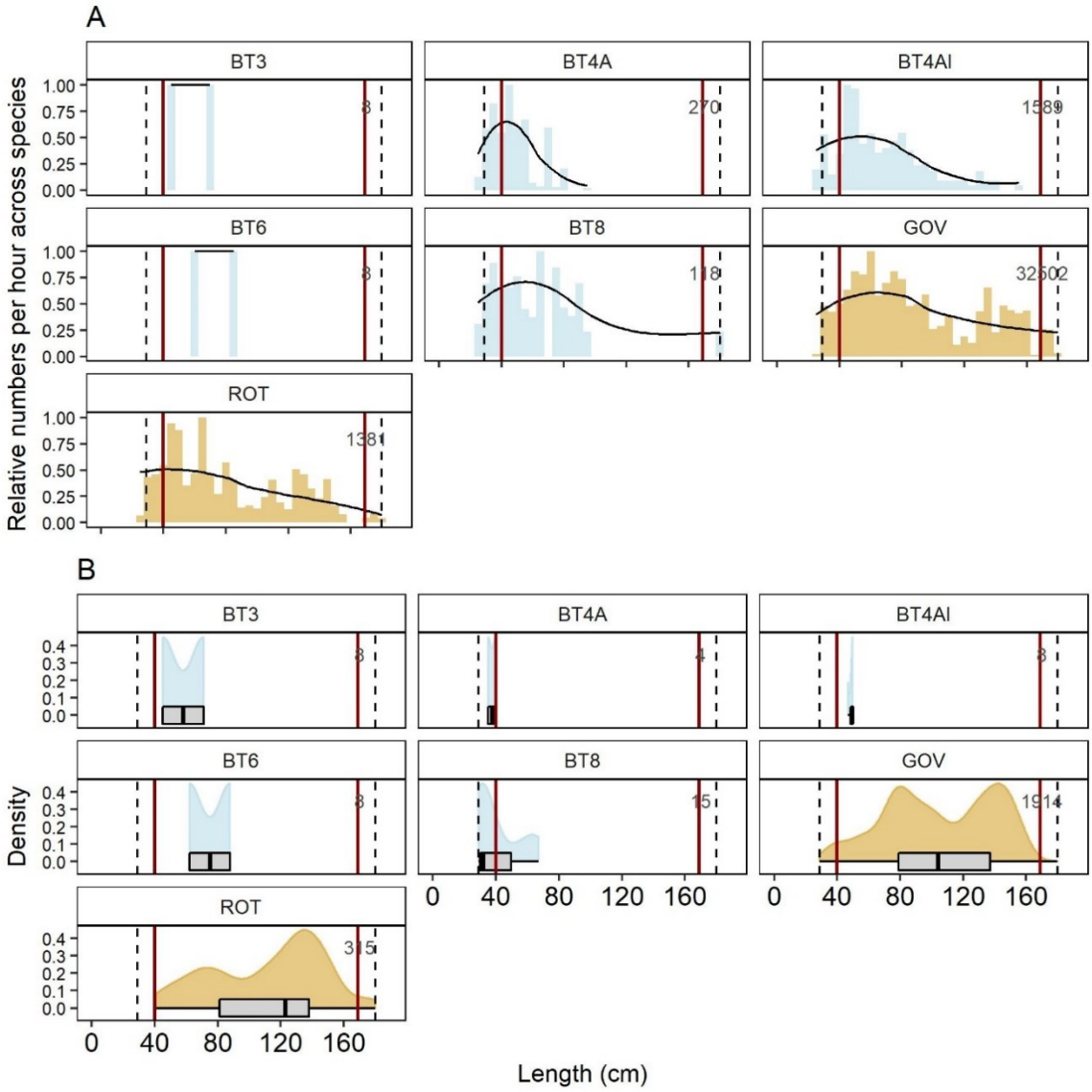

Fig. F29: Gear selectivity analysis for the Tope Shark. a) Shows the relative numbers caught by gear type for all fish species in scientific surveys as a histogram with a bin width of 5 cm length intervals and a smoother line (black). Based on a) comparable gears were selected (gear types with golden bars). b) Shows the numbers caught by gear type for the Tope Shark as flat violin plots. The vertical dotted lines are the minimum and maximum size caught of this elasmobranch species in the scientific surveys, the vertical red lines indicate maximum size at birth and the smallest maximum size reported in literature. The numbers in the plots show the sample size per gear type.

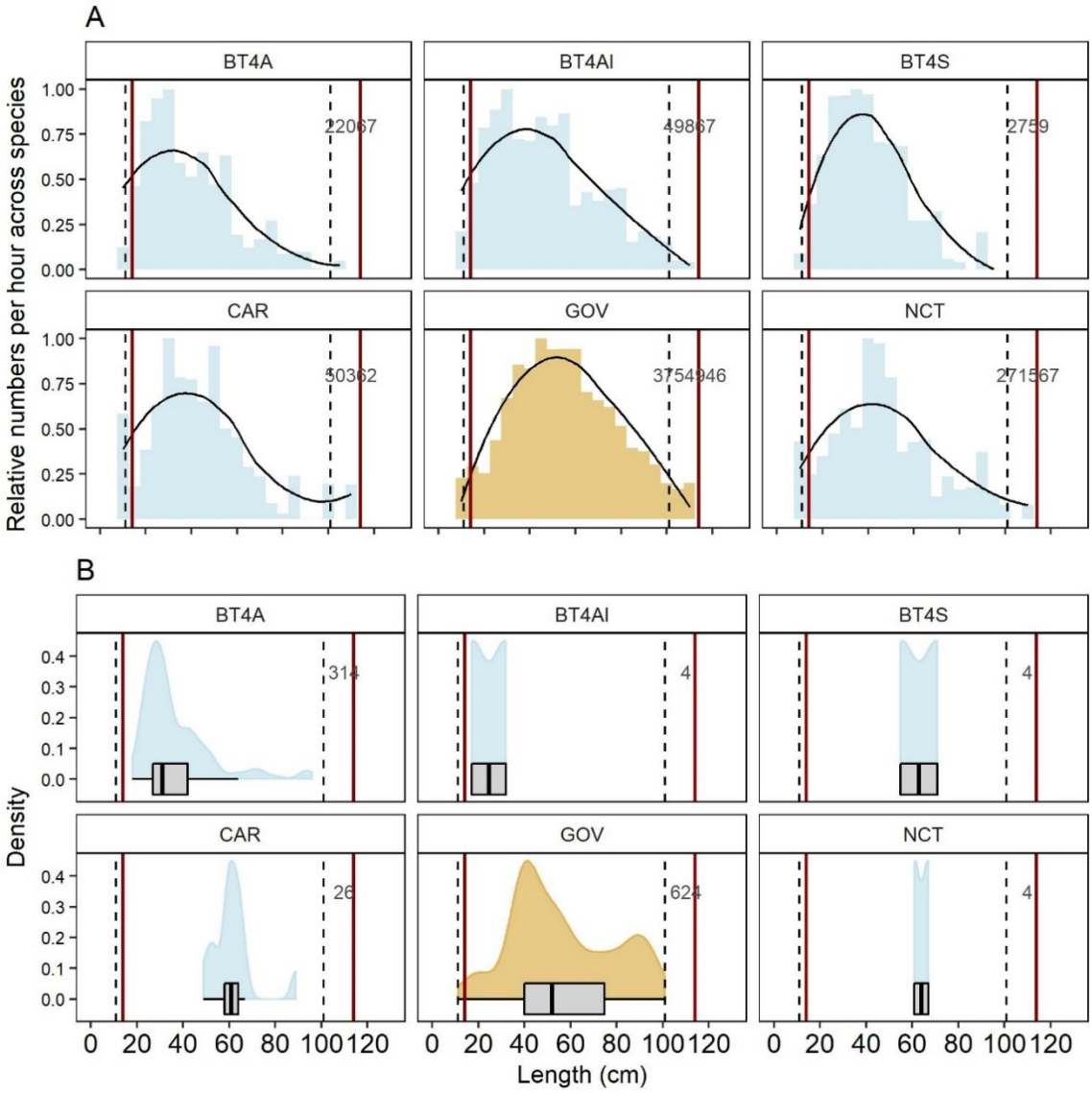

Fig. F30: Gear selectivity analysis for the Undulate Skate. a) Shows the relative numbers caught by gear type for all fish species in scientific surveys as a histogram with a bin width of 5 cm length intervals and a smoother line (black). Based on a) comparable gears were selected (gear types with golden bars). b) Shows the numbers caught by gear type for the Undulate Skate as flat violin plots. The vertical dotted lines are the minimum and maximum size caught of this elasmobranch species in the scientific surveys, the vertical red lines indicate maximum size at birth and the smallest maximum size reported in literature. The numbers in the plots show the sample size per gear type.

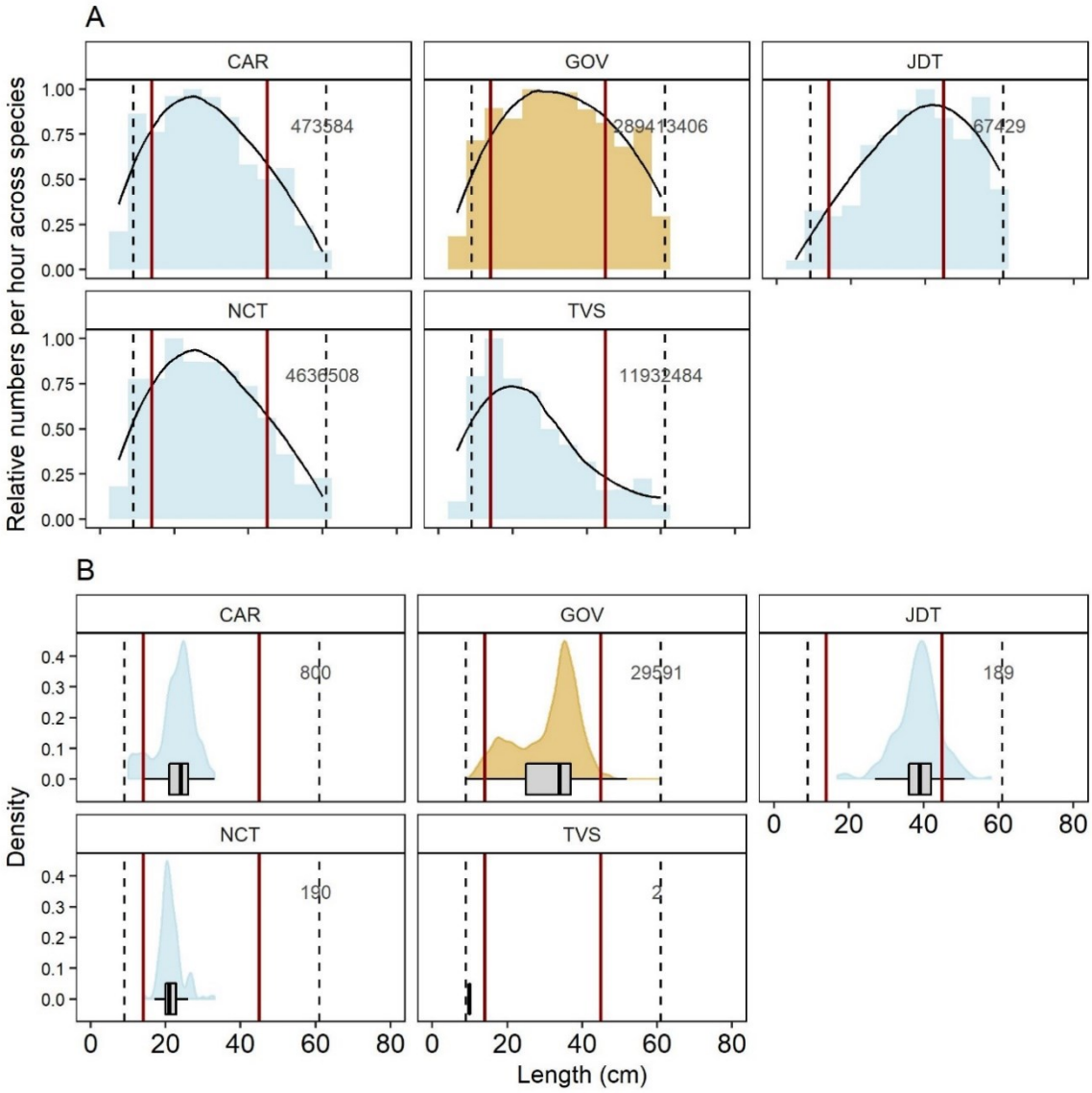

Fig. F31: Gear selectivity analysis for the Velvet Belly. a) Shows the relative numbers caught by gear type for all fish species in scientific surveys as a histogram with a bin width of 5 cm length intervals and a smoother line (black). Based on a) comparable gears were selected (gear types with golden bars). b) Shows the numbers caught by gear type for the Velvet Belly as flat violin plots. The vertical dotted lines are the minimum and maximum size caught of this elasmobranch species in the scientific surveys, the vertical red lines indicate maximum size at birth and the smallest maximum size reported in literature. The numbers in the plots show the sample size per gear type.

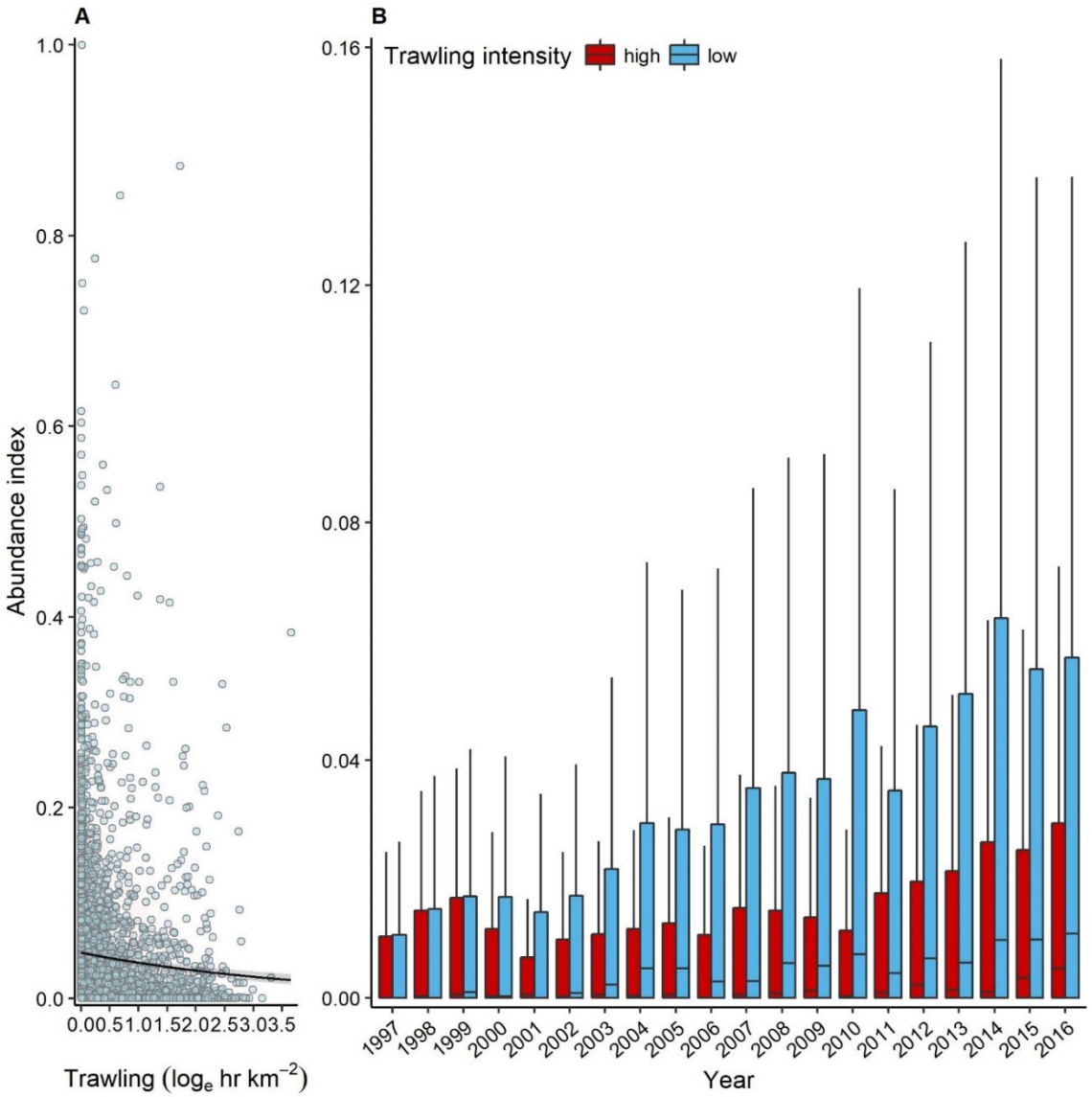

Fig. F32: Fine scale relationship between elasmobranch abundance and commercial trawling. A) Abundance index (scaled multi-species catch per unit effort) versus commercial trawling intensity (log_e+1 hr km^{-2}) per 0.1˚ longitude x 0.1˚ latitude grids over the whole study area. The black line shows the average relationship with 95% confidence limits in grey, obtained from a beta regression with variable dispersion (slope = -0.26 (-0.35 – -0.18), p<<0.0001). The predicted decline in elasmobranch abundance from zero to the maximum observed commercial trawling intensity was 60%. **B)** The temporal trend of elasmobranch abundance (multi-species catch per unit effort) is shown for grids with high (upper quartile) versus low (lower quartile) commercial trawling intensity.

Table F1: Details on International Union for Conservation of Nature marine protected area categories. Given are the primary objectives, the regulations regarding human interaction with the marine protected area (MPA) or resource extraction from the MPA and additional details. All information was taken from 2018 IUCN, International Union for Conservation of Nature. (https://www.iucn.org/theme/protected-areas/about/protected-areas-categories/) and Day et al. 2012. Guidelines for applying the IUCN Protected Area Management Categories to Marine Protected Areas (https://cmsdata.iucn.org/downloads/uicn_categoriesamp_eng.pdf).

IUCN category	Primary objectives	Human interactions and extraction of resources	Additional details
Ia: Strict Nature Reserve	"To conserve regionally, nationally or globally outstanding ecosystems, species (occurrences or aggregations) and/or geodiversity features: these attributes will have been formed mostly or entirely by non-human forces and will be degraded or destroyed when subjected to all but very light human impact."	In order to insure minimal disturbance, these areas should generally be managed to ensure low visitation by humans (particularly in marine environments). These areas should also, in general, be free of modern human disturbances, including minimizing management intervention, in order to maintain conservation objectives	These are areas in which human visitation, use and impacts are strictly controlled/limited in order to protect biodiversity, and in some instances geological/geographical features. Sites are considered close to pristine, and must remain so in order to preserve biodiversity richness. As such, areas can be used as a reference for scientific research, however all research must be planned out in order to minimize disturbance
Ib: Wilderness Area	"To protect the long-term ecological integrity of natural areas that are undisturbed by significant human activity, free of modern infrastructure and where natural forces and processes predominate, so that current and future generations have the opportunity to experience such areas."	These areas should generally be free of modern infrastructure, development, extractive and industrial activities, with highly limited or restricted motorized access. Public access is allowed, but limited, given that it does not disrupt the quality of the site. Available resources can be used by indigenous people living at low densities and maintaining a wilderness-based lifestyle within the area given that it aligns with the conservation objectives	These areas should also be large enough to naturally maintain biodiversity and all natural ecological and evolutionary processes to buffer against climate change. Low impact and minimally invasive scientific activities are permitted in the area for research and educational purposes

Table F1. Continued.

IUCN category	Primary objectives	Human interactions and extraction of resources	Additional details
II: National Park	"To protect natural biodiversity along with its underlying ecological structure and supporting environmental processes, and to promote education and recreation." The goal is long-term resilience of the ecosystem as a whole	National Parks, like Wilderness Areas are typically large in order to naturally maintain large-scale ecological processes, remaining in as natural a state as possible, while limiting activities to those that do not significantly affect biological and/or ecological processes, but do promote the economy through tourism. Subsistence resource use by indigenous and local communities can also be maintained as long as the primary objective of protecting the natural biodiversity, ecological structure and environmental processes is upheld	"Category II areas should be more strictly protected where ecological functions and native species composition are relatively intact; surrounding landscapes can have varying degrees of consumptive or non-consumptive uses but should ideally serve as buffers to the protected area."
III: Natural Monument or Feature	"To protect specific outstanding natural features and their associated biodiversity and habitats." Landscapes and seascapes that have undergone major changes should be given biodiversity protection along with protecting natural sites with both a spiritual/cultural AND biological value.	Visitation and recreation within the area is encouraged, however this category is "not aimed at sustainable resource use." Managed similarly to Category II areas. Extraction for scientific purposes and the sustainable resource use by indigenous people may be permitted, if, for the latter, it is in accordance with traditional and cultural values	Natural monuments or features can include: "landforms, seamounts, submarine caverns, caves, ancient groves", etc., and the associated ecology of the area. Important to note that protection in these areas may not be of a whole natural ecosystem, species or habitat, but rather a specific monument/feature and the associated biodiversity
IV: Habitat/Species Management Area	"To maintain, conserve and restore species and habitats while providing a means by which the urban residents may obtain regular contact with nature."	"Whether or not sustainable fishing is allowed in a Category IV MPA or zone will depend on its objectives. In some circumstances, fishing/collecting may be permissible where the resource use does not compromise the ecological/species management objectives of the site"	Category IV areas focus on specifically defined flora/fauna or targeted habitats. Therefore, recreational use within the area can occur given that it does not go against particular site objectives

Table F1. Continued.

IUCN category	Primary objectives	Human interactions and extraction of resources	Additional details
V: Protected Landscape/Seascape	"To protect and sustain important landscapes/seascapes and the associated nature conservation and other values created by interactions with humans through traditional management practices" Other objectives include providing recreational and tourist use for a socio-economic benefit while maintaining these specific cultural landscapes through the conservation of species important to said landscapes, as well as encouraging the conservation of both agrobiodiversity and aquatic biodiversity.	In Category V Protected areas there is an *essential* balanced interaction between people and nature that has either maintained the integrity of the ecosystem, or has reasonably high probability of restoring the integrity. Extraction and human interaction are typically in the form of agriculture, forestry or tourism. Sustainable extractive use of the seascape is typically done by those communities that lie within the protected area	Often, numerous management patterns surrounding Category V areas help maintain buffer zones when these areas are placed alongside strictly protected areas, and act as corridors between multiple other protected areas. As such, Category V areas help limit land and water use around strictly protected areas in order to help maintain the integrity of those surrounding ecosystems
VI: Protected Area with Sustainable Use of Natural Resources	"To protect natural ecosystems and use natural resources sustainably, when conservation and sustainable use can be mutually beneficial."	Generally, a large area designed for the use of sustainable harvest of natural resources, excluding large-scale industrial harvest. Some areas of the Category VI protected areas *may* be designated as no-take zones in order to retain a natural condition	Tourism can be developed as a secondary strategy within these areas given they are part of the socio-economic strategy. Often, *multiple* stakeholders are involved with a Category VI protected area, and therefore governance within the area needs to be improved to reflect this while maintaining the sustainable use of the natural resources

Table F2: Details on the marine protected area types found in the study area. Given are all marine protected area (MPA) types that have been scientifically surveyed for elasmobranchs by the International Council for the Exploration of the Sea (ICES), after applying the criteria outlined in the methods section. The designation is given together with the national name in brackets where appropriate, the sample size, and if it is a national, regional or international type. The general objectives related to conservation, fisheries and elasmobranchs are summarized. Elasmobranch species in bold were part of the species complex analyzed in the present study. Information is also presented on whether the MPA type is specifically highlighted as a network of MPAs, if commercial trawling was present in 2017 (note that the coverage for vessels < 15 m is considered incomplete), if elasmobranchs species were caught in ICES scientific surveys, if a management plan was present or not, the International Union for the Conservation of Nature (IUCN) category, general fishing regulations that apply to this MPA designation type, and the authorized fisheries management body for the whole area or for territorial waters (up to 12 nautical miles) and the Exclusive Economic Zone (EEZ, 12 to 200 nautical miles). Note that within the EEZ the Common Fisheries Policy (CFP) is the authority that manages and regulates fishing. The European Union (EU) member states can request conservation measures to be implemented (such as fishing restrictions) at the European Commission if all affected member states agree on the suggested measures. Generally, the member states remain the authority in territorial waters, if the measures are non-discriminatory, prior consultation of other Member States has taken place, and if the European Commission has not already adopted measures for this area (EU, 2013). Information on designation name and type, management plan and IUCN category were taken from the WDPA database as outlined in the methods.

Designation name and type	Objectives related to species and/or biodiversity protection	Objectives related to fishing	Objectives related to elasmobranchs	Commercial trawling present	Elasmobranchs present
Baltic Sea Protected Area (HELCOM) (n = 42) regional	Protection of species, natural habitats and nature types to conserve biological and genetic diversity, ecological processes and ensure ecological function. The network should protect areas with, inter alia, threatened and/or declining species, important species and habitats, high natural biodiversity and ecological significance	To preserve use of sustainable resources	Priority species: *Lamna nasus* ***Scyliorhinus canicula*** ***Squalus acanthias*** ***Amblyraja radiata*** ***Dipturus batis*** ***Raja montagui***	Yes	No
Marine Conservation Zone (n = 55) national (UK)	to conserve the diversity of nationally rare, threatened and representative habitats and species	social and economic factors can be taken into account	***Raja undulata*** listed as species of conservation importance	Yes	Yes

Table F2. Continued.

Designation name and type	Objectives related to species and/or biodiversity protection	Objectives related to fishing	Objectives related to elasmobranchs	Commercial trawling present	Elasmobranchs present
Marine Nature Park (Parc naturel marin) (n = 4) national (France)	To ensure a healthy state of species and to allow for their key economic functions including spawning, feeding, migrating, resting and nursing.	sustainable development and use of resources	targets, inter alia, threatened species	Yes	Yes
Marine Protected Area (OSPAR) (n = 260) regional	Protect the maritime area against adverse effects of human activities to conserve marine ecosystems and develop strategies, plans or programs for the conservation of biological diversity. To restore adversely affected marine areas when practical	Develop strategies, plans or programs for the sustainable use of biological diversity	Priority species: *Centroscymnus coelolepis* *Centrophorus granulosus* *Centrophorus squamosus* *Cetorhinus maximus* ***Dipturus batis*** ***Raja montagui*** *Lamna nasus* ***Raja clavata*** *Rostroraja alba* ***Squalus acanthias*** *Squatina squatina*	Yes	Yes
National Park (Nationalpark) (n = 1) national (Germany)	Ensure, in a predominant part of the territory, the undisturbed dynamics of natural processes	Predominant part of area should be or become of no or little human influence	None	Yes	No
Nature Conservation Act (Natuurbeschermings wet) (n = 7) national (Netherlands)	Protection, preservation and restoration of biological diversity and reserving and managing valuable landscapes	shall take into account economic requirements	None	Yes	Yes

Table F2. Continued.

Designation name and type	Objectives related to species and/or biodiversity protection	Objectives related to fishing	Objectives related to elasmobranchs	Commercial trawling present	Elasmobranchs present
Nature Conservation Marine Protected Area (n = 29) national (UK)	to conserve marine flora or fauna and habitats	social and economic factors can be taken into account	***Dipturus batis*** *Cetorhinus maximus* *Centrophorus squamosus* *Lamna nasus* *Centroscymnus coelolepis* ***Leucoraja circularis*** ***Squalus acanthias*** are listed as Priority Marine Features	Yes	Yes
Nature Reserve Germany (Naturschutzgebiet) (n = 3) national (Germany)	Special protection of nature and landscape in their entirety or in individual parts for the conservation, development or restoration of habitats, biotopes or communities of certain wild species, inter alia, because of their rarity, special nature or outstanding beauty	None	targets, inter alia, threatened and rare species	Yes	Yes
Site of Community Importance (Habitats Directive) (n = 185) regional	The conservation of natural habitats and wild fauna and flora to contribute towards ensuring biodiversity with measures designated to maintain or restore favorable conservation status	Measures taken shall take economic requirements into account	None	Yes	Yes
Special Protection Area (Birds Directive) (n = 96) regional	Protect naturally occurring wild species of birds and maintain populations at a level which corresponds to their ecological, scientific and cultural requirements	Measures taken shall take economic requirements into account	None	Yes	Yes

Table F2. Continued.

Designation name and type	Management plan		IUCN Category	General fishing regulations	Fisheries management authority
	Yes	No			
Baltic Sea Protected Area (HELCOM) (n = 42) regional	23	19	Not reported	no fisheries management regulation or mandate	HELCOM member states (territorial waters) CFP (EEZ)
Marine Conservation Zone (n = 55) national (UK)	0	55	Not assigned	Fisheries are generally not restricted, but fisheries can be managed if Marine Conservation Zone features are vulnerable to the fishing activities	England and Wales (territorial waters) CFP (EEZ)
Marine Nature Park (Parc naturel marin) (n = 4) national (France)	0	4	V	The sustainable use is allowed, but different zones can specify permitted uses	France (territorial waters) CFP (EEZ)
Marine Protected Area (OSPAR) (n = 260) regional	260	0	Not applicable	no fisheries management regulation or mandate	Member states (territorial waters) CFP (EEZ)
National Park (Nationalpark) (n = 1) national (Germany)	0	1	II	Different zones can specify permitted uses. Fishing is generally allowed, except in small zones where all form of recourse use is banned. In the case of fishery use, areas are to be preserved as habitats for naturally occurring species	Germany (Federal states in territorial waters) CFP (EEZ)
Nature Conservation Act (Natuurbeschermings wet) (n = 7) national	0	7	IV	Fishing is generally allowed but different zones can specify permitted uses, with zone 1 prohibiting fishing	Netherlands (territorial waters) CFP (EEZ)

Table F2. Continued.

Designation name and type	Management plan		IUCN Category	General fishing regulations	Fisheries management authority
	Yes	No			
Nature Conservation Marine Protected Area (n = 29) national (UK)	0	29	IV (n=11) not assigned (n=18)	Fishing is generally allowed, but can be restricted or banned	Scotland (territorial waters) CFP (EEZ)
Nature Reserve Germany (Naturschutzgebiet) (n = 3) national (Germany)	0	3	IV	Fisheries are allowed as long as it considers the objectives for the protection of nature. In the case of fishery use, areas are to be preserved as habitats for naturally occurring species.	Germany (Federal states in territorial waters) CFP (EEZ)
Site of Community Importance (Habitats Directive) (n = 185) regional	56	129	IV (n=2, Belgium) not assigned (n=6, Spain) not reported (n=177)	Fisheries are allowed as long as the achievement of the conservation objectives of the site are not at risk	Member states (territorial waters) CFP (EEZ)
Special Protection Area (Birds Directive) (n = 96) regional	15	81	IV (n=3, Belgium); not assigned (n=1, Spain) not reported (n=92)	Fisheries are allowed as long as the achievement of the conservation objectives of the site are not at risk	Member states (territorial waters) CFP (EEZ)

Table F2. Continued.

Designation name and type	Comments
Baltic Sea Protected Area (HELCOM) (n = 42) regional	Only the elasmobranch species listed under the HELCOM lists of threatened and/or declining species in the Baltic Sea area are given here. The CFP does not apply to Russia, but the study area here did not include Russia.
Marine Conservation Zone (n = 55) national (UK)	Can be designated in English and Welsh territorial and offshore waters. In territorial waters the Marine Management Organisation (MMO) and Inshore Fisheries and Conservation Authorities (IFCA) regulate fisheries management
Marine Nature Park (Parc naturel marin) (n = 4) national (France)	A major objective is to contribute to an improved knowledge of the marine heritage
Marine Protected Area (OSPAR) (n = 260) regional	The OSPAR List of Threatened and/or Declining Species and Habitats has its only purpose in guiding further work on setting priorities for the conservation and protection of marine biodiversity. OSPAR has also designated MPAs in areas beyond national jurisdiction, but these MPAs are outside the study area and not considered here
National Park (Nationalpark) (n = 1) national (Germany)	In Germany all National Parks are classified as IUCN category II
Nature Conservation Act (Natuurbeschermingswet) (n = 7) national (Netherlands)	The Red List of the Netherlands includes *S. acanthias* and *R. montagui* as seriously threatened, *R. clavata* as threatened and D. batis as extinct
Nature Conservation Marine Protected Area (n = 29) national (UK)	Can be designated in Scottish territorial and offshore waters. Marine Scotland regulates fisheries management in Scottish territorial waters
Nature Reserve Germany (Naturschutzgebiet) (n = 3) national (Germany)	In Germany all Nature Reserves are classified as IUCN category IV
Site of Community Importance (Habitats Directive) (n = 185) regional	Forms the Natura 2000 MPA network together with the Bird Directive. They are the pre-requisite step for establishing Special Areas of Conservation (SACs).
Special Protection Area (Birds Directive) (n = 96) regional	Forms the Natura 2000 MPA network together with the Habitat Directive

Table F2. Continued.

Designation name and type	Sources
Baltic Sea Protected Area (HELCOM) (n = 42) regional	http://www.helcom.fi; http://www.helcom.fi/Lists/Publications/BSEP113.pdf; http://www.helcom.fi/Lists/Publications/BSEP105.pdf
Marine Conservation Zone (n = 55) national (UK)	http://jncc.defra.gov.uk/page-4527; http://jncc.defra.gov.uk/PDF/MCZ_FisheriesManagementFactsheet.pdf; https://www.gov.uk/government/publications/2010-to-2015-government-policy-marine-environment/2010-to-2015-government-policy-marine-environment#appendix-4-marine-protected-areas; https://publications.parliament.uk/pa/cm200809/cmbills/137/2009137vol1.pdf
Marine Nature Park (Parc naturel marin) (n = 4) national (France)	Guignier, A. and Prieur, M., 2010. Legal framework for protected areas: France. Guidelines for Protected Areas Legislation. IUCN Environmental Policy and Law Paper, 81. http://www.aires-marines.com/Marine-Protected-Areas/Different-marine-protected-area-categories
Marine Protected Area (OSPAR) (n = 260) regional	https://www.ospar.org; https://www.ospar.org/work-areas/bdc/species-habitats/list-of-threatened-declining-species-habitats
National Park (Nationalpark) (n = 1) national (Germany)	https://www.bfn.de/fileadmin/MDB/documents/themen/monitoring/BNatSchG.PDF; https://www.nationalpark-wattenmeer.de/sh/nationalpark/nutzungen/fischerei ; https://www.bfn.de/fileadmin/MDB/documents/themen/gebietsschutz/IUCN_Kat_Schutzgeb_Richtl_web.pdf; https://www.bfn.de
Nature Conservation Act (Natuurbeschermingswet) (n = 7) national (Netherlands)	http://wetten.overheid.nl/BWBR0037552/2017-01-01; https://zoek.officielebekendmakingen.nl/stcrt-2015-36471.html; http://www.waddenvereniging.nl/wv/images/PDF/ons_werk_2013/VIBEG-accoord.pdf
Nature Conservation Marine Protected Area (n = 29) national (UK)	http://www.legislation.gov.uk/asp/2010/5/pdfs/asp_20100005_en.pdf; http://www.gov.scot/Topics/marine/marine-environment/mpanetwork/faqs; http://jncc.defra.gov.uk/page-5269; http://jncc.defra.gov.uk/pdf/Priority%20Marine%20Features%20in%20Scotlands%20seas.%2024%20July%202014.pdf
Nature Reserve Germany (Naturschutzgebiet) (n = 3) national (Germany)	https://www.bfn.de/fileadmin/MDB/documents/themen/monitoring/BNatSchG.PDF; https://www.bfn.de/fileadmin/MDB/documents/themen/gebietsschutz/IUCN_Kat_Schutzgeb_Richtl_web.pdf; https://www.bfn.de

Table F2. Continued.

Designation name and type	Sources
Site of Community Importance (Habitats Directive) (n = 185) regional	Reker, J., Annunziatellis, A., Mo, G., Tunesi, L., Globevnik, L., Snoj, L., Agnesi, S. and Korpinen, S., 2015. Marine Protected Areas in Europe's Seas. An Overview and Perspectives for the Future. European Environment Agency, Publication Office of the European Union, Luxembourg. https://eur-lex.europa.eu/legal-content/EN/TXT/PDF/?uri=CELEX:31992L0043&from=EN
Special Protection Area (Birds Directive) (n = 96) regional	Reker, J., Annunziatellis, A., Mo, G., Tunesi, L., Globevnik, L., Snoj, L., Agnesi, S. and Korpinen, S., 2015. Marine Protected Areas in Europe's Seas. An Overview and Perspectives for the Future. European Environment Agency, Publication Office of the European Union, Luxembourg. https://eur-lex.europa.eu/legal-content/EN/TXT/PDF/?uri=CELEX:32009L0147&from=EN

Table F3: Comparison of non-commercially trawled versus commercially trawled marine protected area. Given are the numbers of marine protected areas (MPAs) considered in this study, the mean, lower and upper area and designation year, if a management plan was present, how many where classified according to the International Union for Conservation of Nature (IUCN) classifications and for each IUCN classification. Numbers in brackets show percentages.

	MPAs with no trawling	MPAs with trawling
Numbers	295 (41%)	423 (59%)
Mean area (km^2)	5.49	10.46
Area range (km^2)	$2*10^{-7}$-43.8	$1.38*10^{-10}$-44.1
Mean designation year	2005	2008
Designation year range	1933-2016	1983-2016
Management plan present	142 (40%)	214 (60%)
IUCN Category reported	41 (60%)	27 (40%)
IUCN Category Ia	5 (100%)	0 (0%)
IUCN Category II	0 (0%)	1 (100%)
IUCN Category III	1 (100%)	0 (0%)
IUCN Category IV	32 (60%)	21 (40%)
IUCN Category V	3 (43%)	4 (57%)
IUCN Category VI	0 (0%)	1 (100%)

Table F4: Details on elasmobranch species used in this study. Given are the scientific and the common name, the maximum size at birth (max L_0) the smallest maximum size (min L_{max}), the depth range, the International Union for Conservation of Nature (IUCN) status globally and for Europe (CR = critically endangered, EN = endangered, VU = vulnerable, NT = near threatened, LC = least concern), the total number caught per 60 minutes of trawling (Total N), the number of years the species was caught in International Council for the Exploration of the Sea (ICES) scientific surveys and the diet, if possible separated for juveniles (J) and adults (A). Data were taken from the surveys, the IUCN Red List (www.iucnredlist.org), FishBase (http://www.fishbase.org) or Ebert & Stehmann (2013).

Species	Common name	max L_0	min L_{max}	Depth	IUCN Global	IUCN Europe	Total N	Years	Diet
Galeus atlanticus	Atlantic Sawtail Catshark	15	45	170 - 752	NT	NT	5338	17	not available
Deania calcea	Birdbeak Dogfish	34	122	60 - 800	LC	EN	493	4	variety of bony fish, squids, shrimps
Galeus melastomus	Blackmouth Catshark	9	67	38 - 800	LC	LC	217878	20	bottom invertebrates, small mesopelagic bony fishes
Raja brachyura	Blonde Skate	18	100	0 - 380	NT	NT	3082	20	crustaceans (J), cephalopods and small fish (A)
Dipturus batis	Common Skate	22	250	0 - 800	CR	CR	6707	20	benthic invertebrates and fishes, including other skates
Dasyatis pastinaca	Common Stingray	20	250	0 - 250	DD	VU	428	20	demersal invertebrates and fishes
Leucoraja naevus	Cuckoo Skate	10	72	0 - 770	LC	LC	30181	20	crustaceans and polychaetes (J), bony fish (A)
Scyliorhinus stellaris	Nursehound	16	125	0 - 409	NT	NT	5004	20	cephalopods, crustaceans, variety of bony fish including other sharks
Leucoraja circularis	Sandy Skate	9*	120	0 - 800	EN	EN	970	16	benthic invertebrates and small bony fishes
Leucoraja fullonica	Shagreen Skate	8*	100	30 - 800	VU	VU	799	20	benthic invertebrates, bony fishes
Scyliorhinus cnicula	Small Spotted Catshark	11	80	0 - 780	LC	LC	749993	20	variety of bottom invertebrates and bony fishes

Table F4. Continued

Species	Common name	max L_0	min L_{max}	Depth	IUCN Global	IUCN Europe	Total N	Years	Diet
Raja microocellata	Smalleyed Skate	10	91	0 - 117	NT	NT	1883	20	small crustaceans (J), bony fish (A)
Squalus acanthias	Spiny Dogfish	30	121	0 - 800	VU	EN	72910	20	bony fish, variety of invertebrates
Raja montagui	Spotted Skate	10	80	0 - 530	LC	LC	41499	20	crustaceans, small bony fishes
Mustelus asterias	Starry Smoothhound	38	140	0 - 350	LC	NT	17873	20	crustaceans
Raja clavata	Thornback Skate	13	118	0 - 800	NT	NT	29807	20	small crustaceans (J), larger crustaceans and fish (A)
Amblyraja radiata	Thorny Skate	12	61	0 - 800	VU	LC	22134	20	benthic invertebrates, small bottom fishes
Galeorhinus galeus	Tope shark	40	169	0 - 800	VU	VU	2212	20	bony fishes, variety of invertebrates, less commonly other chondrichthyans
Raja undulata	Undulate Skate	14	114	0 - 200	EN	NT	618	20	benthic invertebrates and fishes
Etmopterus spinax	Velvet Belly	14	45	37 - 800	LC	NT	27144	20	crustaceans, bony fish, cephalopods

Table F5: Beta regression model results. Model 1 is the baseline model with abundance index (multi-species catch per unit effort), transformed to lie between 0 and 1, versus commercial trawling hours per area in square kilometers in International Council for the Exploration of the Sea statistical management areas (whole study area divided in rectangles of 1 degree longitude x 0.5 degrees latitude) as covariate of interest and sea bottom temperature in degree Celsius (SBT), mean depth in meter, the km^2 of the statistical management area protected and dominant substrate type in a statistical management area as additional confounding covariates. Substrate type had 8 factor levels (coarse sediment, fine mud, mixed sediment, mud to muddy sand, rocky or other hard substrata, sand, sandy mud to muddy sand, unknown). Models 2 – 4 account for spatial dependence via a Gaussian correlation term. Given are the estimates of the coefficients, the p value, the confidence intervals (CI), the Akaike information criterion (AIC), and the p-value of Moran's I test for spatial autocorrelation (Moran's I < 0.05 indicates spatial dependency). Non-significant covariates were dropped, starting with the least significant until all covariates were significant. The final model utilized to investigate the effect of commercial trawling on relative elasmobranch abundance across species is given in bold. All models are variable dispersion models, commercial trawling per area was $\log_e$ plus 1 transformed, all other continuous covariates were $\log_e$ transformed, as these models had the lowest AIC compared to non-transformed and non-dispersion models (Table F6).

Model	Coefficient	Estimate	P value	2.5% CI	97.5% CI	AIC	Moran's I
1	Intercept	-5.56	0.0000	-7.09	-4.02	-1143.9	0.0000
	log trawl hours per area	-0.77	0.0000	-1.04	-0.50		
	log SBT	1.51	0.0000	0.92	2.09		
	log mean depth	0.21	0.0000	0.11	0.30		
	log area protected	-0.02	0.1660	-0.06	0.01		
	Substrate fine mud	-0.80	0.0005	-1.25	-0.36		
	Substrate mixed	-0.28	0.6141	-1.36	0.80		
	Substrate mud to muddy sand	-1.02	0.0045	-1.73	-0.32		
	Substrate rock or other hard substrata	-0.58	0.0589	-1.19	0.02		
	Substrate sand	-0.57	0.0000	-0.81	-0.33		
	Substrate sandy mud to muddy sand	-0.61	0.0001	-0.92	-0.29		
	Substrate unknown	-1.15	0.0000	-1.61	-0.68		
2	Intercept	-6.66	0.0000	-9.45	-3.87	-1243.0	0.9873
	log trawl hours per area	-0.62	0.0000	-0.91	-0.33		
	log SBT	1.39	0.0101	0.33	2.45		
	log mean depth	0.27	0.0014	0.10	0.44		
	log area protected	0.02	0.1925	-0.01	0.06		
	Substrate fine mud	-0.36	0.1637	-0.87	0.15		
	Substrate mixed	-0.58	0.3113	-1.71	0.55		
	Substrate mud to muddy sand	-0.41	0.4541	-1.48	0.66		
	Substrate rock or other hard substrata	-0.45	0.2001	-1.13	0.24		
	Substrate sand	0.03	0.8435	-0.26	0.32		
	Substrate sandy mud to muddy sand	-0.14	0.4620	-0.52	0.24		
	Substrate unknown	-0.21	0.5036	-0.81	0.40		

Table F5. Continued.

Model	Coefficient	Estimate	P value	2.5% CI	97.5% CI	AIC	Moran's I
3	Intercept	-6.73	0.0000	-9.47	-4.00	-1255.8	0.9890
	log trawl hours per area	-0.63	0.0000	-0.91	-0.34		
	log SBT	1.45	0.0063	0.41	2.48		
	log mean depth	0.25	0.0028	0.08	0.41		
	log area protected	0.02	0.2521	-0.02	0.06		
4	**Intercept**	**-6.61**	**0.0000**	**-9.32**	**-3.91**	**-1262.6**	**0.9861**
	log trawl hours per area	**-0.62**	**0.0000**	**-0.90**	**-0.33**		
	log SBT	**1.46**	**0.0055**	**0.43**	**2.49**		
	log mean depth	**0.23**	**0.0037**	**0.08**	**0.39**		

Table F6: Beta regression model selection. Shown is the full model with abundance index (multi-species catch per unit effort), transformed to lie between 0 and 1, versus the covariates commercial trawling hours per area (km^2) in International Council for the Exploration of the Sea statistical management areas (whole study area divided in rectangles of 1 degree longitude x 0.5 degrees latitude), sea bottom temperature (SBT), mean depth in meter, the km^2 of the statistical management area protected and dominant substrate type in a statistical management area. Substrate type had 8 factor levels (coarse sediment, fine mud, mixed sediment, mud to muddy sand, rocky or other hard substrata, sand, sandy mud to muddy sand, unknown). Tested were all covariates, variable dispersion models (trawl hours per area | trawl hours per area), commercial trawling per area $\log_e$ plus 1 transformed and all other continuous covariates $\log_e$ transformed and a Gaussian spatial correlation term (gau). The selected model is given in bold, based on the lowest the Akaike information criterion (AIC) of all models that had no spatial autocorrelation (Moran's I test for spatial autocorrelation p-value > 0.05).

Model	AIC	Moran's I
~ trawl hours per area + SBT + mean depth + area protected + substrate	-1087.8	0.0000
~ log trawl hours per area + log SBT + log mean depth + log area protected + substrate	-1132.0	0.0000
~ trawl hours per area | trawl hours per area + SBT + mean depth + area protected + substrate	-1090.4	0.0000
~ log trawl hours per area | log trawl hours per area + log SBT + log mean depth + log area protected + substrate	-1143.9	0.0000
~ trawl hours per area + SBT + mean depth + area protected + substrate + gau	-1189.6	0.9792
~ log trawl hours per area + log SBT + log mean depth + log area protected + substrate + gau	-1233.3	0.9735
~ trawl hours per area | trawl hours per area + SBT + mean depth + area protected + substrate + gau	-1190.4	0.9886
~ log trawl hours per area | log trawl hours per area + log SBT + log mean depth + log area protected + substrate + gau	**-1243.0**	**0.9873**

Appendix G
Copyright permissions

Electronic supplement

The copyright permissions for Chapter 2 and Chapter 6 are provided as electronic supplement available from DalSpace (http://dalspace.library.dal.ca).

Bibliography

Aasen, O. (1961) Some Observations on the Biology of the Porbeagle Shark (*Lamna nasus* L.). Vol. 109.

Andrews, A. H., Kerr, L. A., Burgess, G. H. & Cailliet, G. M. (2011) Bomb Radiocarbon and Tag-Recapture Dating of Sandbar Shark (*Carcharhinus plumbeus*). Fishery Bulletin 109, 454–465.

Ardizzone, D., Cailliet, G. M., Natanson, L. J., Andrews, A. H., Kerr, L. A. & Brown, T. A. (2006) Application of Bomb Radiocarbon Chronologies to Shortfin Mako (*Isurus oxyrinchus*) Age Validation. Environmental Biology of Fishes 77, 355–366.

Baker, T. T., Lafferty, R. & Quinn II, T. J. (1991) A General Growth Model for Mark-Recapture Data. Fisheries Research 11, 257–281.

Barneche, D. R., Robertson, D. R., White, C. R. & Marshall, D. J. (2018) Supplementary Materials for Fish Reproductive-Energy Output Increases Disproportionately with Body Size. Science 360, 52pp.

Baum, J. K. & Myers, R. A. (2004) Shifting Baselines and the Decline of Pelagic Sharks in the Gulf of Mexico. Ecology Letters 7, 135–145.

Baum, J. K., Myers, R. A., Kehler, D. G., Worm, B., Harley, S. J. & Doherty, P. A. (2003) Collapse and Conservation of Shark Populations in the Northwest Atlantic. Science 299, 389–392.

Benoît, H. P., Swain, D. P., Hutchings, J. A., Knox, D., Doniol-valcroze, T. & Bourne, C. M. (2018) Evidence for Reproductive Senescence in a Broadly Distributed Harvested Marine Fish. Marine Ecology Progress Series 592, 207–224.

von Bertalanffy, L. (1938) A Quantitative Theory of Organic Growth (Inquiries on Growth Laws. II). Human Biology 10, 181–213.

von Bertalanffy, L. (1960) Principles and Theory of Growth. Fundamental aspects of normal and malignant growth 493, 137–259.

Beverton, R. J. H. (1992) Patterns of Reproductive Strategy Parameters in Some Marine Teleost Fishes. Journal of Fish Biology 41 (Supplement B), 137–160.

Beverton, R. J. H. & Holt, S. J. (1959) A Review of the Lifespans and Mortality Rates of Fish in Nature, and Their Relation to Growth and Other Physiological Characteristics. O'Connor, G. E. W. W. and M., ed. Rome: CIBA Foundation Colloquia on Ageing.

Beyer, J. E., Kirchner, C. H. & Holtzhausen, J. A. (1999) A Method to Determine Size-Specific Natural Mortality Applied to Westcoast Steenbras (*Lithognathus aureti*) in Namibia. Fisheries Research 41, 133–153.

Boerder, K., Schiller, L. & Worm, B. (2019) Not All Who Wander Are Lost: Improving Spatial Protection for Large Pelagic Fishes. Marine Policy 105, 80–90.

C. Boettiger, D. T. Lang and P. C. Wainwright. "rfishbase: exploring, manipulating and visualizing FishBase data from R". Journal of Fish Biology 81.6 (Nov. 2012), pp. 2030-2039. DOI:10.1111/j.1095-8649.2012.03464.x

Bond, M. E., Babcock, E. A., Pikitch, E. K., Abercrombie, D. L., Lamb, N. F. & Chapman, D. D. (2012) Reef Sharks Exhibit Site-Fidelity and Higher Relative Abundance in Marine Reserves on the Mesoamerican Barrier Reef. PLoS ONE 7, 1–14.

Bond, M. E., Valentin-Albanese, J., Babcock, E. A., Abercrombie, D., Lamb, N. F., Miranda, A., Pikitch, E. K. & Chapman, D. D. (2017) Abundance and Size Structure of a Reef Shark Population within a Marine Reserve Has Remained Stable for More than a Decade. Marine Ecology Progress Series.

Bonham, K., Sanford, F. B., Clegg, W., & Bucher, G. C. (1949). Biological and vitamin A studies of dogfish landed in the State of Washington (*Squalus suckleyi*). Washington Department of Fisheries Report, 49, 83-114.

Braccini, M. & Taylor, S. (2016) The Spatial Segregation Patterns of Sharks from Western. Royal Society Open Science 3: 160306, 1–7.

Brodziak, J., Ianelli, J., Lorenzen, K. & Methot Jr., R. D. (2011) Estimating Natural Mortality in Stock Assessment Applications. Vol. 119.

Bubley, W. J., Kneebone, J., Sulikowski, J. A. & Tsang, P. C. W. (2012) Reassessment of Spiny Dogfish *Squalus acanthias* Age and Growth Using Vertebrae and Dorsal-Fin Spines. Journal of Fish Biology 80, 1300–1319.

Du Buit, M. H. (1977) Age et Croissance de *Raja batis* et de *Raja naevus* En Mer Celtique. ICES Journal of Marine Science 37, 261–265.

Cadima, E.L. (2003) Fish stock assessment manual. FAO Fisheries Technical Paper, 393.

Cailliet, G. M. (1990) Age and Growth Elasmobranch Age Determination and Verification : An Updated Review.

Cailliet, G. M. (2015) Perspectives on Elasmobranch Life-History Studies: A Focus on Age Validation and Relevance to Fishery Management. Journal of Fish Biology 87, 1271–1292.

Cailliet, G. M. & Goldman, K. J. (2004) Age Determination and Validation in Chondrichthyan Fishes. In Biology of Sharks and Their Relatives pp. 399–447.

Cailliet, G. M., Mollet, H. F., Pittenger, G. G., Bedford, D. & Natanson, L. J. (1992) Growth and Demography of the Pacific Angle Shark (*Squatina californica*), Based upon Tag Returns off California. Marine and Freshwater Research 43, 1313–1330.

Cailliet, G. M., Smith, W. D., Mollet, H. F. & Goldman, K. J. (2006) Age and Growth Studies of Chondrichthyan Fishes: The Need for Consistency in Terminology, Verification, Validation, and Growth Function Fitting. Environmental Biology of Fishes 77, 211–228.

Camhi, M., Fowler, S., Musick, J., Bräutigam, A. & Fordham, S. (1998) Sharks and Their Relatives - Ecology and Conservation. Gland, Switzerland and Cambridge, UK: IUCN/SSC Shark Specialist Group. IUCN.

Campana, S., Marks, L., Joyce, W., Hurley, P., Showell, M. & Kulka, D. (1999) An Analytical Assessment of the Porbeagle Shark (*Lamna nasus*) Population in the Northwest Atlantic. Canadian Stock Assessment Secretariat Research Document.

Campana, S. E. (2001) Accuracy, Precision and Quality Control in Age Determination, Including a Review of the Use and Abuse of Age Validation Methods. Journal of Fish Biology 59, 197–242.

Campana, S. E. (2014) Age Determination of Elasmobranchs with Special Reference to Mediterranean Species: A Technical Manual. Rome.

Campana, S. E., Natanson, L. J. & Myklevoll, S. (2002) Bomb Dating and Age Determination of Large Pelagic Sharks. Canadian Journal of Fisheries and Aquatic Sciences 59, 450–455.

Campana, S. E., Joyce, W. & Kulka, D. W. (2009) Growth and Reproduction of Spiny Dogfish off the Eastern Coast of Canada, Including Inferences on Stock Structure. In Biology and Management of Dogfish Sharks (Gallucci, V. F., McFarlane, G. A., Bargmann, G. G., eds), pp. 195–208 Bethesda Maryland: American Fisheries Society.

Capape, C., Ben Souissi, J., Mejri, H., Guelorget, O. & Hemida, F. (2005) The Reproductive Biology of the School Shark, *Galeorhinus galeus* Linnaeus 1758 (Chondrichthyes: Triakidae), from the Maghreb Shore (Southern Mediterranean). Acta Adriatica 46, 109–124.

Capapé, C. & Mellinger, J. (1988) Nouvelles Données Sur La Biologie de La Reproduction Du Milandre, *Galeorhinus galeus* (Linné, 1758), (Pisces, Triakidae) Des Côtes Tunisiennes. Cahiers de Biologie Marine 29, 135–146.

Carlisle, A., Tickler, D., Dale, J., Ferretti, F., Curnick, D., Chapple, T., Schallert, R., Castleton, M. & Block, B. (2019) Estimating Space Use of Mobile Fishes in a Large Marine Protected Area with Methodological Considerations in Acoustic Array Design. Frontiers in Marine Science 6, 1–17.

Carlson, J. K., Sulikowski, J. R. & Baremore, I. E. (2006) Do Differences in Life History Exist for Blacktip Sharks, *Carcharhinus limbatus*, from the United States South Atlantic Bight and Eastern Gulf of Mexico? Environmental Biology of Fishes 77, 279–292.

Casini, M., Eero, M., Carlshamre, S. & Lovgren, J. (2016) Original Article Using Alternative Biological Information in Stock Assessment: Condition-Corrected Natural Mortality of Eastern Baltic Cod. ICES Journal of Marine Science 73, 2625–2631.

Cassoff, R. M., Campana, S. E. & Myklevoll, S. (2007) Changes in Baseline Growth and Maturation Parameters of Northwest Atlantic Porbeagle, *Lamna nasus*, Following Heavy Exploitation. Canadian Journal of Fisheries and Aquatic Sciences 64, 19–29.

Castro, J. I. (2011). The sharks of north America. Oxford University Press.

Charnov, E. L., Berrigan, D. & Shine, R. (1993) The M/k Ratio Is the Same for Fish and Reptiles. The American Naturalist 142, 707–711.

Charnov, E. L., Gislason, H. & Pope, J. G. (2013) Evolutionary Assembly Rules for Fish Life Histories. Fish and Fisheries 14, 213–224.

Cheilari, A. & Rätz, H. J. (2009) The Effect of Natural Mortality on the Estimation of Stock State Parameters and Derived References for Sustainable Fisheries Management.

Chen, S. & Watanabe, S. (1989) Age Dependence of Natural in Fish Population Mortality Coefficient Dynamics. Nippon Suisan Gakkaishi 55, 205–208.

Clark, W. G. (1999) Effects of an Erroneous Natural Mortality Rate on a Simple Age-Structured Stock Assessment. Canadian Journal of Fisheries and Aquatic Sciences 56, 1721–1731.

Claudet, J., Osenberg, C. W., Domenici, P., Badalamenti, F., Milazzo, M., Falcón, J. M., Bertocci, I., Benedetti-Cecchi, L., García-Charton, J.-A., Goñi, R., et al. (2010) Marine Reserves : Fish Life History and Ecological Traits Matter. Ecological Applications 20, 830–839.

Conrath, C. L. (2005) Reproductive Biology. Musick, J. A., Bonfil, R., eds. Food and Agriculture Organization.

Cook, R., Fariñas-Franco, J. M., Gell, F. R., Holt, R. H. F., Holt, T., Lindenbaum, C., Porter, J. S., Seed, R., Skates, L. R., Stringell, T. B., et al. (2013) The Substantial First Impact of Bottom Fishing on Rare Biodiversity Hotspots: A Dilemma for Evidence-Based Conservation. PLoS ONE 8, 1–10.

Cortes, E. (1998) Demographic Analysis as an Aid in Shark Stock Assessment and Management. 39, 199–208.

Cortes, E. (2000) Life History Patterns and Correlations in Sharks. Reviews in Fisheries Science 8, 299–344.

Cortes, E. (2002) Incorporating Uncertainty into Demographic Modeling: Application to Shark Populations and Their Conservation. Conservation Biology 16, 1048–1062.

Cramp, J. E., Simpfendorfer, C. A. & Pressey, R. L. (2018) Beware Silent Waning of Shark Protection. Science 360, 723.

Cribari-Neto, F. & Zeileis, A. (2010) Journal of Statistical Software. Journal of Statistical Software 34, 1–24.

Davidson, L. N. K. & Dulvy, N. K. (2017) Global Marine Protected Areas to Prevent Extinctions. Nature Ecology & Evolution 1, 1–6.

Day, J., Dudley, N., Hockings, M., Holmes, G., Laffoley, D., Stolton, S. & Wells, S. (2012) Guidelines for Applying the IUCN Protected Area Management Categories to Marine Protected Areas. Gland, Switzerland: IUCN.

Deroba, J. J. & Schueller, A. M. (2013) Performance of Stock Assessments with Misspecified Age- and Time-Varying Natural Mortality. Fisheries Research 146, 27–40.

DFO. (2017) Recovery Potential Assessment for Winter Skate (*Leucoraja ocellata*): Eastern Scotian Shelf and Newfoundland Population.

Dulvy, N. K., Fowler, S. L., Musick, J. A., Cavanagh, R. D., Kyne, P. M., Harrison, L. R., Carlson, J. K., Davidson, L. N. K., Fordham, S. V., Francis, M. P., et al. (2014) Extinction Risk and Conservation of the World's Sharks and Rays. eLife 3:e00590, 34p.

Dureuil, M. (2013) Status and Conservation of Sharks in the Northeast Atlantic, Christian-Albrechts-Universitat zu Kiel.

Dureuil, M. & Worm, B. (2015) Estimating Growth from Tagging Data: An Application to North-East Atlantic Tope Shark *Galeorhinus galeus*. Journal of Fish Biology 87, 1389–1410.

Dureuil, M., Towner, A. V., Ciolfi, L. G. & Beck, L. A. (2015) A Computer-Aided Framework for Subsurface Identification of White Shark Pigment Patterns. African Journal of Marine Science 37, 363–371.

Ebert, D. A. & Stehmann, M. F. W. (2013) Sharks, Batoids and Chimaeras of the North Atlantic. Rome.

Edgar, G. J., Stuart-Smith, R. D., Willis, T. J., Kininmonth, S., Baker, S. C., Banks, S., Barrett, N. S., Becerro, M. A., Bernard, A. T. F., Berkhout, J., et al. (2014) Global Conservation Outcomes Depend on Marine Protected Areas with Five Key Features. Nature 506, 216–220.

Edwards, R. R. C. (1980) Aspects of the Population Dynamics and Ecology of the White Spotted Stingaree, *Urolophus paucimaculatus* Dixon, in Port Phillip Bay, Victoria. Australian Journal of Marine and Freshwater Research 31, 459–467.

EFSA (2013). European Federation of Sea Anglers Acceptable Species & European Records. The tope (*Galeorhinus galeus*). Available at http://www.efsa.co.uk/record/tope.htm (last accessed 21 September 2013).

Eigaard, O. R., Bastardie, F., Hintzen, N. T., Buhl-Mortensen, L., Buhl-Mortensen, P., Catarino, R., Dinesen, G. E., Egekvist, J., Fock, H. O., Geitner, K., et al. (2017) The Footprint of Bottom Trawling in European Waters: Distribution, Intensity, and Seabed Integrity. ICES Journal of Marine Science 74, 847–865.

Ellis, J. R., Cruz-Martínez, A., Rackham, B. D. & Rogers, S. I. (2005) The Distribution of Chondrichthyan Fishes around the British Isles and Implications for Conservation. Journal of Northwest Atlantic Fishery Science 35, 195–213.

Escalle, L., Speed, C. W., Meekan, M. G. & White, W. T. (2015) Restricted Movements and Mangrove Dependency of the Nervous Shark *Carcharhinus cautus* in Nearshore Coastal Waters. Journal of Fish Biology 87, 323–341.

Espinoza, M., Cappo, M., Heupel, M. R., Tobin, A. J. & Simpfendorfer, C. A. (2014) Quantifying Shark Distribution Patterns and Species-Habitat Associations: Implications of Marine Park Zoning. PLoS ONE 9.

EU (2002) European Union, Directive 2002/59/EC of the European Parliament and of the Council of 27 June 2002 establishing a Community vessel traffic monitoring and information system and repealing Council Directive 93/75/EEC, OJ L208/10.

EU (2013) European Union, Regulation (EU) No 1380/2013 of the European Parliament and of the council of 11 December 2013, on the Common Fisheries Policy, amending Council Regulations (EC) No 1954/2003 and (EC) No 1224/2009 and repealing Council Regulations (EC) No 2371/2002 and (EC) No 639/2004 and Council Decision 2004/585/EC, L 354/22.

EU (2016) European Union, Regulation (EU) 2016/2336 of the European parliament and of the council of 14 December 2016 establishing specific conditions for fishing for deep-sea stocks in the north-east Atlantic and provisions for fishing in international waters of the north-east Atlantic and repealing Council Regulation (EC) No 2347/2002.

European Union. (2016) The EU in the World 2016 Edition, 2016th ed. Helene, S., Wolff, P., eds. Luxembourg: European Union.

Eveson, J. P., Polacheck, T. & Laslett, G. M. (2007) Consequences of Assuming an Incorrect Error Structure in von Bertalanffy Growth Models: A Simulation Study. Canadian Journal of Fisheries and Aquatic Sciences 64, 602–617.

Fabens, A. J. (1965) Properties and Fitting of the von Bertalanffy Growth Curve. Growth 29, 265–289.

Fahy, E. (1989) Growth Parameters of Rays (Batoidei) in Irish Waters, from Material Examined in Commercial Catches. ICES Document CM 59, 1–11.

Farrell, E. D. (2010) The Life History and Population Biology of the Starry Smoothhound, *Mustelus asterias*, in the Northeast Atlantic Ocean, University College Dublin.

Farrell, E. D., Mariani, S. & Clarke, M. W. (2010) Age and Growth Estimates for the Starry Smoothhound (*Mustelus asterias*) in the Northeast Atlantic Ocean. ICES Journal of Marine Science 67, 931–939.

Fernandes, P. G., Ralph, G. M., Nieto, A., Criado, M. G., Vasilakopoulos, P., Maravelias, Christos. D. Cook, R. M., Pollom, R. A., Kovačić, M., Pollard, D., Farrell, E. D., et al. (2017) Coherent Assessments of Europe's Marine Fishes Show Regional Divergence and Megafauna Loss. Nature Ecology & Evolution 1, 1–8.

Ferreira, B. P. & Vooren, C. M. (1991) Age, Growth, and Structure of Vertebra in the School Shark *Galeorhinus galeus* (Linnaeus, 1758) from Southern Brazil. Fishery Bulletin 89, 19–31.

Ferretti, F., Myers, R. A., Serena, F. & Lotze, H. K. (2008) Loss of Large Predatory Sharks from the Mediterranean Sea. Conservation Biology 22, 952–964.

Ferretti, F., Worm, B., Britten, G. L., Heithaus, M. R. & Lotze, H. (2010) Patterns and Ecosystem Consequences of Shark Declines in the Ocean. Ecology Letters 13, 1055–1071.

Finucci, B., Dunn, M. R. & Arnold, R. (2019) Using Length – Mass Relationships to Estimate Life History: An Application to Deep-Sea Fishes. Canadian Journal of Fisheries and Aquatic Sciences 76, 723–739.

Fox, J. & Weisberg, S. (2011). An R Companion to Applied Regression, 2nd edn. Thousand Oaks: Sage. Available at http://socserv.socsci.mcmaster.ca/jfox/Books/Companion (last accessed 15 January 2015). 2009/WGEF/wgef_2009.pdf (last accessed 13 September 2013).

Francis, M. P. (2006) Morphometric Minefields — towards a Measurement Standard for Chondrichthyan Fishes. Environmental Biology of Fishes 77, 407–421.

Francis, M. P. & Mulligan, K. P. (1998) Age and Growth of New Zealand School Shark, *Galeorhinus galeus*. New Zealand Journal of Marine and Freshwater Research 32, 427–440.

Francis, M. P., Campana, S. E. & Jones, C. M. (2007) Age Under-Estimation in New Zealand Porbeagle Sharks (*Lamna nasus*): Is There an Upper Limit to Ages That Can Be Determined from Shark Vertebrae? Marine and Freshwater Research 58, 10–23.

Francis, M. P., Natanson, L. J. & Campana, S. E. (2008) The Biology and Ecology of the Porbeagle Shark, *Lamna nasus*. In Sharks of the Open Ocean Biology, Fisheries and Conservation (Camhi, M. D., Pikitch, E. K., Babcock, E. A., eds), pp. 105–113 Oxford: Blackwell Publishing Ltd.

Francis, R. I. C. C. (1988a) Are Growth Parameters Estimated from Tagging and Age-Length Data Comparable? Canadian Journal of Fisheries and Aquatic Sciences 45, 936–942.

Francis, R. I. C. C. (1988b) Maximum Likelihood Estimation of Growth and Growth Variability from Tagging Data. New Zealand Journal of Marine and Freshwater Research 22, 43–51.

Frisk, M. G., Miller, T. J. & Fogarty, M. J. (2001) Estimation and Analysis of Biological Parameters in Elasmobranch Fishes: A Comparative Life History Study. Canadian Journal of Fisheries and Aquatic Sciences 58, 969–981.

Froese, R. (2006) Cube Law, Condition Factor and Weight – Length Relationships: History, Meta-Analysis and Recommendations. Journal of Applied Ichthyology 22, 241–253.

Froese, R. & Binohlan, C. (2000) Empirical Relationships to Estimate Asymptotic Length, Length at First Maturity and Length at Maximum Yield per Recruit in Fishes, with a Simple Method to Evaluate Length Frequency Data. Journal of Fish Biology 56, 758–773.

Froese, R. & Luna, S. (2004) No Relationship between Fecundity and Annual Reproductive Rate in Bony Fish. Acta Ichthyologica et Piscatoria 34, 11–20.

Froese, R. & Pauly, D. (2013) Fish Stocks. Encyclopedia of Biodiversity: Second Edition 3, 477–487.

Froese, R. & Pauly, D. (2018) FishBase www.fishbase.org (accessed Feb 6, 2018).

Froese, R., Stern-Pirlot, A., Winker, H. & Gascuel, D. (2008) Size Matters: How Single-Species Management Can Contribute to Ecosystem-Based Fisheries Management. Fisheries Research 92, 231–241.

Froese, R., Winker, H., Gascuel, D., Sumaila, U. R. & Pauly, D. (2016) Minimizing the Impact of Fishing. Fish and Fisheries 173, 785–802.

Froese, R., Winker, H., Coro, G., Demirel, N., Tsikliras, A. C., Dimarchopoulou, D., Scarcella, G., Probst, W. N., Dureuil, M. & Pauly, D. (2018) A New Approach for Estimating Stock Status from Length Frequency Data. ICES Journal of Marine Science 75, 2004–2015.

Froese, R., Winker, H., Coro, G., Demirel, N., Tsikliras, A. C., Dimarchopoulou, D., Scarcella, G., Probst, W. N., Dureuil, M. & Pauly, D. (2019) Reply On the Pile-up Effect and Priors for L Inf and M / K : Response to a Comment by Hordyk et Al . on " A New Approach for Estimating Stock Status from Length Frequency Data ". ICES Journal of Marine Science 76, 461–465.

Gallagher, A. J., Wagner, D. N., Irschick, D. J. & Hammerschlag, N. (2014) Body Condition Predicts Energy Stores in Apex Predatory Sharks. Conservation Physiology 2, 1–8.

Gallagher, M. J., Nolan, C. P. & Jeal, F. (2005) Age, Growth and Maturity of the Commercial Ray Species from the Irish Sea. Journal of Northwest Atlantic Fishery Science 35, 47–66.

Gallucci, V. F., Saila, S. B., Gustafson, D. J. & B.J., R. (1996) Stock Assessment: Quantitative Methods and Applications for Small Scale Fisheries. Boca Raton: CRC Press.

Gallucci, V. F., Taylor, I. G. & Erzini, K. (2006) Conservation and Management of Exploited Shark Populations Based on Reproductive Value. Canadian Journal of Fisheries and Aquatic Sciences 63, 931–942.

Garla, R. C., Chapman, D. D., Wetherbee, B. M. & Shivji, M. (2006) Movement Patterns of Young Caribbean Reef Sharks, *Carcharhinus perezi*, at Fernando de Noronha Archipelago, Brazil:

The Potential of Marine Protected Areas for Conservation of a Nursery Ground. Marine Biology.

Gelman, A., Carlin, J. B., Stern, H. S., Dunson, D. B., Vehtari, A., & Rubin, D. B. (2014). Bayesian data analysis. Third Edition Chapman and Hall/CRC.

George, J. C., Bada, J., Zeh, J., Scott, L., Brown, S. E., O'Hara, T. & Suydam, R. (1999) Age and Growth Estimates of Bowhead Whales (*Balaena mysticetus*) via Aspartic Acid Racemization. Canadian Journal of Zoology 77, 571–580.

Germanov, E. S., Bejder, L., Chabanne, D. B. H., Dharmadi, D., Hendrawan, I. G., Marshall, A. D., Pierce, S. J., van Keulen, M., Loneragan, N. R. & Stewart, J. D. (2019) Contrasting Habitat Use and Population Dynamics of Reef Manta Rays Within the Nusa Penida Marine Protected Area, Indonesia. Frontiers in Marine Science 6, 1–17.

Gislason, H., Daan, N., Rice, J. C. & Pope, J. G. (2010) Size, Growth, Temperature and the Natural Mortality of Marine Fish. Fish and Fisheries 11, 149–158.

Goldman, K. J., Cailliet, G. M., Andrews, A. H. & Natanson, L. J. (2012) Assessing the Age and Growth of Chondrichthyan Fishes. In Biology of Sharks and Their Relatives pp. 423–451.

Graham, F., Rynne, P., Estevanez, M., Luo, J., Ault, J. S. & Hammerschlag, N. (2016) Use of Marine Protected Areas and Exclusive Economic Zones in the Subtropical Western North Atlantic Ocean by Large Highly Mobile Sharks. Diversity and Distributions 22, 534–546.

Grant, C. J., Sandland, R. L. & Olsen, A. M. (1979) Estimation of Growth, Mortality and Yield per Recruit of the Australian School Shark, *Galeorhinus australis* (Macleay), from Tag Recoveries. Australian Journal of Marine and Freshwater Research 30, 625–637.

Gruber, S. H., De Marignac, J. R. & Hoenig, J. M. (2001) Survival of Juvenile Lemon Sharks at Bimini, Bahamas, Estimated by Mark–Depletion Experiments. Transactions of the American Fisheries Society 130, 376–384.

Gulland, J. A. (1971) The Fish Resources of the Ocean. Gulland, J. A., ed. 23 Rosemount Avenue, West Byfleet, Surrey, England: Fishing News (Books) Ltd.

Gulland, J. A. & Holt, S. J. (1959) Estimation of Growth Parameters for Data at Unequal Time Intervals. ICES Journal of Marine Science 25, 47–49.

Haddon, M. 2011. Modeling and quantitative methods in fisheries. Second edition, Chapman & Hall/CRC, New York, London, Taylor and Francis Group.

Hamady, L. L., Natanson, L. J., Skomal, G. B. & Thorrold, S. R. (2014) Vertebral Bomb Radiocarbon Suggests Extreme Longevity in White Sharks. PLoS ONE 9.

Hammerschlag, N. & Sulikowski, J. (2011) Killing for Conservation: The Need for Alternatives to Lethal Sampling of Apex Predatory Sharks. Endangered Species Research 14, 135–140.

Hammerschlag, N., Skubel, R. A., Sulikowski, J., Irschick, D. J., & Gallagher, A. J. (2018). A comparison of reproductive and energetic states in a marine apex predator (the tiger shark, *Galeocerdo cuvier*). Physiological and Biochemical Zoology, 91(4), 933-942.

Hammond, T. R. & Ellis, J. R. (2005) Bayesian Assessment of Northeast Atlantic Spurdog Using a Stock Production Model, with Prior for Intrinsic Population Growth Rate Set by Demographic Methods. Journal of Northwest Atlantic Fishery Science 35, 299–308.

Harry, A. V. (2017) Evidence for Systemic Age Underestimation in Shark and Ray Ageing Studies. Fish and Fisheries 1–16.

Hearn, W. S. & Polacheck, T. (2003) Estimating Long-Term Growth-Rate Changes of Southern Bluefin Tuna (*Thunnus maccoyii*) from Two Periods of Tag-Return Data. Fishery Bulletin 101, 58–74.

Henderson, A. C., Flannery, K. & Dunne, J. (2003) Biological Observations on Shark Species Taken in Commercial Fisheries to the West of Ireland. Biology and Environment: Proceedings of the Royal Irish Academy 103B, 1–7.

Heupel, M. R. & Simpfendorfer, C. A. (2002) Estimation of Mortality of Juvenile Blacktip Sharks, *Carcharhinus limbatus*, within a Nursery Area Using Telemetry Data. Canadian Journal of Fisheries and Aquatic Sciences 59, 624–632.

Heupel, M. R. & Simpfendorfer, C. A. (2011) Estuarine Nursery Areas Provide a Low-Mortality Environment for Young Bull Sharks *Carcharhinus leucas*. Marine Ecology Progress Series 433, 237–244.

Hewitt, D. A. & Hoenig, J. M. (2005) Comparison Of Two Approaches For Estimating Natural Mortality Based On Longevity. Fishery Bulletin 103, 433–437.

Hewitt, D. A., Lambert, D. M., Hoenig, J. M., Lipcius, R. N., Bunnel, D. B. & Miller, T. J. (2007) Direct and Indirect Estimates of Natural Mortality for Chesapeake Bay Blue Crab. Transactions of the American Fisheries Society 136, 1030–1040.

Hisano, M., Connolly, S. R. & Robbins, W. D. (2011) Population Growth Rates of Reef Sharks with and without Fishing on the Great Barrier Reef: Robust Estimation with Multiple Models. PLoS ONE 6, e25028.

Hoenig, J. (1983) Empirical Use of Longevity Data to Estimate Mortality Rates. Fishery Bulletin 82, 898–903.

Hoenig, J. M. (1982) A Compilation of Mortality and Longevity Estimates for Fish, Mollusks, and Cetaceans, with a Bibliography of Comparative Life History Studies. Kingston, Rhode Island.

Hoenig, J. M. & Gruber, S. H. (1990) Life-History Patterns in the Elasmobranchs: Implications for Fisheries Management. Vol. 90.

Hoenig, J. M., Barrowman, N. J., Hearn, W. S. & Pollock, K. H. (1998) Multiyear Tagging Studies Incorporating Fishing Effort Data. Canadian Journal of Fisheries and Aquatic Sciences 55, 1466–1476.

Hoenig, J. M., Then, A. Y.-H., Babcock, E. A., Hall, N. G., Hewitt, D. A. & Hesp, S. A. (2016) The Logic of Comparative Life History Studies for Estimating Key Parameters, with a Focus on Natural Mortality Rate. ICES Journal of Marine Science 73, 2453–2467.

Hoffman, M. D., and A. Gelman. 2014. “The No-U-Turn Sampler: Adaptively Setting Path Lengths in Hamiltonian Monte Carlo.” Journal of Machine Learning Research 15 (1), 1593–1623.

Holden, M. J. & Horrod, R. G. (1979) The Migrations of Tope, *Galeorhinus galeus* (L), in the Eastern North Atlantic as Determined by Tagging. Journal du Conseil International pour l’ Exploration de la Mer 38, 314–317.

Hordyk, A., Ono, K., Sainsbury, K., Loneragan, N. & Prince, J. (2015) Some Explorations of the Life History Ratios to Describe Length Composition, Spawning-per-Recruit, and the Spawning Potential Ratio. ICES Journal of Marine Science 72, 204–216.

Huynh, Q. C., Beckensteiner, J., Carleton, L. M., Marcek, B. J., Nepal KC, V., Peterson, C. D., Wood, M. A. & Hoenig, J. M. (2018) Comparative Performance of Three Length-Based Mortality Estimators. Marine and Coastal Fisheries: Dynamics, Management, and Ecosystem Science 10, 298–313.

ICES. (2009) Report of the Joint Meeting between ICES Working Group on Elasmobranch Fishes (WGEF) and ICCAT Shark Subgroup. Copenhagen, Denmark.

ICES. (2014) Report of the Working Group on Elasmobranch Fishes (WGEF). Lisbon, Portugal.

ICES. (2016) Report of the Workshop on Guidance on How Pressure Maps of Fishing Intensity Contribute to an Assessment of the State of Seabed Habitats (WKFBI). ICES HQ, Copenhagen, Denmark.

ICES. (2017a) EU Request on Indicators of the Pressure and Impact of Bottom-Contacting Fishing Gear on the Seabed, and of Trade-Offs in the Catch and the Value of Landings. ICES special request advice 1–29.

ICES. (2017b) Report of the Working Group on Elasmobranch Fishes.

Ingle, D. I., Natanson, L. J. & Porter, M. E. (2018) Mechanical Behavior of Shark Vertebral Centra at Biologically Relevant Strains. Journal of Experimental Biology 221, jeb188318.

Irschick, D. J. & Hammerschlag, N. (2014) A New Metric for Measuring Condition in Large Predatory Sharks. Journal of Fish Biology 85, 917–926.

IUCN. (2018) Applying IUCN's Global Conservation Standards to Marine Protected Areas (MPA).

James, I. R. (1991) Estimation of von Bertalanffy Growth Curve Parameters from Recapture Data. Biometrics 47, 1519–1530.

Jensen, A. L. (1985) Relations Among Net Reproductive Rate and Life History Parameters for Lake Whitefish (*Coregonus clupeaformis*). Canadian Journal of Fisheries and Aquatic Sciences 42, 164–168.

Jensen, A. L. (1996) Beverton and Holt Life History Invariants Result from Optimal Trade-off of Reproduction and Survival. Canadian Journal of Fisheries and Aquatic Sciences 53, 820–822.

Johannes, R. E. (1998) The Case for Data-Less Marine Resource Management: Examples from Tropical Nearshore Finfisheries. 5347, 243–246.

Johnson, K. F., Monnahan, C. C., McGilliard, C. R., Vert-pre, K. A., Anderson, S. C., Cunningham, C. J., Hurtado-Ferro, F., Licandeo, R. R., Muradian, M. L., Ono, K., et al. (2015) Time-Varying Natural Mortality in Fisheries Stock Assessment Models: Identifying a Default Approach. ICES Journal of Marine Science 72, 137–150.

Jones, K. R., Venter, O., Fuller, R. A., Allan, J. R., Maxwell, S. L., Negret, P. J. & Watson, J. E. M. (2018) One-Third of Global Protected Land Is under Intense Human Pressure. Science 360, 788–791.

Jones, O. R., Gaillard, J.-M., Tuljapurkar, S., Alho, J. S., Armitage, K. B., Becker, P. H. & Bize, P. (2008) Senescence Rates Are Determined by Ranking on the Fast – Slow Life-History Continuum. Ecology Letters 11, 664–673.

Kalish, J. M. & Johnstone, J. (2001) Determination of School Shark Age Based on Analysis of Radiocarbon in Vertebral Collagen. Vol. 93. Final Report FRDC Project.

Kenchington, T. J. (2014) Natural Mortality Estimators for Information-Limited Fisheries. Fish and Fisheries 15, 533–562.

Ketchen, K. S. (1972) Size at Maturity, Fecundity, and Embryonic Growth of the Spiny Dogfish (*Squalus acanthias*) in British Columbia Waters. Journal of the Fisheries Board of Canada 29, 1717–1723.

Kimura, D. K. (1980) Likelihood Methods for the von Bertalanffy Growth Curve. Fishery Bulletin 77, 765–776.

Kimura, D. K. (2008) Extending the von Bertalanffy Growth Model Using Explanatory Variables. Canadian Journal of Fisheries and Aquatic Sciences 65, 1879–1891.

Kimura, D. K., Shimada, A. M. & Lowe, S. A. (1993) Estimating von Bertalanffy Growth-Parameters of Sablefish *Anoplopoma fimbria* and Pacific Cod *Gadus macrocephalus* Using Tag-Recapture Data. Fishery Bulletin 91, 271–280.

Kindsvater, H. K., Mangel, M., Reynolds, J. D. & Dulvy, N. K. (2016) Ten Principles from Evolutionary Ecology Essential for Effective Marine Conservation. Ecology and Evolution 6, 2125–2138.

Kindsvater, H. K., Dulvy, N. K., Horswill, C., Juan-Jorda, M.-J., Mangel, M. & Matthiopoulos, J. (2018) Overcoming the Data Crisis in Biodiversity Conservation. Trends in Ecology & Evolution 33, 676–688.

Kinney, M. J., Wells, R. J. D. & Kohin, S. (2016) Oxytetracycline Age Validation of an Adult Shortfin Mako Shark *Isurus oxyrinchus* after 6 Years at Liberty. Journal of Fish Biology 89, 1828–1833.

Knip, D. M., Heupel, M. R. & Simpfendorfer, C. A. (2012a) Evaluating Marine Protected Areas for the Conservation of Tropical Coastal Sharks. Biological Conservation 148, 200–209.

Knip, D. M., Heupel, M. R. & Simpfendorfer, C. A. (2012b) Mortality Rates for Two Shark Species Occupying a Shared Coastal Environment. Fisheries Research 125–126, 184–189.

Kohler, N. E. & Turner, P. A. (2001) Shark Tagging: A Review of Conventional Methods and Studies. Environmental Biology of Fishes 60, 191–223.

Kohler, N. E., Casey, J. G. & Turner, P. A. (1996) Length-Length and Length-Weight Relationships for 13 Shark Species from the Western North Atlantic. Narragansett.

Kristensen, Kasper, Anders Nielsen, Casper W. Berg, Hans Skaug, and Bradley M. Bell. (2016). “TMB: Automatic Differentiation and Laplace Approximation.” Journal of Statistical Software 70 (5): 21.

Kroodsma, D. A., Mayorga, J., Hochberg, T., Miller, N. A., Boerder, K., Ferretti, F., Wilson, A., Bergman, B., White, T. D., Block, B. A., et al. (2018) Tracking the Global Footprint of Fisheries. Science 359, 904–908.

Kyne, P. M., Jabado, R. W., Rigby, C. L., Dharmadi, Gore, M. A., Pollock, C. M., Herman, K. B., Cheok, J., Ebert, D. A., Simpfendorfer, C. A., et al. (2019) The Thin Edge of the Wedge: Extremely High Extinction Risk in Wedgefishes and Giant Guitarfishes. bioRxiv 595462.

Laslett, G. M., Eveson, J. P. & Polacheck, T. (2002) A Flexible Maximum Likelihood Approach for Fitting Growth Curves to Tag & Recapture Data. Canadian Journal of Fisheries and Aquatic Sciences 59, 976–986.

Last, P., Naylor, G., Séret, B., White, W., de Carvalho, M., & Stehmann, M. (Eds.). (2016). Rays of the World. CSIRO publishing.

Lee, H., Maunder, M. N., Piner, K. R. & Methot, R. D. (2011) Estimating Natural Mortality within a Fisheries Stock Assessment Model: An Evaluation Using Simulation Analysis Based on Twelve Stock Assessments. Fisheries Research 109, 89–94.

Legendre, P., 2018. lmodel2: Model II Regression. R package version 1.7-3. https://CRAN.R-project.org/package=lmodel2

Lenth, R., 2018. emmeans: Estimated Marginal Means, aka Least-Squares Means. R package version 1.1.3. https://CRAN.R-project.org/package=emmeans

Lenth, R.V., 2016. Least-Squares Means: The R Package lsmeans. Journal of Statistical Software, 69(1), 1-33. doi:10.18637/jss.v069.i01

Lessa, R., Batista, V. S. & Santana, F. M. (2016) Close to Extinction? The Collapse of the Endemic Daggernose Shark (*Isogomphodon oxyrhynchus*) off Brazil. Global Ecology and Conservation 7, 70–81.

Lester, N. P., Shuter, B. J. & Abrams, P. A. (2004) Interpreting the von Bertalanffy Model of Somatic Growth in Fishes: The Cost of Reproduction. Proceedings of the Royal Society of London. Series B: Biological Sciences 271, 1625–1631.

Liu, K., Chin, C., Chen, C. & Chang, J. (2015) Estimating Finite Rate of Population Increase for Sharks Based on Vital Parameters. PLoS ONE 10, e0143008.

Lombardi-Carlson, L. A. (2007) Life History Traits of Bonnethead Sharks, *Sphyrna tiburo*, from the Eastern Gulf of Mexico.

Lorenzen, K. (1996) The Relationship between Body Weight and Natural Mortality in Juvenile and Adult Fish: A Comparison of Natural Ecosystems and Aquaculture. Journal of Fish Biology 49, 627–647.

Lorenzen, K. (2000) Allometry of Natural Mortality as a Basis for Assessing Optimal Release Size in Fish-Stocking Programmes. Canadian Journal of Fisheries and Aquatic Sciences 57, 2374–2381.

Lucifora, L. O., Menni, R. C., & Escalante, A. H. (2002). Reproductive ecology and abundance of the sand tiger shark, *Carcharias taurus*, from the southwestern Atlantic. ICES Journal of Marine Science, 59(3), 553-561.

Maceina, M. J. & Sammons, S. M. (2016) Assessing the Accuracy of Published Natural Mortality Estimators Using Rates Determined from Five Unexploited Freshwater Fish Populations. North American Journal of Fisheries Management 36, 433–446.

Magris, R. A. & Pressey, R. L. (2018) Marine Protected Areas: Just for Show? Science 360, 723–727.

Maindonald, J.H., and Braun, J.W. (2015). DAAG: Data Analysis and Graphics Data and Functions. R package version 1.22. https://CRAN.R-project.org/package=DAAG

Maller, R. A. & deBoer, E. S. (1988) An Analysis of Two Methods of Fitting the von Bertalanffy Curve to Capture-Recapture Data. Australian Journal of Marine and Freshwater Research 39, 459–466.

Manning, M. J. & Francis, M. P. (2005) Age and Growth of Blue Shark (*Prionace glauca*) from the New Zealand Exclusive Economic Zone. New Zealand Fisheries Assessment Report 26, 52.

Maunder, M. N. & Wong, R. A. (2011) Approaches for Estimating Natural Mortality: Application to Summer Flounder (*Paralichthys dentatus*) in the US Mid-Atlantic. Fisheries Research 111, 92–99.

Mcauley, R. B., Simpfendorfer, C. A. & Hall, N. G. (2007) A Method for Evaluating the Impacts of Fishing Mortality and Stochastic Influences on the Demography of Two Long-Lived Shark Stocks. ICES Journal of Marine Science 64, 1710–1722.

McAuley, R. B., Simpfendorfer, C. A., Hyndes, G. A., Allison, R. R., Chidlow, J. A., Newman, S. J. & Lenanton, R. C. J. (2006) Validated Age and Growth of the Sandbar Shark, *Carcharhinus plumbeus* (Nardo 1827) in the Waters off Western Australia. Environmental Biology of Fishes 77, 385–400.

McCord, M. E. (2005) Aspects of the Ecology and Management of the Soupfin Shark (*Galeorhinus galeus*) in South Africa, Rhodes University, Grahamston, South Africa.

McCoy, M. W. (2008) Predicting Natural Mortality Rates of Plants and Animals. Ecological Letters 11, 710–716.

McCulloch, C.E., Searle, S.R. (2000). Generalized, Linear, and Mixed Models. Wiley, Chichester, New York.

Mccully, S. R., Scott, F. & Ellis, J. R. (2012) Lengths at Maturity and Conversion Factors for Skates (Rajidae) around the British Isles, with an Analysis of Data in the Literature. ICES Journal of Marine Science 69, 1812–1822.

McPhie, R. P. & Campana, S. E. (2009) Reproductive Characteristics and Population Decline of Four Species of Skate (Rajidae) off the Eastern Coast of Canada. Journal of Fish Biology 75, 223–246.

Meyer, C. G., O'Malley, J. M., Papastamatiou, Y. P., Dale, J. J., Hutchinson, M. R., Anderson, J. M., Royer, M. A. & Holland, K. N. (2014) Growth and Maximum Size of Tiger Sharks (*Galeocerdo cuvier)* in Hawaii. PLoS ONE 9.

Mollie et al. 2017, glmmTMB balances speed and flexibility among packages for zero-inflated generalized linear mixed modeling. R J. 9, 378–400.

Moreau, J., Bambino, C. & Pauly, D. (1986) Indices of Overall Growth Performance of 100 Tilapia (Cichlidae) Populations. Maclean, J. L., Dizon, L. B., Hosillo, L. V., eds. Manila, Philippines.

Moulton, P. L., Saddlier, S. R. & Knuckey, I. A. (1989) New Time-at-Liberty Record Set by Tagged School Shark *Galeorhinus galeus* Caught off Southern Australia. North American Journal of Fisheries Management 9, 254–255.

Moulton, P. L., Walker, T. I. & Saddlier, S. R. (1992) Age and Growth Studies of Gummy Shark, *Mustelus antarcticus* (Giinther), and School Shark, *Galeorhinus galeus* (Linnaeus), from Southern Australian Waters. Australian Journal of Marine and Freshwater Research 43, 1241–1267.

Musick, J. A. (1999) Criteria to Define Extinction Risk in Marine Fishes. The American Fisheries Society Initiative 24, 6–14.

Nadon, M. O. & Ault, J. S. (2016) A Stepwise Stochastic Simulation Approach to Estimate Life History Parameters for Data-Poor Fisheries. Canadian Journal of Fisheries and Aquatic Sciences 73, 1–11.

Nammack, M. F., Musick, J. A. & Colvocoresses, J. A. (1985) Life History of Spiny Dogfish off the Northeastern United States. Transactions of the American Fisheries Society 114, 367–376.

Natanson, L. J. & Cailliet, G. M. (1990) Vertebral Growth Zone Deposition in Pacific Angel Sharks. Copeia 1133–1145.

Natanson, L. J., Mello, J. J. & Campana, S. E. (2002) Validated Age and Growth of the Porbeagle Shark (*Lamna nasus*) in the Western North Atlantic Ocean. Fishery Bulletin 100, 266–278.

Natanson, L. J., Kohler, N. E., Ardizzone, D., Cailliet, G. M., Wintner, S. P. & Mollet, H. F. (2006) Validated Age and Growth Estimates for the Shortfin Mako, *Isurus oxyrinchus*, in the North Atlantic Ocean. Environmental Biology of Fishes 77, 367–383.

Natanson, L. J., Gervelis, B. J., Winton, M. V., Hamady, L. L., Gulak, S. J. B. & Carlson, J. K. (2014) Validated Age and Growth Estimates for *Carcharhinus obscurus* in the Northwestern Atlantic Ocean, with Pre- and Post Management Growth Comparisons. Environmental Biology of Fishes 97, 881–896.

Natanson, L. J., Skomal, G. B., Hoffmann, S. L., Porter, M. E., Goldman, K. J. & Serra, D. (2018) Age and Growth of Sharks: Do Vertebral Band Pairs Record Age? Marine and Freshwater Research 69, 1440–1452.

Nelson, G. A. (2013). fishmethods: Fishery Science Methods and Models in R. R package version 1.5-0. Available at http://CRAN.R-project.org/package=fishmethods (last accessed 17 January 2015).

Nielsen, J., Steffensen, J. F., Christiansen, J. S., Heinemeier, J., Simon, M., Steffensen, K. F., Ramsey, C. B., Olsen, J., Bushnell, P. G., Hedeholm, R. B., et al. (2016) Eye Lens Radiocarbon Reveals Centuries of Longevity in the Greenland Shark (*Somniosus microcephalus).* Science 353, 702–704.

Nieto, A., Ralph, G. M., Comeros-Raynal, M. T., Kemp, J., Criado, M. G., Allen, D. J., Dulvy, N. K., Walls, R. H. L., Russell, B., Pollard, D., et al. (2015) European Red List of Marine Fishes. Luxembourg: Publications Office of the European Union.

Nussey, D. H., Froy, H., Lemaitre, J.-F., Gaillard, J.-M. & Austad, S. N. (2013) Senescence in Natural Populations of Animals: Widespread Evidence and Its Implications for Bio-Gerontology. Ageing Research Reviews 12, 214–225.

Officer, R. A., Gason, A. S., Walker, T. I. & Clement, J. G. (1996) Sources of Variation in Counts of Growth Increments in Vertebrae from Gummy Shark, *Mustelus antarcticus*, and School Shark, *Galeorhinus galeus*: Implications for Age Determination. Canadian Journal of Fisheries and Aquatic Sciences 53, 1765–1777.

Ohsumi, S. (1979) Interspecies Relationships among Some Biological Parameters in Cetaceans and Estimation of the Natural Mortality Coefficient of the Southern Hemisphere Minke Whale. Report of the International Whaling Commission 29, 397–406.

Olsen, A. M. (1954) The Biology, Migration, and Growth Rate of the School Shark, *Galeorhinus australis* (Macleay) (Carcharhanidae) in South-Eastern Australian Waters. Australian Journal of Marine and Freshwater Research 5, 353–410.

Olsen, A. M. (1984) Synopsis of Biological Data on the School Shark, *Galeorhinus australis* (Macleay 1881). In FAO Fisheries Synopsis pp. 1–42.

Pante, E. & Simon-Bouhet, B. (2013) Marmap: A Package for Importing, Plotting and Analyzing Bathymetric and Topographic Data in R. PLoS ONE 8, 6–9.

Pardo, S. A., Cooper, A. B. & Dulvy, N. K. (2013) Avoiding Fishy Growth Curves. Methods in Ecology and Evolution 4, 353–360.

Pauly, D. (1979) Gill Size and Temperature as Governing Factors in Fish Growth: A Generalization of von Bertalanffy's Growth Formula. Berichte aus dem Institut für Meereskunde an der Christian-Albrechts-Universität Kiel 63, 1–156.

Pauly, D. (1980) On the Interrelationships between Natural Mortality, Growth Parameters, and Mean Environmental Temperature in 175 Fish Stocks. ICES Journal of Marine Science 39, 175–192.

Pauly, D. (1984) Fish Population Dynamics in Tropical Waters: A Manual for Use with Programmable Calculators. In WorldFish.

Pauly, D. & Gaschutz, G. (1979) A Simple Method for Fitting Oscillating Length Growth Data, with a Program for Pocket Calculators. ICES CM 6, 1–26.

Pauly, D. & Munro, J. L. (1984) Once More on the Comparison of Growth in Fish and Invertebrates. Fishbyte 2, 1–21.

Pauly, D. & Soriano, M. L. (1986) Some Practical Extensions to Beverton and Holt's Relative Yield-Per-Recruit Model*. Manila, Philippines.

Pauly, D. & Morgan, G. R. (1987) Length-Based Methods in Fisheries Research.

Pauly, D., Soriano-Bartz, M., Moreau, J. & Jarre-Teichmann, A. (1992) A New Model Accounting for Seasonal Cessation of Growth in Fishes. Australian Journal of Marine and Freshwater Research 43, 1151–1156.

Pauly, D., Moreau, J. & Gayanilo, J. F. C. (1996) A New Method for Comparing the Growth Performance of Fishes, Applied to Wild and Farmed Tilapias. In: The Third International Symposium on Tilapia in Aquaculture, ICLARM Conf. Proc. 41. Biometry pp. 433–441 San Francisco: W.H. Freeman and Company.

Peres, M. B. & Vooren, C. M. (1991) Sexual Development, Reproductive Cycle, and Fecundity of the School Shark *Galeorhinus galeus* off Southern Brazil. Fishery Bulletin 89, 655–667.

Peterson, I. & Wroblewski, S. (1984) Mortality Rate of Fishes in the Pelagic Ecosystem. Canadian Journal of Fisheries and Aquatic Sciences 41, 1117–1120.

Pilling, G. M., Kirkwood, G. P. & Walker, S. G. (2002) An Improved Method for Estimating Individual Growth Variability in Fish, and the Correlation between von Bertalanffy Growth Parameters. Canadian Journal of Fisheries and Aquatic Sciences 59, 424–432.

Le Port, A., Lavery, S. & Montgomery, J. C. (2012) Conservation of Coastal Stingrays: Seasonal Abundance and Population Structure of the Short-Tailed Stingray *Dasyatis brevicaudata* at a Marine Protected Area. ICES Journal of Marine Science 69, 1427–1435.

Powter, D. M. & Gladstone, W. (2008) Demographic Analysis of the Port Jackson Shark *Heterodontus portusjacksoni* in the Coastal Waters of Eastern Australia. Marine 59, 444–455.

Pratt, H. (1979) Reproduction in the Blue Shark, *Prionace glauca*. Fishery Bulletin 77, 445–470.

Prince, J. & Hordyk, A. (2018) What to Do When You Have Almost Nothing: A Simple Quantitative Prescription for Managing Extremely Data-Poor Fisheries. Fish and Fisheries 224–238.

Prince, J., Hordyk, A., Valencia, S. R., Loneragan, N. & Sainsbury, K. (2015) Revisiting the Concept of Beverton–Holt Life-History Invariants with the Aim of Informing Data-Poor Fisheries Assessment. ICES Journal of Marine Science 72, 194–203.

Punt, A., Smith, D. C. & Koopman, M. T. (2005) Using Information for 'data-Rich' Species to Inform Assessments of 'Data-Poor' Species through Bayesian Stock Assessment Methods.

R Core Team (2013). R: A language and environment for statistical computing. Available at http://www.R-project.org/ (last accessed 21 January 2015).

R Core Team, 2017. R: A language and environment for statistical computing. R Foundation for Statistical Computing, Vienna, Austria. URL https://www.R-project.org/.

Reker, J., Annunziatellis, A., Mo, G., Tunesi, L., Globevnik, L., Snoj, L., Agnesi, S. & Korpinen, S. (2015) Marine Protected Areas in Europe's Seas - An Overview And Perspectives for the Future. Copenhagen.

Ricard, D., Minto, C., Jensen, O. P. & Baum, J. K. (2012) Examining the Knowledge Base and Status of Commercially Exploited Marine Species with the RAM Legacy Stock Assessment Database. Fish and Fisheries 13, 380–398.

Ricker, W. E. (1979) Growth Rates and Models. Academic Press Inc. Vol. 8.

Roff, D. A. (1984) The Evolution of Life History Parameters in Teleosts. Canadian Journal of Fisheries and Aquatic Sciences 41, 989–1000.

Roff, G., Brown, C. J., Priest, M. A. & Mumby, P. J. (2018) Decline of Coastal Apex Shark Populations over the Past Half Century. Communications Biology 1, 1–11.

Ryland, J. S. & Ajayi, T. O. (1984) Growth and Population Dynamics of Three Raja Species (Batoidei) in Carmarthen Bay, British Isles. ICES Journal of Marine Science 41, 111–120.

Sainsbury, K. J. (1980) Effect of Individual Variability on the von Bertalanffy Growth Equation. Canadian Journal of Fisheries and Aquatic Sciences 37, 241–247.

Sguotti, C., Lynam, C. P., García-Carreras, B., Ellis, J. R. & Engelhard, G. H. (2016) Distribution of Skates and Sharks in the North Sea: 112 Years of Change. Global Change Biology 22, 2729–2743.

Da Silva, C., Kerwath, S. E., Attwood, C. G., Thorstad, E. B., Cowley, P. D., Økland, F., Wilke, C. G. & Næsje, T. F. (2013) Quantifying the Degree of Protection Afforded by a No-Take Marine Reserve on an Exploited Shark. African Journal of Marine Science 35, 57–66.

Simpfendorfer, C. A. (1993) Age and Growth of the Australian Sharpnose Shark, *Rhizoprionodon taylori*, from North Queensland, Australia. Environmental Biology of Fishes 36, 233–241.

Simpfendorfer, C. A. (1999) Mortality Estimates and Demographic Analysis for the Australian Sharpnose Shark, *Rhizoprionodon taylori*, from Northern Australia. Fishery Bulletin 97, 978–986.

Simpfendorfer, C. A. (2000) Growth Rates of Juvenile Dusky Sharks, *Carcharhinus obscurus* (Lesueur, 1818), from Southwestern Australia Estimated from Tag-Recapture Data. Fishery Bulletin 98, 811–822.

Simpfendorfer, C. A. & Dulvy, N. K. (2017) Bright Spots of Sustainable Shark Fishing. Current Biology 27, R83–R102.

Simpfendorfer, C. A., Bonfil, R. & Latour, R. J. (2005) Mortality Estimation. Vol. 474.

Sims, S. E. (1984) An Analysis of the Effect of Errors in the Natural Mortality Rate on Stock-Size Estimates Using Virtual Population Analysis (Cohort Analysis). ICES Journal of Marine Science 41, 149–153.

SISP 1-IBTS VIII, 2012. International Council for the Exploration of the Sea, “Manual for the International Bottom Trawl Surveys. Series of ICES Survey Protocols”.

Skomal, G. B. & Natanson, L. J. (2003) Age and Growth of the Blue Shark (*Prionace glauca*) in the North Atlantic Ocean. Fishery Bulletin 101, 627–639.

Smart, J. J., Chin, A., Tobin, A. . J. & Simpfendorfer, C. A. (2016) Multimodel Approaches in Shark and Ray Growth Studies: Strengths, Weaknesses and the Future. Fish and Fisheries 17, 955–971.

Smith, S. E., Au, D. W. & Show, C. (1998) Intrinsic Rebound Potentials of 26 Species of Pacific Sharks. Marine and Freshwater Research 49, 663–678.

Smithson, M. & Verkuilen, J. (2006) A Better Lemon Squeezer? Maximum-Likelihood Regression with Beta-Distributed Dependent Variables. Psychological Methods 11, 54–71.

Soetaert, K. (2009). rootSolve: Nonlinear root finding, equilibrium and steady-state analysis of ordinary differential equations. Available at http://cran.r-project.org/web/packages/rootSolve/index.html (last accessed 21 January 2015).

Somers, I. F. (1988) On a Seasonally Oscillating Growth Function. Fishbyte 6, 8–11.

de Souza, E. N., Boerder, K., Matwin, S. & Worm, B. (2016) Improving Fishing Pattern Detection from Satellite AIS Using Data Mining and Machine Learning. PLoS ONE 11, 1–20.

Sparre, P. & Venema, S. C. (1999) Introduction to Tropical Fish Stock Assessment. Part 1: Manual. FAO Fisheries Technical Paper 306, 1–407.

Speed, C. W., Cappo, M. & Meekan, M. G. (2018) Evidence for Rapid Recovery of Shark Populations within a Coral Reef Marine Protected Area. Biological Conservation 220, 308–319.

SSTP (2010). Scottish Shark Tagging Programme. Progress Report December. Available at http://www.ssacn.org/wp-content/pdf/readroom/2010b%20SSTP%20Progress%20Report%20Dec.pdf (last accessed 17 September 2015).

Stevens, J. D. (1990) Further Results from a Tagging Study of Pelagic Sharks in the North-East Atlantic. Journal of the Marine Biological Association of the UK 70, 707–720.

Stevens, J. D. (2008) The Biology and Ecology of the Shortfin Mako Shark, *Isurus oxyrinchus*. In Sharks of the Open Ocean Biology, Fisheries and Conservation (Camhi, M. D., Pikitch, E. K., Babcock, E. A., eds), pp. 87–94 Oxford: Blackwell Publishing Ltd.

Stevens, J. D. & McLoughlin, K. J. (1991) Distribution, Size and Sex Composition, Reproductive Biology and Diet of Sharks from Northern Australia. Australian Journal of Marine and Freshwater Research 42, 151–199.

Stevens, J. D., Bonfil, R., Dulvy, N. K. & Walker, P. A. (2000) The Effects of Fishing on Sharks, Rays, and Chimaeras (Chondrichthyans), and the Implications for Marine Ecosystems. ICES Journal of Marine Science 57, 476–494.

Stone, H. (2017). Shark LF data. BIO 2017/09/30, provided on 30 September 2017.

Taylor, C. C. (1958) Cod Growth and Temperature. ICES Journal of Marine Science 23, 366–370.

Taylor, I. G., Gertseva, V., Methot Jr., R. D. & Maunder, M. N. (2013) A Stock – Recruitment Relationship Based on Pre-Recruit Survival, Illustrated with Application to Spiny Dogfish Shark. Fisheries Research 142, 15–21.

Then, A. Y., Hoenig, J. M., Hall, N. G. & Hewitt, D. A. (2015) Evaluating the Predictive Performance of Empirical Estimators of Natural Mortality Rate Using Information on over 200 Fish Species. ICES Journal of Marine Science 72, 82–92.

Thorson, J. T., Munch, S. B., Cope, J. M. & Gao, J. (2017) Predicting Life History Parameters for All Fishes Worldwide. Ecological Applications 27, 2262–2276.

Thrush, S. F. & Dayton, P. K. (2002) Disturbance to Marine Benthic Habitats by Trawling and Dredging: Implications for Marine Biodiversity. Annual Review of Ecology and Systematics 33, 449–473.

Tovar-Ávila, J., Troynikov, V. S., Walker, T. I. & Day, R. W. (2009) Use of Stochastic Models to Estimate the Growth of the Port Jackson Shark, *Heterodontus portusjacksoni*, off Eastern Victoria, Australia. Fisheries Research 95, 230–235.

Vega, N. M., Gallucci, V. F., Hauser, L. & Franks, J. (2009) Differences in Growth in the Spiny Dogfish over a Latitudinal Gradient in the Northeast Pacific .In Biology and Management of Dogfish Sharks (Gallucci, V. F., McFarlane, G. A., Bargmann, G., eds), pp. 169–180.

Vetter, E. F. (1988) Estimation of Natural Mortality in Fish Stocks: A Review. Fishery Bulletin 86, 25–43.

Walker, P. A. (1999) Fleeting Images Dynamics of North Sea Ray Populations, University of Amsterdam.

Walker, T. I. (2007) Spatial and Temporal Variation in the Reproductive Biology of Gummy Shark *Mustelus antarcticus* (Chondrichthyes: Triakidae) Harvested off Southern Australia. Marine and Freshwater Research 58, 67–97.

Walker, T. I., Brown, L. P. & Clement, J. G. (2001) Age Validation from Tagged School and Gummy Sharks Injected with Oxytetracycline. Queenscliff, Victoria, Australia.

Walker, T. I., Cavanagh, R. D., Stevens, J. D., Carlisle, A. B., Chiaramonte, G. E., Domingo, A., Ebert, D. A., Mancusi, C. M., Massa, A., McCord, M., et al. (2006) *Galeorhinus galeus*, Tope http://dx.doi.org/10.2305/IUCN.UK.2006.RLTS.T39352A10212764.en (accessed Jul 18, 2019).

Walther, B. A. & Moore, J. L. (2005) The Concepts of Bias, Precision and Accuracy, and Their Use in Testing the Performance of Species Richness Estimators, with a Literature Review of Estimator Performance. Ecography 28, 815–829.

Wang, Y.-G. (1999) Estimating Equations for Parameters in Stochastic Growth Models from Tag-Recapture Data. Biometrics 55, 900–903.

Wang, Y. (1998) An Improved Fabens Method for Estimation of Growth Parameters in the von Bertalanffy Model with Individual Asymptotes. Canadian Journal of Fisheries and Aquatic Sciences 55, 397–400.

Wang, Y. & Thomas, M. R. (1995) Accounting for Individual Variability in the von Bertalanffy Growth Model. Canadian Journal of Fisheries and Aquatic Sciences 52, 1368–1375.

Ward-Paige, C. A. & Worm, B. (2017) Global Evaluation of Shark Sanctuaries. Global Environmental Change 47, 174–189.

Ward-Paige, C. A., Keith, D. M., Worm, B. & Lotze, H. K. (2012) Recovery Potential and Conservation Options for Elasmobranchs. Journal of Fish Biology 80, 1844–1869.

WCC-2016-Rec-102-EN. (2016) Protected Areas and Other Areas Important for Biodiversity in Relation to Environmentally Damaging Industrial Activities and Infrastructure Development.

Wells, D. R. J., Smith, S. E., Kohin, S., Freund, E., Spear, N. & Ramon, D. A. (2013) Age Validation of Juvenile Shortfin Mako (*Isurus oxyrinchus*) Tagged and Marked with Oxytetracycline off Southern California. Fishery Bulletin 111, 147–160.

White, T. D., Carlisle, A. B., Kroodsma, D. A., Block, B. A., Casagrandi, R., De Leo, G. A., Gatto, M., Micheli, F. & Mccauley, D. J. (2017) Assessing the Effectiveness of a Large Marine Protected Area for Reef Shark Conservation. Biological Conservation 207, 64–71.

Worm, B. (2017) How to Heal an Ocean. Nature 543, 630–631.

Worm, B., Davis, B., Kettemer, L., Ward-Paige, C. A., Chapman, D., Heithaus, M. R., Kessel, S. T. & Gruber, S. H. (2013) Global Catches, Exploitation Rates, and Rebuilding Options for Sharks. Marine Policy 40, 194–204.

Yin, Y., Aeberhard, W. H., Smith, S. J. & Mills Flemming, J. (2019) Identifiable State-Space Models: A Case Study of the Bay of Fundy Sea Scallop Fishery. Canadian Journal of Statistics 47, 27–45.

Yokoi, H., Ijima, H., Ohshimo, S. & Yokawa, K. (2017) Impact of Biology Knowledge on the Conservation and Management of Large Pelagic Sharks. Scientific Reports 7, 14pp.

Zhang, Z., Lessard, J. & Campbell, A. (2009) Use of Bayesian Hierarchical Models to Estimate Northern Abalone, Haliotis Kamtschatkana, Growth Parameters from Tag-Recapture Data. Fisheries Research 95, 289–295.

Zhou, S., Yin, S., Thorson, J. T., Smith, A. D. M. & Fuller, M. (2012) Linking Fishing Mortality Reference Points to Life History Traits: An Empirical Study. Canadian Journal of Fisheries and Aquatic Sciences 69, 1292–1301.